A thesis

entitled

THE MAGNETOCRYSTALLINE ANISOTROPY AND OTHER MAGNETIC PROPERTIES OF FERROMAGNETIC METALS

by

Peter Martin Wallis, BSc.,A.R.C.S.

Submitted for the

Degree of Doctor of Philosophy

of the

University of London

Imperial College of Science and Technology

London

1965

ABSTRACT

The work described in this thesis is concerned with the temperature dependence of the magnetocrystalline anisotropy of nickel and gadolinium and with certain related magnetic properties such as domain structure and magnetostriction. The anisotropy measurements on nickel permitted the determination of both the first (K_1) and second (K_2) anisotropy constants.

The most difficult measurement was that of the second anisotropy constant - at room temperature existing measurements of K_2 differed even as to sign and no attempt had previously been made to determine its variation with temperature. The magnitude of K_2 was obtained directly by measuring the torque on a disc-shaped single-crystal specimen oriented parallel to a (111) plane. K_1 does not contribute to the torque in this plane and the contribution from K_2 is itself small, even with a relatively large specimen. Spurious torques arising from inadequacies in the torque measuring system can therefore be important and they were overcome only after a novel form of torque meter had been developed. Measurements of K_2 and K_1 for nickel and gadolinium were made within the temperature range 92°K to 347°K.

The data obtained for nickel revealed an unexpected variation of torque with inverse field at low temperatures. This necessitated a detailed and original calculation of the

magnetization process (including the effect of the specimen demagnetizing factor) and led to a modification to the usual extrapolation procedure for determining anisotropy constants.

The agreement between calculation and experiment was so good that predictions could be made about a related magnetic phenomenon, namely magnetostriction, and these predictions were verified by further experimental measurements.

Finally, the apparatus and measuring techniques were employed to investigate the anisotropy of gadolinium in the interesting temperature range in which the directions of easy magnetization lie on the surface of a cone surrounding the hexagonal axis. These measurements are fully described together with some related observations of domains on this material.

C O N T E N T S

1

INTRODUCTION

1.1 Intrinsic Magnetization 8

1.2 Technical Magnetization 25

1.3 Anisotropy 32

1.4 The Temperature Dependence of Magnetocrystalline Anisotropy in Cubic Crystals 39

1.5 Magnetostriction in Ferromagnetic Single Crystal Materials 49

2

THE MAGNETIZATION PROCESS

2.1 Anisotropy 59

2.2 The (111) Plane for Nickel 67

2.3 Magnetostriction 78

2.4 Magnetostriction in the (111) Plane for Nickel 81

3

DESIGN OF APPARATUS AND SPECIMEN PREPARATION

3.1 The Torque Meter 90

3.2 Apparatus for Temperature Control and Auxiliary Apparatus 102

3.3 Preparation of the Nickel Specimen 112

3.4 Preparation of the Gadolinium Specimen 123

3.5 Preparation of the Magnetic Colloid 125

4

EXPERIMENTAL MEASUREMENTS AND RESULTS

4.1 Preliminary and Other Checks on Performance of Apparatus 128

4.2 Magnetocrystalline Anisotropy Constants, K_1 and K_2 for Nickel 139

4.3 Forced Magnetostriction in Nickel in the (111) Plane 150

4.4 Torque Measurements on Gadolinium 159

4.5 Domain Observations on Gadolinium..... 165

5

NUMERICAL RESULTS

5.1 Anisotropy Measurements, (111) Nickel 170

5.2 Anisotropy Measurements, (110) Nickel 172

5.3 Anisotropy Measurements on Gadolinium 174

5.4 Magnetostriction Measurements on (111) Nickel 176

TABLES 5.1 - 5.12 179

6

DISCUSSION OF RESULTS AND CONCLUSIONS

6.1 The Anisotropy Measurements 199

6.2 The Theory for the Magnetization Process in the (111) Plane 204

6.3 Magnetostriction Measurements on Nickel 207

6.4 Anisotropy Measurements on Gadolinium 209

6.5 Domain Observations on Gadolinium 211

6.6 Proposals for Further Research 212

ACKNOWLEGEMENTS 216

REFERENCES 217

APPENDIX

CHAPTER ONE.

I N T R O D U C T I O N

The work described in this thesis is concerned with the temperature dependence of the magnetocrystalline anisotropy of nickel and gadolinium, and with certain related magnetic properties such as domain structures and magnetostriction. The anisotropy measurements on nickel permitted the determination of both the first (K_1) and second (K_2) anisotropy constants.

Prior to the present investigation there was little agreement between previous measurements of the second anisotropy constant of nickel. In fact different workers reported values of differing signs and the accurate measurement of this constant is only achieved with difficulty. The most reliable method of determining anisotropy constants is by measurement of the torque on a single crystal disc of the metal when it is subjected to a saturating magnetic field. If, as is customary, the disc is chosen to have its surface parallel to a (110) plane, then both K_1 and K_2 may be obtained from one set of measurements. However the contribution to the torque from K_2 is at least an order of magnitude smaller than that from K_1 and it may in fact be smaller than the experimental uncertainties involved, so that such determinations of K_2 are unreliable. A specimen with a (111) plane parallel to the disc surface may, however, be used to measure K_2 alone, and although K_1 does not contribute to the torque in this plane, the contribution from K_2 is itself small, even with a relatively large specimen. Spurious torques arising from inadequacies in the torque measuring system are therefore important and they were overcome only after a novel form

of torque meter had been developed.

To obtain the anisotropy constant from the torque measurements, the normal procedure is to plot the torque amplitude against the reciprocal of the field. Extrapolation to the intercept $\frac{1}{H} = 0$ then gives the torque amplitude at infinite field, which is required since only then is the direction of the magnetization coincident with the applied field direction. Under these circumstances the anisotropy constants may be easily extracted from the torque data. Measurements of K_2 and K_1 for nickel and gadolinium were made within the temperature range $92^{\circ}K$ to $347^{\circ}K$.

The data obtained for nickel revealed an unexpected variation of torque with inverse field at low temperatures. This necessitated a detailed and original calculation of the magnetization process (including the effect of the specimen demagnetizing factor) and led to a modification to the usual extrapolation procedure for determining anisotropy constants.

The agreement between calculation and experiment was so good that predictions could be made about a related magnetic phenomenon, namely magnetostriction, and these predictions were verified by further experimental measurements.

However, before the details of these anisotropy and magnetostriction measurements are dealt with, the background theory is presented in this chapter. First, the intrinsic and technical magnetization of ferromagnets are considered in § 1.1 and § 1.2 and, secondly, these considerations are extended to include existing theories of anisotropy and magnetostriction in § 1.3 to § 1.5.

§1.1 Intrinsic Magnetization.

Magnetic phenomena in ferromagnetic metals arise from the orbital motion and spin of the electrons within the material. A circulation of charge is equivalent to a current loop and therefore to a magnetic dipole, and it maybe shown clasically that the magnetic moment of this dipole is

$$\underset{\sim}{\mu}_e = - g \frac{e}{2mc} \underset{\sim}{j} \qquad (1.1)$$

where $\underset{\sim}{j}$ is the angular momentum of the electron.

Here g is a factor that depends on the details of the electronic motion: it is equal to two if the angular momentum of the electron is due to its spin alone, and is unity when there is only orbital motion. The magnetic properties of a material thus stem from the angular momentum of its electrons.

From the Pauli exclusion principle, it may be shown that complete electron shells of a free atom have no overall angular momentum and so it might be thought that these electrons could not contribute to the magnetic moment of the atoms. In fact, however, the orbital motion of each individual electron causes it to precess in a magnetic field and this precession gives rise to a very small magnetic moment directed in opposition to the applied

field. All the electrons on the atom contribute to this effect, which is known as diamagnetism, regardless of their electronic configuration. However, the diamagnetic moment is very small and is therefore only noticeable when the atom has no incomplete electron shells and therefore no overall angular momentum, or when there are unfilled shells with paired electron spins. When there are unfilled electron shells with unpaired electron spins (each with μ_e given by equation I.I) the resultant magnetic moment on the atom masks the diamagnetic moment. Such electronic configurations occur in the transition elements; for example, iron, cobalt and nickel have respectively 4, 3 and 2 unpaired 3d - electrons per free atom. The rare-earth metal gadolinium, which is also ferromagnetic at room temperature, has 7 unpaired 4f-electrons per free atom.

In the solid, the outer electron shells of each atom interact so that, for instance in iron, cobalt and nickel, the outer electrons are no longer bound but become conduction electrons and the average number of unpaired spins per atom is then no longer an integer. Further, the orbital motion of the electrons in a solid is found to be frozen in, or 'quenched' by the internal electric field produced by the atoms. Hence the orbital magnetic moments of the unpaired electrons can not rotate under the influence of an applied magnetic field and their overall magnetic moment becomes statistically almost zero.

This fact is confirmed by experiments which measure the g-factor (equation 1.1), and which give $g \simeq 1.9$ for iron, cobalt and nickel showing that the magnetic moment arises predominently from the spin angular momentum in these metals. The magnetic moment of each atom may thus be considered to be due just to the unpaired spins on that atom, while the orbital magnetic moments may be ignored.

At high temperatures and with zero applied field, the thermal agitation causes the spin vector $\underline{S}$, and hence the magnetic moment $\underline{\mu}$, of each atom to be oriented randomly with respect to its neighbour and no resultant magnetic moment ensues. If a field is applied the average spin distribution of the atoms is modified since each spin experiences a torque tending to turn it towards the field direction and a magnetic moment may be induced. Below the Curie point, the disordering thermal energy is less important so that the spins tend to align and an overall magnetic moment arises even with no applied field. The interaction energy between a spin and its neighbours may be represented by the energy of a spin in a very powerful internal magnetic field (known as the molecular field) proportional to the magnetization of the material. This is a reasonable approximation since a molecular field represents the result of a co-operative interaction of the spins and the magnetization measures the extent of this co-operation.

Weiss (1907), first postulated the existance of a molecular field and showed that, under suitable conditions, this could lead to the production of a spontaneous magnetization. The molecular field theory which will now be considered, follows Weiss, but is modified to accomodate the requirements of quantum mechanics.

§ 1.1.1. Molecular Field Theory.

It is assumed that the electrons responsible for ferromagnetism are bound to each atom as though the atoms were isolated. The influence of neighbouring atoms on the behaviour of the electrons is then allowed for by assuming that Maxwell-Boltzmann statistics are obeyed, and by introducing the Weiss molecular field. Thus no specific interaction between neighbouring spins is introduced although the collective effect of such an interaction is employed.

The magnetic moment $\underline{\mu}$, of an atom may be written

$$\underline{\mu} = - g \frac{\mu_\beta}{\hbar} \underline{J} \qquad (1.2)$$

where $\mu_\beta = e\hbar/2mc$, g is given by

$$g = 1 + \frac{J(J+1) + S(S+1) - L(L+1)}{2J(J+1)} \qquad (1.3)$$

where S, L and J are the spin, orbit and total angular momentum quantum numbers of the atom measured in units

of π. It is assumed that Russell-Saunders coupling occurs so that $\underline{J} = \underline{L} + \underline{S}$. On application of a magnetic field $\underline{H}$ in the z direction, the magnetic potential energy of the atom due to the magnetic moment of the electron is given by

$$E = -\underline{\mu} \cdot \underline{H} \, . \tag{1.4}$$

The angular momentum vector $\underline{J}$ precesses about the z axis and as a result of spatial quantisation it may only have positions in space such that its component along the z direction has one of $(2J + 1)$ discrete values, namely

$$J_z = J, \; J - 1, \; \ldots\ldots\ldots, \; - J + 2, \; - J + 1, \; - J, \tag{1.5}$$

so that the potential energy may have one of $(2J + 1)$ values given by

$$E = g \mu_\beta \; H \; J_z \tag{1.6}$$

If now the problem is simplified by assuming that the orbital angular momentum does not contribute significantly to the total magnetic moment of the electron, so that $L = 0$, and we take $J = S = \frac{1}{2}$, (since this is the simplest case), then $g = 2$ and J_z may take only the values $\pm \frac{1}{2}$, leading to two energy states E_{+z} and E_{-z}, given, from (1.6), by

$$\begin{aligned} E_{+z} &= + \mu_\beta \; H \\ E_{-z} &= - \mu_\beta \; H \, . \end{aligned} \tag{1.7}$$

If it is further assumed that the Maxwell-Boltzmann statistics are obeyed for a collection of these atoms, then the

.....

number of atoms per unit volume N_{+z}, with energy E_{+z}, will be given by

$$N_{+z} = a\, e^{-\mu_\beta H/kT} \tag{1.8}$$

and similarly,

$$N_{-z} = a\, e^{+\mu_\beta H/kT} \tag{1.9}$$

and since $N_{+z} + N_{-z} = N$, the total number of atoms per unit volume, the constant a is given by

$$a = \frac{N}{e^{+\mu_\beta H/kT} + e^{-\mu_\beta H/kT}} \tag{1.10}$$

and the average magnetic moment along the z axis, $\langle \mu_z \rangle$ will be given by

$$\langle \mu_z \rangle = \frac{1}{N}\left\{ N_{+z}\ (-\mu_\beta) + N_{-z}\ (+\mu_\beta) \right\}$$

$$= \mu_\beta \frac{e^{+\mu_\beta H/kT} - e^{-\mu_\beta H/kT}}{e^{+\mu_\beta H/kT} + e^{-\mu_\beta H/kT}}$$

$$= \mu_\beta \tanh\left(\frac{\mu_\beta H}{kT}\right). \tag{1.11}$$

The magnetic moment per unit volume I_s is thus given by

$$I_s = I_o \tanh\left(\frac{\mu_\beta H}{kT}\right), \tag{1.12}$$

where $I_o = N\mu_\beta$.

For the more general case with $S \neq \frac{1}{2}$, $L \neq 0$ so that $g \neq 2$, the magnetization becomes

$$I_s = N \frac{\sum_{J_z} g\mu_\beta J_z \, e^{+g\mu_\beta J_z H/kT}}{\sum_{J_z} e^{g\mu_\beta J_z H/kT}} \qquad (1.13)$$

This expression can be rewritten in the form

$$I_s = I_o \; B_J(x) \qquad (1.14)$$

where $I_o = N g\mu_\beta J$, is the magnetization at absolute zero, $B_J(x)$ is the Brillouin function given by

$$B_J(x) = \left(\frac{2J+1}{2J}\right)\coth\left(\frac{(2Jx+x)}{2J}\right) - \frac{1}{2J}\coth\left(\frac{x}{2J}\right), \qquad (1.15)$$

and

$$x = \frac{(g\mu_\beta JH)}{kT}$$

Since nothing has yet been introduced into the working which allows for the effect of the interaction energy between spins, equation 1.14 is appropriate to paramagnetic materials. Thus, in accordance with the correspondence principle, it can be seen that equation 1.14 reverts to the classical Langevin solution for paramagnetic materials in the limit of very large J. For materials which are ferromagnetic at room temperature, and which thus have a non-zero or spontaneous magnetization even in zero applied field, the above theory is clearly inadequate (except at high temperatures above the Curie point). The co-operative effect of the interaction between spins is introduced, as

indicated above, by postulating an internal molecular field, whose magnitude is proportional to the magnetization. Thus, the applied field H, is replaced by $H + \lambda I_s$, where λ is the molecular field parameter. When this is done, the magnetization is still given by equation 1.14 but the variable x is now

$$x = \frac{g\mu_\beta J (\lambda I_s + H)}{kT} \qquad (1.17)$$

Equations 1.14 and 1.17 are two simultaneous equations for x that can be solved to give I_s as a function of temperature. Solutions in normalised form, taken from Bozorth (1951), are shown in figure 1.1 together with experimental curves for iron, nickel and cobalt. In these solutions H has been neglected in comparison with I_s and $\underline{J}$ has been taken equal to $\underline{S}$. From figure 1.1 it can be seen that experimental points for nickel, iron and cobalt agree well with the theoretical curves for J = ½ or 1, while for gadolinium the experimental data co-incides more nearly with the curve for $J = \frac{7}{2}$,(Nigh , Legvold, Spedding, 1963)in agreement with the expected values for J in these metals. The curve $J = \infty$, which is the classical limit of the quantum mechanical modification to the Weiss theory, does not in general agree very well with the experimental data.

The Curie temperature T_c, may be obtained by equating

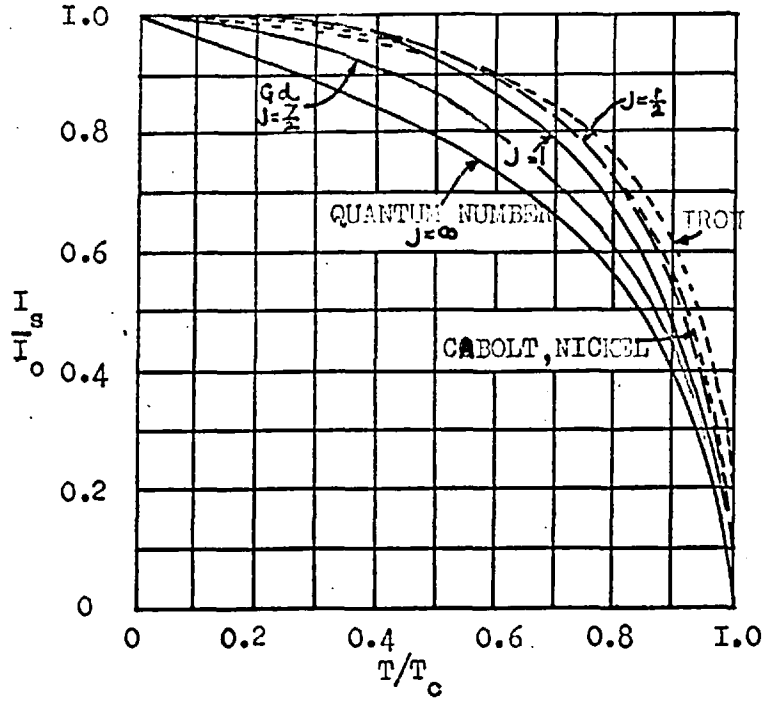


Figure I.I Temperature dependence of the saturation magnetization of iron, cobalt and nickel, compared with theory.

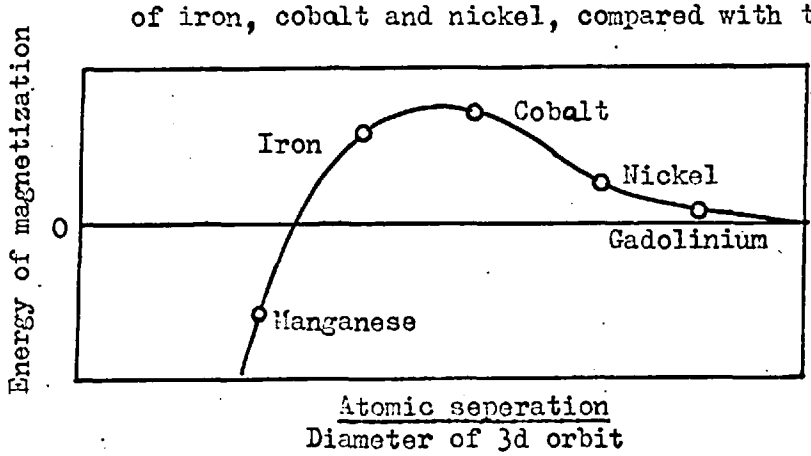


Figure I.2 Bethe's interaction energy curve.

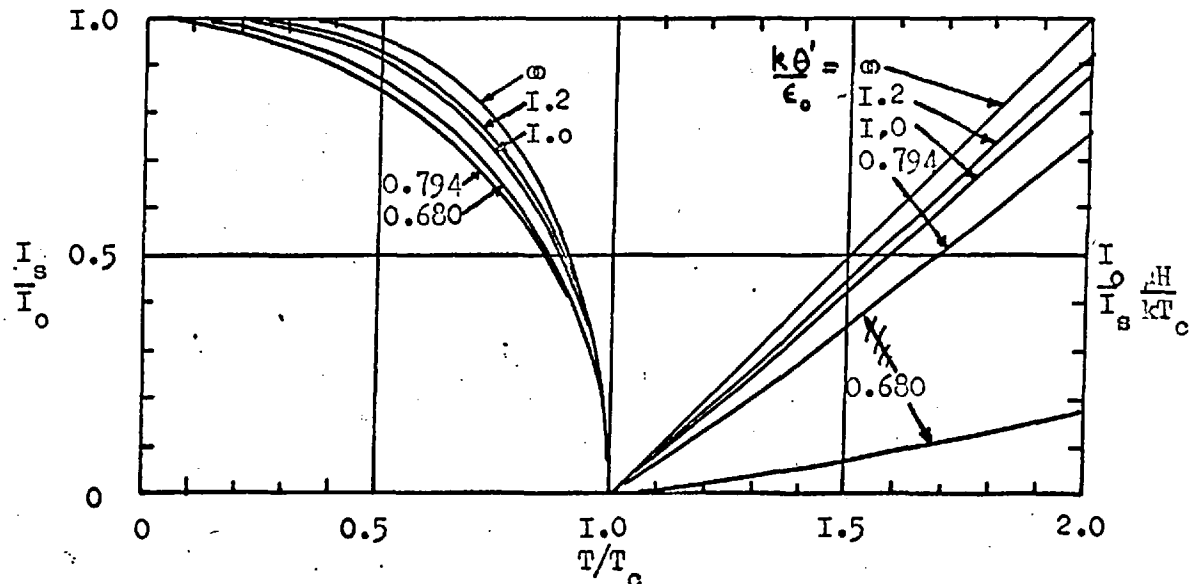


Figure I.3 Stoner's magnetization curves.

the slopes of the two curves given by equations 1.14 and 1.17 (with $\underline{J} = \underline{S}$) at $x = o$. The Brilloin function $B_s(x)$ approximates, for small x, to

$$B_S(x) = \frac{(S + 1)x}{3S}, \tag{1.18}$$

so that

$$T_c = \frac{N g^2 \mu_\beta^2 \, S(S+1)\lambda}{3k} = C\lambda \tag{1.19}$$

and it can be seen that the Curie temperature is proportional to the molecular field parameter, λ.

Above the Curie temperature ferromagnetic materials become paramagnetic and the susceptibility $\chi = \frac{I_s}{H}$, may be obtained from the equation

$$I_s = I_o B_s(x), \tag{1.20}$$

or approximately, for small x,

$$I_s \approx \frac{I_o (S + 1)x}{3S}. \tag{1.21}$$

Rewriting equation 1.21 using 1.17 with $J = S$ gives

$$I_s \approx \frac{C(H + \lambda I_s)}{T} \tag{1.22}$$

or, with 1.19, the Curie-Weiss law

$$\chi = \frac{C}{T - T_c} \tag{1.23}$$

In practice the susceptibility plotted against $\frac{1}{T}$ gives a substantially straight line which on extrapolation

intersects the T axis at $T = T_c'$, a value slightly greater than T_c, the temperature at which the magnetization disappears. An explanation for the slight curve of $1/\chi$ versus T near the Curie point was given by Weiss in (1948) on the basis of the formation of parallel spin clusters. In the above theory it is assumed that the molecular field is proportional to the average magnetization through λ, but in practice it is more likely that the molecular field at a given point arises only from nearby spins so that the magnetic moment of the electron will line up with neighbouring spins if this is different from the direction of the average magnetization. Clusters of parallel spins then find it energetically more favourable to deviate from the average magnetization direction and the Curie point is lowered. It can be seen that this is reasonable since the magnetization direction of each parallel spin cluster will still be deflected from the average magnetization direction by the thermal agitation, but now the co-operative interaction must operate between neighbouring clusters and therefore must operate over longer distances. The cooperative interaction is known to be a short-range effect so that the interaction energy between clusters will be reduced and the Curie point will be lowered. As the temperature increases above the Curie point the clusters disappear and the $\frac{1}{\chi}$ versus T plot approaches the straight line given by

the original theory.

§ 1.1.2. The Heisenberg Exchange Integral.

The quantum mechanical explanation of the molecular field postulated by Weiss was given by Heisenberg in 1928, in terms of the energy of exchange

$$W = -2 \sum_{i>j} J_{ij}\, \underline{S}_i \cdot \underline{S}_j, \qquad (1.24)$$

between two electrons i and j with spin vectors $\underline{S}_i$ and $\underline{S}_j$ respectively. Here J_{ij}, the quantum-mechanical exchange integral between the two spins, is related to the overlap between the two charge distributions and is given by the overlap integral

$$J_{ij} = \int \psi^*_i (\underline{r}_1)\, \psi_j (\underline{r}_1)\, H_{12}\, \psi^*_j (\underline{r}_2)\, \psi_i (\underline{r}_2)\, d\underline{r}_1 d\underline{r}_2, \qquad (1.25)$$

where ψ_i and ψ_j are the state wave functions describing the electrons (numbered 1 + 2) in positions $\underline{r}_1$ and $\underline{r}_2$ while H_{12} is the interaction Hamiltonian $\frac{e^2}{\underline{r}_1 - \underline{r}_2}$. Since the exchange energy must be a minimum for stability, the spins will, from (1.24), line up parallel or anti-parallel depending on whether J_{ij} is positive or negative respectively. Calculations of the exchange integral show that this mechanism is capable of giving a large enough interaction energy between spins to explain ferromagnetism. (Ordinary electrostatic and magnetic interactions between

spins give an interaction energy which is many orders of magnitude too small. This mechanism thus explains the large values of λ needed in e.g. equation 1.19 and today it is generally accepted as correct.

Heisenberg used Heitler-London type wave functions for the 3d electrons localised around the crystal atoms thus assuming that the 3d electrons were tightly bound to their respective atoms. Approximate calculations by Bethe (1933) showed how the exchange interaction depends on the interatomic distance, J being negative for small separations and giving rise to antiferromagnetism, positive for greater atomic separations leading to ferromagnetism, and becoming very small for distances of 2 or 3 times the normal nearest-neighbour separation in crystals. The variation of the exchange interaction energy or energy of magnetization with the ratio of the interatomic distance in the crystal to the diameter of the 3d orbit is shown in figure 1.2 (Hozelitz 1952). An alternative approach to the problem of ferromagnetism in metals was initiated by Slater (1936 a, b) and by Stoner (1933, 1938) and was based on what is known as the free, itinerant or collective electron model.

§ 1.1.3 Collective Electron Model

Slater and Stoner's calculations required a

knowledge of the electronic band structure for the metal concerned. Slater originally extrapolated the data then available for copper to obtain an approximate result for nickel. Slater and Stoner followed Weiss by assuming that the exchange interaction could be represented by a molecular field proportional to the magnetization which meant that the two energy bands, representing the energy distribution of the 3d electrons with positive and negative spins, were displaced by an energy proportional to the difference in the number of electrons in the two bands. The assumption was also made that the shape of the bands at the high energy end was parabolic in form. Stoner obtained the reduced magnetization curve of $\frac{I_s}{I_o}$ against $\frac{T}{T_c}$, shown in figures 1,3 by finding the distribution of electrons with minimum total energy at any given temperature. In the figure $k\Theta'$ is the measure of the ex-change energy, while ϵ_o is the energy level of the top of the unfilled 3d band when the exchange energy is zero. The curves on the right-hand side of the figure give the variation of the reciprocal susceptibility versus reduced temperature, and exhibit a slight curvature near the Curie point, as is observed experimentally, Further advances using this model, in some cases modified to take into account the mutual repulsion of the electrons, have been made by Slater (1959), Stoner (1951), Wohlfarth (1953, 1958), Friedel (1955, 1958), and others. The theories require

initially a knowledge of the band structure of the metal concerned and Callaway (1958) has reviewed the appropriate calculations.

§ 1.1.4 Spin-Wave Theory.

An alternative approach to the mechanism of ferromagnetism at low temperatures was made by Bloch (1932) and by Holstein and Primakoff (1940) with the introduction of spin-wave theory. Here the correct exchange coupling is used rather than the molecular field coupling and spin deviations are assumed to be propogated through the crystal. The theory may be understood from a classical standpoint by imagining the total electronic spin on each atom of a ferromagnetic crystal to be perfectly aligned parallel with its neighbours. If a reversed spin is then introduced and the constraint on it subsequently removed, the spin will not remain in the position that it is placed, but will be propogated through the crystal lattice owing to the exchange coupling between it and its neighbours. The initial disturbance therefore travels through the crystal by spin deviations and forms what is known as a spin-wave, or more correctly a spin wave-packet. Clearly, however, spin-waves do not obey classical laws of superposition since two spin-wave reversals on the same atom will produce a normal spin and not a reversal of double magnitude. In general spin-waves interact and

scatter one another, so that such spin-wave theories only apply to low spin-wave concentrations, and hence to temperatures near absolute zero. Van Kranendonk (1950 a, b) introduced a modified spin-wave theory, (known as the spin-deviation theory) which allows for the fact that the spin-waves scatter one another, and he was thus able to extend the range of spin-wave theory to higher temperatures. Originally, Bloch assumed that the exchange coupling was isotropic, however, Holstein and Primakoff introduced anisotropic coupling which depended on the directions of the two spins $\underline{S}_i$ and $\underline{S}_j$ with respect to the line joining them. Clasically the magnetic spin-spin interaction is given by the dipolar term

$$\sum_{j>i} D_{ij}\left\{(\underline{S}_i \cdot \underline{S}_j) - \frac{3(\underline{S}_i \cdot \underline{r}_{ij})(\underline{S}_j \cdot \underline{r}_{ij})}{r_{ij}^2}\right\}, \qquad (1.26)$$

where

$$D'_{ij} = \frac{g^2 \mu_\beta^2}{r_{ij}^3}, \qquad (1.27)$$

and where r_{ij} is the vector connecting the atoms i and j.

In practice the interaction is nonclassical; it arises indirectly from spin-orbit coupling (Van Vleck 1937) and the constant D'_{ij} must be replaced by a much larger term, D_{ij}, known as the pseudopolar coupling constant. For atomic spins with $S>\frac{1}{2}$, pseudoquadrupolar and higher terms

must be introduced. Bloch (1932) and Holstein and Primakoff (1940) used quantum-mechanical theory based on the use of creation and annihilation operators, while a semi-classical approach has been developed by Heller and Kramers (1934) and Klein and Smith (1950).

One important result of the spin-wave theory is Bloch's $T^{3/2}$ law which describes the variation of the magnetization, I, near absolute zero, namely

$$I = I_o \left\{ 1 + C\left(\frac{kT}{J}\right)^{3/2} \right\}, \qquad (1.28)$$

where I_o is the magnetization at absolute zero, J is the exchange integral and C is a constant equal to 0.1174 for a simple cubic structure, 0.0587 for a body-centred cube structure, and 0.0294 for a face-centred cubic lattice. It is found that experimental measurements of the magnetization at low temperatures are in fairly good agreement with Bloch's law (e.g. Rode and Herrman, 1964). At first sight, because the spin wave theory assumed the Heitler-London or Heisenberg model of localised spins at regularly spaced lattice sites, it might be thought that the results of the theory applied only to nonconducting ferrimagnets and antiferromagnets. However, Herring and Kittel (1951) have shown that it may be applied to conducting ferromagnets as well.

There are at present numerous different theories

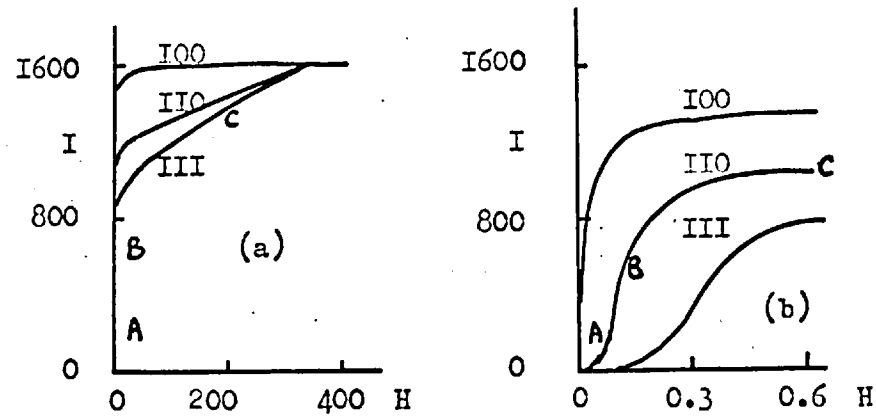
on the role that the 3d electrons play in the magnetic properties of the transition metals, which are founded on the basic concepts of the free or itinerant, and the bound, 3d electrons. The present state of the many theories has been dealt with by Herring (1960).

§ 1.2 Technical Magnetization.

Weiss, in 1907, postulated the existence of magnetic domains to explain the fact that while iron, for instance, has as intrinsic or spontaneous magnetization of 1,700 gauss, it is apparently not normally magnetized. He suggested that the magnetization within a domain should have the saturation value, but that there should be equal numbers of these domains lying in opposite directions so that no total magnetic moment arose. The existence of domains was first confirmed experimentally by Bitter (1931) using the powder pattern technique. The direction in which the spins prefer to lie with respect of the crystal lattice depends on the position of the minima in the anisotropy energy density surface for the particular material concerned. In iron the easy directions, that is the directions in which the material is most easily magnetized, are along the <100> crystallographic directions. In nickel the <111> directions are easy directions, while in cobalt the hexagonal axis is the preferred axis. In gadolinium, just below the Curie point, the hexagonal axis is the easy direction, but at

lower temperatures the direction of easy magnetization lies on the surface of a cone about the hexagonal axis, and the semiangle of the cone varies with temperature.

The shape of the magnetization curves observed experimentally thus depends on the direction in which the magnetizing field is applied, and the overall behaviour of the curve of magnetization versus field can be explained in terms of domain wall movements at lower fields, followed by the spin directions turning towards the applied field direction for high fields. Typical mgnetization curves are shown in figures 14a and b for three 3.85% silicon-iron single crystals (Williams 1937) with the regions of different magnetization processes marked. The crystals were cut in the form of picture frames so that for a particular specimen all four sides of the frame lay parallel to the same type of crystallographic direction. Coils were then wound round the sides of the frame so that the magnetization could be measured by the same method as is commonly used for ring cores of polycrystalline material. RegionA is known as the region of intial permeability and here the magnetization changes by reversible 180° domain wall movements. In this region the domain walls are considered as being pinned by impurities or dislocations so that when the applied field is removed the walls return to their former positions. In region B, the magnetization proceeds by irreversible



Figures I.4a,b. Magnetization curves for 3.85% silicon-iron single crystals at high and low field strengths.

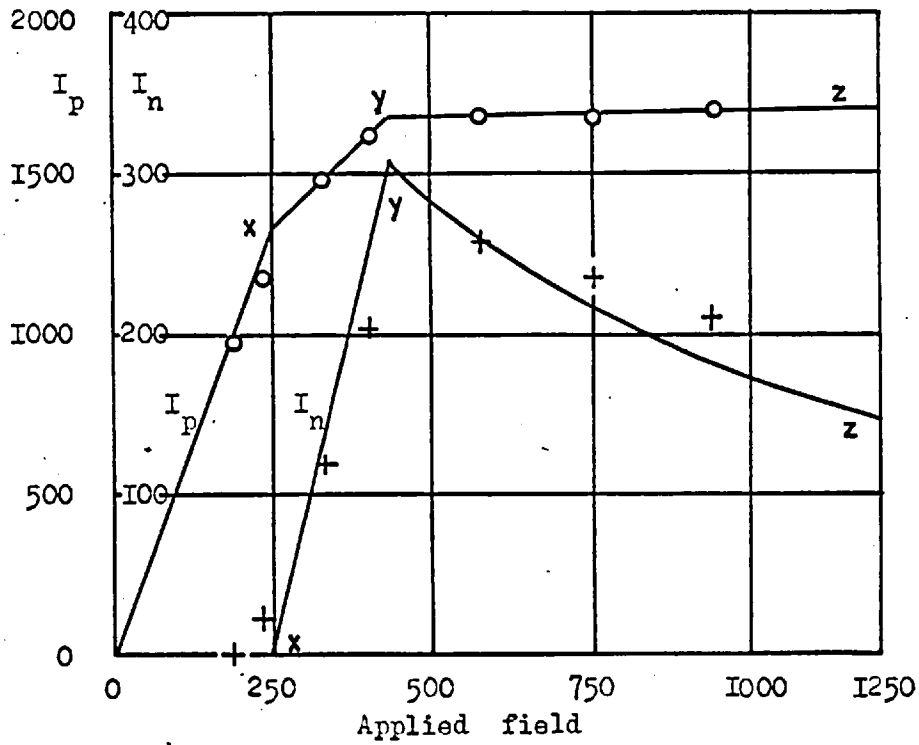


Figure I.5. Calculated magnetization curves for an oblate spheroid of iron, equatorial plane (I00). Applied field at 20° to [I00]. Experimental points from Honda and Kaya (I926).

180^{o} and 90^{o} domain wall movement and it is in this region that Barkhausen noise is most noticeable since it is caused by sudden flux changes due to domain walls jumping from one stable position to another. In region C the material is in a single domain state; that is with all domains lying parallel to the easy direction nearest to the direction of the applied field. The magnetization may then only increase by the rotation of the domains towards the applied field. For single crystal materials the variation of the magnetization, I, with the applied field, H, (e.g. see fig. 1.4 a, b) in region C, may fairly easily be calculated for the principal crystallographic directions if the demagnetizing energy of the specimen is ignored.

Let H and I_s make angles Θ_o and Δ with the easy direction [100] in an iron single crystal. Then the torque due to the field on the I_s vector must exactly balance the restoring torque on I_s due to the anisotropy energy E_c, and if I_s always lies in the same plane as the [100] direction and $\underline{H}$ then,

$$H\, I_s \sin(\Theta_o - \Delta) = \frac{dE_c}{d\Delta} \quad . \qquad (1.29)$$

When $\underline{H}$ is parallel to a <110> direction, $\Theta_o = \frac{\pi}{4}$, and from the expression for the cubic anisotropy energy density (e.g. § 1,3, eqn. 1.33)

$$\frac{dE_c}{d\Delta} = \frac{K_1}{2} \sin 4\Delta, \qquad (1.30)$$

So that the two equations may be obtained

$$H = \frac{K_1 \sin 4\Delta}{2I_s \sin(\frac{\pi}{4} - \Delta)} \qquad (1.31)$$

$$I = I_o \cos(\frac{\pi}{4} - \Delta).$$

from which the I versus H curve may be plotted with Δ as a parameter. In order to obtain the field necessary to magnetize the single crystal to saturation in the <110> direction, Δ must be put equal to $\frac{\pi}{4}$, which gives

$$H_{sat} = \frac{2K_1}{I_s} . \qquad (1.32)$$

The appropriate equations (e.g. Stoner 1950) for the case of H applied in a <111> direction and for the corresponding directions in Nickel may be derived using similar arguments to those applied in the case just considered.

Neel (1944 a, b) and independently Lawton and Stewart (1948) drew attention to the important influence that the demagnetizing energy of a specimen has, in general, on the magnetization processes below saturation. They assumed that the domain magnetization vectors always lie along the direction of the lowest energy minimum. The position of the minimum is determined by the anisotropy of the crystal and the applied and demagnetizing field

energies. This means that the state of magnetization for a given applied field is determined by minimising the energy of the specimen with respect to both the magnetization directions of the domains and the volume (number) of the domains in a given direction.

For example, suppose that a small external field is applied in a direction which is slightly closer to one of two easy directions (e.g. let $\underline{H}$ lie in a $\{100\}$ plane near a $<110>$ direction in a $\{100\}$ disc of iron so that $\underline{H}$ lies almost midway between the two nearest $<100>$ easy directions). All the domains do not then lie parallel to the easy direction closest to the applied field direction since the demagnetizing energy of the specimen would become $\frac{1}{2}N I_s^2$ (where N is the demagnetizing factor). This contribution to the energy of the specimen is reduced if there are still a number of domains in the other (apparently) less favourable easy direction so that the demagnetizing energy is just $\frac{1}{2}N I^2$ where I is the resultant magnetization vector ($I < I_s$). Clearly the way in which the total volume of the domains is divided between the two easy directions depends not only on the magnitude and direction of the applied field but also on the shape of the specimen.

This example illustrates the basic processes that occur: in larger fields, of course, the directions of the

domains also rotate towards the effective field direction.

Neel and Lawton and Stewart showed that, in general, as the applied field increases from zero, the magnetization of a single-crystal specimen will go through a number of distinct phases, distinguished by the number of different vectors that are needed to specify the magnetization directions of the domains. Thus an iron-like specimen will go through four distinct regions: a six-vector region (domains along the <100> easy directions) for H = 0, and three-, two- and one-vector regions for H> 0, corresponding to domains lying in, or near to, the three, two and one nearest easy directions to the field direction.

From figure 1.5, taken from Lawton and Stewart (1948), it can be seen that agreement between the experimental points and their theory is good. The experimental points (from Honda and Kaya 1926) are for the components of the magnetization parallel (I_p) and normal (I_n) to the applied field in an oblate spheroid of iron with a {100} equatorial plane. The field was applied at an angle of 20° to the [100] direction, the demagnetizing factor was N = 0.184 and Lawton and Stewart assumed that $K_1 = 4.2 \times 10^5$ erg cm^{-3} and I_s = 1720 gauss. The three-, two- and one-vector regions are indicated respectively by ox, xy and yz. It can be seen that the experimental points follow a curve

that is more rounded than the curve predicted by the theory, and it is probable that this discrepancy is due to the effects of internal strains in the specimen (Stoner 1950).

§ 1.3 Anisotropy.

It is intended briefly to review those less recent and now well established theories of magnetic anisotropy which are applicable to metals, as opposed to insulating magnetic materials. In fact the treatment of anisotropy in insulators has received somewhat more attention, probably because there is less uncertainty involved in determining the electronic configuration of each atom since all the electrons must be bound. In conductors, the outer shells of electrons of the isolated atom disappear in the metal to become conduction electrons. The exact extent to which the electron is responsible for the magnetization of the material and is also involved in conduction has proved difficult to determine. Nevertheless this work is primarily concerned with metals, so that this section has been limited to the consideration of just those theories which are applicable.

The magnetic free energy of ferromagnetic single-crystal materials is found to vary with the direction of the magnetization vector: the part that varies is known as the magnetocrystalline anisotropy energy and is commonly

described by the phenomenological expressions

$$E_c = K_o + K_1 (\alpha_1^2 \alpha_2^2 + \alpha_2^2 \alpha_3^2 + \alpha_3^2 \alpha_1^2) + K_2(\alpha_1^2 \alpha_2^2 \alpha_3^2)+\ldots, \tag{1.33}$$

for the crystals with cubic symmetry and,

$$E_h = K_o' + K_1' \sin^2 \phi + K_2' \sin^4 \phi + \ldots , \tag{1.34}$$

for crystals with hexagonal symmetry. Here the K's are the anisotropy constants, while ϕ or the α's describe the direction of the magnetization relative to the crystallographic axes. The form of these equations is determined purely by the crystal symmetry involved. From the theoretical standpoint, anisotropy is believed to arise from what is known as spin-orbit coupling. The normal Heisenberg exchange energy between two atoms with spins $\underline{S}_i$ and $\underline{S}_j$ is discussed in section 1.1 and is given by

$$- 2 J_{ij} \underline{S}_i \underline{S}_j . \tag{1.35}$$

It cannot lead to any anisotropy since the expression is independent of the direction of the crystallographic axes. In the derivation of equation 1.35, Heisenberg assumed that the contribution of the orbital angular momentum to the total angular momentum is quenched, and although the mechanism by which this occurs is not fully understood, the quenching may be confirmed by measurement of the g-factor, (the spectroscopic splitting factor). For

complete quenching of the orbital moment, g = 2 and it is in fact close to this figure for most ferromagnetic metals; for example, in nickel g≈ 1.9. This indicates that quenching is very nearly, but not quite, complete, so that there can still be some interaction between the orbital angular momentum vectors of two adjacent atoms. This interaction will be anisotropic in nature since it will depend upon the angles that the orbital momentum vectors make with the line joining the two atoms, and hence in general it will depend on the direction of the vector with respect to the crystal lattice. Interaction of the spin of the electron with its orbital angular momentum (spin-orbit coupling) will then lead to an anisotropic exchange coupling between the spins of the two adjacent atoms. Mathematically this appears as an anisotropic variation of J, the exchange integral, which represents the degree of overlap between the wave functions of the two spins. Before the importance of spin-orbit coupling was appreciated, early efforts (Mahajani 1929) were directed towards the purely classical interaction between the magnetic dipole moments of the spinning electrons and it was found that although a cubic array of dipoles aligned parallel could not give rise to any anisotropy (although a hexagonal array could) a similarly aligned cubic array of magnetic quadrupoles could yield some anisotropy. The evaluation of the anisotropy constants

gave a value for K_1 which was too small by a factor of 10^3. Van Vleck (1937, 1956, 1959), who enlarged some earlier ideas of Bloch and Gentile (1931), obtained the first derivation for the anisotropy constants using the concept of spin-orbit coupling. He considered the possible contributions to the anisotropy energy from the dipole-dipole, quadrupole- quadrupole, and high order couplings. The classical potential energy between two spinning electrons, with spin vectors $\underline{S}_i$ and $\underline{S}_j$, is given by the following expression representing dipole-dipole coupling,

$$\frac{g^2\mu^2}{r_{ij}^3}\beta\left\{\underline{S}_i\cdot\underline{S}_j - \frac{3(\underline{S}_i\cdot\underline{r}_{ij}\,\underline{S}_j\cdot\underline{r}_{ij})}{r_{ij}^2}\right\}, \qquad (1.36)$$

where μ_β is the Bohr magneton, and $\underline{r}_{ij}$ is the vector joining atoms i and j. Van Vleck found that using quantum-mechanics he could obtain the same form of coupling between the two spins, but with a different constant, D_{ij}, not equal to the classical constant. Similarly, higher order coupling could be represented by an expression similar in form to a simple type of quadropole-quadrupole coupling energy, thus

$$Q_{ij}\left\{(\underline{S}_i\cdot\underline{r}_{ij})^2\ (\underline{S}_j\cdot\underline{r}_{ij})^2\right\}. \qquad (1.37)$$

Here D_{ij} and Q_{ij} are known as the pseudo-dipolar and the pseudo-quadrupolar coupling constants. Van Vleck showed that there could be no pseudoquadrupole coupling unless

the total spin vector $\underline{S}$ was greater than ½(i.e. S = 1 or greater). While pseudo-hexapole coupling was excluded unless $\underline{S}$ was greater than 1. (i.e. S = $\frac{3}{2}$ or greater). Now for iron it was found experimentally that S = 1 or possibly $\frac{3}{2}$ so that quadrupole-quadrupole coupling was admissible. However for nickel, S is probably exactly ½, and Van Vleck had therefore to find some other explanation, since for parallel spins and dipole-dipole coupling no anisotropy arises in a cubic lattice. His explanation was that, in practice, owing to thermal agitation and hence deviation from perfect alignment, dipole-dipole coupling of the spins may still give rise to some anisotropy in nickel. Van Vleck (1956) was able to show that, in terms of orders of magnitude,

$$D_{ij} \approx J (g - 2)^2 \qquad (1.38)$$

while

$$Q_{ij} \approx J (g - 2)^4 \qquad (1.39)$$

It can be seen that this is reasonable since the term (g-2) represents the degree to which orbital angular momentum is not quenched. In nickel, where the normal dipole-dipole interaction given by equation 1.36 is not allowed, the calculations were extended to include second order perturbations to represent the effect of thermal agitation on the spins and then it was found that

$$K_1 \approx \frac{D_{ij}^2}{J} \approx J (g - 2)^4 \qquad (1.40)$$

which is the same order of magnitude as the contribution to K_1 from quadrupole-quadrupole coupling. In practice these estimates give good agreement with experimentally observed values. For the case of a material with hexagonal symmetry, dipole-dipole coupling is not disallowed so

$$K_1 \approx D_{ij} \approx J(g - 2)^2, \qquad (1.41)$$

which gives a value for K_1 about 50 times too large in the case of cobalt.

Van Vleck's theory gives a definite prediction for the sign of K_1 for crystals of cubic symmetry only if the pseudodipolar coupling is used to explain the anisotropy. This is because D_{ij} is raised to the second power in the second-order dipole-dipole coupling, so that, although he is unable to determine the sign of the constants D_{ij} and Q_{ij}, this cannot effect the sign of the estimate for K_1. He found that K_1 should be positive for the simple cubic structures and negative for body-centred cubic or face-centred cubic structures. This would be acceptable for nickel with a negative K_1 since only second order pseudo-dipolar coupling is expected. For iron, with a positive K_1, the pseudo-dipolar coupling is not expected to be the main cause of anisotropy, and since the sign of quadrupole-quadrupole coupling is unknown, the experimental evidence could still fit the facts. Van Vleck did not seriously attempt to determine the magnitude of K_2 since

the choice of the order of coupling and the perturbation order of the coupling chosen is much less restricted than it is for K_1. Because of the difficulty in determining the constants D_{ij} and Q_{ij}, it was not possible to obtain more than an order of magnitude value for K_1. However Van Vleck did obtain expressions for the temperature variation of K_1 in terms of the temperature variation of the magnetization, and this is further discussed in the next section.

To try to overcome the problem of solving Heisenberg's many electron model rigorously, Brooks (1940), attempted to solve the problem of anisotropy using the itinerant electron model of Stoner and Slater. It should be noted that this model is not such a good approximation to the state of the tightly bound 3d electrons as is the Heisenberg model. Brooks used a spin orbit interaction with the itinerant electron model to obtain the correct sign and estimate of the magnitude of K_1 for both nickel and iron at or near the absolute zero of temperature, but again owing to the complexity of the theory he was unable to obtain results at temperatures other than absolute zero. Fletcher (1954) extended the calculations of Brooks by removing the major approximations involved, and by using the calculated form of the energy distribution of the d electrons in nickel. Fletcher obtained a value for K_1 in nickel of -5×10^7

erg. cm^{-3} at absolute zero which is probably still somewhat too great.

Joenk (1963) extended the calculations of Van Vleck, after modifying them with spin-wave theory, to obtain values for K_2 at absolute zero. Joenk's calculations are discussed further in chapter six.

§ 1.4 The Temperature Dependence of Magnetocrystalline Anisotropy in Cubic Crystals.

It is generally believed (Akulov 1936, Van Vleck 1937, Keffer 1955, Zener 1954, Brenner 1957, Carr 1958a) that the greater part of the temperature variation of the anisotropy constants K_1 and K_2, used in the equation describing the magnetocrystalline anisotropy energy density, arises from thermal fluctuations of the neighbouring anisotropically coupled spins from their positions at the absolute zero of temperature. Figure 1.6 shows the variation of K_1 for iron, nickel and cobalt, compared with the variation of the reduced magnetization with temperature. Akulov showed that if all the individual spins were assumed to be aligned parallel to one another, but were allowed to collectively deviate from the direction of the applied magnetic field and to precess round this field direction, then the law

$$\frac{K_1(T)}{K_1(0)} = \left\{ \frac{I(T)}{I(0)} \right\}^n \qquad (1.42)$$

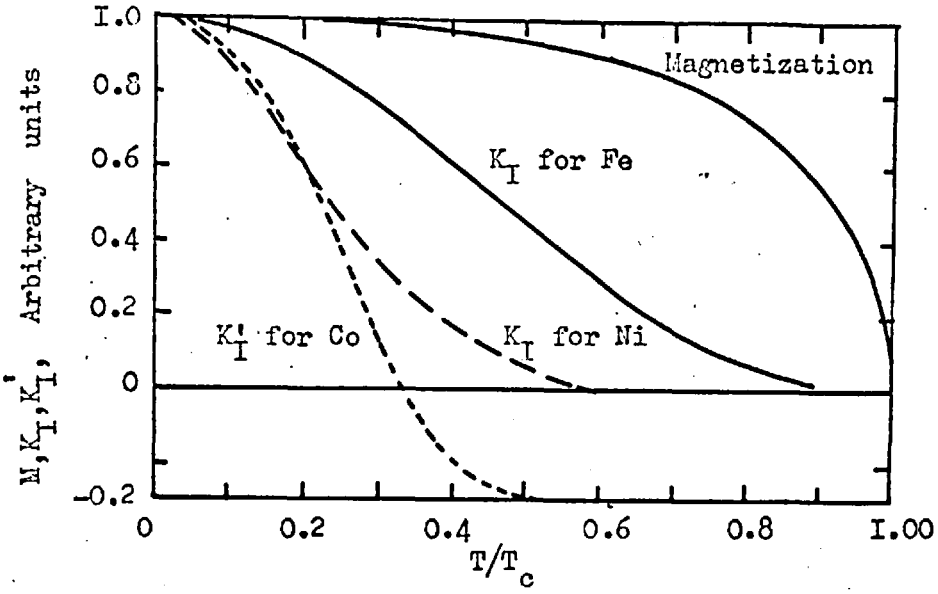


Figure I.6 Dependence of anisotropy energy and magnetization on temperature in iron cobalt and nickel.

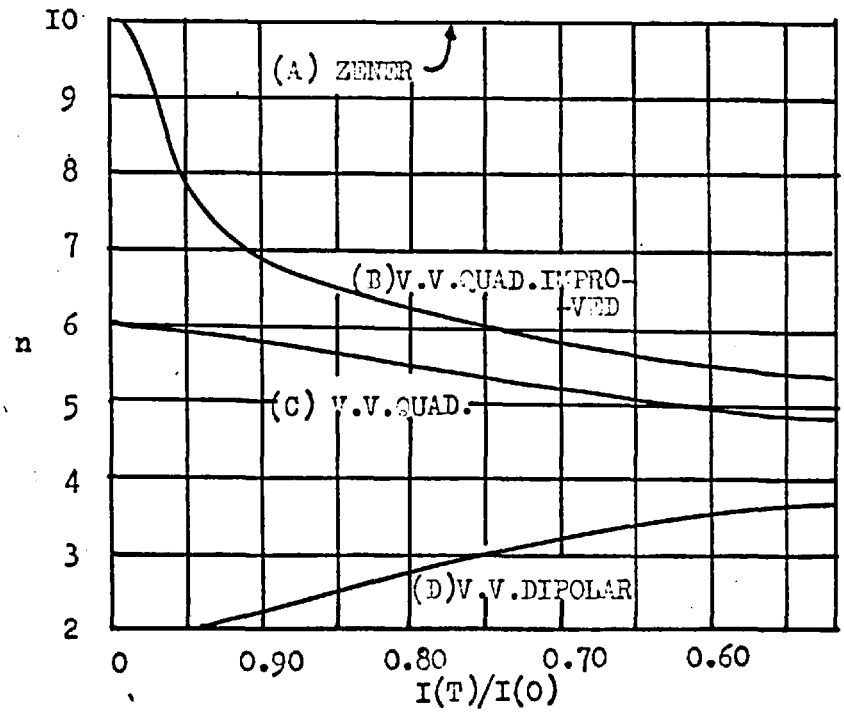


Figure I.7 Theoretical values of the exponent n defined by the relation $K_I(T)/K_I(0) = [M(T)/M(0)]^n$ plotted against $M(T)/M(0)$.

would hold where I(T) is the bulk magnetization at temperature T, and n = 10. The rather drastic assumption that all the spins were aligned parallel can only hold near absolute zero.

The variation of anisotropy with magnetization is of direct interest when the temperature variation of anisotropy is under consideration, since the variation of magnetization with temperature is well known and understood. Hence, a study of the variation of anisotropy with magnetization determines in principle the required variation of anisotropy with temperature, and at the same time facilitates theoretical manipulation.

For some time it was thought that the experimental data for iron obeyed this law with n = 10, with considerable accuracy. However, the recent and careful measurements of Graham (1958), who used somewhat higher measuring fields than earlier workers, with correspondingly greater accuracy, indicate a power law with n = 4 for iron for temperatures lying below room temperature. Graham also notes that some measurements made by Bozorth in 1952, but then unpublished, also indicate that n ≈ 5 for iron. For nickel, experimental measurements had for some time been widely misquoted as giving a power law variation of about n = 20. In any case, because K_1 for nickel changes sign above room temperature, before finally disappearing

at the Curie temperature, a power law cannot exactly fit the experimental data. However a power law with n = 50 is a much better approximation to the available data for low temperatures than n = 20, as was first pointed out by Carr (1958a), and subsequently confirmed by Keffer and Oguchi (1960).

Van Vleck, using the concept of the Weiss molecular field, was able to obtain the temperature variation of the contribution to the first anisotropy constant from pseudodipole and pseudoquadrupole coupling separately. His results were given in the form of numerical tables. Figure 1.7, is taken from Keffer's paper in which he expresses Van Vleck's results in the form of equation 1.42. The graphs show the variation of n, the power of the reduced magnetization, against the reduced magnetization itself. It can be seen that the curve (C), which is derived from the temperature variation of the pseudoquadrupole interaction, leads to a power law (equation 1.42) with an exponent lying between 5 and 6. Keffer pointed out that this should represent the behaviour of the anisotropy at high temperatures near T_c where there is less correlation between neighbouring spins. Curve (B) represents the same pseudoquadrupole contribution calculated by Van Vleck by treating the interaction between a pair of atoms rigorously, but using a molecular field to represent the interaction between the pair of atoms and the rest

of the crystal. It can be seen that at low temperatures, where there is expected to be considerable correlation between the spins on adjacent atoms, the exponent n approaches 10. The contribution due to dipole-dipole coupling is shown by curve (D) and as can be seen, this contribution becomes smaller as the temperature is lowered; this is because it arises from a second-order effect or thermal perturbation of the spins from parallel alignment. Keffer showed that the spin wave model of Holstein and Primakoff produces the same type of variation of n from 10 at low temperatures to 6 at higher temperatures as obtained by Van Vleck, although, of course, spin wave theory does not strictly hold at temperatures other than near absolute zero.

Zener derived the temperature variation of the anisotropy constants using a purely classical model with two basic assumptions, namely that the atomic coupling constants were independent of temperature and that over the whole range of temperatures for which the theory was expected to hold, there was short-range correlation between spins. The second assumption is realistic since neutron defraction studies (Shull 1955) indicate that there is still a relatively large correlation over small regions even at the Curie point. It is thus supposed that small regions of undefined volume exist in which the magnetization has the saturation value appropriate to the absolute zero of

temperature, but with the direction randomly deflected from that of the spontaneous bulk magnetization. Within each small region the spins are supposed to be aligned exactly parallel. The anisotropy energy of each region is taken to be given by

$$e = k_1 (\alpha_1^2 \alpha_2^2 + \alpha_2^2 \alpha_3^2 + \alpha_3^2 \alpha_1^2) + k_2 (\alpha_1^2 \alpha_2^2 \alpha_3^2) + \ldots \quad (1.43)$$

where the direction cosines, α, refer to the direction of a local magnetization, and $k_1 = K_1(0)$ and $k_2 = K_2(0)$, and are the values of K_1 and K_2 in equation 1.42 for $T = 0$, that is k_1 and k_2 are not supposed to vary with temperature.

Zener expresses the anisotropy equation 1.43 in the form

$$E = \sum_n E_n S_n (\alpha_1 \alpha_2 \alpha_3), \quad (1.44)$$

where S_n is a surface harmonic of degree n. Birss (1964 a) enumerates, in detail, the relationships that exist between the anisotropy constants of equations 1.33 and 1.34, and the constants employed in this type of representation of the anisotropy energy. In particular it should be noted that

$$S_4 = (\alpha_1^2 \alpha_2^2 + \alpha_2^2 \alpha_3^2 + \alpha_3^2 \alpha_1^2 - \tfrac{1}{3}) \quad (1.45)$$

and

$$S_6 = \alpha_1^2 \alpha_2^2 \alpha_3^2 - \tfrac{1}{11} (\alpha_1^2 \alpha_2^2 + \alpha_2^2 \alpha_3^2 + \alpha_3^2 \alpha_1^2) + \tfrac{2}{231} \quad (1.46)$$

Zener then assumes that the local magnetization vector (α_1, α_2, α_3) undergoes random fluctuations, described by a random walk function, from the average direction $\underline{\alpha}_1$, $\underline{\alpha}_2$, $\underline{\alpha}_3$ of the bulk magnetization. The average anisotropy energy represented by equation 1.43, which may be written

$$E = \sum_n E_n(T)\, S_n\,(\underline{\alpha}_1,\ \underline{\alpha}_2,\ \underline{\alpha}_3), \qquad (1.47)$$

and which is appropriate to the bulk magnetization, may then be obtained by averaging equation 1.44 with respect to the random walk function. His first step was to express the surface harmonics $S_n(\alpha_1, \alpha_2, \alpha_3)$ in terms of spherical harmonics Y_n^m, thus,

$$S_n = \sum_{m=-n}^{n} C_m\, Y_n^m\,(\theta, \psi)\ . \qquad (1.48)$$

where θ and ψ represent the polar co-ordinates of the local magnetization vectors (α_1, α_2, α_3) with respect to the bulk ~~of the~~ magnetization ($\underline{\alpha}_1$, $\underline{\alpha}_2$, $\underline{\alpha}_3$). Then because the random walk function is symmetrical about ($\underline{\alpha}_1$, $\underline{\alpha}_2$, $\underline{\alpha}_3$), he averaged out the ψ terms and rewrote the averaged function $\langle S_n \rangle$ in terms of Legendre polynomials P_n (cos θ), thus,

$$\langle S_n \rangle = C_o\, P_n\,(\cos\theta) \qquad (1.49)$$

and showed that $C_o = S_n\,(\underline{\alpha}_1\ \underline{\alpha}_2\ \underline{\alpha}_3)$ by considering the particular case $\theta = 0$. Zener then averaged P_n (cos θ) with respect to the random walk function and found that this averaged function, written $\langle P_n\,(\cos\theta)\rangle_{RW}$, was given by

$$\langle P_n(\cos\theta)\rangle_{RW} = e^{-n(n+1)\tau}. \qquad (1.50)$$

The parameter τ was eliminated by obtaining the equation

$$\frac{I_s(T)}{I_s(0)} = \langle P_1(\cos\theta)\rangle_{RW}, \qquad (1.51)$$

which takes account of the fact that the magnitude of the bulk magnetization at a temperature T must depend on the average angle between the $I_s(0)$ direction and the $I_s(T)$ direction. Thus

$$\left\{\frac{I_s(T)}{I_s(0)}\right\}_{\text{measured}} = \langle\cos\theta\rangle, \qquad (1.52)$$

so that

$$\frac{I_s(T)}{I_s(0)} = e^{-2\tau} \qquad (1.53)$$

Hence

$$P_n\langle(\cos\theta)\rangle_{RW} = \left\{\frac{I_s(T)}{I_s(0)}\right\}^{\frac{n(n+1)}{2}}, \qquad (1.54)$$

and finally

$$\langle S_n\rangle_{RW} = \left\{\frac{I_s(T)}{I_s(0)}\right\}^{\frac{n(n+1)}{2}} S_n(\underline{\alpha}_1, \underline{\alpha}_2, \underline{\alpha}_3). \qquad (1.55)$$

From (1.55) it can be seen that

$$\frac{E_n(T)}{E_n(0)} = \left\{\frac{I_s(T)}{I_s(0)}\right\}^{\frac{n(n+1)}{2}}, \qquad (1.56)$$

and this leads to the tenth power law for K_1 since [Birss (1964)] ,

$$\frac{E_4(T)}{E_4(0)} = \frac{K_1(T) + \frac{1}{11} K_2(T)}{K_1(0) + \frac{1}{11} K_2(0)} \approx \frac{K_1(T)}{K_1(0)} , \qquad (1.57)$$

for $\frac{1}{11} K_2 \ll K_1$. It also leads to a 21st power law for K_2.

Brenner (1957) and Carr (1958a) pointed out that it is somewhat artificial to choose a random walk function for the statistical variation in the direction of the local magnetization vector and that a Boltzmann distribution might be considered more satisfactory. Following Carr, it can be seen from Zener's theory outlined above that

$$\frac{E_4(T)}{E_4(0)} = \langle P_4 (\cos \theta) \rangle \qquad (1.58)$$

The averaging of $P_4(\cos \theta)$ may now alternatively be done with respect ot a Boltzmann distribution in a molecular field as indicated below;

$$\langle P_4(\cos \theta) \rangle = \frac{\int_o^{\pi} P_4(\cos\theta)\, e^{\alpha \cos \theta} \sin\theta \, d\theta}{\int_o^{\pi} e^{\alpha \cos \theta} \sin \theta \, d\theta} \qquad (1.59)$$

where $\alpha(T)$ is given by

$$\alpha(T) = b \frac{I_s}{kT} , \qquad (1.60)$$

and b is a constant depending on the molecular field parameter and the average magnetization of the spins. Carr then showed that

$$P_4 (\cos\theta) = 1 + \frac{35}{\alpha^2} - \frac{10}{\alpha} + \frac{105}{\alpha^3} \left\{ \frac{I_s(T)}{I_s(0)} \right\} \qquad (1.61)$$

and, when α is obtained from the measured values of $\frac{I_s(T)}{I_s(0)}$ using the equation:

$$\left\{\frac{I_s(T)}{I_s(0)}\right\}_{measured} = \coth\alpha - \frac{1}{\alpha}, \qquad (1.62)$$

Carr found that $\langle P_4(\cos\theta)\rangle$ agreed very closely with Zener's tenth power law. This is in contrast to the work of Brenner, who used the values of $\frac{I_s(T)}{I_s(0)}$ obtained from the standard theoretical Langevin-Weiss temperature variation of magnetization, and whose values did not agree with Zener's tenth power law. By assuming a Boltzmann distribution for the spin directions, Birss (1964) has shown that even if no correlation exists between spins, the tenth power law still holds for K_1 at temperatures near absolute zero.

As has already been indicated, there is considerable discrepancy between the power laws and the experimental data for both iron and nickel. The most obvious reasons for the discrepancy appear to lie in the assumption that the k's in equation 1.43 are independent of temperature. It was assumed that they had the values $K_1(0)$, $K_2(0)$ etc., but in fact it is unlikely that the k_n are independent of temperature since they must be functions of the spin-orbit coupling which is itself probably a function of temperature. In fact, if k_1 for nickel is assumed to be a linear function of the reduced temperature (Carr 1958a), the theoretical variation of K_1 may be fitted to the experimental data with

some success. However, there appears to be, as yet, no theoretical justification for this assumption.

Another reason for the disagreement between theory and experiment may arise from the fact that the averaging processes followed in deriving equation 1.56 are only applicable if the material is under constant strain. In practice, the experimental data is obtained under conditions of constant stress, so that both the isotropic volume change due to thermal expansion, and the anisotropic volume change due to magnetostriction must be taken into account. Brenner (1957) has investigated the effect of thermal expansion alone, which he found did not adequately explain the discrepancy. Birss (1964) has shown how the theory must be modified to take account of the effect of both the isotropic and anisotropic volume changes. The subject is discussed further in the next section.

§ 1.5 Magnetostriction in Ferromagnetic Single Crystal Materials

Magnetostriction may be defined somewhat loosley as the variation in the dimensions of a sample arising due to changes in the technical magnetization. In fact this definition includes two other small but distinct effects, more accurately described under the headings of the forced magnetostriction and the form effect, which will also be dealt with further in this section.

Since a ferromagnetic sample, below its Curie point, normally consists of a number of domains within which the magnetization has its saturation value I_s, the magnetostriction must be associated with an anisotropic strain of each domain. This being so, it is more fundamental, and also somewhat easier, to deal with the magnetostriction in single crystal materials, since in principle the magnetostriction can be obtained for polycrystalline specimens by a suitable averaging process.

It can be quite easily seen in a qualitative manner how magnetostriction may arise when the magnetocrystalline anisotropy energy is a function of the state of strain of the crystal lattice. Under these conditions the specimen may be expected to deform to lower the anisotropy energy so that the observed magnetostriction will be the strain for which the sum of the anisotropic and elastic energies is a minimum.

A phenomenological equation has been developed (Akulov 1928, 1930, Gans and Von Harlem 1933, Vautier 1954) which describes the dependence of the saturation magnetostriction on the direction of the magnetization vector $(\alpha_1, \alpha_2, \alpha_3)$, and measuring direction $(\beta_1, \beta_2, \beta_3)$. The form of such an equation is determined solely by the requirements of the crystal symmetry involved. For cubic crystals the expression may be written

$$\lambda = A_o + A_1 S(\alpha_1^2 \beta_1^2) + A_2 S(\alpha_1 \alpha_2 \beta_1 \beta_2)$$
$$+ A_3 S(\alpha_1^2 \alpha_2^2) + A_4 S(\alpha_1^4 \beta_1^2) + A_5 S(\alpha_1 \alpha_2 \alpha_3 \beta_1 \beta_2)$$
$$+ A_6 S(\alpha_1^6 \beta_1^2) + A_7 S(\alpha_1^3 \alpha_2^3 \beta_1 \beta_2)$$
$$+ A_8 S(\alpha_1^4 \alpha_2 \beta_1 \beta_2) + A_9 \alpha_1^2 \alpha_2^2 \alpha_3^2 \quad , \qquad (1.63)$$

where the A_n are constants and where the operator S ( ) stands for the sum of the three terms given by the cyclic permutation of the suffixes on the term within the brackets. Equation 1.63 describes the magnetostriction at saturation and, because of the experimental difficulty of exactly reproducing the ideal demagnetized state, measurements are normally made between different saturated states. Equation 1.63 may be manipulated so that the constants A_n can be determined from these measurements and this is done in chapter 2 for the crystal orientations which are more commonly used. From a theoretical point of view, the constants A_n, must be functions of the elastic constants of the material and must also be functions of the rate of change of the magnetocrystalline anisotropy with strain. The latter may be expressed as a power series in $(\alpha_1, \alpha_2, \alpha_3)$, and when this is done the coefficients of the series are known as the magneto-elastic coupling constants. Furthermore, it is then clear that, in principle, the constants A_n, must be related to the fundamental interatomic forces which give rise to the anisotropy energy. However,

in practice this may only be done if an adequate theory of anisotropy exists, and, as has been seen in section 1.3, this is as yet not the case. It is therefore not surprising that theoretical calculations (Vonsovsky 1940, Katayama 1951, Gusev 1954, Flecher 1955) of the A_n have not proved particularly successful. The saturation magnetostriction constants may, however, be written in terms of the magento-elastic constants (Birss 1959), which themselves may be empirically determined and in order for these general derivations to hold it is necessary that the magnetization, the magnetic field within the test specimen and the strain components should be uniform throughout the volume of the specimen. It is found in practice that these rather special requirements are met if the specimen is saturated as a single domain by a uniform external field and with the specimen in the form of an ellipsoid . If this is done the internal field and hence the demagnetizing field will be uniform. The strain components will not be exactly uniform owing to a small contribution from the form effect, which will now be examined. The form effect arises from the interaction of the demagnetizing field energy with the elastic and magnetic energies of the sample. In practice, because the form effect and the spontaneous magnetostriction are both small, they are treated independently of one another so that the form effect is considered as arising just from the interaction of the demagnetizing energy and

the elastic energy. Since the magnitude of the demagnetizing field is a function of the shape of the sample, a strain will occur in such a way as to lower the demagnetizing field and hence the associated energy, and this deformation will be opposed by the eleastic restoring forces in the sample. The equilibrium deformation may then, in principle, be calculated by minimizing the sum of the elastic and demagnetizing energies, if the components of strain are uniform throughout the sample.

However, Brown (1953) showed that the form effect could be considered as being due to tractions everywhere normal to the surface, a condition which cannot, in general, give rise to a uniform distribution of strain. Gersdorf (1961) has made calculations of the form effect for single-crystal spheroids.

In the region well below technical saturation where the magnetization of the specimen is in a multi-domain state, a single vector can no longer be used to describe the direction of the magnetization, so that the theoretical interpretation of the magnetostriction below technical saturation involves the evaluation of the contributions to the total magnetostriction of a number of differently oriented domains. Birss and Lee (1961) extended the work of Akulov (1929) and Heisenberg (1931)

who calculated the magnetostriction for iron crystals as a function of the reduced magnetization in the three principal crystalographic directions. Birss and Lee assumed that the magnetostriction of each domain could be described by an equation of the form 1.63, but terminated after the first two terms. They assumed that the strains of each of the individual domains could be added algebraically after multiplication by a weighting factor proportional to the volume of the domains, to give the total magnetostriction. The case of an {001} oblate spheroid was considered, with the external applied field and measuring directions making arbitrary angles with the <110> direction in the {100} plane. The magnetostriction was calculated over a range of fields from saturation down to the point where the two vectors disappeared, that is the region where the magnetization vectors of all the domains lie parallel with either of the two easy directions lying nearest to the field direction. The relative volumes of domains lying in these two directions was calculated from the theory of Lawton and Stewart (1948) who showed that these volumes must be distributed in a way such as to keep the internal field parallel with the <110> direction. It was shown that their theory was in a reasonable agreement with the experimental variation of the magnetostriction below

saturation.

In applied fields well above saturation, it is found that a small strain occurs, that is proportional to the applied field and this has been called the forced magnetostriction. The experimental measurements[(Von Auwers (1933), Kornetzki (1934), Calhourn and Carr (1955)], have shown that although in iron for instance, the effect is predominantly a volume change, the effect exhibits a small amount of anisotropy, and a phenomenological equation may be readily developed from equation 1.63, by assuming the constants, A_n, to be linear functions of the applied field. (Carr 1958a, Birss 1959). The forced magnetostriction is believed to arise as a direct consequence of forced magnetization, an effect that occurs when the applied field is large enough to be comparable with the effective molecular field arising from the exchange coupling between spins. The applied field may then increase the degree of alignment of the spins and hence increase the magnetization. The effect is found in practice to be large only near the Curie point, in agreement with the above ideas.

It was expected (Kittel, 1959) that the variation of the saturation magnetostriction with temperature might be treated in an analogous way to the theoretical

treatment of the temperature variation of anisotropy, dealt with in section (1.4). In that theory, for reasons of expediency, the variation of K_1 with magnetization, rather than with temperature, was calculated theoretically and it can be seen that this was sufficient since the variation of magnetization with temperature is well known. Thus Kittel and Van Vleck (1960), showed that in the same way, the magneto-elastic constants might be calculated as functions of the reduced magnetization, by the extension of the general theory (Van Vleck, 1959) for the variation of the anisotropy constant K_1 with temperature.

Specifically, if the magneto-eleastic constants are defined by

[see e.g. Birss (1959)],

$$V_1^o = Lo + L_1 \alpha_1^2 + L_2 \alpha_1^4 + L_3 \alpha_2^2 \alpha_3^2$$

$$V_2^o = L_o + L_1 \alpha_2^2 + L_2 \alpha_2^4 + L_3 \alpha_3^2 \alpha_1^2$$

$$V_3^o = L_o + L_1 \alpha_3^2 + L_2 \alpha_3^4 + L_3 \alpha_1^2 \alpha_2^2$$

$$V_4^o = M_o \alpha_2\alpha_3 + M_1 \alpha_1^2\alpha_2\alpha_3$$

$$V_5^o = M_o \alpha_3\alpha_1 + M_1 \alpha_2^2\alpha_3\alpha_1$$

$$V_6^o = M_o \alpha_1\alpha_2 + M_1 \alpha_3^2\alpha_1\alpha_2 , \qquad (1.64)$$

their predicted temperature dependence is given by;

$$L_1(T) = [L_1(0)+\tfrac{6}{7}L_2(0)+\tfrac{1}{7}L_3(0)]\,\zeta^3 - [\tfrac{6}{7}L_2(0)+\tfrac{1}{7}L_3(0)]\zeta^{10}$$

$$L_2(T) = [L_2(0)]\,\zeta^{10}$$

$$L_3(T) = [L_3(0)]\,\zeta^{10}$$

$$M_o(T) = [M_o(0) + \tfrac{1}{7} M_1(0)]\,\zeta^3 - \tfrac{1}{7}[M_1(0)]\zeta^{10}$$

$$M_1(T) = [M_1(0)]\zeta^{10} \qquad (1.65)$$

where ζ is the reduced magnetization. It should be pointed out that the calculation of Kittel and Van Vleck is appropriate to constant lattice strain, whereas the reduced magnetization refers to constant stress. The state of strain of a crystalline lattice at temperature T differs from that at T = 0 partly because of thermal expansion and partly because of magnetostriction. The normal thermal expansion is supplemented by a change in magnetostriction with temperature to give a deformation of the lattice which is principally an isotropic volume strain, $\omega = \omega(T)$, but is partly an anisotropic deformation that depends on the direction of the magnetiztion. Since, however, it is observed experimentally that, for the ferromagnetic metals at least (See Callen and Callen 1960), the

magnitude of the saturation magnetization depends on ω but not on the direction of the magnetization relative to the crystal lattice, it is possible to express the spontaneous magnetization $I_s(T,\omega)$, at temperature T and volume strain ω, approximately in the form

$$I_s(T,\omega) = I_s(T,0) + \frac{\partial I_s(T,\omega)}{\partial \omega}\,\omega \qquad (1.66)$$

where $\omega(0) = 0$. The quantity observed experimentally,

$$\zeta = I_s(T,\omega)/I_s(0,0), \qquad (1.67)$$

should therefore be replaced in equations (85) by either

$$I_s(T,\omega)/I_s(0,\omega) \text{ or } I_s(T,0)/I_s(0,0), \qquad (1.68)$$

that is by

$$\zeta' = \zeta - \frac{1}{I_s(0,0)}\,\frac{\partial I_s(T,\omega)}{\partial \omega}\,\omega . \qquad (1.69)$$

Similar calculations of the temperature dependence of the magneto-elastic coupling constants for hexagonal materials have been performed by Birss and Wallis (1963) and these are included as appendix A1.

Chapter Two

THE MAGNETIZATION PROCESS.

§ 2.1 Anisotropy.

The general stages through which the magnetization of a ferro-magnetic material passes as an external magnetic field is applied have been described in the introduction. The exact process by which the magnetization vector is turned from an easy direction towards the field direction in high fields is of interest and will now be considered in more detail.

§ 2.1.1 In general terms the exact direction in which the magnetization vector lies is dependent on a balance between the coupling of the electron spins with the atomic lattice and with the applied and demagnetizing magnetic fields. The energy density due to the spin-lattice coupling may be expressed at saturation by a power series in the direction cosines ($\alpha_1, \alpha_2, \alpha_3$) specifying the magnetization vector I_s. The form of the power series may be obtained by considering the crystal symmetry involved [Akulov (1928, 1930), Gans and Von Harlem (1933)] . For crystals with cubic symmetry, terms in odd powers of α_i may not be included since the direction specified by $+\alpha_i$ is equivalent in the crystal to that specified by $-\alpha_i$. Similarly, since the three cubic axies are equivalent, the terms of the power series must be invariant with the interchange of any two of the α_i's. Further, since $\alpha_1^2 + \alpha_2^2 + \alpha_3^2 = 1$, the second order term is isotopic so that the series must start with the fourth order term

$$\alpha_1^4 + \alpha_2^4 + \alpha_3^4 = 1 - 2(\alpha_1^2\alpha_2^2 + \alpha_2^2\alpha_3^2 + \alpha_3^2\alpha_1^2).$$

(Further relationships of this type, used in deriving this and higher order terms are listed by Birss 1964). Thus the magneto-crystalline anisotropy energy density, E, for a ferromagnetic material with cubic symmetry is given by;

$$E = K_o + K_1(\alpha_1^2\alpha_2^2 + \alpha_2^2\alpha_3^2 + \alpha_3^2\alpha_1^2) + K_2(\alpha_1^2\alpha_2^2\alpha_3^2) + \ldots\ldots \qquad (2.1)$$

where K_1, K_2, etc. are the cubic anisotropy constants.

In the case of a hexagonal crystal, similar considerations lead to the following expression for the anisotropy energy density, (Mason 1954),

$$E = K_o' + K_1' \sin^2\phi + K_2' \sin^4\phi + K_3' \sin^6\phi + K_4' \sin^6\theta \cos 6\phi + \ldots. \qquad (2.2)$$

where ϕ and θ, are the angles that I_s makes respectively with the c-axis and between the projection of I_s and an a-axis in the basal plane, and K_1', K_2', etc. are the hexagonal anisotropy constants.

The coupling energy, E_H, between the electron spins and the magnetic field, H, is given by

$$E_H = -\underline{H} \cdot \underline{I}_s \qquad (2.3)$$

The energy, per unit volume, E_d, due to the demagnetizing field depends on the particular shape considered. For an

ellipsoid, chosen because the internal field and magnetization are uniform in a uniform applied field,

$$E_d = \tfrac{1}{2} (N_1 I_1^2 + N_2 I_2^2 + N_3 I_3^2)$$

where N_1, N_2, N_3 and I_1, I_2, and I_3, are the demagnetising factors and the magnetization components along the three principal ellipsoid axes. The equilibrium position that the I_s vector takes up is such as to minimise the total free energy, E_f, of the crystal, given by

$$E_f = E + E_H + E_d, \qquad (2.5)$$

and the direction of the I_s vector is thus a function of the anisotropy constants, the magnitude of the saturation magnetization, the applied field and the specimen demagnetizing factors. The last of these four factors depends entirely on the shape of the specimen and if this closely approximates to, or is exactly, a surface of the second degree, the demagnetizing factors are well known [e.g. Stoner (1945), and Osborne (1945)]. The magnitude of the saturation magnetization is substantially constant with applied field and its variation with temperature is usually well-known from standard magnetisation measurements. The anisotropy constants which are again, in general, a function of temperature, may be measured by a number of techniques, the most important of which is direct torque measurements.

For cubic ferromagnetic single crystal materials,

such as iron and nickel, samples oriented in the three principal crystalographic planes [i.e. the (100), (110), and the (111) planes] are important, since in these planes the magnetization processes may be specified by relatively simple expressions. For torque measurements, samples usually take the form of oblate spheroids with the two major axes in the chosen principal plane. A surface of the second degree is desirable to ensure that at saturation the magnetization is uniform over the whole volume of the sample. In practice a thin disc is often used, which approximates fairly well to a thin oblate spheroid when the diameter is more than ten times the thickness. For a specimen oriented in the (100) plane and in a high enough field so that the magnetization is in a single domain regime, it can be seen from equation 2.1 that

$$E = -\frac{K_1}{8}\cos 4\psi \qquad (2.6)$$

where ψ is measured in the (100) plane <u>from</u> a [001] direction <u>to</u> the I_s vector. If a magnetic field H is applied in a direction making an angle β' with a [001] direction then,

$$E_H = -I_s H \cos(\beta' - \psi) \qquad (2.7)$$

and,

$$E = +\frac{1}{2} I_s^2 N, \qquad (2.8)$$

where N is the demagnetizing factor in the plane of the disc.

The torque, L, on I_s is given by $-\frac{\partial E_F}{\partial \psi}$, so that

$$L = -\tfrac{1}{2}K_1 \sin 4\psi + HI_s \sin(\beta' - \psi) \qquad (2.9)$$

and to minimise the total energy for equilibrium L = 0, when ψ is determined by equation 2.9. The torque, Γ, on the specimen is given by $+\frac{\partial E}{\partial \psi}$ so that,

$$\Gamma = \tfrac{1}{2}K_1 \sin 4\psi = HI_s \sin(\beta' - \psi) \qquad (2.10)$$

By measuring Γ, the anisotropy constant K_1 can, in principle, be found at any field above that needed to provide saturation, and in general a graphical solution of equation 2.10 first suggested by Bozorth and Williams (1941) may be used. Then for very large fields $\psi = \beta'$ so that

$$\Gamma = \tfrac{1}{2}K_1 \sin 4\beta' \qquad (2.11)$$

A procedure often used to obtain K_1 from experimental data is to plot the sin $4\beta'$ component of the torque curve (Γ versus β) against $\frac{1}{H}$ and then to extrapolate the curve to the origin to obtain the effective value of K_1 at infinite field. Alternatively a first order correction may be made to the torque curve at large but finite fields so that it approximates to the curve at an infinite field (Bozorth 1954). The procedure involves displacing points on the torque curve parallel to the β - axis by amounts $\frac{\Gamma}{HI_s}$. A similar theoretical analysis to that given above may be applied to a (110) disc to obtain the torque on the specimen as a function of both K_1 and K_2 at high fields. Thus from equation 2.1 and 2.5, at very large fields,

$$\Gamma = \left(\frac{\partial E}{\partial \psi}\right)_{\psi=\beta'} = \frac{K_1}{8}(2\sin 2\beta' + 3\sin 4\beta') + \frac{K_2}{64}(\sin 2\beta' + 4\sin 4\beta' - 3\sin 6\beta') \qquad (2.12)$$

where θ and β' are measured in the (110) plane from an [001] direction. The graphical solution used by Bozorth and Williams (1941), for lower fields may be used in the (110) plane but the problem is somewhat more complicated since the magnetization in this plane is the resultant of two symmetrically directed I_s vectors lying on either side of the (110) plane.

The case of a disc oriented in a (111) plane, is somewhat more complicated than the two foregoing cases since even at high fields the magnetization vector does not lie in the (111) plane and its direction must be specified by two variables. Nevertheless, for very large fields

$$\Gamma = \left(\frac{\partial E}{\partial \theta}\right)_{\theta=\beta'} = \frac{K_2}{18}\sin 6\beta' \qquad (2.13)$$

where θ and β' are measured in the (111) plane from an [110] direction.

It has been shown that in general the position of the magnetization vector at high fields may be determined if the anisotropy constants are known, and the methods by which these constants are obtained from torque measurements have been outlined. For nickel the first anisotropy

constant K_1, has been measured many times and its value is well-known [Bozorth (1951)]. For the second anisotropy constant K_2, however many widely different values have been obtained in the past (see table, Chapter 6.) presumably owing to the difficult experimental techniques required. However, the (111) plane is eminently suitable for measuring this constant, since, as indicated above, the torque curves at very large fields depend only on K_2 But it is found, in practice, that sufficiently large fields may not be obtained so that some understanding of the magnetization process for this orientation, at high fields is desirable. This is attempted in section 2.2.

§2.1.2. The magnetization processes that occur in gadolinium are of interest since it has been reported [Corner, Roe & Taylor (1962) and Graham (1962) (1963), (1964)] that, over a substantial temperature range below the Curie point, the easy directions lie on the surface of a cone surrounding the hexagonal axis. The way in which the cone angle varies with the temperature may most easily be investigated with a single crystal disc of the material orientated so that the hexagonal axis lies in the plane of the disc. Using the anisotropy energy density given by equation 2.2 and ignoring terms involving constants higher than K_2', the torque on the specimen for infinite fields becomes

$$\Gamma = \frac{\partial E}{\partial \phi} = K_1' \sin 2\phi + K_2' (\sin 2\phi - \tfrac{1}{2} \sin 4\phi). \quad (2.14)$$

The torque is of course, zero in the two perpendicular directions $\phi = 0$, and $\phi = \pi/2, 3\pi/2$. However, if K_1' and K_2' are of opposite signs and $|K_1'| < |2K_2'|$, then the torque is also zero when $\phi = \phi_E$, where

$$\cos 2\phi_E = \frac{K_1' + K_2'}{K_2'} \qquad (2.15)$$

and ϕ_E is the semi-angle of the cone of easy magnetization directions. In the experiments which were made on gadolinium, it was found to be inconvenient to measure full torque curves, although it was possible to measure the slope of the torque curve near the position of zero torque. The reasons for the method of measurement adopted are dealt with in Chapter 4, section 4.3. The slope of the torque curve at positions of zero torque is given by

$$\frac{\partial \Gamma}{\partial \phi} = 2K_1' \qquad (\text{at } \phi = 0) \qquad (2.16)$$

and by

$$\frac{\partial \Gamma}{\partial \phi} = -2K_1' - 4K_2', \qquad (\text{at } \phi = \pi/2) \qquad (2.17)$$

Hence by measuring the slope of the torque curves at these two positions for high fields and extrapolating to infinite fields the effective values of K_1' and K_2' may be obtained. The cone angle ϕ_E can similarly be obtained by measuring the angular position of the appropriate torque zero for high fields and again extrapolating to infinite fields. In practice, however, these measurements vary

appreciably with the applied field, even at high fields, so that the extrapolation is unreliable.

§ 2.2 The (111) plane for Nickel.

As indicated in section 2.1.1, the (111) plane is the most favourable plane in which to measure torque curves to obtain the second anisotropy constant K_2, since in this plane, at very high fields, there should be no contribution to the measured torque from K_1. In the (100) and (110) planes the measured torque depends only weakly on K_2 so that even small experimental uncertainties in the measurements lead to quite large errors in K_2. It is for this reason, that the orientation of the plane must be chosen to eliminate any contributions from K_1. In section 2.1.1 it was also indicated that if the applied field is not infinitely large the magnetization does not, in general, lie in the (111) plane so that further analysis is desirable in order that the experimental torque curves may be properly interpreted. To this end the free energy, given by equation 2.5, is first obtained in terms of the anisotropy, demagnetizing, and field energies. The equilibrium position of the magnetization vector is then determined by minimising the free energy.

The energy equation 2.1 for E refers the direction cosines α_1, α_2, α_3, to three rectangular cartesian axes x', y', z' parallel to the cubic

crystallographic axes. It is more convenient to re-arrange these axes as shown in figure 2.1 so that the new axes x, y, z, coincide respectively with $[1\bar{1}0]$, $[11\bar{2}]$, $[111]$ crystalographic directions. If the I_s vector is then specified by the polar and azimuthal angles ϕ and θ respectively, such that ϕ is measured <u>from</u> the $[1\bar{1}0]$ direction <u>to</u> the projection of I_s in the plane, while θ is measured <u>from</u> the [111] direction <u>to</u> I_s, then the direction cosines $\alpha_1, \alpha_2, \alpha_3$, become,

$$\alpha_1 = \frac{1}{\sqrt{6}}[\sqrt{3}\sin\theta\cos\phi + \sin\theta\sin\phi + \sqrt{2}\cos\theta]$$

$$\alpha_2 = \frac{1}{\sqrt{6}}[-\sqrt{3}\sin\theta\cos\phi + \sin\theta\sin\phi + \sqrt{2}\cos\theta]$$

$$\alpha_3 = \frac{1}{\sqrt{6}}[-2\sin\theta\sin\phi + \sqrt{2}\cos\theta], \qquad (2.18)$$

and it may easily be shown that ;

$$E = K_o + \frac{K_1}{36}[12 - 3\sin^4\theta - 6\sin^2 2\theta - 6\sqrt{2}\sin^2\theta \sin 2\theta \sin 3\phi]$$
$$+ \frac{K_2}{108}[4 - 3\sin^4\theta - \sin^6\theta\cos 6\phi - 6\sin^2 2\theta$$
$$- 6\sqrt{2}\sin^2\theta\sin 2\theta\sin 3\phi + 6\sin^2 2\theta\sin^2\theta$$
$$+ 3\sqrt{2}\sin^4\theta\sin 2\theta\sin 3\phi + 2\sqrt{2}\sin^3 2\theta\sin 3\phi]. \qquad (2.19)$$

The magnetic field energy E_H is

$$E_H = -I_s H(\alpha_1\beta'_1 + \alpha_2\beta'_2 + \alpha_3\beta'_3) \qquad (2.20)$$

where β'_1, β'_2, β'_3, are the direction cosines of the magnetic field in the [111] plane and are given by equations 2.18 with

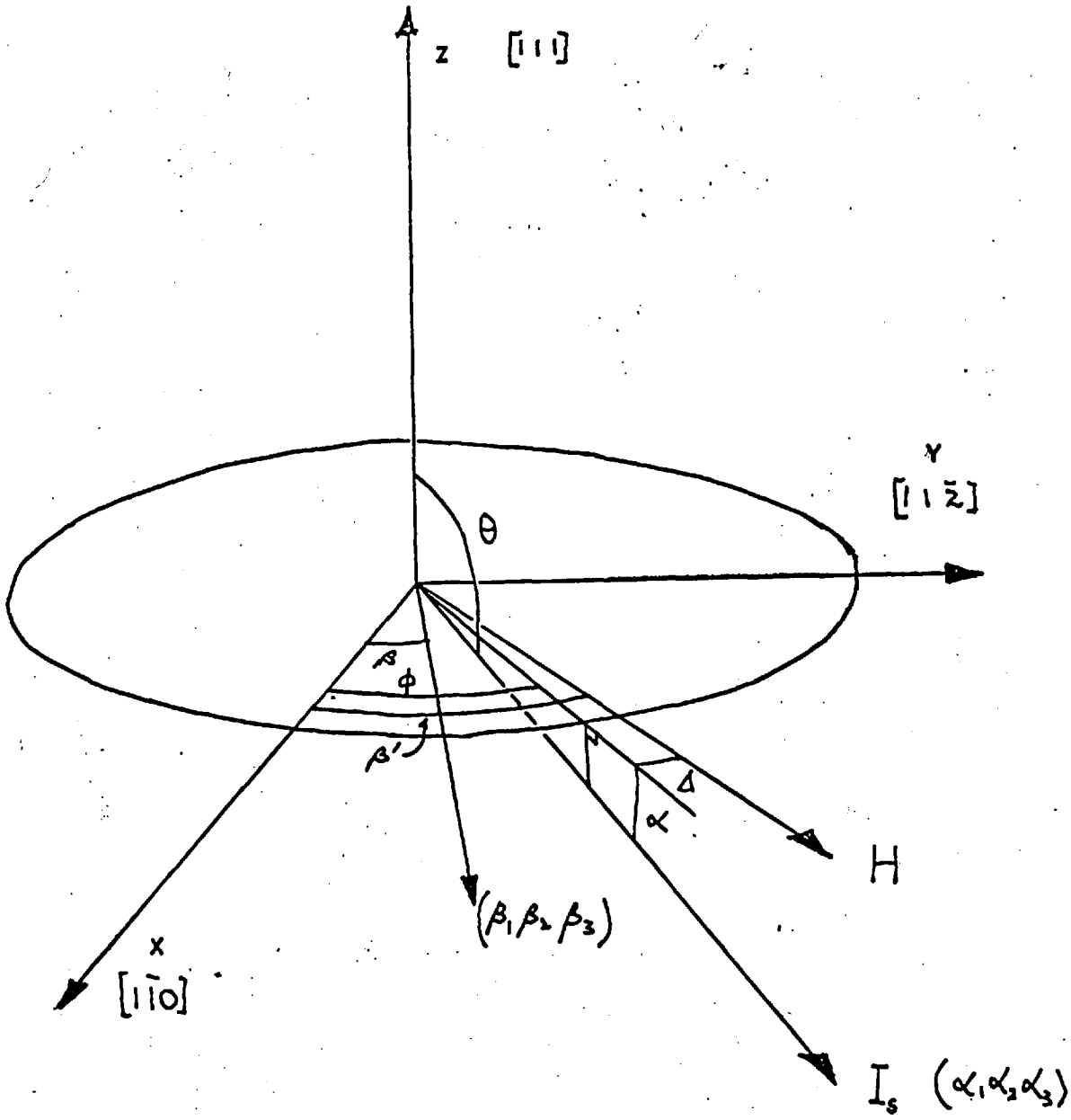


Figure 2.I

POSITION OF AXES FOR (III) THEORY

$\phi = \beta'$ and $\theta = \pi/2$. Thus

$$E_H = -I_s H \sin\theta \cos(\phi - \beta'). \qquad (2.21)$$

Further, the demagnetizing energy E_d, for an oblate spheroid with demagnetizing factor N in the plane of an equivalent disc, is given by

$$E_d = \tfrac{1}{2} I_s^2 [N_x \alpha_x^2 + N_y \alpha_y^2 + N_z \alpha_z^2] \qquad (2.22)$$

where α_x, α_y, α_z are the direction cosines of I_s relative to axes x, y, z. Then, since $N_x = N_y = N$ from the symmetry of the oblate spheroid, and $N_z = (4\pi - 2N)$,

$$E_d = \tfrac{1}{2} I_s^2 [N + (4\pi - 3N)\cos^2\theta] . \qquad (2.23)$$

The free energy of the system is given by equation 2.5 and the direction of the magnetization vector will be such as to minimize E, so that θ and ϕ are determined by the simultaneous equations,

$$\left(\frac{\partial E_F}{\partial \theta}\right)_\phi = 0 \text{ and } \left(\frac{\partial E_F}{\partial \phi}\right)_\theta = 0 . \qquad (2.24)$$

To simplify the solution of these two equations when H is large but finite, the following substitution may be made;

$$\phi = \beta' - \Delta , \qquad (2.25)$$

and

$$\theta = \pi/2 + \alpha , \qquad (2.26)$$

so that α and Δ are small angles. If it is assumed that α and Δ are so small that

$$\sin n\Delta = n\Delta$$
$$\sin n\alpha = n\alpha$$
$$\cos n\alpha = \cos n\Delta = 1,$$

for $n \leq 6$, then equations 2.24 may be written in the form

$$(h + k_1)\alpha + k_2\alpha\Delta + k_3\Delta + k_4 = 0, \qquad (2.27)$$

$$k_5\alpha + k_6\alpha\Delta + (k_7 - h)\Delta + k_8 = 0, \qquad (2.28)$$

where

$$h = H I_s,$$
$$k_1 = -\frac{K_1+K_2}{9} + \frac{K_2}{18}\cos 6\beta' + I_s^2 (4\pi - 3N),$$
$$k_2 = \frac{K_2}{3}\sin 6\beta',$$
$$k_3 = -\sqrt{2}\left(K_1 + \frac{K_2}{6}\right)\cos 3\beta',$$
$$k_4 = \frac{\sqrt{2}}{3}\left(K_1 + \frac{K_2}{6}\right)\sin 3\beta',$$
$$k_5 = \sqrt{2}\left(K_1 + \frac{K_2}{6}\right)\cos 3\beta',$$
$$k_6 = 3\sqrt{2}\left(K_1 + \frac{K_2}{6}\right)\sin 3\beta',$$
$$k_7 = -\frac{K_2}{3}\cos 6\beta',$$
$$k_8 = +\frac{K_2}{18}\sin 6\beta'. \qquad (2.29)$$

Solving equations 2.27 and 2.28 simultaneously for Δ gives

$$\Delta = \frac{-k_8 (h + k_1) + k_4 k_5}{(k_7 - h)(h + k_1) - k_3k_5 - k_4k_6 + k_2k_8} \qquad (2.30)$$

which, using equations 2.29, may be written in the form

$$\Delta = \frac{\frac{K_2}{18}\sin 6\beta' - \frac{1}{3}\frac{\left(K_1 + \frac{K_2}{6}\right)^2}{(h + k_1)}\sin 6\beta'}{h\left\{1 + \frac{k_5}{h} - \frac{1}{h(h+k_1)}(k_3k_5 + k_4k_6 - k_2k_8)\right\}}. \qquad (2.31)$$

If the terms of the order $\frac{K}{h}$ in the square brackets in the denominator are neglected in favour of unity, then the final, high-field, solution for Δ is

$$\Delta = \frac{1}{h}\left\{ + \frac{K_2}{18} - \frac{1}{3}\ \frac{(K_1 + \frac{K_2}{6})^2}{h + k_1} \right\} \sin 6\beta'. \qquad (2.32)$$

It should be noted that $k_1 \approx -K_1 + I_s^2 (4\pi - 3N)$, since the term in I_s^2 is an order of magnitude greater than K_1 for the specimen form used in the experiments and the terms in K_2 may therefore be neglected since $K_2 < K_1$.

The torque on I_s, in the (111) plane, is given by $-\frac{\partial E}{\partial \beta'}$ and at equilibrium this is equal to $+\frac{\partial E_H}{\partial \beta'}$, so that the torque about the axis of the disc, Γ, is given by either $+\frac{\partial E}{\partial \beta'}$ or $-\frac{\partial E_H}{\partial \beta'}$. It may therefore be seen from equation 2.21 that the torque on the specimen is simply $+ h\Delta$.

As a better approximation than $\frac{K}{h} \ll 1$, the denominator of equation 2.30 may be expanded binomially, so that it is only necessary to assume $\frac{K}{h} < 1$. If this is done the following equation may be obtained after some manipulation

$$\Delta = \frac{1}{h}\left\{ \frac{K_2}{18} - \frac{1}{3}\ \frac{(K_1 + \frac{K_2}{6})^2}{h + k_1} \right\}\left\{ 1 + \frac{K_2^2}{108h\,(h+k_1)} \right\} \sin 6\beta' + \left\{ \text{terms of order } \frac{K}{h} \right\} \sin 12\beta' + \ldots \qquad (2.33)$$

Inspection of equations 2.29 shows that k_1 contains a small term, $\frac{K_2}{18}\cos 6\beta'$. However if $\frac{1}{h}\left(1+\frac{k_1}{h}\right)^{-1}$ is expanded binomially as before, it may be seen that this term can only give rise to a small correction with an angular dependence of $12\beta'$. Hence the expression 2.33 may be rewritten in the form

$$\Delta h = \Gamma = \Gamma_6 \sin 6\beta' + \Gamma_{12} \sin 12\beta' + \ldots\ldots \tag{2.34}$$

$$\text{where } \Gamma_6 = \left\{\frac{K_2}{18} - \frac{1}{3}\frac{\left(K_1 + \frac{1}{6}K_2\right)^2}{h + k_1'}\right\}\left\{1 + \frac{K_2^2}{108\, h(h+k_1')}\right\} \tag{2.35}$$

$$\text{and } k_1' = k_1 - \frac{K_2}{18}\cos 6\beta'. \tag{2.36}$$

To facilitate comparison of expression 2.35 with experimental measurements, the measured torque values may be subjected to Fourier analysis, so that the $6\beta'$ component may be compared directly with Γ_6.

The angle α, which measures the extent to which the I_s vector lies out of the (111) plane, may be found from the simultaneous equations 2.27 and 2.28, in the same way as for Δ, to be,

$$\alpha = \frac{-\sqrt{2}}{3}\,\frac{\left(K_1 + \frac{1}{6}K_2\right)}{h + k_1}\left\{1 - \frac{\frac{K_2}{3}\cos^2 3\beta'}{h + \frac{K_2}{3}\cos 6\beta'}\right\}\sin 3\beta' \tag{2.37}$$

At high fields, this equation becomes

$$\alpha = \frac{-\sqrt{2}}{3}\,\frac{\left(K_1 + \frac{K_2}{6}\right)}{h + k_1}\sin 3\beta'. \tag{2.38}$$

It will be shown in chapter 4, that in fact equation 2.32, which predicts Δ, can only be fitted to the experimental data above applied fields of the order of 6 koe. Hence it is reasonable to suppose that α, given by equation 2.38, will also be a good approximation only above this field value. However, the experimental measurements give Δ directly since the measured torque is just $h\Delta$. Hence if the experimental torque is represented by a Fourier series

$$\Gamma_{expt} = \sum_{n=1}^{\infty} A_{2n} \sin 2n\beta', \qquad (2.39)$$

so that the $6\beta'$ component of Δ becomes $\frac{A_6 \sin 6\beta'}{h}$,

equation 2.27 becomes, when $K_2\Delta$ is ignored in comparison with $(h + k_1)$,

$$\alpha_1 = \frac{-\frac{\sqrt{2}}{3}(K_1 + \frac{1}{6}K_2)\left[1 - \frac{6A_6}{h}\cos^2 3\beta'\right]\sin 3\beta'}{h + k_1} \qquad (2.40)$$

and equation 2.28 becomes, when $k_6\Delta$ is ignored in comparison with k_5,

$$\alpha_2 = -\sqrt{2}\left[\frac{\frac{K_2}{18} + A_6\left(1 - \frac{K_2}{3h}\cos 6\beta'\right)}{(K_1 + \frac{1}{6}K_2)}\right]\sin 3\beta' \qquad (2.41)$$

Clearly neither equation 2.40 nor 2.41 exactly represent α below 6 kOe, since the Δ which simultaneously satisfies equations 2.27 and 2.28 is different from the equilibrium Δ measured directly from experiment. However, in the absence of a better expression for α below 6 kOe,

equations 2.40 and 2.41 give a reasonable indication of the expected variation of α .

The foregoing analysis for α and Δ is only strictly correct at very high fields, and in fact the approximations made may be expected to hold well for applied fields in excess of 5 k Oe. At lower fields, the measured values of Δ , and the estimated values of α , become large enough so that the approximations $\sin n\theta = n\theta$, and $\cos n\theta = 1$, , are no longer sufficiently good for the higher values of n used (i.e. n = 6). To test whether these approximations will explain the disagreement of theory and experiment below about 6 kOe the analysis has been extended to higher powers of α and Δ , by writing $\cos n\theta = 1 - \frac{n^2\theta^2}{2}$.

Accordingly the simultaneous equations 2.27 and 2.28 now become;

$$\alpha^2 k_9 + \alpha(h + k_1) + \alpha\Delta\ k_2 - \alpha^2\Delta\ \frac{h}{2} + \Delta\ k_3 + \Delta^2\ k_{10} + k_4 = 0 \qquad (2.42)$$

$$\alpha^2 k_{11} + \alpha^2\ \frac{\Delta h}{2} + \alpha\ k_5 + \alpha\Delta\ k_6 + \Delta\ (k_7 - h) + \Delta^2\ k_{12} + k_8 = 0 \qquad (2.43)$$

where terms in $\alpha\Delta^2$ and $\alpha\Delta^2$ have been ignored except when they are multiplied by h. The constants k_1 to k_8 are given by equations 2.29 while

$$k_9 = -\frac{5\sqrt{2}}{3}\ (K_1 + \frac{K_2}{3})\ \sin 3\beta'$$

$$k_{10} = -\frac{3\sqrt{2}}{2}\ (K_1 + \frac{K_2}{6})\ \sin 3\beta' \ , \qquad (2.44)$$

$$k_{11} = -\frac{1}{6}K_2 \sin 6\beta',$$

$$k_{12} = -K_2 \sin 6\beta'. \qquad (2.44)$$

It is convenient to consider equations 2.42 and 2.43 in the form

$$\alpha^2 a_1 + \alpha b_1 + c_1 = 0$$

and

$$\alpha^2 a_2 + \alpha b_2 + c_2 = 0,$$

so that upon solving these simultaneous equations separately for α and equating the two solutions, it may easily be shown that the following expression is obeyed ;

$$(a_1c_2 - a_2c_1)^2 + (a_1b_2 - a_2b_1)(b_2c_1 - b_1c_2) = 0.$$

Elimination of α from equations 2.42 and 2.43 thus gives an equation of the form

$$A^2 + BC = 0, \qquad (2.45)$$

where A, B, and C are the following functions of Δ

$$A=[k_9][k_8+\Delta^2 k_{12}+\Delta(k_7-h)]-[k_{11}+\frac{\Delta h}{2}][\Delta^2 k_{10}+\Delta k_3+k_4],$$

$$B=[k_9][k_5+\Delta k_6]-(k_{11}+\frac{\Delta h}{2})[-\frac{\Delta^2}{2}h+\Delta k_2+h+k_1],$$

$$C=[k_5+\Delta k_6][\Delta^2 k_{10}+\Delta k_3+k_4]-[-\frac{\Delta^2}{2}h+\Delta k_2+(h+k_1)][k_8+\Delta^2 k_{12}+\Delta(k_7-h)].$$

It may be seen that at high fields, $A^2 \ll BC$, so that $C \simeq 0$, since $B \neq 0$. Then treating C as a quadratic in Δ yields the following equation;

$$\Delta^2\left\{ -\frac{9}{2}\left(K_1 + \frac{1}{6}K_2\right)^2 + \frac{13}{36}hk_2\right\} \sin 6\beta'$$

$$+ \Delta\left\{ -\frac{1}{108}K_2^2 - (h + k_1)(k_7 - h)\right\}$$

$$+ \left\{ +\frac{1}{3}\left(K_1 + \frac{1}{6}K_2\right)^2 - (h + k_1)\frac{1}{18}K_2\right\} \sin 6\beta' = C \simeq 0. \qquad (2.46)$$

The solution for Δ is then approximately

$$\Delta = \frac{\sin 6\beta'}{h}\left[\frac{1}{18}K_2 - \frac{\frac{1}{3}\left(K_1 + \frac{1}{6}K_2\right)^2}{h + k_1} - \frac{1}{6}K_2\left\{\frac{\frac{1}{3}\left(K_1 + \frac{1}{6}K_2\right)^2}{h + k_1} - \frac{1}{18}K_2\right\}^2 - \frac{}{h^3(h+k_1)} \cdots\cdots\right] \qquad (2.47)$$

Evaluation of the third term in equation 2.47 at 92°K, shows that for H = 2 x 10^3 oersted, the estimated Δ is reduced by only 2.5% from the value obtained from equation 2.32. This correction term may therefore be neglected for fields of 2 x 10^3 oersteds upwards so that equation 2.46 becomes

$$C \simeq \Delta h\,(h + k_1) + \left\{\frac{1}{3}\left(K_1 + \frac{1}{6}K_2\right)^2 - (h + k_1)\frac{1}{18}K_2\right\} \sin 6\beta'.$$

Then from equation 2.45,

$$\Delta = \frac{1}{h}\left[+\frac{1}{18}K_2 - \frac{\frac{1}{3}\left(K_1 + \frac{1}{6}K_2\right)^2}{h + k_1}\right] \sin 6\beta' - \frac{A^2}{B(h + k_1)} \qquad (2.48)$$

The experimental values of Δ may be used to evaluate the term $\frac{A^2}{B(h + k_1)}$ numerically. It is of the order of 0.3 x 10^3 dyn. cms. at 92°k for a field of 2 x 10^3 oersted, so that this correction is also negligible at these fields. It is thus clear that the approximation used in the original theory (first order in α and Δ) appears to hold quite well

down to 2 x 10^3 oersted, so that the cause of the observed divergence of the theory and experiment at higher fields may not be explained in this way.

§ 2.3 Magnetostriction.

The phenomenological equation (1.75) appropriate to a material with cubic symmetry referred to in section 1.5, may be replaced by an equation terminating after the 6th term,

$$\lambda = B_o + B_1 S(\alpha_1^2 \beta_1^2) + B_2 S(\alpha_1 \alpha_2 \beta_1 \beta_2) \qquad (2.49)$$
$$+ B_3 S(\alpha_1^2 \alpha_2^2) + B_4 S(\alpha_1^4 \beta_1^2) + B_5 S(\alpha_1 \alpha_2 \alpha_3^2 \beta_1 \beta_2),$$

which is generally believed (Birss 1959) to be consistent with the experimental data. An even shorter equation

$$\lambda = C_o + C_1 S(\alpha_1^2 \beta_1^2) + C_2 S(\alpha_1 \alpha_2 \beta_1 \beta_2). \qquad (2.50)$$

may be used to represent the experimental data for nickel.

These equations represent the saturation deformation, λ, from an unmagnetized (or non magnetic) reference state which is found to be, in practice, an unsatisfactory reference state from which to make measurements since to unmagnetize the specimen its temperature must be raised above the Curie point. To overcome this difficulty, the constant, A_o (B_o or C_o), which is isotropic, may be measured independently of the constants A_n (e.g. by

measuring the deformation of the specimen as the temperature passes through the Curie point); the constants A_n may then be obtained by making measurements between two saturated states. It should be noted that, contrary to much past practice, the demagnetized state (that is the state when there is no overall magnetization owing to the presence of equal numbers of domains in opposite easy directions) is not a satisfactory reference state either, since the distribution of domains in this state may depend on the method of demagnetization used (Lee 1955), and hence it cannot be a unique state common to different measurements and specimens.

To obtain the saturation magnetostriction corresponding to a demagnetized specimen, it is usually assumed that there are equal numbers of domains in each easy direction, and this state is known as the ideal demagnetized state. If the assumption is made that the magnetostrictive strains of the individual domains may be added together algebraically, after multiplication by a factor proportional to their volumes, the deformation λ_i of an ideally demagnetized specimen becomes

$$\lambda_i = B_o + \frac{1}{3} B_1 + \frac{1}{3} B_4$$

for iron and

$$\lambda_i = B_o + \frac{1}{3} B_1 + \frac{1}{3} B_3 + \frac{1}{9} B_4 \qquad (2.51)$$

for nickel.

The magnetostrictive strain, Λ, $(=\lambda - \lambda_i)$ referred to the ideal demagnetized state, may then be obtained by subtracting equations 2.51 from equation 2.49. The resulting equation for Λ is more often quoted in the form first given by Becker and Döring (1939) where B_1, B_2, $(B_3 - \frac{2}{3} B_4)$, B_4, B_5 are replaced by h_1, $2\ h_2$, h_3, h_4 and $2\ h_5$ respectively.

If equation 2.50, is used for the evaluation of measurements between different saturated states, the saturation magnetostriction may be written in a particularly simple form, (Birss 1959);

$$\lambda_x - \lambda_o = q\ (\cos 2\theta - 1) + 2r \sin 2\beta \sin 2\theta. \qquad (2.52)$$

which applies, when the magnetization and measuring direction both lie in one of the three principal crystallographic planes. For convenience the three planes used are the (001), $(1\bar{1}0)$, or $(1\bar{1}1)$ planes where β is the angle that the measuring direction makes from a [110] direction, and θ is the angle between the measuring direction and the magnetization vector. The sign of these angles is such that β and θ are positive when measured in a direction from the (110) direction towards $[1\bar{1}0]$, [001] and [112] directions in the (001), $(1\bar{1}0)$ and $(1\bar{1}1)$ planes respectively. The functions $q\ (\beta)$ and $r\ (\beta)$ are different in the three planes and are given by

(001) plane $\quad 8q = (2\,C_1 + C_2) - (2\,C_1 - C_2)\cos 4\beta$,

$\quad 8r = (2\,C_1 - C_2)\cos 2\beta$,

(1$\bar{1}$0) plane $\quad 32q = (6\,C_1 + 5\,C_2) - (2\,C_1 - C_2)(2\cos 2\beta - 3\cos 4\beta)$,

$\quad 32r = (2C_1 - C_2)(1 - 3\cos 2\beta)$,

(1$\bar{1}$1) plane $\quad 6q = (C_1 + C_2)$,

$\quad r = 0.$ (2.53)

From equation 2.52 it can be seen that two measurements are usually enough to determine C_1 and C_2 if it is assumed that equation 2.50 is exact, as opposed to being the first three terms of a series. For example, in the (001) plane, with $\beta = 0$, $x = \frac{\pi}{2}$, $\lambda_x - \lambda_o = -\frac{1}{2} C_2$ and if $\beta = \frac{\pi}{4}$ with $x = \frac{\pi}{2}$, $\lambda_x - \lambda_o = -C_1$. In the (111) plane equation 2.52 becomes

$$\lambda_x - \lambda_o = \frac{(C_1 + C_2)}{6} \quad (\mathrm{Cos}\ 2x - 1) \qquad (2.54)$$

so that it is not possible to measure C_1 and C_2 separately in this plane. The detailed behaviour of the magnetization processes that occur in the (111) plane, at high fields will now be considered.

§2.4 Magnetostriction in the (111) plane for Nickel.

In section 2.2 equations were developed that gave the dependence of the direction of the saturation magnetization vector on the field for high fields in the (111) plane. The information may be used to predict the high field variation

of the magnetostriction with field in the same plane.

The saturation magnetostriction for nickel may be represented by equation 2.50, and the direction cosines $(\alpha_1, \alpha_2, \alpha_3)$ of the magnetization vector are given by equations 2.18. The direction cosines $(\beta_1, \beta_2, \beta_3)$ of the measuring direction are given by equations 2.18, with $\phi = \frac{\pi}{2}, \theta = \beta$ and are thus;

$$\beta_1 = \frac{1}{\sqrt{6}} \left(\sqrt{3} \cos\beta + \sin\beta \right)$$
$$\beta_2 = \frac{1}{\sqrt{6}} \left(-\sqrt{3} \cos\beta + \sin\beta \right)$$
$$\beta_3 = \frac{1}{\sqrt{6}} \left(-2 \sin\beta \right) \qquad (2.55)$$

where β is the angle between the measuring direction and the [110] direction in the (111) plane. Substitution of equations 2.18 and 2.55 into equation 2.50 gives

$$\lambda = C_o + \frac{C_1}{6} \left[2 + \sin^2\theta \cos 2(\phi - \beta) + \sqrt{2} \sin 2\theta \sin(2\beta + \phi) \right] + \frac{C_2}{12} \left[1 - 3\cos^2\theta + 2\sin^2\theta \cos 2(\phi - \beta) - \sqrt{2} \sin 2\theta \sin(2\beta + \phi) \right]. \qquad (2.56)$$

The substitutions $\theta = \frac{\pi}{2} + \alpha$, and $\phi = \beta' - \Delta$ may be made with β' representing the angle between the [110] direction and $\underline{H}$, and the approximation that at high fields both α and Δ are small may be applied. If this is done and if all terms other than the first order in and Δ are neglected, equation 2.56 becomes

$$\lambda = C_o + \frac{C_1}{6}[2 + \cos 2(\beta' - \beta) + 2\Delta \sin 2(\beta' - \beta) - 2\sqrt{2}\alpha \sin(2\beta + \beta')] + \frac{C_2}{12}[1 - 2\cos 2(\beta' - \beta) + 4\Delta \sin 2(\beta' - \beta) + 2\sqrt{2}\alpha \sin(2\beta + \beta')]$$

and this may be regrouped to collect terms independent of, and dependent on α and Δ. Thus,

$$\lambda = C_o + \frac{C_1}{3} + \frac{C_2}{12} + \frac{1}{6}(C_1 + C_2)\cos 2(\beta' - \beta) + \frac{1}{3}(C_1 + C_2)\Delta \sin 2(\beta' - \beta) - \frac{\sqrt{2}}{3}(C_1 - \frac{C_2}{2})\alpha \sin(\beta' + 2\beta) \qquad (2.58)$$

Measurements of the variation of the magnetostriction with field for high fields may thus be interpreted in terms of the variation of α and Δ, the angles specifying the direction of the I_s vector, which should be in agreement with the results from torque measurements.

Further deductions may be made from equation 2.58 to find the most profitable measuring and field directions for experimental measurements of α and Δ from the magnetostriction. It would, of course, be desirable to measure the contributions to the saturation magnetostriction from α and Δ separately, and inspection of equation 2.58 will yield the conditions under which this may be done. First, however it is helpful to rewrite α and Δ in a form that takes account of their angular dependence as determined by equations 2.32 and 2.38, namely,

$$\Delta = A_{\Delta} \sin 6\beta'$$

$$\alpha = A_{\alpha} \sin 3\beta'. \qquad (2.59)$$

Then, to measure the contribution due to Δ alone, the following conditions must apply

$$\beta' = n\pi - 3\beta, \text{ but } \beta' \neq \frac{n\pi}{2} + \beta \qquad (2.60)$$

or

$$\beta' = \frac{n\pi}{3}, \text{ but } \beta' \neq \frac{n\pi}{6},$$

where $n = 0, \pm 1, \pm 2, \pm 3, \ldots$ etc. Similarly, to measure α alone,

$$\beta' = \frac{n\pi}{2} + \beta \text{ but } \beta' \neq n\pi - 2\beta \qquad (2.61)$$

or

$$\beta' = \frac{n\pi}{6} \text{ but } \beta' \neq \frac{n\pi}{3},$$

are the conditions that must be complied with. To illustrate these conditions, the angular dependence in the field direction, of the last two terms of equation 2.58 have been plotted in figures 2.2 a, b, c for $\beta = 7.5^{\circ}$, 15°, 30°. It can then be seen at a glance that for $\beta = 15^{\circ}$ and 30°, only the terms in α may be measured alone, while for $\beta = 7.5^{\circ}$ there are positions of β' where the terms in α and Δ may be measured alone.

The variation with field of equation 2.58 is small and may be partially masked by the forced magnetostriction [Carr (1958) and Birss (1959)] which arises from variation of the magnetostriction constants with field, and by the magnetocaloric heating effect which gives rise to a

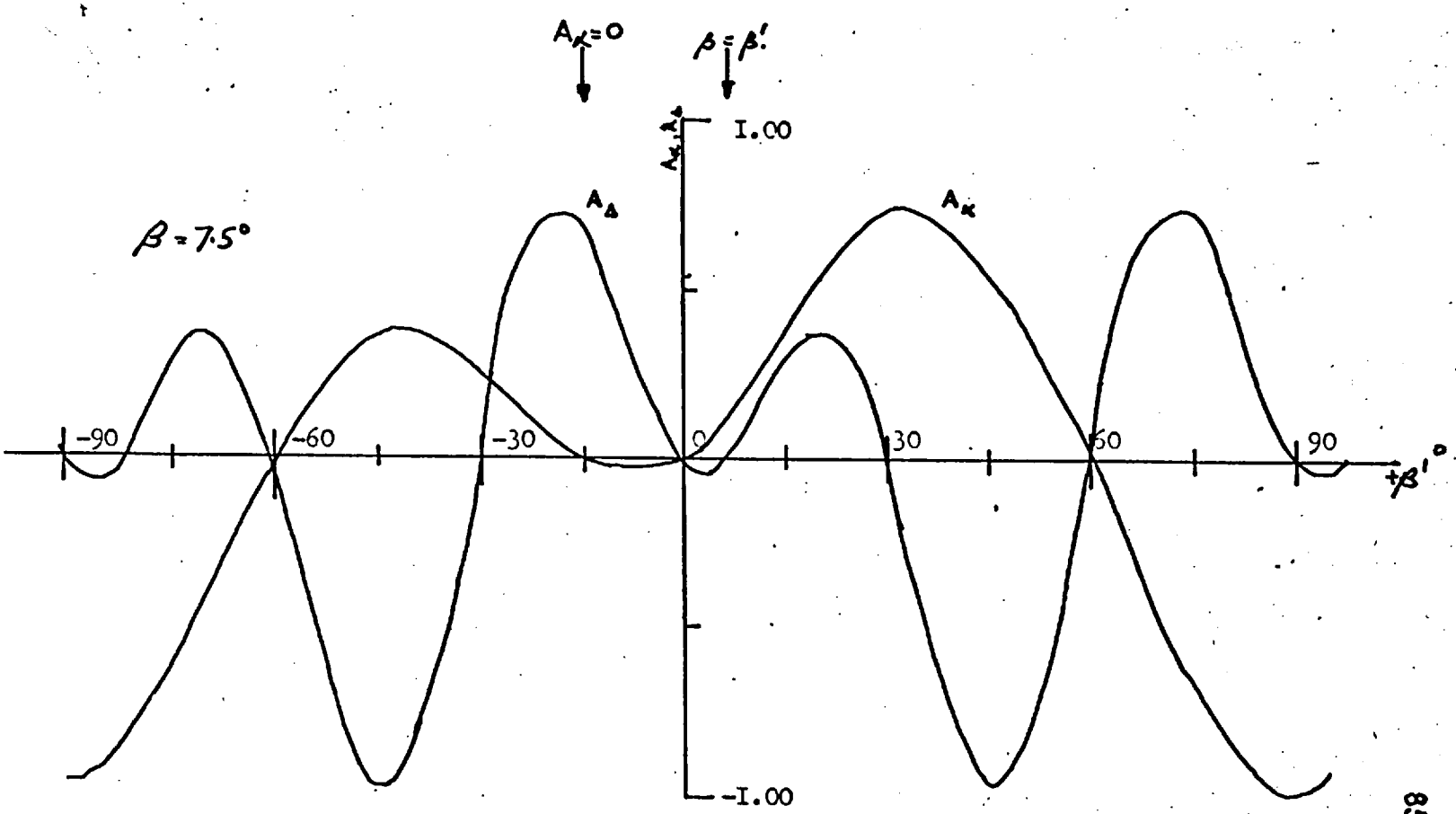


Figure 2.2a

ANGULAR DEPENDENCE OF A_α AND A_Δ

$A_\alpha = \sin(\beta'+2\beta)\sin 3\beta'$, $A_\Delta = \sin 2(\beta'-\beta)\sin 6\beta'$.

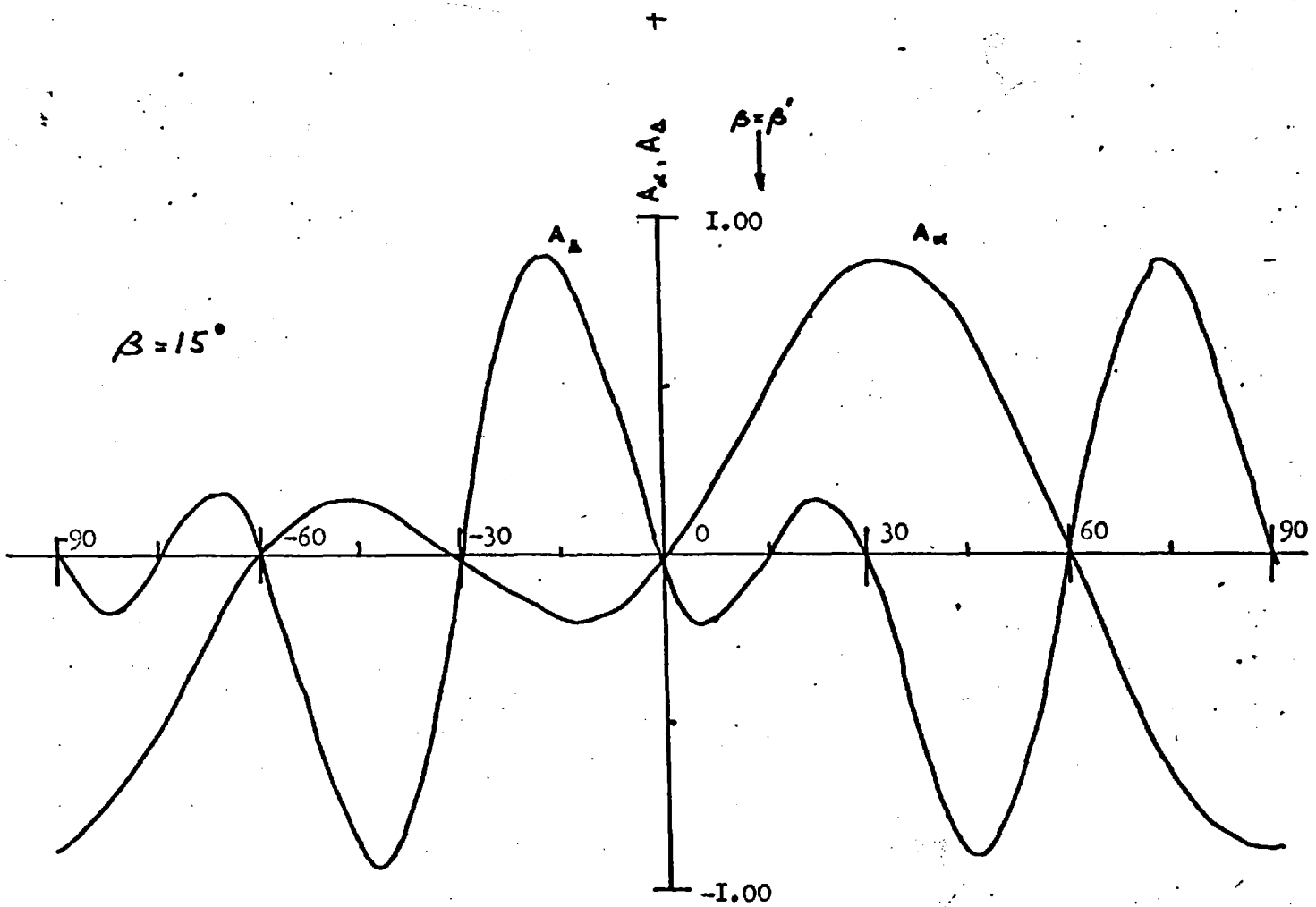


Figure 2.2b

ANGULAR DEPENDENCE OF A_α AND A_Δ

$A_\alpha = \sin(\beta'+2\beta')\sin 3\beta'$, $A_\Delta = \sin 2(\beta'-\beta)\sin 6\beta'$.

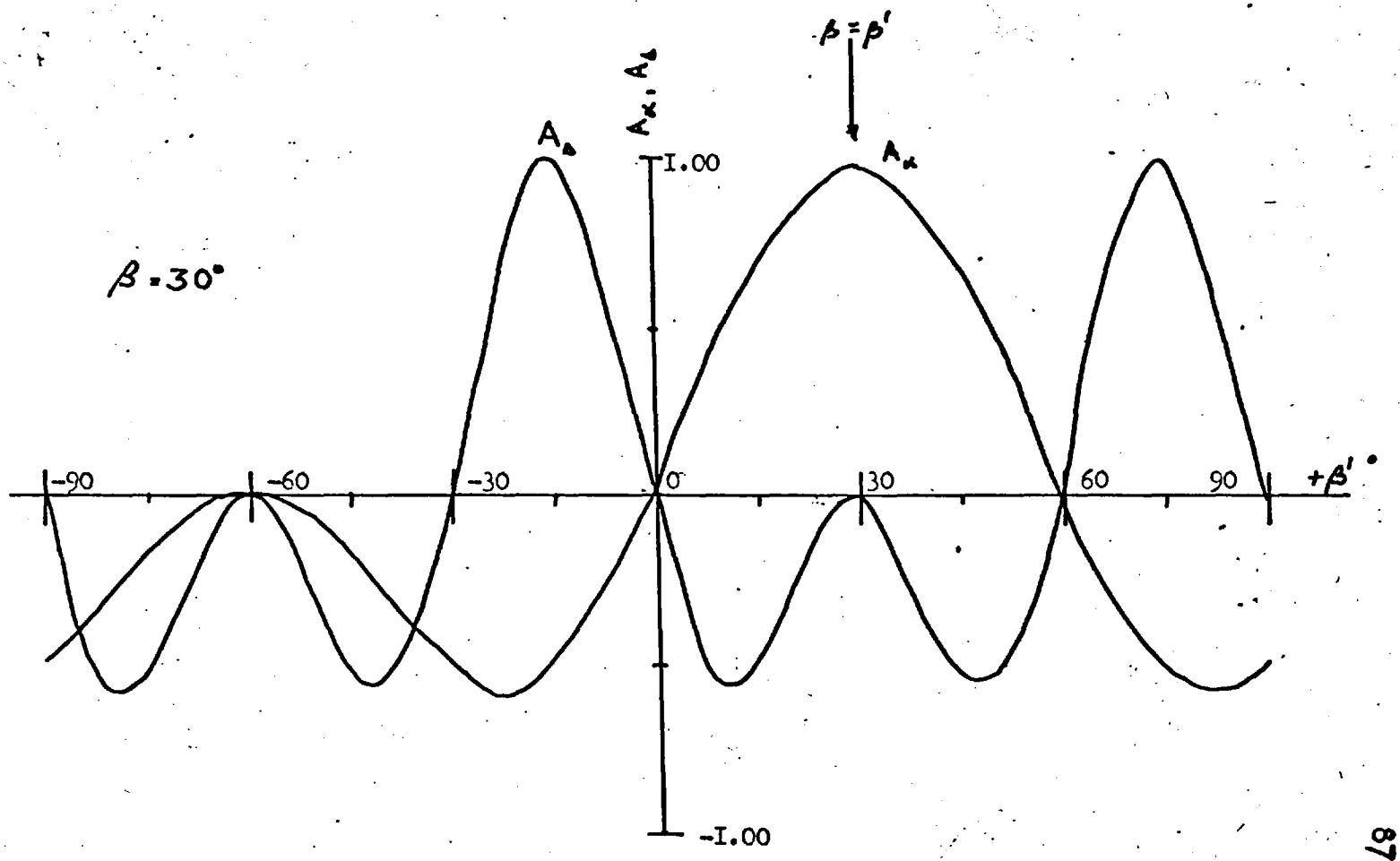


Figure 2.2c

ANGULAR DEPENDENCE OF A_α AND A_Δ

$A_\alpha = \sin(\beta' + 2\beta)\sin 3\beta'$, $A_\Delta = \sin 2(\beta' - \beta)\sin 6\beta'$.

transient deformation when the applied field magnitude is changed.

It is customary to assume that the magnetostriction constants vary linearly with field so that, for instance, C_1 may be replaced by $C_1 + C_1' H$, where C_1' is the forced magnetostriction constant. The change in the saturation magnetostriction $\delta\lambda$, that arises from a change in field δH $(= H_2 - H_1)$ is then given by

$$\begin{aligned}\delta\lambda = \delta H \Big[& C_o' + \tfrac{1}{3}C_1' + \tfrac{1}{12}C_2' + \tfrac{1}{6}(C_1' + C_2')\cos 2(\beta' - \beta) \\ & + \tfrac{1}{3}(C_1 + C_2)\delta\Delta \sin 2(\beta' - \beta) + \tfrac{1}{3}(C_1' + C_2') \\ & (\Delta_2 H_2 - \Delta_1 H_1) \sin 2(\beta' - \beta) \\ & - \tfrac{\sqrt{2}}{3}(C_1 - \tfrac{1}{2}C_2)\delta\alpha \sin(\beta' + 2\beta) - \tfrac{\sqrt{2}}{3}(C_1' - \tfrac{1}{2}C_2') \\ & (\alpha_2 H_2 - \alpha_1 H_1)\sin(\beta' + 2\beta) \Big] \end{aligned} \qquad (2.62)$$

where $\delta\Delta = \Delta_2 - \Delta_1$ and $\delta\alpha = \alpha_2 - \alpha_1$. Then if the values of the magnetostriction for values of β' given by $\beta' = 30^\circ$, $30^\circ + 45^\circ$, $30^\circ + 90^\circ$, are denoted by λ_{30}, λ_{75} and λ_{120}, when $\beta = 30^\circ$,

$$\begin{aligned}\tfrac{3}{2}\delta\lambda_{120} - \tfrac{1}{2}\delta\lambda_{30} - \delta\lambda_{75} = & -\tfrac{1}{3}(C_1' + C_2')\delta H \\ & - \tfrac{1}{3}(C_1 + C_2)\delta\Delta - \tfrac{1}{3}(C_1' + C_2')(\Delta_2 H_2 - \Delta_1 H_1) \end{aligned} \qquad (2.63)$$

and

$$\delta\lambda_{120} - \delta\lambda_{30} = -\frac{1}{3}(C_1' + C_2')\delta H + \frac{\sqrt{2}}{3}(C_1 - \tfrac{1}{2}C_2)\delta\alpha$$

$$+ \frac{\sqrt{2}}{3}(C_1' - \tfrac{1}{2}C_2')(\alpha_2 H_2 - \alpha_1 H_1) \qquad (2.64)$$

In principle, equations 2.63 and 2.64 enable the forced magnetostriction constants C_1' and C_2' to be determined. However, in practice, the last terms of both equation 2.63 and 2.64 are negligible so that it is only possible to measure the sum $C_1' + C_2'$.

Chapter Three

DESIGN OF APPARATUS AND SPECIMEN PREPARATION

§3.1 The Torque Meters

The method chosen to determine the magnetocrystalline anisotropy constants of nickel involved the measurement of small torques developed about the symmetry axis of a disc-shaped specimen (described in 3.3) when a uniform magnetic field was applied in the plane of the disc. A number of different torque meters or torque magnetometers, all of which may be used for such measurements, have been described in the literature. A common type (Sato and Chandrasekhar 1956), consisting of specimen holder with mirror attached, torsion suspension and torsion head, suffers from certain disadvantages. For stable measurement of a complete torque curve, the elastic constant of the suspension must be greater than a limiting value determined by the volume of the specimen and the slope of the torque curve (Harrison 1955). The maximum sensitivity is therefore limited for stable operation. Although this system is basically simple, it would appear that considerable care and patience are needed to obtain accurate results.

These difficulties are reduced, although not eliminated, in a somewhat different type of apparatus first described by Craft, Donahoe and Love (1955) and subsequently modified and improved by others including Penoyer (1956) and Pearson (1957 , 1959). The specimen is suspended from the coil of a moving-coil galvanometer and the torque developed in the specimen is balanced by passing a current through the galvanometer coil. Automatic balancing is achieved by the use of feedback and the sensitivity of this type of instrument appears to be about one centimeter of deflection of the indicating instrument per dyne-cm. The same principle (of balancing torque against electromagnetic force) is used, with a much higher sensitivity, to measure the anisotropy of thin films (Humphrey and Johnston 1963), but the system is necessarily

complex and the apparatus is cumbersome.

In another type of torque magnetometer (Miller 1950), the specimen is supported by an axle mounted in bearings. A phosphor bronze strip, wrapped once round the axle and kept under tension, converts the torque on the axle to a tangential force on the strip, which is directly measured with a commercial force-measuring device that operates on the strain gauge principle. The maximum sensitivity is of the order of 10^{3} centimeters per dyne-cm. Friction in the bearings limits the sensitivity, and an error is present due to the rotation of the specimen when torque is applied. The torque magnetometer described by Aldenkamp, Marks and Zijlstra (1960) avoids bearing friction by the use of a special torsion suspension incorporating three phosphor bronze strips between two discs. This arrangement makes the suspension relatively rigid to lateral displacements. A differential transformer and commercial displacement meter are used to measure the relative rotation between the two discs. It is claimed that there is a negligible rotation of the pecimen and that the maximum sensitivity is about 6×10^{-2} centimeters per dyne-cm.

On considering these various arrangements it became apparent that a more convenient torque meter might be developed using the principle employed in resistance strain gauges. Such a development is attractive because it allows a particularly simple experimental arrangement in which the fractional resistance change resulting from a torque developed in the specimen, may be measured easily and accurately with a Wheatstone bridge. No feedback network is necessary for stable operation, nor is there a limit in this respect, to the maximum working sensitivity. The configuration of resistance wires adopted in this torque meter gives a number of desirable features, namely:

(1) positive location of the specimen in the magnetic field, with negligible rotation on application of torque;

(2) insensivity to unwanted translational forces and torques;

(3) insensitivity to small changes in ambient temperature and pressure;

(4) ease of temperature control and stabilization due to the small volume of the torque meter (about 12 cm^3);

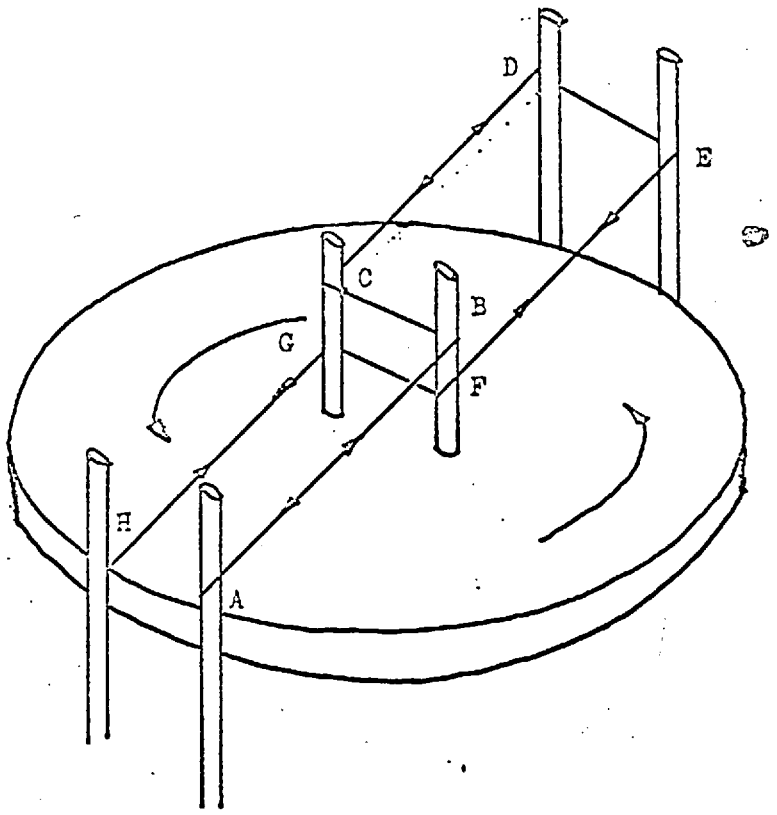
(5) absence of friction e.g. from supporting bearings, (since support is entirely by elastic means);

(6) linearity between the output from the Wheatstone bridge and the torque to be measured.

The use of semi-conductor strain-gauge elements was considered because they exhibit a much greater resistance change for the same strain. However, the sensing element in the torque meter has to measure stress rather than strain, and high sensitivity is achieved with a small area of cross-section, so that a large strain, and hence a large resistance change, accompanies a given stress. Semiconducting materials are generally stiffer than wire so that for a given cross section and stress there is less strain. Further factors favouring the use of strain gauge wires are that they are readily available, that they are much easier to manipulate than semiconductor elements of the same cross-section, and that the magneto- resistance of these wires is small when compared with galvanomagnetic effects in semiconductors.

§3.1.1. Considerations in the Design of the Torque Meter.

The basic construction of the torque mater is shown in figure 3.1. The prestressed resistance wires ABCD and EFGH form two adjacent arms of a Wheatstone bridge. A torque about the axis



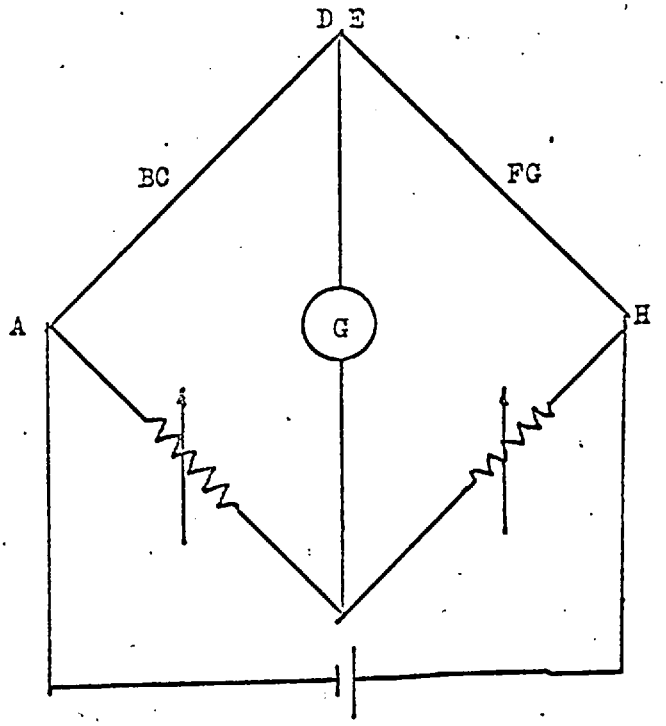


Figure 3.1

TORQUE METER PRINCIPLE

of the disc, transmitted by the two central supports (CF and BG) increases the stress in one arm and decreases the stress in the other. Since the resistance of the two arms varies linearly with the stress provided the elastic limit of the wire is not exceeded, small torques produce a proportional out-of-balance current in the galvanometer G. Inspection of figure 3.1 shows that if a translational force were applied parallel to the direction AB then sections AB and GH would be increased in length and sections CD and EF would be decreased in length. There would thus be no overall change in the length of either arm ABCD or cf arm EFGH, and consequently no change in the bridge balance point would occur. A translational force perpendicular to AB would increase the length of all four sections by the same amount, again leading to no change in the balance point of the bridge. Further inspection shows that torques about the two diameters of the disc parallel and perpendicular to the direction of the resistance wires also leave the balance point of the bridge unaltered. This design also compensates automatically for changes in resistance due to the magnetoresistance of the wires in a magnetic field and due to small changes of temperature.

Consider a wire of length ℓ and resistance R. If its volume and resistivity remain constant and its length is increased by $\Delta\ell$, it can easily be shown that

$$\Delta R/R = 2\,\Delta l/l. \qquad (3.1)$$

In practice, neither of these conditions is satisfied: since the volume does not remain constant and the resistivity of the wire changes with deformation, the factor 2 must be replaced by a number, G, called the gauge factor, which is usually nearer 2.2. If a force F is applied to a wire of cross section πr^2 then,

$$F = \pi r^2 E\,\Delta l/l\ ,$$

where E is Youngs modulus, and

$$\Delta R/R = G/\pi r^2 E. \qquad (3.2)$$

Now consider the configuration of figure 3.1 and let a force F in each of the four wires counteract a torque L developed in the specimen. If the separation of the two central supports

is 2d, then $L = 4Fd$ and

$$\Delta R/R = GL/4\pi r^2 d \qquad (3.3)$$

Furthermore, it can be shown that for a bridge with bridge current 2i, galvanometer resistance R_G and each arm of resistance R, the galvanometer current is

$$i_G = i\Delta R/2(R + R_G) \qquad (3.4)$$

where ΔR is a small change of resistance in one of the bridge arms such that $\Delta R << R$. In the present case both arms change by ΔR but in opposite senses, giving an effective change of $2\Delta R$ in one arm, whence

$$i_G = i RGL/4(R + R_G)\pi r^2 Ed \qquad (3.5)$$

Under these conditions, the galvanometer current i_G is therefore proportional to the torque.

The upper and lower limits to the torque that can be measured, depend respectively on the breaking strain or elastic limit of the wire and on the smallest value of galvanometer current that can be measured in practice. The upper limit thus depends on the type of wire available. The wire used was Nichrome wire with a diameter of about 0.0027 cm, a Youngs modulus of 18×10^{-11} dyne-cm^{-2} and an estimated elastic limit of 2×10^{9} dyne-cm^{-2} (corresponding to a fractional change of the resistance of 2.4×10^{-3}). The lower limit of $\frac{\Delta R}{R}$ is more difficult to estimate, since it depends on the amount of amplification that can, in practice, be applied to the out-of-balance signal from the Wheatstone bridge. Electrostatic and electromagnetic pick-up and electrical noise originating from temperature instability, electrical contacts, thermal e.m.f.'s and mechanical vibration, limit the maximum sensitivity. A conservative estimate of the lower limits of $\frac{\Delta R}{R}$ for a normal bridge circuit with complicated auxiliary apparatus would be about 10^{-6}, although this limit could be extended, probably by one or two orders of magnitude, depending on the amount of care taken in

reducing noise and the efficiency of the amplifying equipment used.

It may be seen from equation 3.3 that these practical limits (of 10^{-3} and 10^{-6}) between which $\frac{\Delta R}{R}$ may be measured, define upper and lower limits of torque, depending on the factor, d, which is half the separation of the support wires. The value of d, used in the torque meter was 0.2 centimeters, so that the approximate range of torque that could be measured was from 4×10^{3} to 4 dyne-cms. Because of obvious geometrical and mechanical limitations the factor d, cannot be reduced by more than about one order of magnitude, although it could be increased in size to a limit determined only by the maximum desirably size of the apparatus. The lower limit of torque that could be measured with the strain gauge wire used was therefore between about 10^{-1} and 10^{-2} dyne-cms.

For the bridge circuit used, in which $R = 60\Omega$, $R_G = 40\Omega$ and $i = 10$ mA., equation 3.4 gives the galvanometer currents corresponding to the upper and lower limits of torque as 6 μA. and 6×10^{-3} μA. The galvanometer used was a Tinsley type 4500 LS, for which these currents give deflections at 2 meters of 1300 centimeters and 1.3 centimeters respectively (this corresponds to an overall sensitivity of about 3 dyne-cms. per centimeter deflection). In practice, a galvanometer amplifier with almost full negative feedback is inserted between the bridge and the galvanometer so that the sensitivity can easily be varied. A simple calculation using equations 3.1 and 3.2 indicates that when the elastic limit of the wires is approached, say at 10^{9} dyne-cms.$^{-2}$, then $\frac{\Delta \ell}{\ell} \simeq 5 \times 10^{-4}$. Since $\ell \simeq 0.5$ cms and $\Delta \ell \simeq 2.5 \times 10^{-4}$ cms, the maximum rotation of the specimen is then about 10^{-3} radians, that is about 3 mins. of arc.

For unwanted torques and translational forces to have no effect on the balance of the bridge, it is important that the wires should be parallel and of the same length, resistance and elasticity. These conditions can never be perfectly fulfilled in practice but careful construction does reduce unwanted effects to a tolerable level. In particular it was found to be important that the two parallel planes containing the resistance wires AB CD and EFGH (figure 3.1) should be as close together as possible. If this is not done, more torque is transmitted to the arm EFGH, nearer to the specimen, due to the flexibility of the specimen support wires. For the same reason, under these circumstances the proper compensation of unwanted effects is not achieved either.

§ 3.12 The Mechanical Lay-out of the Torque Meters.

The mechanical layout of the first torque meter that was made is shown in figure 3.2. The second torque meter, which was basically the same but which was modified to facilitate calibration under working conditions, is shown in figure 3.3. Since a wire cannot be compressed by pressure on its ends, all four wires have to be prestressed, ideally to half the elastic limit. This was done by forcing the two halves of clamp A apart with the differential screw so that the support wires B were made to flex from their bases. The torque from the specimen H in the specimen holder C, was then transmitted via the specimen support wires D to produce a strain in the resistance wires E. When not in use the clamp A was closed, removing the stress from the resistance wires and clamping the wires D supporting the specimen holder so that, for instance, the specimen could be changed without risk of damage occurring. In the first model the phosphor bronze suspension wire J attached between the calibration head F and the specimen holder C was of circular section and was used for calibration purposes. A photograph, one centimeter in diameter, of a circular protractor was cemented centrally on to the top of

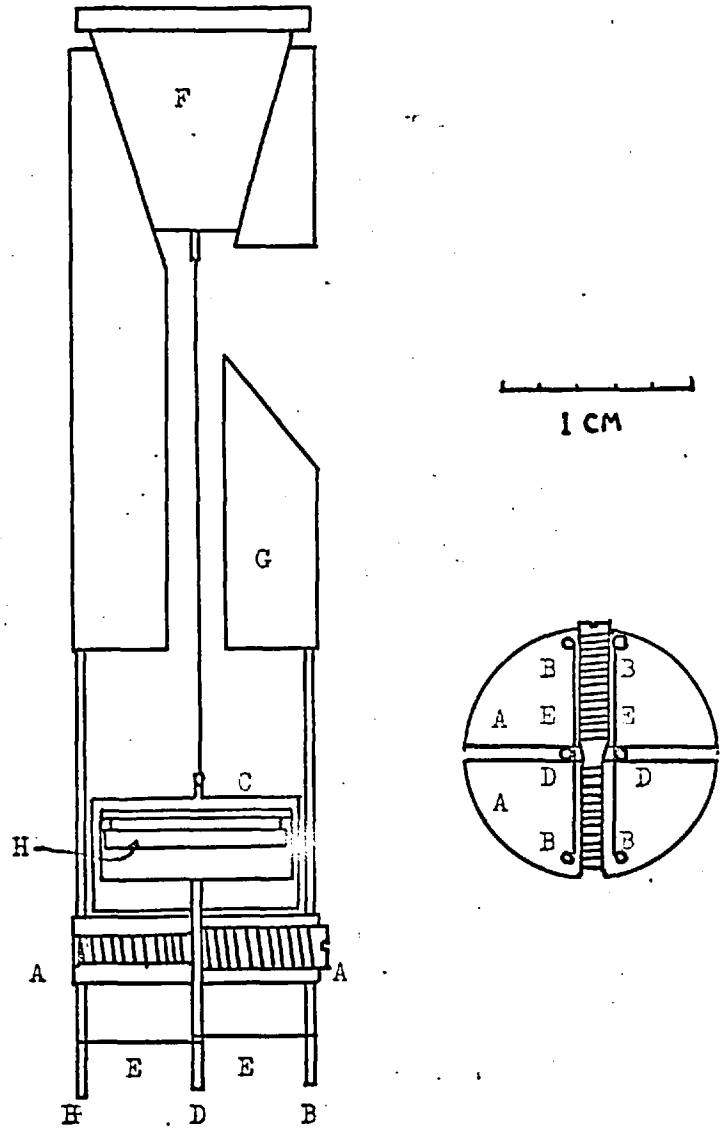


Figure 3.2

MECHANICAL LAYOUT OF FIRST TORQUE METER

(A) Clamp jaws, (B)(D) Support wires, (C) Specimen holder, (E) Resistance wires, (F)Torque head, (G) Main body of torque meter, (H) Specimen.

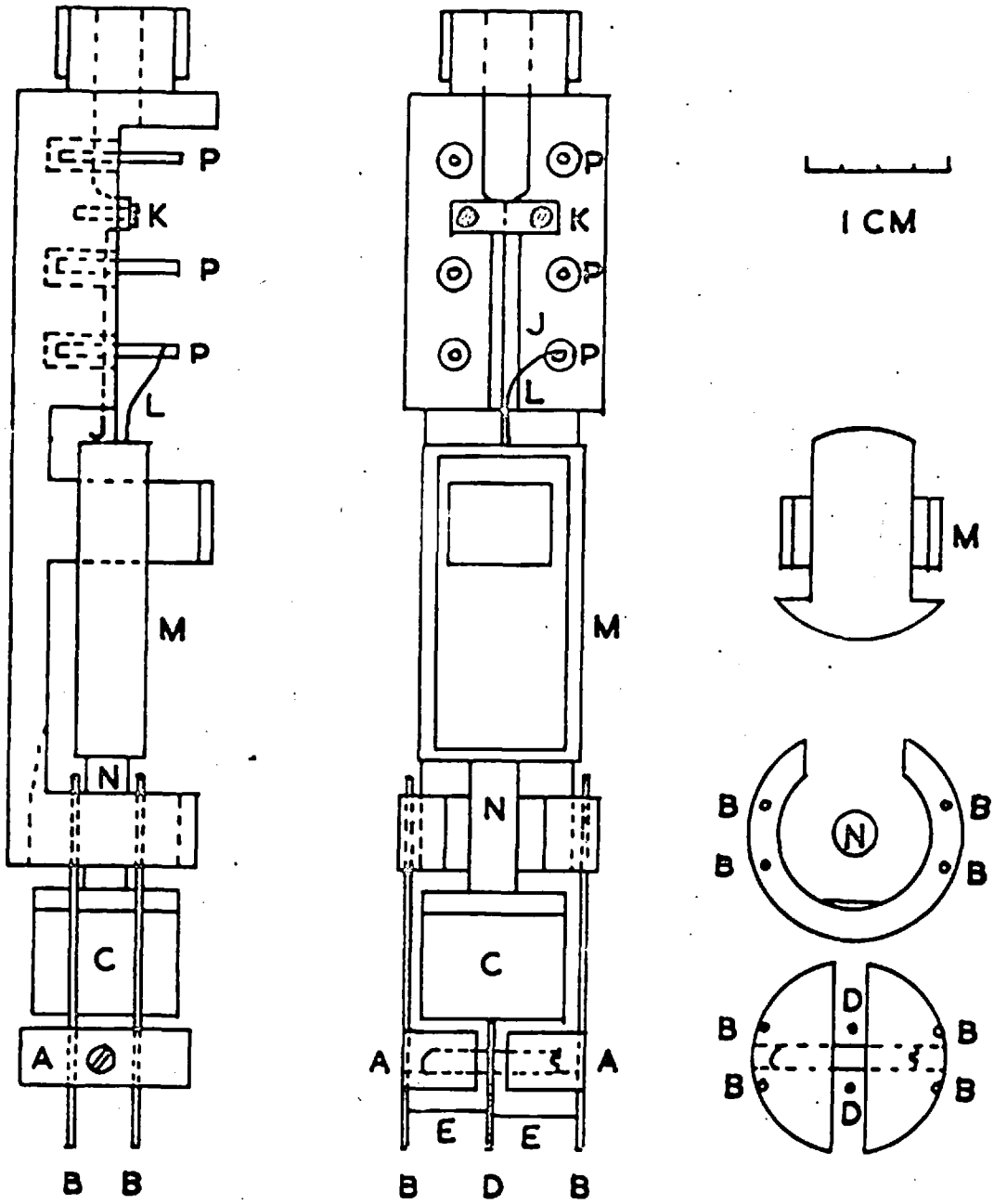


Figure 3.3

MECHANICAL LAYOUT OF SECOND TORQUE METER

(A)Clamp jaws, (B,D)Support wires, (C)Specimen holder, (E)Resistance wires, (J)Phosphor bronze filament, (K)Filament clamp, (L)Silver ligament, (M)Calibration coil, (N)Brass rod, (P)Soldering post, (Q)Threaded stud.

the torque head. Thus the angular rotation of the head could be measured accurately with the aid of a microscope. A thin coating of Araldite on the support wires B and D insulated them from the resistance wires E. The ends of these resistance wires were terminated mechanically at the tops of the support wires B by wrapping them once round the support wires and then coating them with Durafix. Soldering tags, which were spot-welded to the ends of the resistance wires E prior to assembly, were then soldered to copper soldering posts (not shown in the diagram for the sake of clarity). The soldering posts were let into the clamp jaws A and were insulated from them by Paxolin bushes. Electrical connections from the Wheatstone bridge were made to these soldering posts. A port was provided in the main body G of the instrument, so that the phosphor bronze suspension could be unsoldered and replaced. To gain access to the specimen H, the specimen holder G was made in two halves. In operation these were secured with smears of Durofix which could be readily dissolved in acetone when the specimen was to be changed. Within the specimen holder, the specimen was mounted on a thin rubber pad to provide a small degree of flexibility in the plane of the specimen.

The method of calibration used in this model proved quite satisfactory for measurements near room temperature. However, at other temperatures the variation of the modulus of rigidity of the torsion filament with temperature must be found by a separate experiment and a rather inconvenient temperature control set up would be required for calibration purposes since the torque head would have to be rotated at the calibration temperature. In the second torque meter, the configuration of the strain gauge wires, specimen holder and clamp jaws was not modified in principle. However, the method of applying a known torque to calibrate the meter was changed. Because measurements were always made in a large uniform magnetic field, it was feasible to connect a rectangular coil rigidly to the

specimen holder C (figure 3.3) and to use the torque developed in the coil when it carried a current in the magnetic field to calibrate the torque meter directly. Because this calibration technique was used, it was important that the flux through the coil from the demagnetising field of the specimen should be negligible compared with the applied magnetic field. The lower end of the coil and the specimen holder were therefore connected by a massive brass rod some 9mms long. The top end of the coil was connected to a flattened phosphor bronze filament J which acted both as a suspension and as an electrical connection to the coil. The other electrical connection to the coil was made by a silver ligament: this was situated at the top of the coil and was connected between the coil and an insulated solder post. The dimensions of these ligaments were chosen so that they would cause a negligible error in the measurement of the torque, bearing in mind the small, but finite, rotation of the specimen.

A modification was also made to the method of terminating the strain sensing resistance wires at the outer support posts B. Originally the posts were insulated with a thin layer of Araldite and the resistance wire was wound around them and anchored with Durafix. Electrical connections were then made separately to the free unstressed end of the resistance wire. This method had the advantage that the state of stress of the wire could not effect the contact resistance of the electrical connection, but it required a fairly substantial length of non-active resistance wire. This led to a reduction in sensitivity and also to rather clumsy arrangements for connection of the leads to the Wheatstone bridge. The modification was to use enamelled constantan wire (22 s.w.g.) for the support posts, so that there was no electrical connection between them and the body of the torque meter. The strain sensing resistance wire could then be soldered directly to the support posts, connections from the solder

posts at the top of the torque meter being made to the other free projecting ends of the support posts. In practice it was found that with carefully soldered joints the effect of strain on the contact resistance at the joint was not troublesome. The same method of changing the specimen was used as before. The clamp jaws were contracted by the differential screw, relieving the stress in the resistance wires E and clamping the support wires D. The base of the specimen holder with the specimen attached, together with coil and suspension filaments, could then be withdrawn through the port in the body of the torque meter, after the clamp K has been loosened to free the support filament E.

§3.2 The Apparatus for Temperature Control and Auxiliary Apparatus.

The earlier measurements were carried out with a 4" Newport water-cooled electromagnet (with cylindrical pole pieces) mounted on a turntable. To facilitate access to the experimental equipment, the magnet and turntable were placed on a trolley and rails as shown in figure 3.4. The design of the pair of wheels on one side of the trolley and the corresponding rail permitted the magnet to be withdrawn from the experimental equipment and replaced accurately after withdrawal. This arrangement permitted small translational adjustments of the position of the magnet relative to the remaining experimental equipment and parallel to the direction of the rails. Horizontal translational motion perpendicular to this direction was accomplished with the aid of a slide supporting the temperature control equipment, while the three supporting adjustment screws allowed vertical movement and alignment of the temperature control equipment. Later experiments were conducted with the aid of a 7" Newport water-cooled electromagnet with conical pole tips, again mounted on a turntable. The same trolley was used as before, but a slide which permitted control of lateral displacement

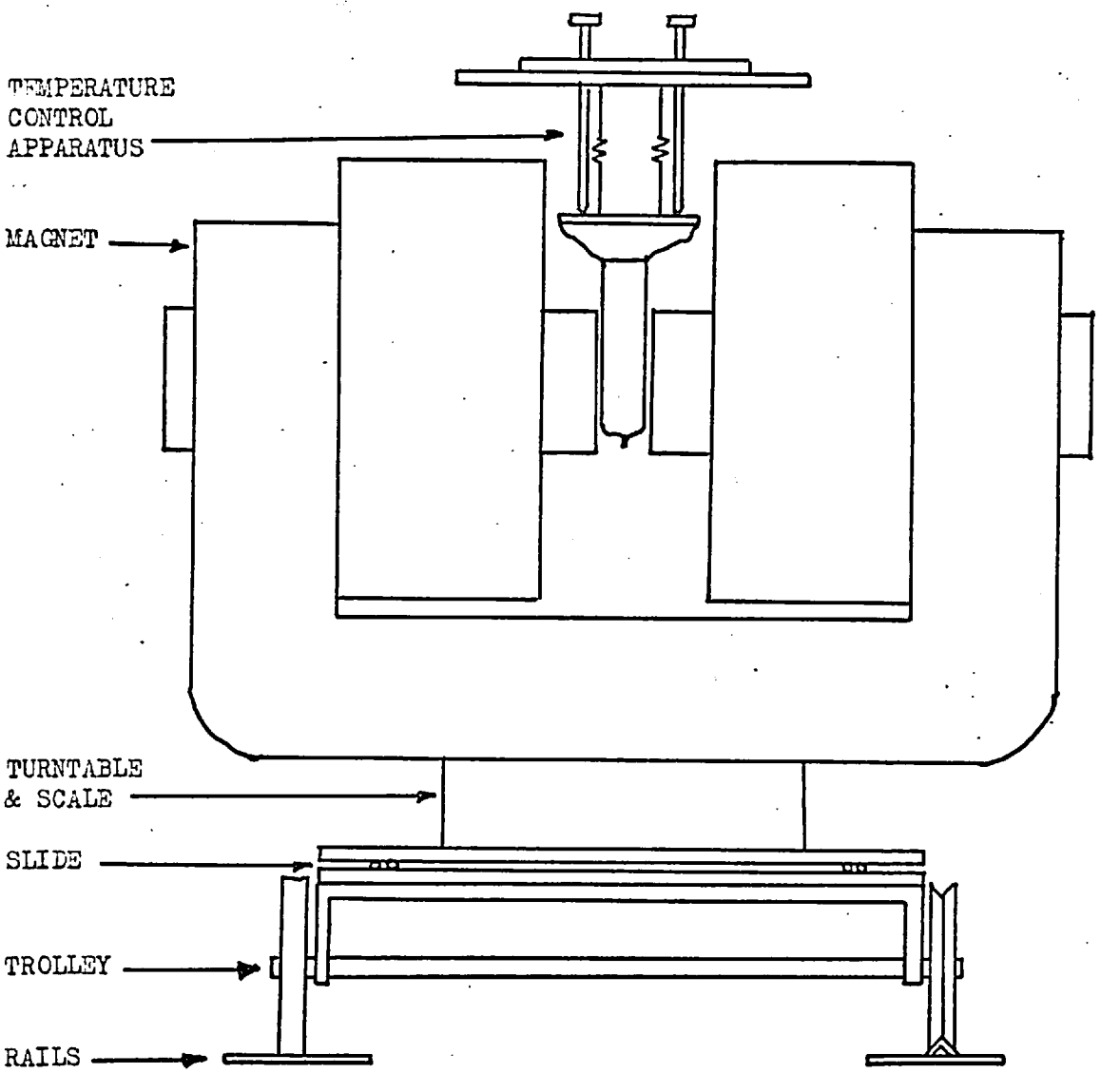


Figure 3.4

AUXILIARY APPARATUS

over about 2" was inserted between the trolley and the magnet turntable. The provision of two degrees of translational freedom thus ensured that the magnet and turntable could be accurately positioned with respect to the remaining apparatus, while the provision for vertical movement and alignment was provided on the temperature control equipment by a similar arrangment to that used with the 4" magnet.

Preliminary measurements made with the smaller magnet used a temperature control system based on thermoelectric cooling modules. These were manufactured by De La Rue under the trade name of Frigistors and were constructed from p- and n-type semi-conducting bismuth telluride. The smallest module available consisted of 4 couples, and it was claimed that it would achieve a temperature difference of 62°C between the hot and cold junctions with no heat pumped, or would pump 3.5 watts of heat for zero temperature difference between the junctions. These figures are based on the assumption that the hot junctions are held at 27°C with a current of 15 amps and a voltage of about 0.4 volts across the device.

The preliminary experimental set up, shown in figure 3.5, employed two thermoelectric cooling stages operated in cascade. The hot junctions of the first-stage modules were thus cooled by the cold junctions of the second stage modules. The hot junctions of the second stage were

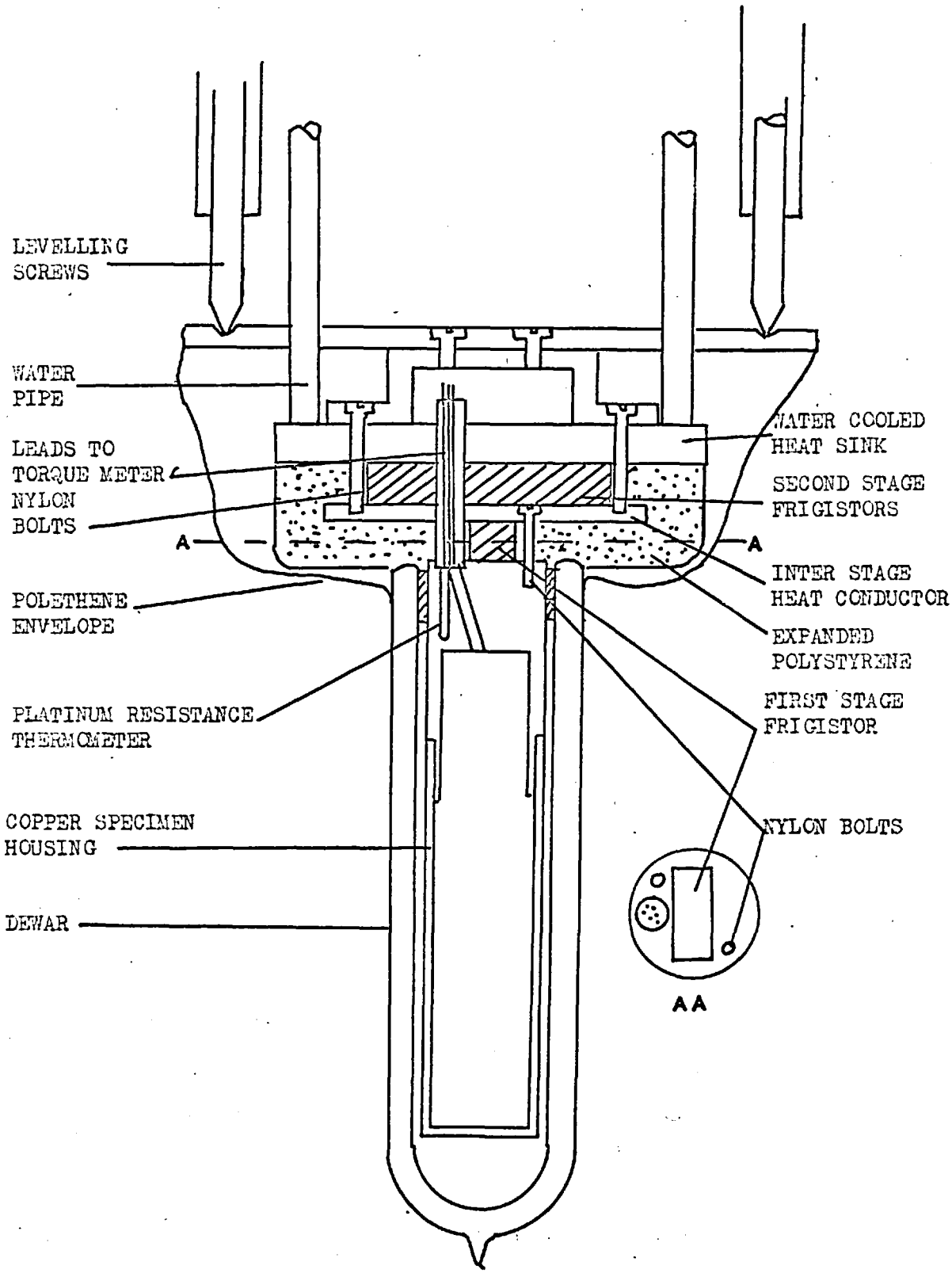


Figure 3.5

PRELIMINARY TEMPERATURE CONTROL APPARATUS

then water cooled. Because Joule heat is generated within the thermocouple, it can be seen that even with no heat pumped and therefore with the maximum temperature difference realised across the first-stage modules, the second stage must still pump a substantial quantity of heat. In order to achieve a reasonable temperature difference across the second stage, the heat pumped per module must be kept low, and the ratio of second to first stage modules should ideally be large. A ratio of 5:1 was chosen in the preliminary equipment as being a reasonable compromise between expense and efficiency and as giving an overall theoretical maximum temperature difference of about 90°C for no heat pumped. From figure 3.5 it can be seen that the two stages are clamped together via the interstage heat conductor, between the water-cooled second-stage heat sink and the copper specimen housing. Nylon bolts were used to reduce heat losses by conduction. Heat losses were further reduced by the use of the dewar surrounding the specimen housing and by lagging the remaining exposed surfaces with expanded polystyrene. A polythene envelope was found to be necessary to reduce condensation. A platinum resistance thermometer located in the specimen housing was connected, in series with an adjustable resistance, in one arm of an a.c. Wheatstone bridge circuit, as indicated in figure 3.6. The out-of-balance a.c. signal from the bridge was amplified and used continuously to control a direct current power supply to the thermoelectric cooling devices. The full circuit for this bridge amplifier and

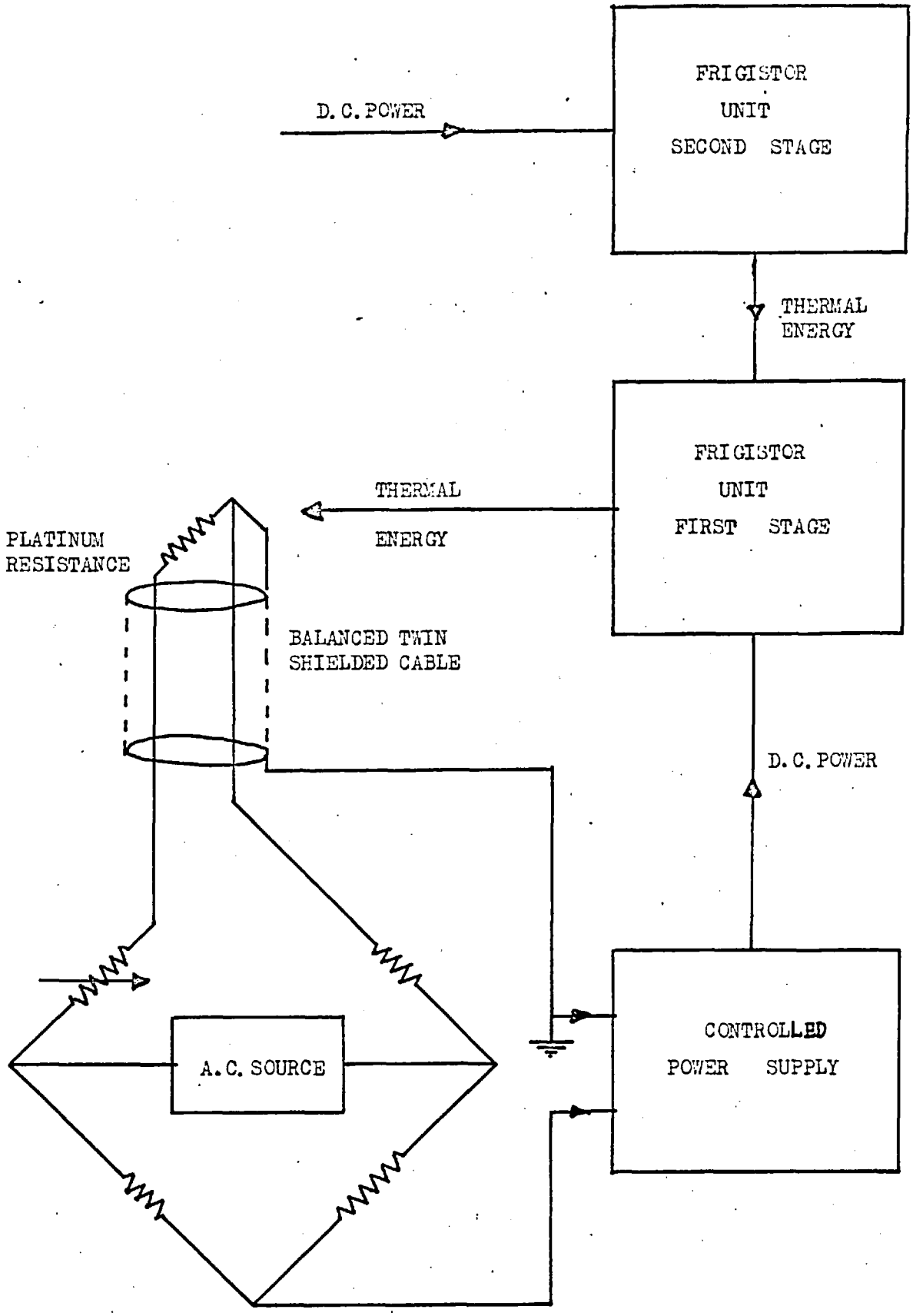
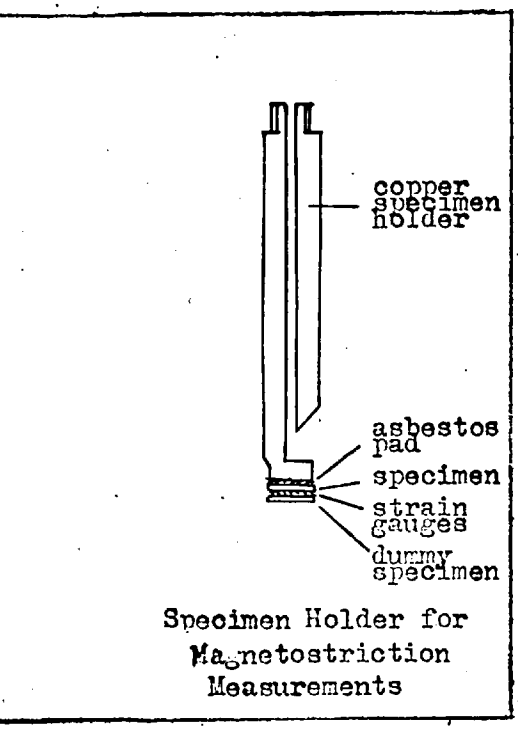


Figure 3.6
PLATINUM RESISTANCE THERMOMETER CIRCUIT

d.c. supply is shown in appendix B. The value of the resistance in series with the platinum resistance thermometer determined the temperature at which the system stabilized, and this particular configuration had the advantage that the output impedance of the bridge at or near balance did not vary with temperature. However, the sensitivity of the bridge to changes in temperature decreased with temperature and hence the resistance of the platinum thermometer was reduced. Nevertheless this type of system was found to be capable of holding the temperature of the specimen housing constant to within about 1/50th to 1/20th of a degree centigrade over a range from room temperature to liquid-air temperature. The lowest temperature at which measurements were made with this equipment was, however, only about -60°C. Lower temperatures could be obtained, but this took a long time and excessive condensation was troublesome. Temperatures above the ambient could be obtained by reversing the current through the Frigistors and then an upper limit of about 100°C was set by the melting point of the solder used in their construction.

The modified temperature control system shown in figure 5.7, had about three times the heat pumping capacity of the first model and this reduced the time required to reach thermal equilibrium. The whole system was enclosed in an evacuated envelope (g) which eliminated



Specimen Holder for Magnetostriction Measurements

Figure 3.7
Apparatus for Temperature Control
a, first-stage cooling modules,
b, second-stage cooling modules
c, specimen housing,
d, interstage heat conductor,
e, second-stage heat conductor,
f, brass rings,
g, vacuum vessel,
h, drill hole for platinum resistance thermometer,
i, space for specimen holder or torque meter,
j, polythene tube,
k, polythene tube,
w, electrical heaters.

condensation and reduced heat losses. By the use of liquid air or water cooling for the second-stage hot junctions (e), the temperature range was extended from + 100°C down to liquid-air temperatures. From figure 3.7 it can be seen that the same cascade principle of operation was used as before, except that the three identical units were symmetrically arranged round the central copper specimen housing (c). Nylon bolts were used only to clamp the second stage module (b) in position. Paths by which heat could be conducted across the modules were eliminated in the first stage by bolting the three units to the two brass rings (f) to force the three first stage modules (a) inwards against the hexagonal faces of the torque meter housing (c). The ratio of the numbers of modules in the first and second stages was changed to 1:6 to increase the maximum temperature difference across the second stage modules. The only paths by which stray heat could be conducted to the first stage were then via leads to the measuring equipment in the specimen housing, the leads to the platinum resistance thermometer (located in drill hole (h) and thermocouple, and the polythene tube (j). Heat transfer by the leads was kept small by reducing their diameters as far as was practicable. The polythene tube (j) was used to control the atmosphere within the specimen housing to improve heat transfer. Heat transfer by radiation from the first stage was reduced as much as

possible by periodically cleaning the copper specimen housing in chromic acid, to ensure low surface emissivity. Heat transfer by convection was reduced, as already mentioned, by evacuating the polished brass vacuum vessel surrounding the temperature control unit to between 10^{-4} and 10^{-5} mm. of mercury. A conventional system comprising diffusion and backing pumps and Penning gauge was employed to produce and measure this vacuum. Water or liquid air was circulated to the second-stage heat conductors within the vacuum vessel via three polythene tubes (k). Conventional rubber O-ring vacuum seals were used at the entry of the polythene tubes to the vacuum vessel. To prevent the breakdown of these seals when liquid air was in use, electrical heaters (w) dissipating about 15 watts each were used.

The temperature control circuit was the same as that described for the preliminary apparatus except that the controlled d.c. power was supplied to only the first stage thermoelectric cooling modules. A separate supply of d.c. power to the second stage could be controlled manually.

The liquid air supply to the apparatus operated in a semi-continuous manner because the sizes of the three reservoirs attached to the second-stage hot junction conductors (e in the figure) were small. Liquid air, conducted by a transfer tube from a large 25 litre storage

dewar, was introduced into the three reservoirs, by 1/8th in. bore copper tubes penetrating via the polythene tubes (k) almost to the lower ends of the reservoirs. The three open ends of the polythene tubes were thus left free for the efflux of boil-off gas. A thermocouple, located near the top of one of the three reservoirs, controlled the liquid-air level in the following way. The output from a conventional potentiometer that measured the thermocouple e.m.f. operated a Cambridge spot galvanometer. A phototransistor, attached to the galvanometer scale at a position appropriate to the temperature of liquid air, controlled the air pressure inside the large storage dewar by means of a relay and compressed-air valve.

§3.3 Preparation of the Nickel Specimen.

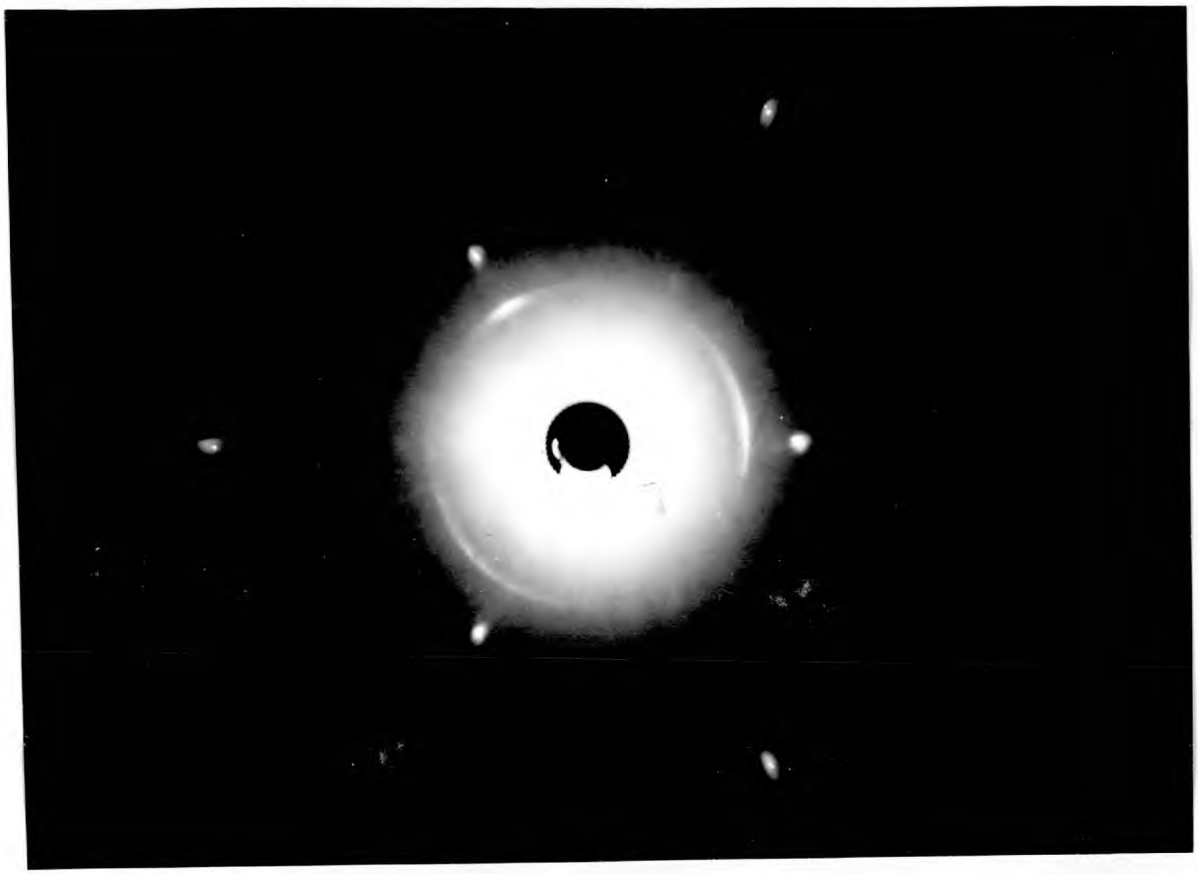
The sample of pure nickel, from which the (111) specimen was to be cut, was in the form of a thin slightly irregular slab, about 1.5 x 1.5 x 0.3 cms. It was believed to be substantially a single crystal with a (111) plane approximately parallel to the surface of the slab. A rough orientation had been carried out at the Mullard's Research Laboratories (Salford), where a small flat had been ground on the surface of the slab to within 1° of the (111) plane. The specimen was required in the form of a disc with the symmetry axis coincident with a (111) direction. To this end, the nickel slab was

first etched to reveal the prescence of any grain boundaries and then oriented by means of X-rays so that a flat surface could be ground and polished to within 15 minutes of a true (111) plane. A second surface was then ground on the back of the slab parallel to within 6 minutes of the first surface. Finally a disc was spark-cut from the slab to give the required specimen.

§3.3.1. X-Ray Orientation.

X-rays emitted from a copper target were available for purposes of orientation and, because the crystal was about 0.3 cms thick, only back reflection could be used. A Laue back-reflection camera was employed on a Phillips-type camera mount. The film size was 16 x 12 cms. and the working distance between the crystal and the film plane was 3 cms. The camera holder contained a horizontal turntable with goniometer head free to rotate about two perpendicular horizontal axes and translate along two perpendicular horizontal directions. There were also two arms rotating coaxially with the turntable and supporting respectively an illuminated slit with collimator, and a telescope with cross hairs. Finally there were mountings for the film-holder and X-ray collimator. The normal proceedure for setting up the apparatus was to rotate the telescope until it was coaxial with the X-ray collimator when the telescope was locked in this position. The crystal was mounted with plasticine on the goniometer

head which was adjusted until an image of the slit in the collimator, reflected from the surface of the crystal that was being inspected, coincided with the crosshairs in the telescope, when the collimator and the telescope were 90^{o} apart. At the same time, the goniometer was adjusted both to make a reference edge of the crystal parallel to the vertical cross-hair in the telescope and to make the surface of the crystal coincide with the intersection of the crosshairs in the telescope while also coinciding with the axis of rotation of the turntable. After rotation of the turntable by 135^{o}, the equipment was set up as required with the crystal surface perpendicular to the X-ray beam and 3 cms from the film plane. After exposure, the resulting negatives (an example of which is shown in plate 3.1) were analysed in the following way. The circular ring was interpreted as being due to diffraction of the copper Kα (λ = 1.542 Å) line by the randomly oriented surface crystallites created during grinding operations. The plane of the reciprocal lattice shown in figure 3.8 was drawn out to scale, together with a circle representing the cross section of the sphere of reflection with a diameter for copper Kα radiation of wavelength 1.542Å It was found to pass exactly through a 331 point which requires an angle of $22^{o}0'$ between incident and reflected beams and agrees well with the angle subtended by the diffraction ring. The discrete spots on the negative were then identified by comparing



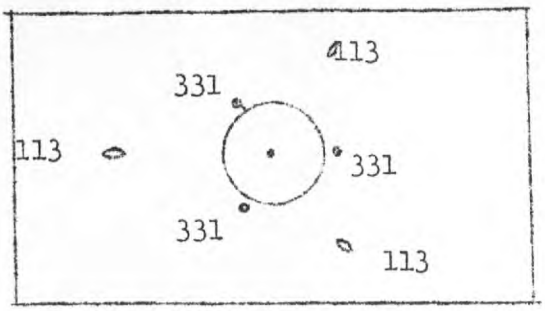


Plate 3.1

X RAY PHOTOGRAPH

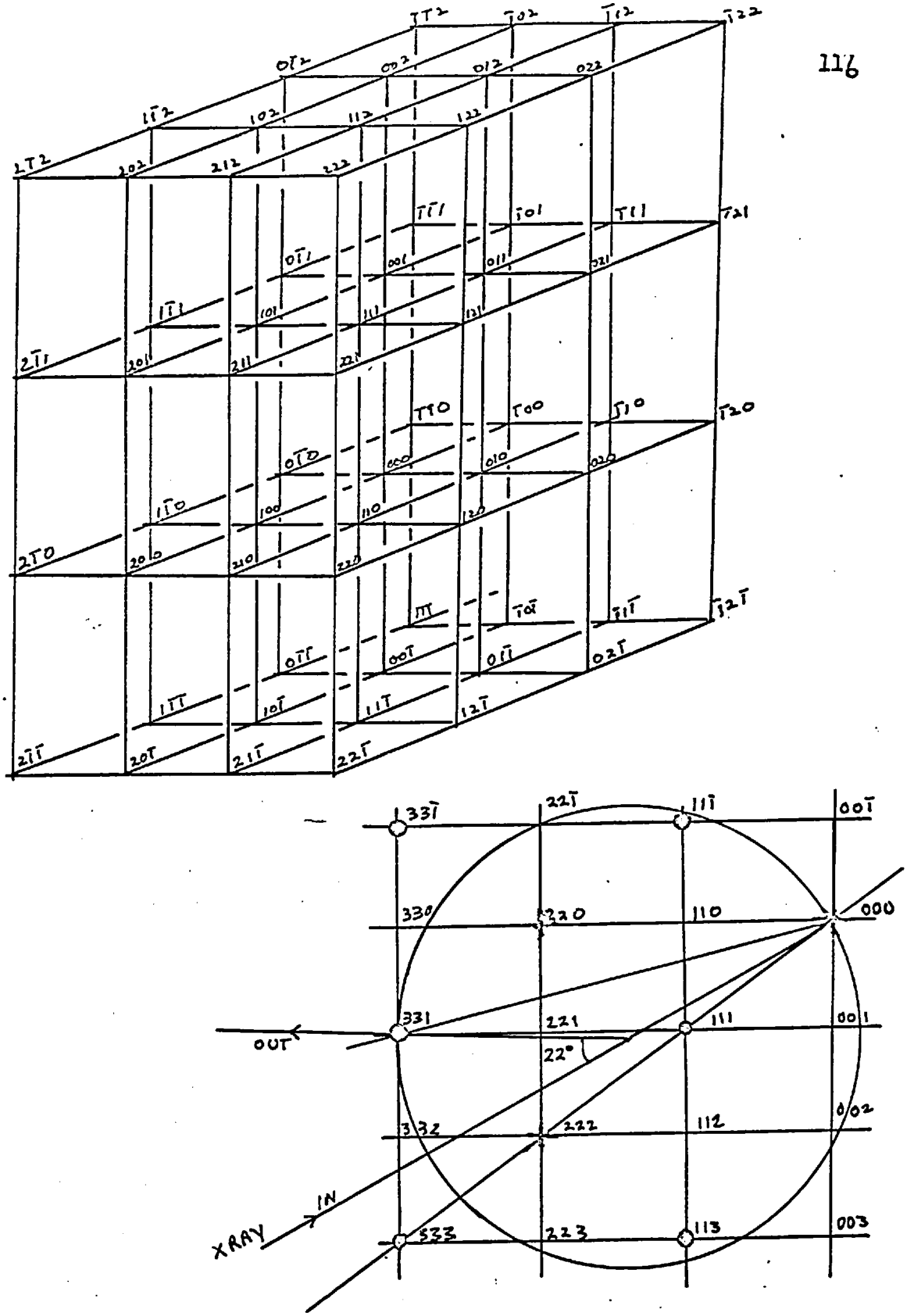


Figure 3.8 RECIPROCAL LATTICE AND CONSTRUCTION TO IDENTIFY POWDER RING

the measured angles with those possible as reflections due to refraction of white radiation at (113) and (331) type planes, as indicated on the plate. The exact angle between the X-ray beam (and hence the crystal surface) could then be obtained graphically in the following way. The origin of the reciprocal lattice was imagined at the centre of a sphere, radius R, with a [111] direction as a diameter. Suppose the three symetrically placed 331 points on the reciprocal lattice subtend angles θ with the [111] direction at the origin and let the three measured angles between the 331 spots on the plate and the X-ray beam be Φ_1 Φ_2 Φ_3 Then circles drawn on the surface of the sphere with centres at the 331 points, and diameters subtending half the measured angles $\frac{\Phi_1}{2}$ $\frac{\Phi_2}{2}$ $\frac{\Phi_3}{2}$ intersect to give the position of the X-ray beam. To make a graphical solution possible, the stereographic projection of the sphere onto the equatorial plane was used as shown in figure 3.9. Circles and arcs are projected as such, although their centres move, and angles of intersection between great circles are reproduced as angles between straight lines on the projection plane. The position of the centre of a projected circle was found using the formulae:

$$s_i = \frac{R}{2}\left[\tan\left(\tfrac{1}{2}\theta + \tfrac{1}{4}\Phi_i\right) + \tan\left(\tfrac{1}{2}\theta - \tfrac{1}{4}\Phi_i\right)\right] ,$$

where s_i was the distance of the centre of a projected

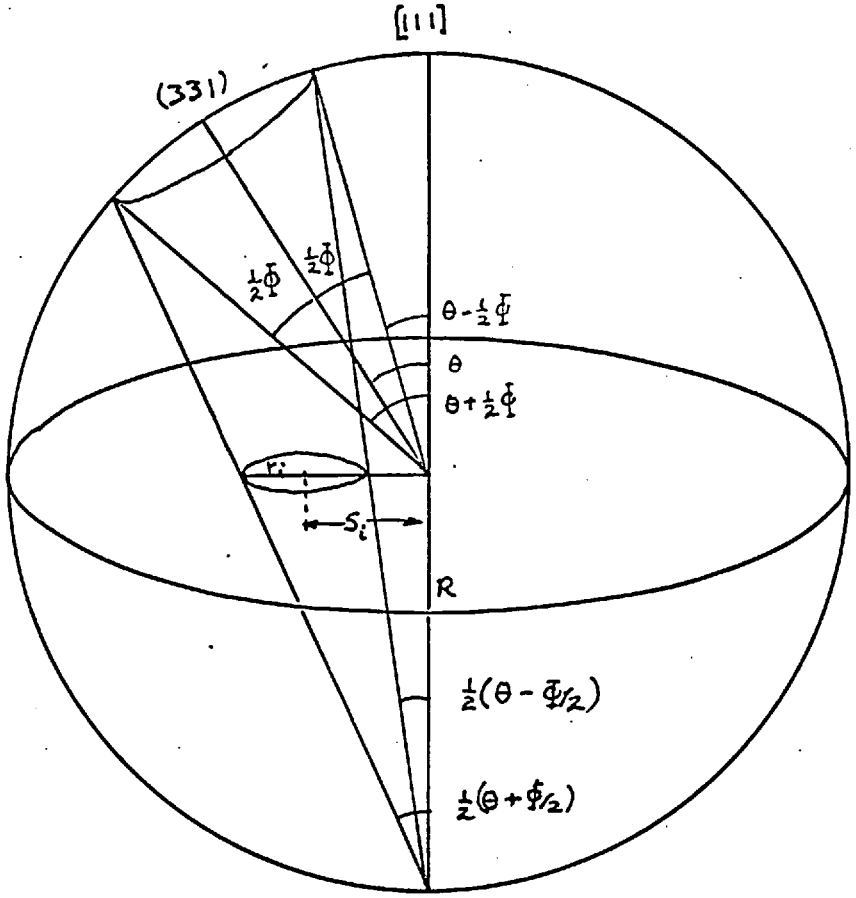


Figure 3.9

THE STEREOGRAPHIC PROJECTION

circle from the centre of the sphere, and R was the radius of the sphere. The radius, r_i, of a projected circle was then given by

$$r_i = \frac{R}{2}\left[\tan\left(\tfrac{1}{2}\theta + \tfrac{1}{4}\Phi_i\right) - \tan\left(\tfrac{1}{2}\theta - \tfrac{1}{4}\Phi_i\right)\right].$$

The point of intersection of the three arcs then gave the position of the X-ray beam relative to the [111] direction, and it only remained to measure the separation between these two points on the graphical solution and convert this to the error angle. The direction of the error relative to the reference direction on the crystal was easily found by direct comparison of the graphical solution with the original negative.

§3.3.2 Grinding and Orientation Procedure.

The jig shown in figure 3.10 was devised so that grinding and polishing could be done by hand. In use the speciman was mounted in shellac in the brass specimen cup (d) which was attached to the central sliding rod (b) via a universal ball joint (a). The sliding rod was locked in position with the crystal surface slightly proud of the jig face (e). The jig face and the crystal were then ground simultaneously on abrasive paper supported on a flat plate of glass (f). The jig face thus defined the grinding plane and the following technique was used to orient the crystal relative to this plane before grinding commenced. The jig, with specimen, was supported with its

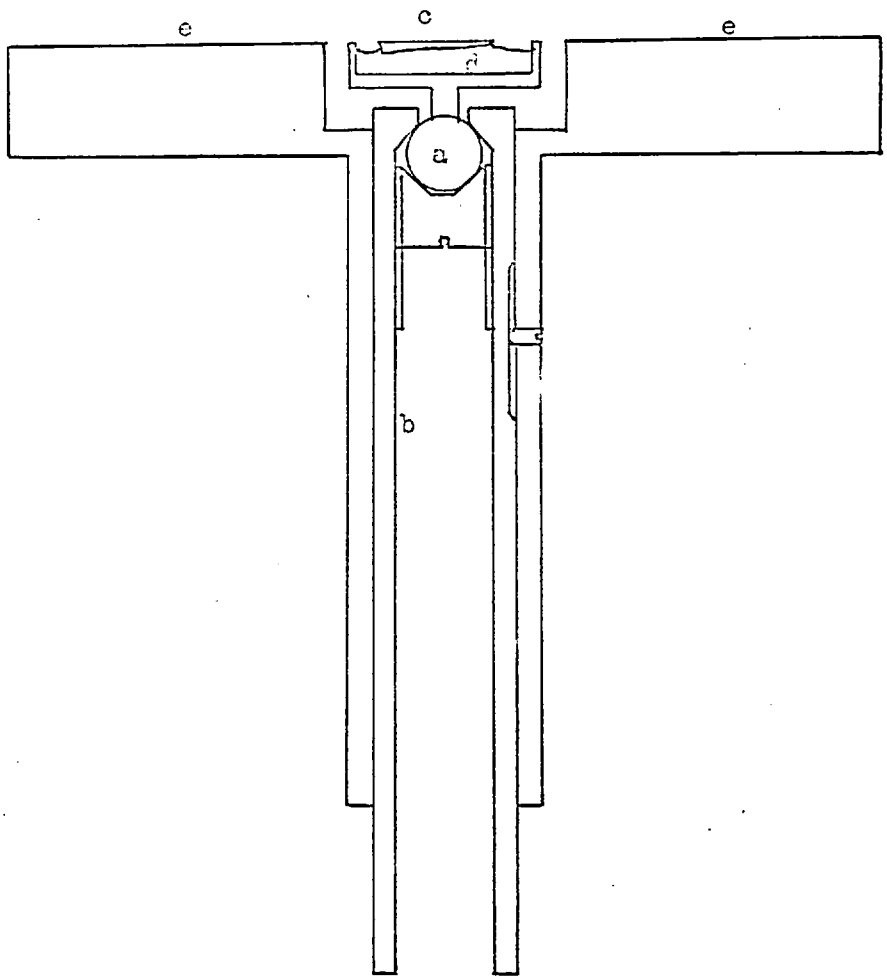


Figure 3.10

GRINDING JIG

(a) Ball joint, (b) Sliding rod, (c) Specimen, (d) Specimen cup, (e) Jig face.

axis horizontal on a spectrometer turntable. The collimator and telescope of the spectrometer were designed to have an aperture large enough for light from an illuminated pin hole in the collimator to fall on both the crystal plane under observation and the polished surface of the jig face. With the collimator adjusted to give a parallel beam of light, and the telescope focused at infinity, two images of the pin hole could be seen in the telescope field of view reflected from the specimen and the jig face. The specimen cup could then be adjusted on its universal ball joint and locked in the required position to give the correction to the plane, as indicated by the X-ray diffraction analysis. In order that small corrections could be achieved accurately, the turntable was rotated by a micrometer screw bearing on an arm connected to the turntable. In practice dampened grade 0000 abrasive paper was found to permit quite high grinding speeds while giving a good reflecting surface on both the nickel specimen surface and the steel jig face.

In order to grind the back face of the crystal parallel with the front face, already aligned, the central sliding rod of the jig was replaced by one with a flat end. This end was then ground until its plane was parallel with the jig face. The crystal was then attached with shellac, with the aligned face in contact with the end of the rod, and grinding was continued until the crystal was of the required thickness. The error in alignment between the back and front faces of the

of the crystal was measured optically on the x-ray camera holder and was found to be less than 6 minutes of arc.

The diffraction photographs gave the orientation, relative to a reference edge on the crystal, of the [112] directions lying in the (111) plane. Hence it was possible, before the specimen disc was cut from the crystal, to inscribe on the (111) plane, a line giving the [112] direction. This was done by mounting the crystal in Shellac at the centre of the turntable. A travelling microscope was mounted in such a way that it bridged the turntable and could be used to traverse the crystal face. By first rotating the table so that the microscope objective traversed along the reference edge of the crystal, and then rotating the turntable by the angle given by the X-ray data the objective could be made to traverse the crystal face parallel to a 112 direction. The objective lens was then replaced by a brass blank carrying a scribe, and the traverse across the crystal face was made to give the reference line. A spark-cutting machine with a hollow cylindrical copper tool of the correct internal diameter was used to cut the disc from the prepared nickel slab, because this method leaves the specimen substantially free from strain. The area from which the disc was cut was selected after a number of X-ray photographs over the whole surface had been inspected to find the least disturbed area. The weight and dimensions of the disc were : Weight 0.7662 grms, diameter 1.006 cm., and thickness 0.1110 cm.

§3.4 Preparation of the Gadolinium Specimen.

A single crystal specimen of gadolinium was made available by K.J. Tauer and A. Marotta and was in the form of a roughly rectangular thin parallel sided slab with two somewhat rounded corners (see plate 3.2). The plane in which the parallel faces lay was perpendicular to a $[11\bar{2}0]$ direction, while the c-axis was perpendicular to one of the slab edges. The specimen was subjected to a preliminary etch to reveal the position of unwanted crystallites. The etchant used was Nital (1% HNO_3 (specific gravity 1.42) in absolute alcohol) and was one of a number recommended by Spedding and Danne (1961). The crystal surface was swabbed with this etchant until the grain boundaries shown in plate 3.2 were observed. Subsequently a reference line was scribed on the crystal surface, parallel to a reference edge, and a disc was spark-cut as indicated by the broken circle superimposed on the photograph. The techniques used for inscribing the reference line and for spark cutting were the same as those described for the corresponding operations on the (111) nickel single crystal (section 3.3.3). The disc was subsequently used for torque measurements while the detached corner, marked (a) on the plate, was further prepared for domain observations which required a well polished surface free from any surface layers that might prohibit the observation of domains. Electropolishing was investigated since this operation has been used successfully in the preparation of surfaces on cobalt, iron and nickel for domain observation and has been used on gadolinium for shaping purposes (Corner, Roe and Taylor 1962).

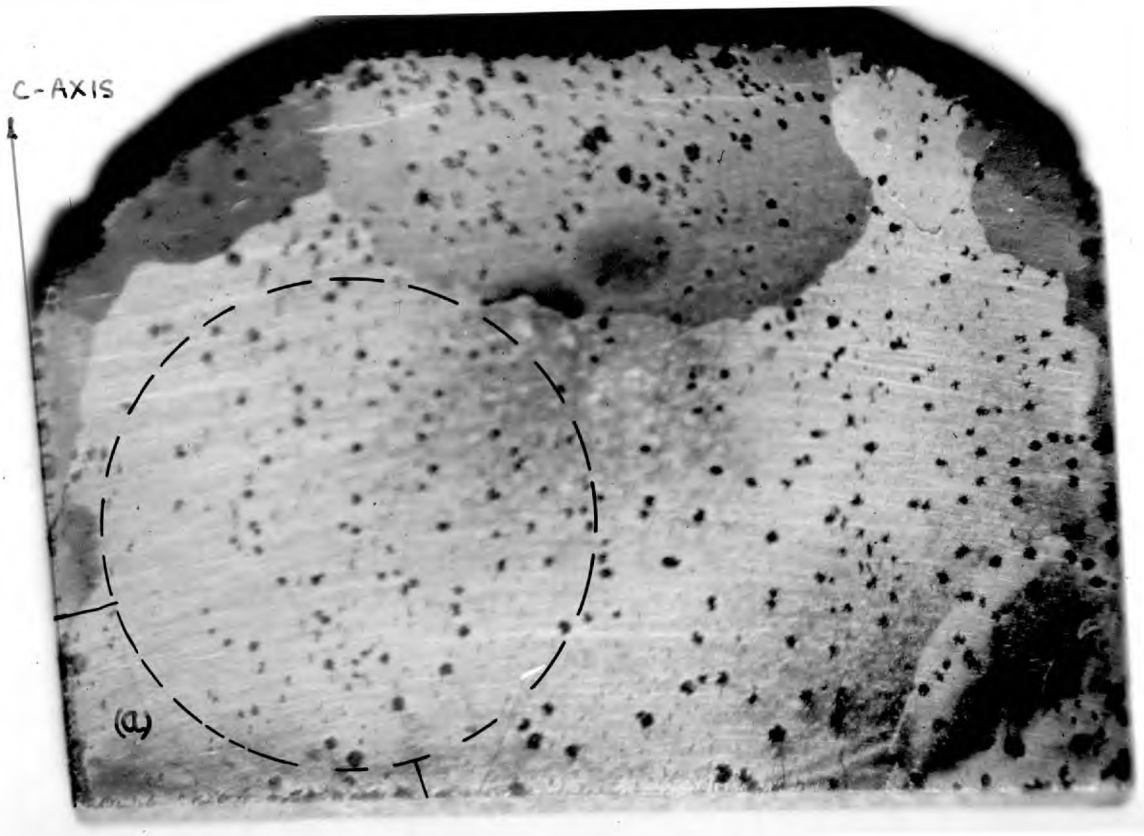


Plate 3.2 GADOLINIUM SINGLE CRYSTAL SPECIMEN

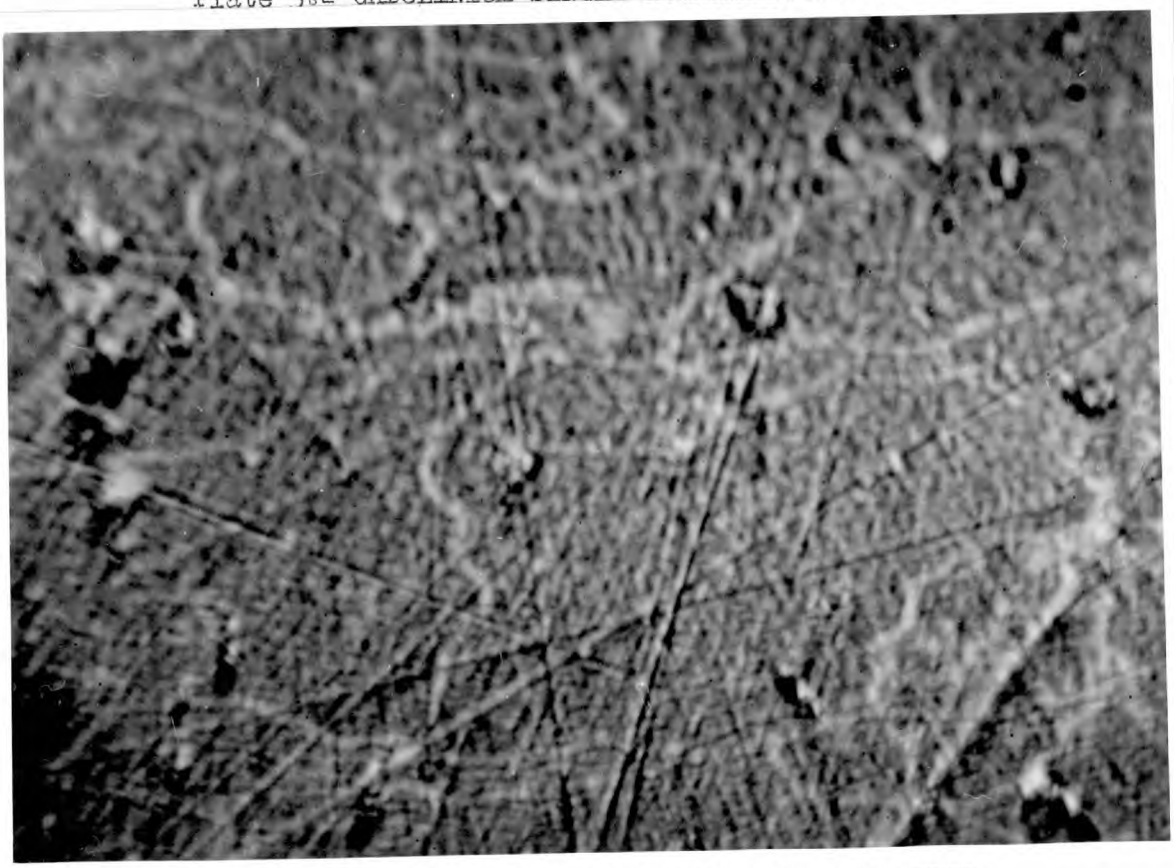


Plate 3.3 GRAIN BOUNDARIES ON POLYCRYSTALLINE GADOLINIUM

However, none of the methods tried for electro-polishing gadolinium for the observation of domains was considered satisfactory and the apparatus shown in figure 3.11 was therefore set up for ion-bombardment of the specimen held in the jaws of a copper specimen clamp. A vacuum of 20-30 microns was maintained within the bell-jar, while argon gas was permitted to leak slowly into the system. The specimen and clamp were held at a negative potential of 2 Kv. relative to earth, with a current flowing of between 0.1 and 0.2 mA. per square centimeter of cathode. Heat was removed from the specimen by a thick copper conductor and external fins. A test specimen of pure polycrystalline gadolinium was first polished by hand with a diamond paste having a paraffin type base. Subsequently the specimen was ion-bombarded for about 4 hours in the apparatus under the conditions just described. Inspection under a microscope then revealed the grain boundaries shown in plate 3.3, indicating that the process had had the required effect. The single crystal specimen was subsequently prepared in a similar manner. On removal from the vacuum system, it was immediately placed under Xylene to avoid deterioration of the surface.

§ 3.5 Preparation of the Magnetic Colloid.

It was found that colloids prepared with the normal base e.g. water (Bitter 1931, Elmore 1938, Bozorth 1951, Craik & Griffiths 1956, Garrood 1962) and with acetone (Gustard 1964) attacked the prepared surface of the specimen and were thus unsuitable. However, the technique used by Gustard for preparation of colloids in acetone was modified by replacing

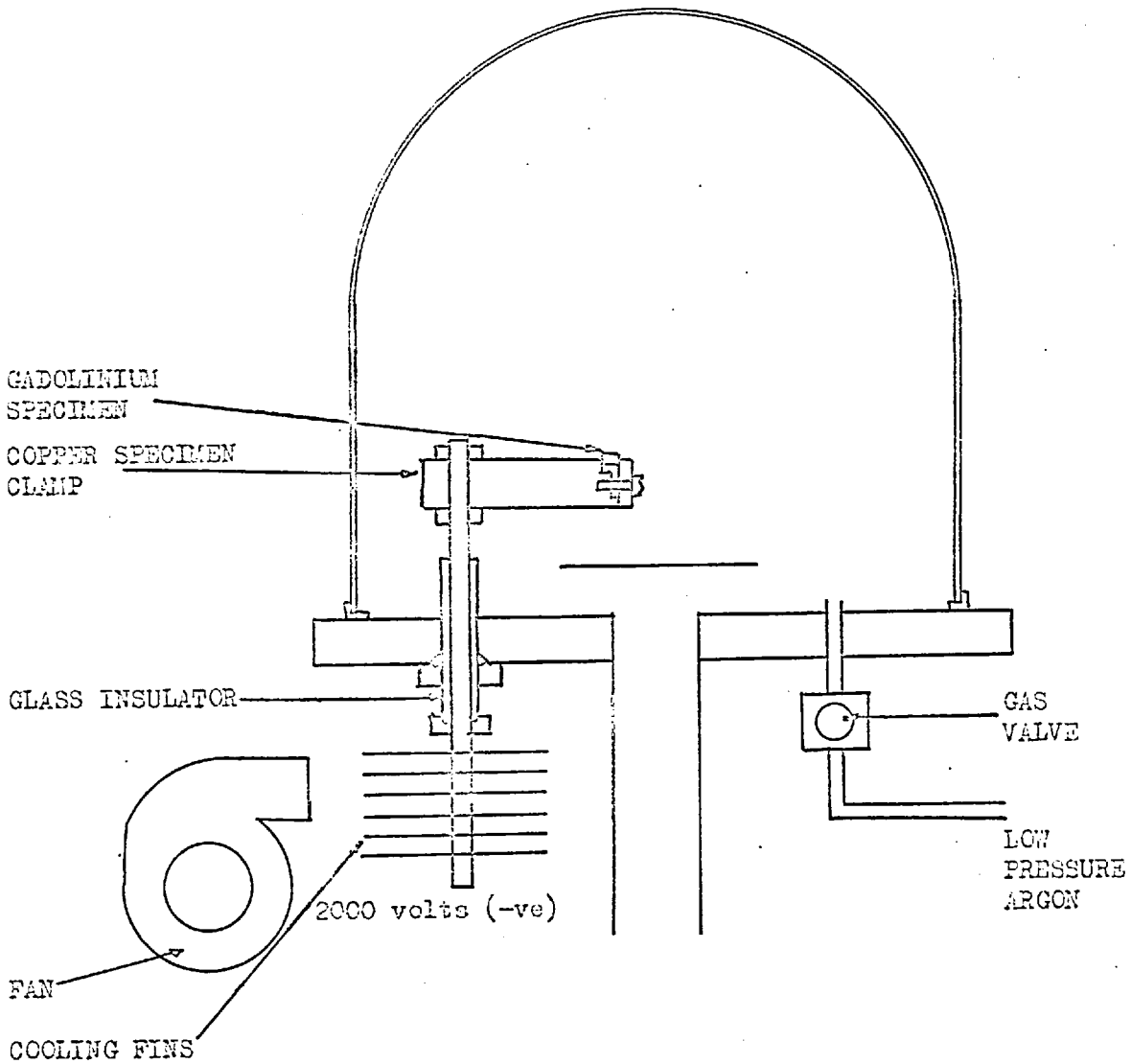


Figure 3.11
ION BOMBARDMENT APPARATUS

acetone with Xylene and was used with some success. The colloid was made in the following way from solutions of 2.78 grms. of $FeSO_4$, 5.40 grms of $FeCl_3$, and 5.20 grms of KOH, each in 50cc of distilled water. To 16 cc. of boiling KOH solution, 12 cc. of a 1:1 mixture of the $FeCl_3$ and $FeSO_4$ solutions was added. Boiling was continued with frequent stirring for 45 minutes (Garrood 1962) in a magnetic field of about 1600 oe. The resulting precipitate was then filtered, washed in distilled water, in ethyl alcohol and in Xylene, and finally dispersed in a 50 milli-molar concentration of Aerosol O.T. ($C_{20}\ H_{37}\ O_7\ SNa$) in Xylene. After ultrasonic agitation, the colloid was separated from the remaining precipitate to be used for domain observations.

Chapter Four

EXPERIMENTAL MEASUREMENTS AND RESULTS.

§4.1 Preliminary and Other Checks on Performance of Apparatus.

Before reliable measurements of anisotropy or magnetostriction could be made, it was necessary to carry out a number of preliminary and other checks on the performance of the apparatus involved. These are discussed here before the details of the measuring procedure are described.

§4.1.1 The Torque Meter.

Anisotropy measurements could only be made if the torque meter was deemed to be satisfactory in respect of the configuration of the strain gauge wires, the method of mounting the specimen, the method of predicting the sense of the torque, the calibration techniques and their reliability, and the overall performance of the torque meter. It is convenient to consider these desiderata separately.

§4.1.1.1 Preliminary tests on the original torque meter were first performed to verify the theoretical analysis of the performance of the configuration of the strain gauge wire. This analysis predicted (equation 3.5) that the fractional charge in resistance, $\Delta \frac{R}{R}$, of the resistance wires should vary lineally with the applied torque Γ. To test this, the

torque head (F in figure 3.2) was rotated to apply a torque to the strain-sensing resistance wires via the torsion suspension and specimen holder. A photograph, 1 cm. in diameter, of a circular protractor was cemented centrally onto the torque head, so that the angles through which the torque head had been rotated could be accurately measured with the aid of a low-power microscope. The applied torque caused a deflection on the Wheatstone bridge output galvanometer. This deflection was cancelled by adjustment of one of the two external bridge arm resistances (R in figure 4.4) from which the fractional change in resistance was obtained. The dependence of $\frac{\Delta R}{R}$ on the rotation of the torque head was found to be linear as shown in figure 4.1. The elastic constants of the torsion suspension were found by measuring the period of small oscillations of a body of known moment of inertia supported by a known length of the suspension. Hence the torque meter could be calibrated without relying on the strict validity of equation 3.5. The operation of the torque meter depended on the prestressing of the strain-sensing resistance wires, which was accomplished by the use of the differential screw between the two clamp jaws (A) in figures 3.2 and 3.3). The two halves of the differential screw in the original torque meter were threaded with 10 and 11 B.A. dies, so that the relative movement of the clamp jaws depended on the difference in pitch of these two thread sizes. In the modified torque meter the two thread sizes were changed to 7 and 8 B.A. To prestress the wires the clamp jaws were then

ROTATION OF TORQUE HEAD (1 unit = 7.51 dyn-cm)
15
10
5
-5
-10
-15
0.001
0.002
0.003
$\frac{\Delta R}{R}$ $\Omega \times 10^2$
0.004

Figure 4J

opened until the resistance wires were seen to be strained. The operation of the torque meter was not particularly sensitive to the amount of stress applied by the clamp jaws as long as this was in excess of the stress in the resistance wires caused by the torque being measured by the system.

It was important to know the amount of rotation of the specimen holder that occurred in practice when a torque was applied. A small mirror, with a radius of curvature of one meter, was therefore temporarily attached to the specimen holder so that small angular movements could be measured. It was found that a torque of 350 dyne-cms. which corresponds with a typical torque measurement, gave a rotation of the order of 0.1 minutes of arc.

§ 4.1.1.2. Calibration tests on the modified torque meter were concerned with detecting any variation of the sensitivity of the torque meter with the magnitude and direction of the applied magnetic field. The calibration procedure, described in section 4.2.1. was followed to obtain calibration curves of the current through the calibration coil (M in figure 3.3) versus output galvanometer deflection. This was done for different fields over the same range as that for which torque curves were usually measured. However, before plotting the points the values for the calibration coil currents corresponding to different magnetic fields were normalised to give values corresponding to the field of 4,865 oersteds usually used for calibration purposes. This was done by multiplying the calibration coil current by the ratio

of the flux meter readings for the field in question and the normal calibration field of 4,865 oersteds. All the curves thus obtained were found to coincide, showing that there was no measurable variation of the torque meter sensitivity with field. To check that the measurements were valid for other field directions, the above procedure was repeated with different magnet positions. This meant that the flux through the calibration coil was now no longer maximised. However, the procedure was otherwise the same as before, the magnet being turned exactly 90° from the position at which the flux was measured to the position at which the calibration measurements were made. No variation of the sensitivity of the torque meter with field could be found for different field directions.

§4.1.1.3. It was important to know in which direction the output galvanometer would be deflected for a given direction of torque on the specimen holder. The simplest method of obtaining this information was to immerse the torque meter in a cylinder of silicone oil (MS 550) and to note the output galvanometer deflection when the cylinder was rotated. The viscosity of the oil used was such as to give satisfactory results when the cylinder was rotated by hand. The result of this test could be verified by checking the geometry and connections of the torque meter, and noting the output galvanometer deflection when the resistance of the external arms of the Wheatstone-bridge was altered.

§ 4.1.1.4. The specimen was mounted with Durafix in the torque meter specimen holder on a pad of asbestos paper, thus avoiding any undesirable restrictions on the specimen. To check that the asbestos paper and Durafix cement did in fact reduce the constraints on the specimen to an acceptable level, an alternative method of mounting was tested. The specimen was cemented centrally on a slender brass peg (a diameter of about 2 mms.) to reduce the clamped volume of the specimen to a minimum. However, no difference in the torque curves obtained was detected so that the original method of mounting was adopted.

4.1.1.5. To test the performance of the torque meter, preliminary measurements were made of the second magneto-crystalline anisotropy constant K_2 of nickel, using the single crystal disc oriented parallel to a (111) plane (section 3.3). For this orientation, even with the relatively large specimen, the torque is small and it may easily be masked by unwanted torques due to inadequacies in the measuring apparatus and from other sources.

The measurements were made using a similar measuring procedure and bridge circuit to those described in 4.2.1. The torque expected should have consisted of an almost pure $\sin 6\theta$ variation. However, it was found that the $\sin 6\theta$ component was small compared with unwanted 2θ and 4θ components (Sato and Chandrasekhar 1956). These may have arisen from a number of sources. Those attributed principally to the specimen are:

(i) misalignment of the disc surfaces relative to the (111) plane. This can occur during the preparation of the disc and should give rise to terms, which depend on K_1 in $\sin 2\theta$, $\cos 2\theta$, $\sin 4\theta$, and $\cos 4\theta$.

(ii) misalignment of the disc (and hence the (111) plane), relative to the magnetic field. This can occur during the assembly of the apparatus and again should give rise to terms up to $\sin 4\theta$ and $\cos 4\theta$ (Tarasov and Bitter 1937).

(iii) any deviation in the shape of the specimen from that assumed, e.g. variation in thickness or deviation from circular profile.

(iv) any included grains of different orientation within the crystal disc, together with internal stresses and consequent additional anisotropy.

Only the first item contains a contribution from the torque-measuring apparatus. However, there may be other contributions due to the malfunctioning of the torque measuring device. In practice it was found that careful alignment of the torque meter in the magnetic field was important in reducing the unwanted 2θ and 4θ variations. Contribution (ii), given above, was, of course, reduced by this careful alignment. It was also found that cancellation of contributions due to unwanted translational forces and torques was not quite complete. Thus careful alignment played an important role in reducing the forces and torques which arose due to the slight non-uniformity of the magnetic field. After the strain-sensing resistance wires had been rewound to obtain the proper compensation (section 3.11), careful alignment was no longer found to be so critical. Figure 4.2 shows a torque curve obtained at room temperature without careful alignment and before effects of unwanted forces and torques were being properly cancelled. For comparison a torque curve obtained by Sato and Chandrasekhar is superimposed. The broken curve gives the 6θ component of both these curves. A fairly typical torque curve, obtained at a temperature of $9{\cdot}5^{\circ}$C

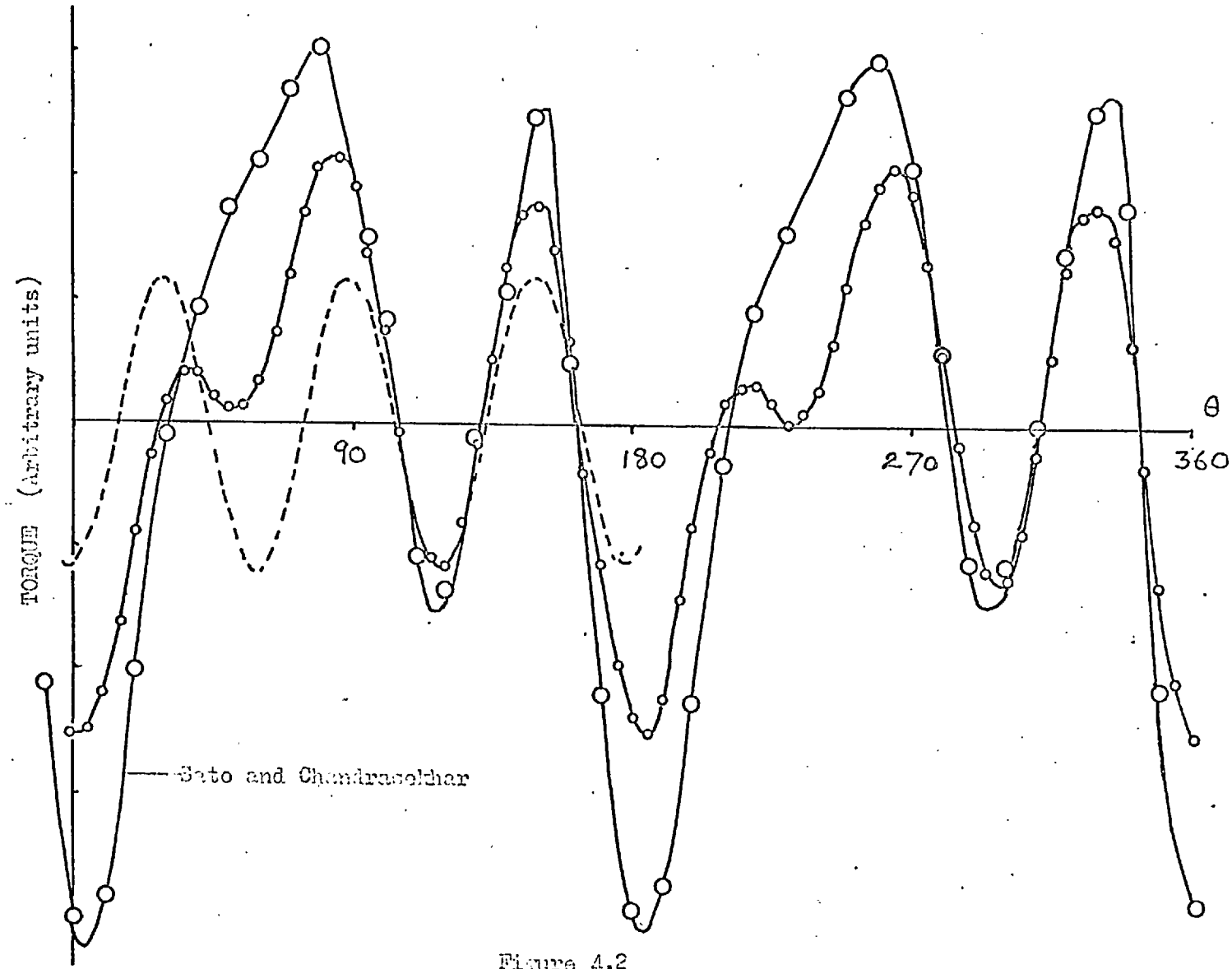

TORQUE (arbitrary units)
θ
90
180
270
360
Seto and Chandrasekhar

Figure 4.2

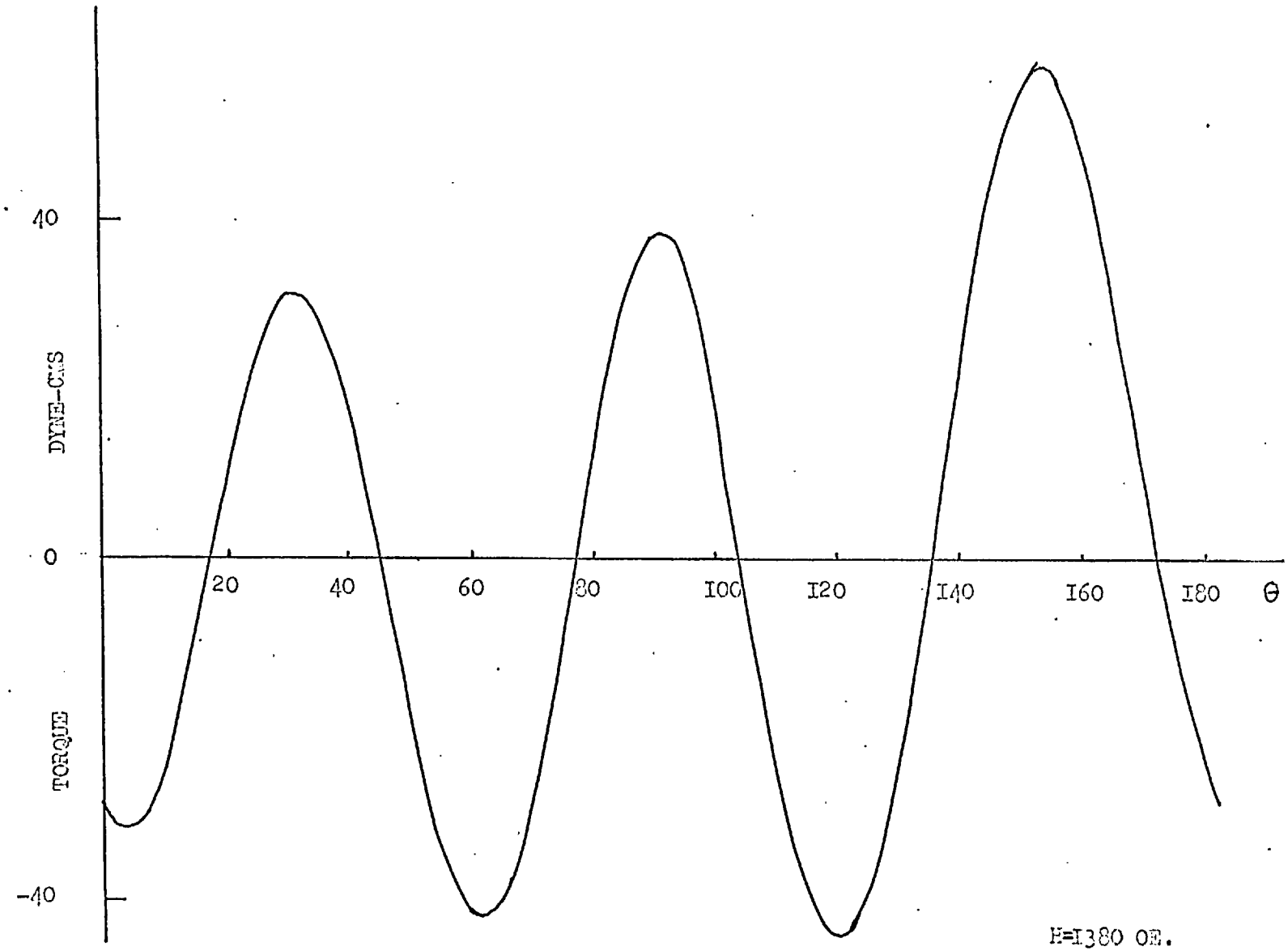


Figure 4.3

A TYPICAL TORQUE CURVE

after careful alignment and with full compensation for unwanted effects, is shown in Figure 4.3.

§4.1.2 The Strain Measuring Apparatus.

The temperature control and auxiliary equipment used for magnotostriction measurements have been described in detail in section 3.2. No modifications were made to this equipment, but the torque meter used for anisotropy measurements was replaced by a copper specimen holder, which is shown inset in figure 3.7.

Before the magnetostriction measurments could be made it was necessary to ensure that the strain measuring equipment was functioning properly. Since the strain gauges were commercial types that had been extensively used for similar measurments it was not necessary to test the operation of the gauges themselves. However, a number of special precautions were taken in their use and these will be considered separately below.

§4.1.2.1. Type 6J strain gauges (manufactured by Tinsley and Co. Ltd.) were used to measure the magnetostrictive strains. A gauge was mounted on the free surface of the specimen with Durafix in the manner recommended by the manufacturers. It was important to know the orientation of the gauge with respect to the reference line scribed on the specimen. Accordingly the

specimen was mounted, face upwards in plasticine, at the centre of a spectrometer turntable. A microscope was mounted vertically above the turntable and a cross hair in the microscope eyepiece was then aligned parallel to the reference line on the specimen and the turntable scale was read. The strain gauge was then affixed and the turntable rotated so that the microscope cross hair was parallel with the strain gauge wires which were visible through the paper strain gauge mounting and which represented the direction of measurement of strain. After again reading the turntable scale, the orientation of the strain gauge relative to the reference direction, and hence to the crystal axies, was known.

§ 4.1.2.2. An identical strain gauge, known as the 'dummy' was placed as close as possible to the first, or active, strain gauge with their measuring directions aligned as nearly parallel as possible. The two gauges were then connected in the two arms of the same Wheatstone bridge circuit that was used for anisotropy measurements (fig. 4.4), so that the change in resistance of the gauges could be measured. The purpose of the dummy gauge was to balance out the change in resistance of the gauges with temperature and with field. Although changes in resistivity with temperature are compensated thereby, the thermal expansion, per degree centigrade was of the order of 10^{-5}, while the fractional change in length due to the magnetostriction was of the order 10^{-6}. Serious drifting of the output galvanometer of the Wheatstone bridge thus resulted from very small temperature

changes and to overcome this difficulty the dummy gauge was cemented to a dummy specimen. Since there are no suitable metals with a coefficient of expansion close to that of nickel, a bi-metallic disc was constructed from copper and aluminium strips, stuck together with Araldite. The thickness of the two strips was adjusted until the effective thermal expansion on the outer surface of the copper strip was equal to that of nickel and this was found to greatly improve the temperature stability of the system.

§ 4.1.2.3. The (111) disc was mounted with Durafix at the end of the specimen holder. An asbestos pad was inserted between the disc and the specimen holder to ensure that the specimen was not unduly strained by its mounting (c.f. § 4.1.1.4)

§ 4.2 Magnetocrystalline Anisotropy Constants K_1 and K_2 for Nickel.

The first and second anisotropy constants were obtained by measuring torque curves on the (111) single-crystal disc , the preparation of which was described in section 3.3. The way in which the torque on the (111) specimen was expected to vary with field was discussed in section 2.2. The theoretical torque curves were therefore fitted to the torque curves obtained experimentally by adjusting the values of K_1 and K_2. Subsequently the values of K_1 were checked by measuring torque curves on a (110) single-crystal disc. The torque meter described in section 3.1 was used for

all torque measurements, in conjunction with the temperature control and auxiliary apparatus described in section 3.2. A number of preliminary tests were peformed on the original and on the modified versions of the torque meter to ensure that they were functioning satisfactorily.

§ 4.2.1 Measurements and Measuring Techniques.

Before torque measurements were taken, the torque meter and temperature control apparatus were aligned as accurately as possible in the centre of the magnet pole gap with the aid of the positioning equipment described in chapter 3. For the earlier experiments using the 4" electromagnet, the relatively large gap used, gave rise to a reduction in the uniformity of the field. [For the smaller magnet the field gradient at a point 0.5 cm. from the centre of the pole gap was approximately twice that of the larger magnet with the same pole gap and field so that correct alignment was found to be fairly critical]. Use of the 7" magnet, with a correspondingly more uniform field, reduced these difficulties. The original unmodified torque meter was used for preliminary measurements at or near room temperature with the first temperature control apparatus described in chapter 3. The purpose of these measurments was to test the principle of operation and to ensure that the system was working correctly. Measurements at other than room temperatures yielded somewhat uncertain results owing to the difficulties of calibration. The methods of calibration and the experiments made with this torque meter have been described in section 4.1.1.

The strain-sensing resistance wires in the torque meter, described in chapter 3, formed two arms of a Wheatstone bridge; the full circuit actually used for torque measurements is shown in figure 4.4. Before measurements were made, the bridge current was always standardised by comparing the e.m.f. across the standard 50Ω resistance with that of the standard cell. Temporary drifting of the balance point often occured after the bridge was initially balanced. Small changes in the balance point could be made to compensate for this effect by adjusting the variable reistance R. The attenuator circuit, between the Tinsley galvanometer-amplifier and the output galvanometer G, was then used to adjust the overall sensitivity of the circuit so that the deflections to be measured on G were of convenient size relative to full-scale deflection. The modified torque meter was calibrated by generating a known torque in the calibration coil attached to the specimen holder. The flux through the coil was first maximised by rotating the electromagnet on its turntable until no deflection was observed at the output galvanometer G when current was passed through the calibration coil. The current supply to the coil was then temporarily replaced by a flux meter and the flux was measured by reversing the current supply to the electromagnet. The magnet was then rotated through exactly 90° to give the position of zero flux through the calibration coil. After reconnection of the calibration current supply, the deflection of the output galvanometer (G) for different calibration currents was recorded. A large-scale graph of these measurements was used for calibration purposes.

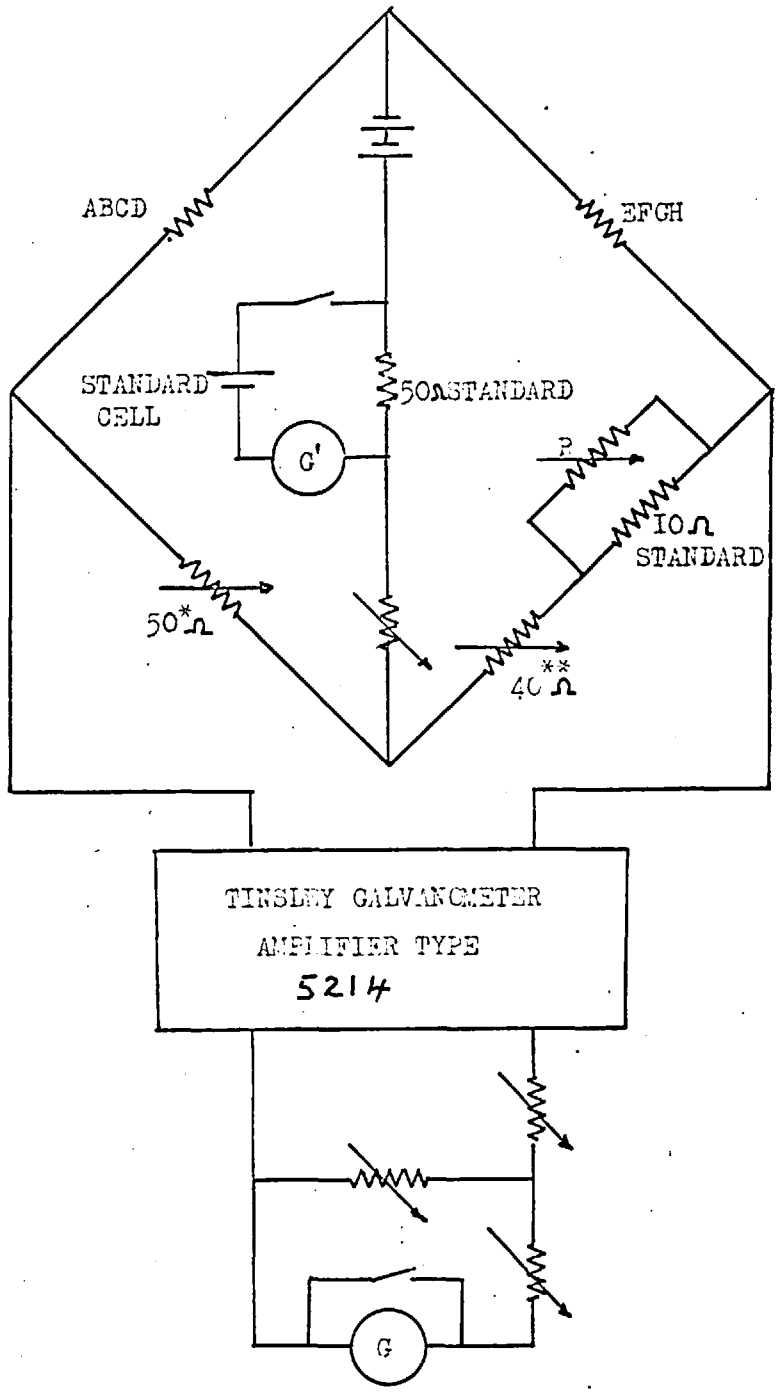


Figure 4.4

BRIDGE CIRCUIT

*, **These resistances were changed to 100Ω and 90Ω respectively for measurements with 100Ω strain gauges replacing ABCD & EFGH.

The torque Γ on the calibration coil was given by

$$\Gamma = \frac{Fi}{20} \text{ dyne-cm.} \qquad (4.1)$$

where i was the calibration current in amperes and F was the net flux change in maxwell turns through the coil.

Torque measurements were then made by noting the output galvanometer deflection for a given magnet position and using the calibration curve and equation 4.1 to obtain the corresponding torque. The procedure used in making torque measurements was to rotate the magnet through 180° in steps of 5°. In order to avoid the effect of drift in measurements above room temperature, where the torque to be measured was small, the output galvanometer reading was taken at the 0° position between each 5° step. The average of successive 0° galvanometer readings was then subtracted from the intervening reading to give the corrected reading, free from drift. At lower temperatures drift was not troublesome and it was found to be sufficiently accurate to repeat the 0° reading only at the end of the 180° run.

A Fourier analysis was performed on the torque curves for the (111) specimen to obtain the $\sin 6\theta$ and $\cos 6\theta$ components ($\sin 2\theta \cos 2\theta$, and $\sin 4\theta$, $\cos 4\theta$ for the (110) specimen) from the arbitrary origin corresponding to 0° on the magnet scale (where θ was the angle given by the magnet scale). The sine and cosine amplitudes were then combined to give the resultant $6\beta'$ amplitude and true origin (or $2\beta'$ and $4\beta'$ variation), where

β' was the true angle of the field from a <110> direction . It then only remained to determine the sign of this amplitude. A test, described in section 4.1.1, was applied to find the sign of the deflection on the galvanometer output scale corresponding to a torque developed by the specimen in the direction of β' increasing on the magnet turntable scale. A torque developed by the specimen in the direction of β' increasing on the magnet scale corresponded to a negative galvanometer deflection. The procedure for torque measurements just described was repeated at a given temperature for a number of different fields up to the maximum field obtainable with the magnet, pole gap, and power supply used. The ranges of field at which measurements were made were from 1,400 oersted to 7,100 oersted and from 1,400 to 14,700 oersted for the 4" and the 7" magnets respectively. All these measurements were repeated at different temperatures over a range from + 70°C to -196°C.

After these measurements had been made, the torque meter was partially dismantled so that the direction of the reference line on the crystal could be found relative to the magnet turntable scale. It was found that the magnet field was parallel with the reference line (a <112> direction in the crystal) when θ on the magnet turntable scale was 20°. This angle corresponded to a postion of zero torque ($\beta' = 30°$) with a negative slope on the torque curve.

§4.2.2 Results.

The results of the measurements described in 4.2.1 are shown in figures 4.5 and 4.6. Figure 4.5 shows the variation of the amplitude of the $6\beta'$ component of the torque curves with field and with temperature. The results are presented in a more detailed numerical form in hapter 5.

The theoretical field dependence of the torque curves at high fields was obtained in section 2.2. Equation 2.32 gave the field dependence of Δ, but it was also shown in that section that the torque on the specimen was given by $h\Delta$ so that

$$\Gamma = \left\{ \frac{1}{18} K_2 - \frac{1}{3} \frac{(K_1 + \frac{1}{6} K_2)^2}{h + k_1} \right\} \sin 6\beta' \qquad (4.2)$$

The amplitude of the curves obtained from equation 4.2 when the correct values of I_s, H and N were inserted was made to fit the experimental points on figure 4.5 by adjusting the magnitude of K_1 and K_2. The curves representing equation 4.2, adjusted for best fit, are shown in figure 4.5 as unbroken curves. The final values of K_1 and K_2 used in the equation are plotted on figure 4.6 against temperature as unbroken lines. The broken curve on figure 4.6 is the variation of K_2, with sign changed, taken from Bozorth's book. It may be seen from equation 4.2 that, since the sign of K_1 is negative, the theoretical equation appropriate to low temperatures may only be fitted to the experimental points when K_2 is negative.

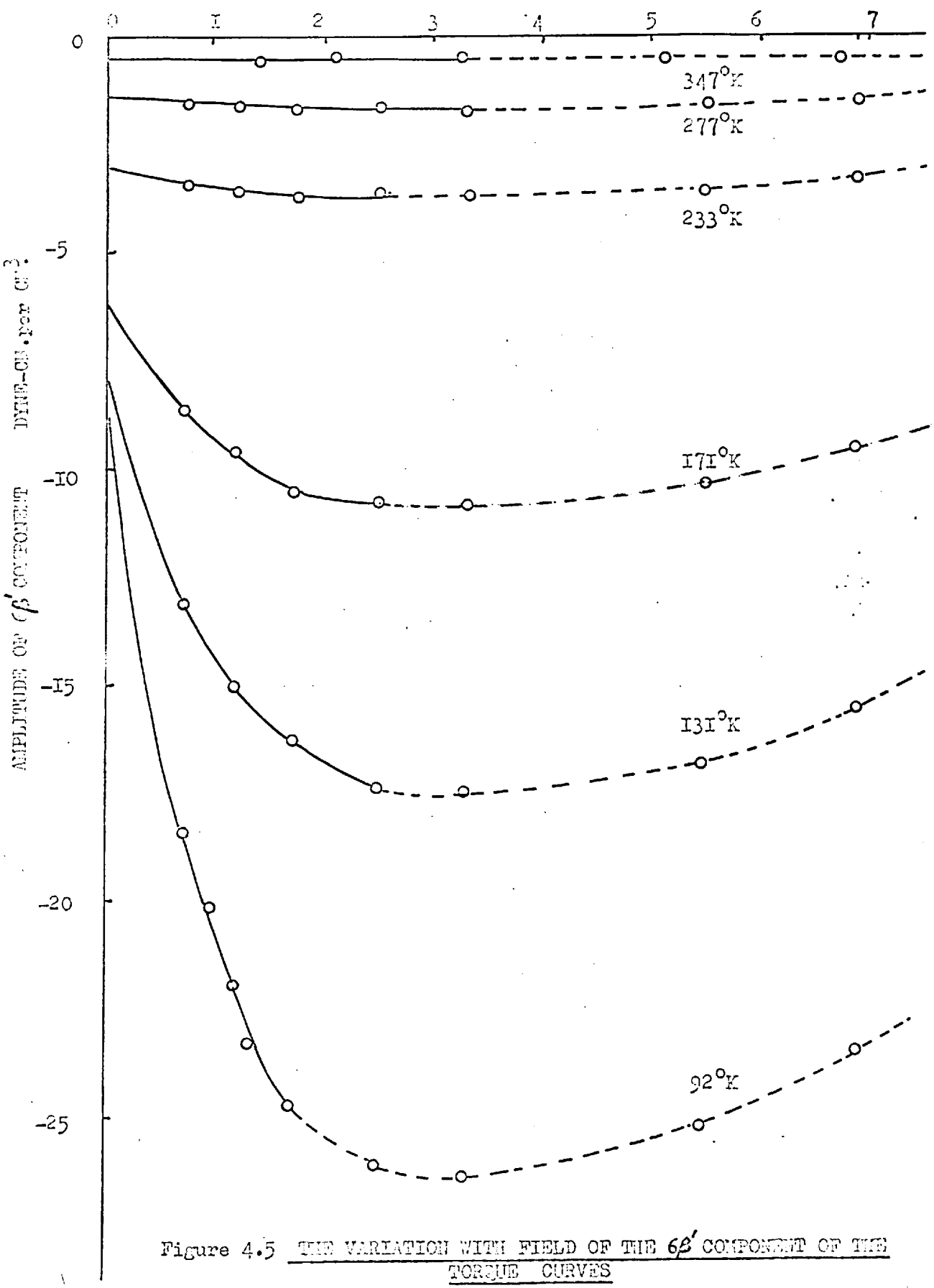


Figure 4.5 THE VARIATION WITH FIELD OF THE 6β' COMPONENT OF THE TORQUE CURVES

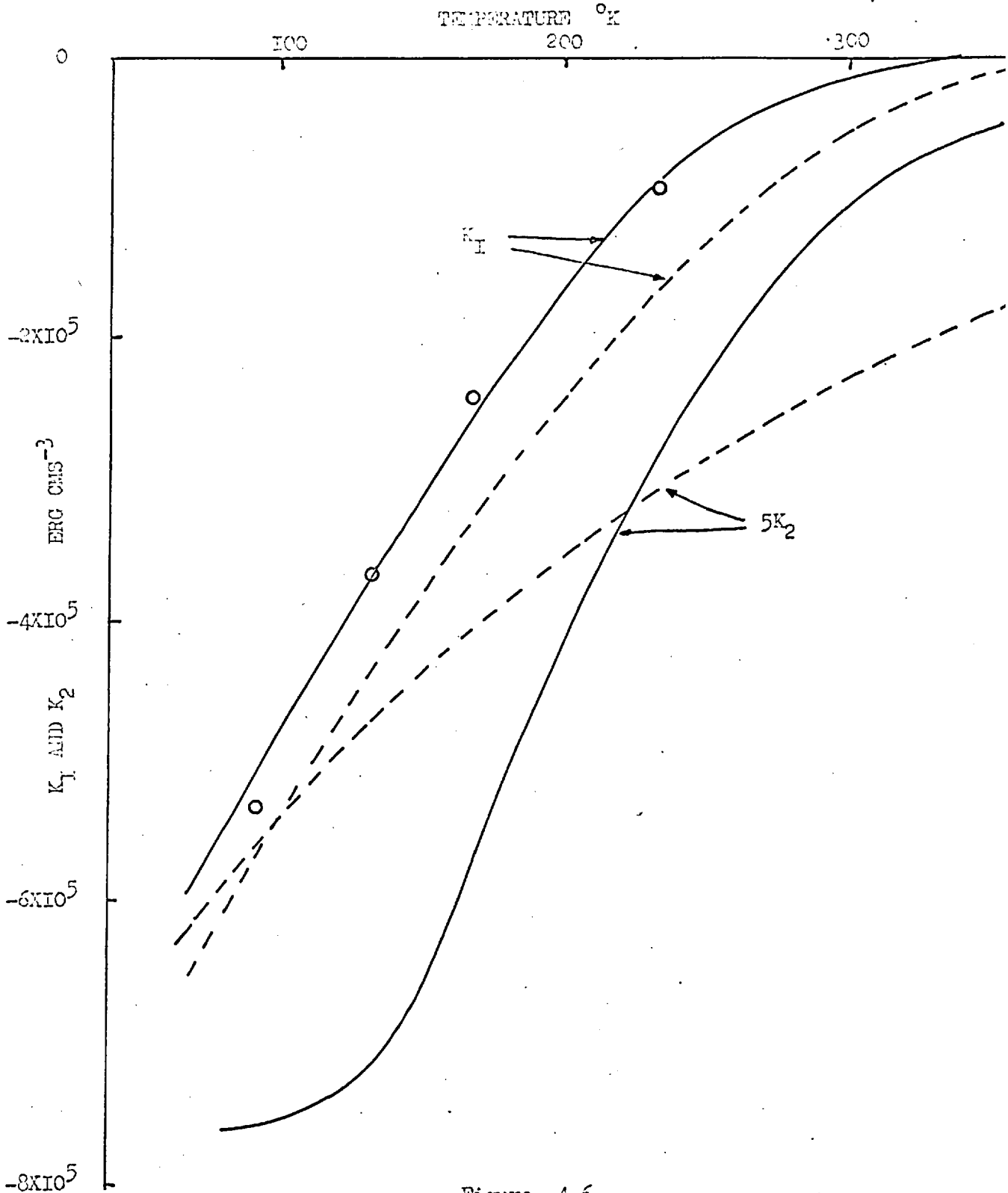


Figure 4.6

THE VARIATION WITH TEMPERATURE OF K_I AND K_2 FOR NICKEL

The relation usually given (Bozorth 1951, Brailsford 1960, Stoner 1950) for the anisotropy torque in high fields is

$$\Gamma = -\frac{dE}{d\phi}, \qquad (4.3)$$

where E is the anisotropy energy density. Γ is the torque exerted on the crystal per unit volume of the crystal and ϕ is the angle (in the plane of which the magnetization rotates) between the direction of magnetization and a fixed direction in the crystal. Since the differentiation is performed relative to axes fixed with respect to the crystal whilst the orientation of the magnetization direction varies relative to the crystal axes, it might reasonably be supposed that equation 4.3 gives the torque on the crystal, in the direction of ϕ increasing, when ϕ is measured from a fixed direction in the crystal to the direction of magnetization. Such optimism would, however, be misplaced for, with this interpretation of the symbols, the torque must be given by

$$\Gamma = +\frac{dE}{d\phi} \qquad (4.4)$$

because it must be in such a direction as to bring an easy direction into coincidence with the field direction when the easy direction makes a small angle with the magnetization. In fact, equation 4.3 gives the torque on the magnetization when the crystal is fixed whilst 4.4 gives the torque on the crystal when the magnetization is fixed (by the direction of the field). The reason that the distinction between 4.3 and 4.4

is often not important is that the torque usually contains a (leading) term involving K_1, the sign of which may, of course, be predicted in advance from the known position of the easy directions. In the (111) plane, however,

$$\Gamma = + \frac{dE}{d\phi} \simeq + \frac{K_2}{18} \sin 6\beta' \qquad (4.5)$$

where β is the angle made by the magnetization in the (111) plane with a <110> direction. The sign of K_2 can not therefore be determined correctly by using equation 4.3 and it is thought that both the direct determinations of K_2 (Sato and Chandrasekhar 1956, and appendix A 3) made at room temperature are in error for this reason. The sign of the torque was known (as explained in § 4.2.1). Further, the correct origin of the sin $6\beta'$ component was found by inspection of the slope of the torque curve for the value of β' for which the field was parallel to the reference direction on the specimen. The sign of K_2 was thus easily verified from the experimental measurements with the aid of equation 4.4

The experimental points on figure 4.6 are the values of K_1 taken from torque measurements on the (110) crystal. These values of K_1 were obtained by Fourier analysis of the torque curves for $2\beta'$ and $4\beta'$ components as explained in § 4.2.1. From the theoretical expression for the torque in a (110) plane above saturation, namely,

$$\Gamma = -\frac{1}{8}K_1(2\sin 2\beta' + 3\sin 4\beta') + \frac{1}{64}K_2(\sin 2\beta' - 4\sin 4\beta' - 3\sin 6\beta'), \qquad (4.6)$$

it can be seen that, if A_2 and A_4 are the amplitudes of the 2β and 4β variations, K_1 is given by

$$K_1 = \frac{8A_2 - 3A_4}{5} \qquad (4.7)$$

The effective values of K_1, found in this way for three different fields, were plotted against $\frac{1}{H}$ and the resulting straight line extrapolated to $\frac{1}{H} = 0$ to obtain the value of K_1 appropriate to infinite field. The procedure described for determining the sign of K_2 was, however, repeated for these measurements which confirmed that K_1 was negative, in agreement with the known directions of the easy magnetization.

§ 4.3 Forced Magnetostriction in nickel in the (111) plane.

At high fields the saturation magnetostriction in the (111) plane will be a function of the variation with field of both α and Δ (section 2.4). The forced magnetostriction will also produce a variation of the magnetostriction with field and this contribution has also been considered in section 2.4. Since both α and Δ have been determined experimentally, the equations derived in section 2.4 may be used to provide information about C_1' and C_2', the forced magnetostriction constants. The results of such measurements will now be considered.

§4.3.1 Measurements and Measuring Techniques.

The measurements were directed towards observing the small change in magnitude of the saturation magnetostriction with the change in the applied field. Since this change was expected to be small compared with the saturation magnetostriction itself, measurements were made from a reference state at a fixed field large enough to saturate the specimen.

To take a set of measurements, the procedure was first to achieve temperature stability, which was indicated by a reduction in the drift of the output galvanometer of the Wheatstone bridge. The magnetic field was then applied in the required direction and the output galvanometer deflections were noted as the field magnitude was changed in a measuring sequence, A, B, A, C, A, D, A ...., measurement A representing the measurement of the magnetostriction of the reference state. It was found that changing the magnetic field rapidly caused slight heating of the specimen with a consequent short term drift superimposed on the steady background drift. The decay time of this thermal fluctuation that occurred with each field change was about 15 seconds. To overcome this effect, the successive measurements were made at intervals of time with a period between measurements of about 1 minute and this was long enough to ensure that the transient drift was negligible. The steady background drift could then be allowed for from the successive measurements of the reference state A.

The fractional change in resistance, $\frac{\Delta R}{R}$, of the active gauge due to the fractional change in length, $\frac{\Delta \ell}{\ell}$, of the specimen was obtained from the deflections of the output galvanometer by using an identical calibration technique to that described in section 4.2.1. The fractional change in length of the specimen due to the magnetostriction was then given by

$$\frac{\Delta \ell}{\ell} = G \frac{\Delta R}{R} \qquad (4.8)$$

where G was the gauge factor.

In order to find the orientation of the applied field relative to the strain gauge and specimen, it was merely necessary to observe the saturation magnetostriction as the magnet was rotated. Then as can be seen from equation 2.58 (remembering that α and Δ are small) there will be a maximum when $\beta = \beta'$, that is when the measuring direction is parallel with the applied field, and a minimum for $\beta = \beta' + \frac{\pi}{2}$.

The measurements were made with the active gauge stuck to the crystal so that $\beta = 30^{\circ} \pm 1^{\circ}$. This orientation was chosen for a number of reasons. First, although choosing $\beta = 30^{\circ}$ does not allow the contributions of both α and Δ to be measured separately, (see figure 2.2 c) it is possible to measure α alone, at $\beta' = 30^{\circ}$, and the sum of α and Δ may then be measured at $\beta' = 75^{\circ}$, so that Δ may be determined. Secondly, at $\beta' = 120^{\circ}$ both α and Δ are zero so that any variation of the magnetostriction constants due to forced

magnetostriction may be determined. Thirdly, it will be noted that these four measuring positions coincide with the extremal and zero points of the overall magnetostriction given by equation 2.58. Hence the ease with which the applied field may be accurately alinged with the specimen was very much improved, which is an important point in view of the rapid angular variation of the magnetostriction due to α and Δ .

§4.3.2. Results.

Measurments were made in the four field directions for extremal and zero overall magnetostriction. A typical set of curves of the variation of the strain of the sample with field measured at 213°K are shown in fig. 4.7. The four curves are superimposed so that the points corresponding to the reference measuring field coincide. Curves a and b represent λ_{30} and λ_{120} respectively while curves c and d represent $\lambda_{30 \pm 45}$ (c.f. section 2.4). Equations 2.63 and 2.64 can in principle be used to evaluate the forced magnetostriction constants. However, it was found that the last term of both equations was negligible when compared with the remaining parts so that it was only possible to measure the sum $C_1' + C_2'$.

The values of α and Δ used in equations 2.63 and 2.64 are shown in figure 4.8.1&2. The values shownhere of Δ were obtained directly from the torque curves (figures 4.2 and 4.3) since the torque is given by $HI_s\Delta$ (see section 2.3). The values of α

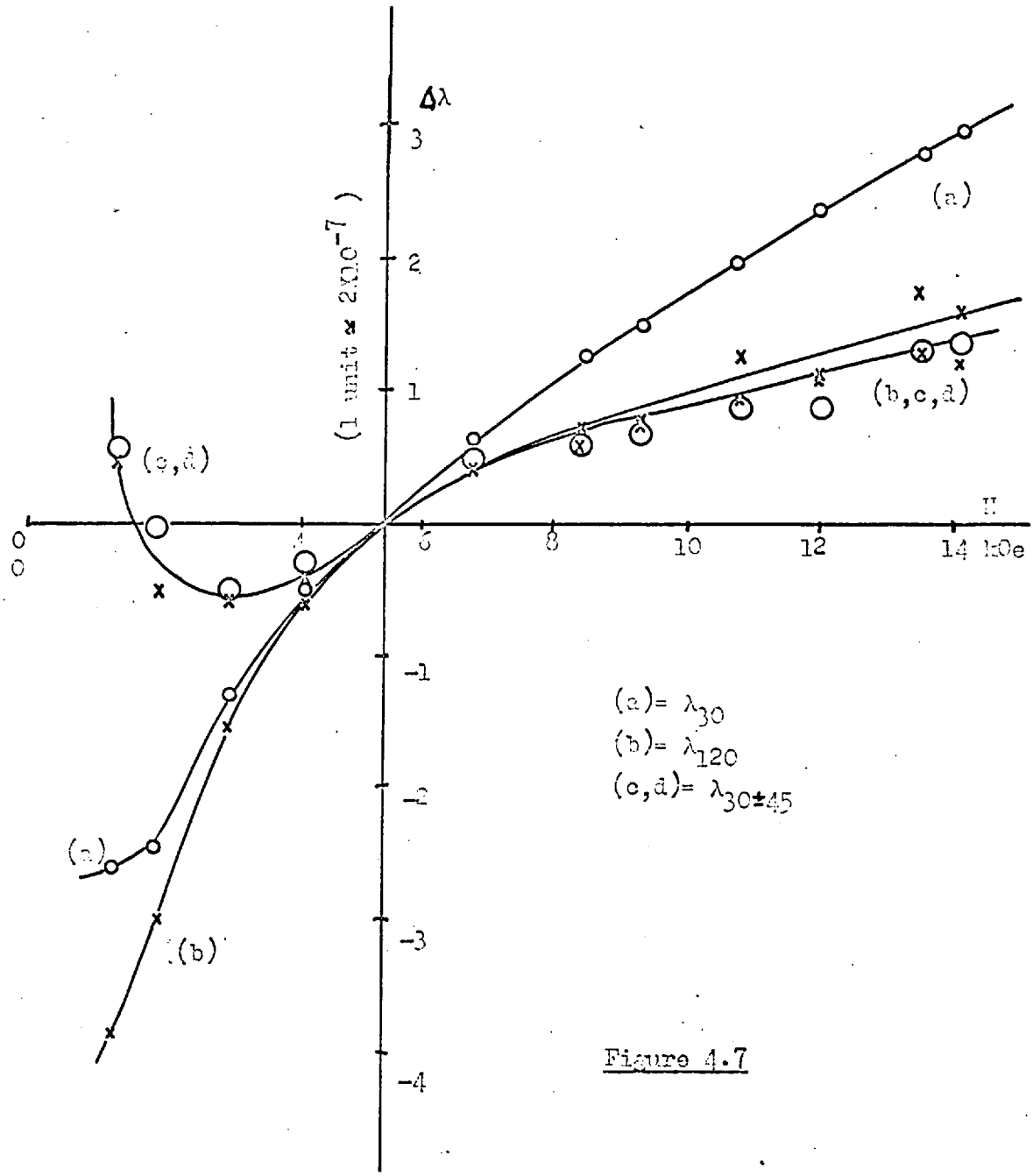

Δλ
(1 unit = 2x10⁻⁷)
3
2
1
-1
-3
-4
(a)
(b,c,d)
(c,d)
(a)
(b)
H
0
0
6
8
10
12
14 kOe
(a)= λ30
(b)= λ120
(c,d)= λ30±45

Figure 4.7

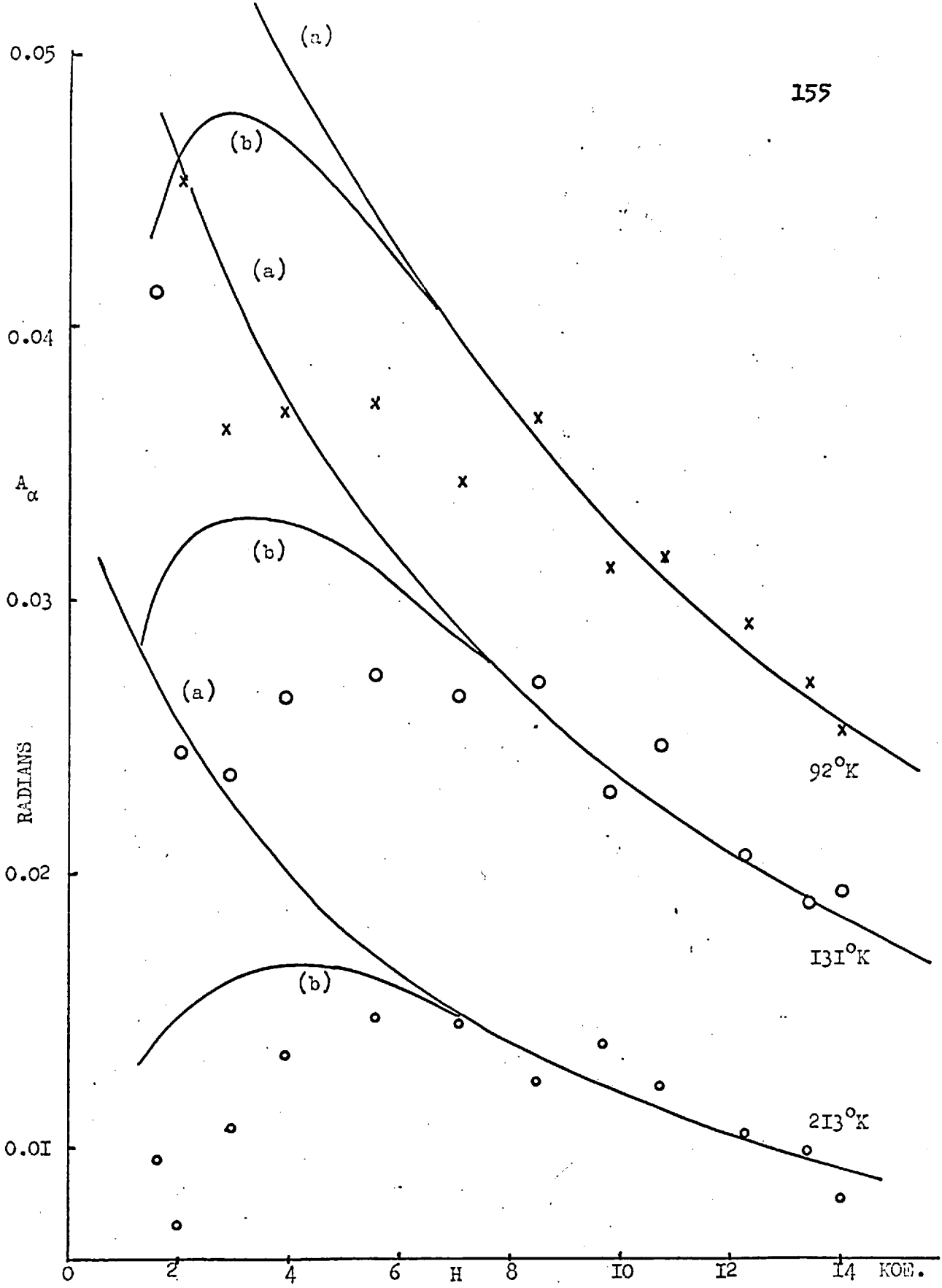


Figure 4.8.1 THE VARIATION WITH FIELD OF A_α

(a),(b), Theoretical curves obtained from equations 2.40 and 2.41 respectively.

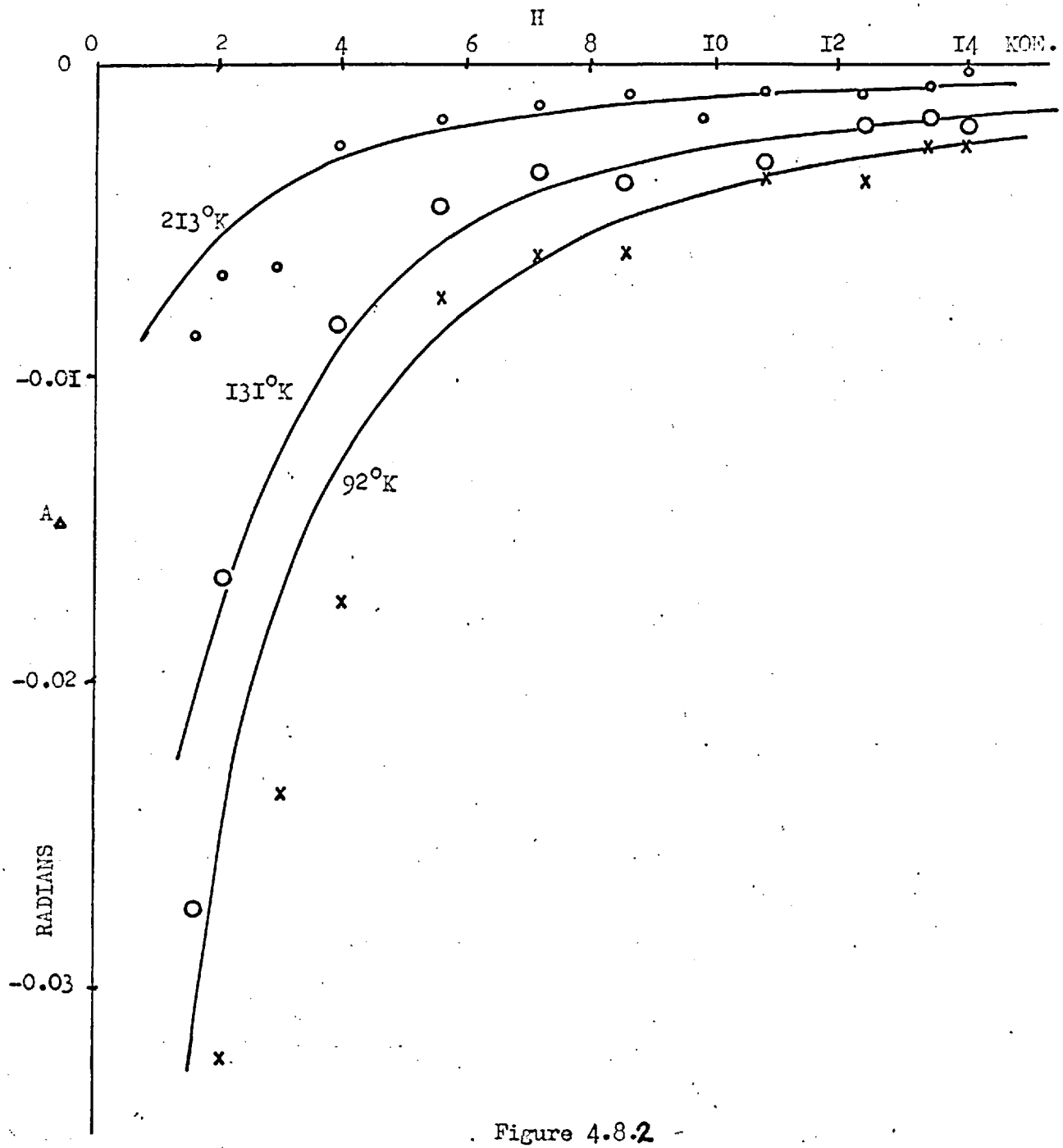


Figure 4.8.2

THE VARIATION WITH FIELD OF A_{Δ}

shown in figures 4.8 were calculated using equations 2.40 and 2.41. The correction terms (proportional to $\frac{6A_6}{h}$ and $\frac{K_2 A_6}{3h}$) in these two equations were neglected.

The effective gauge factor and the resistance of the strain gauges change with temperature, but these quantities must be known for calibration purposes. To obtain this information the quantity $\lambda_{30} - \lambda_{120}$ was measured. From equation 2.58 it can be seen that

$$\lambda_{30} - \lambda_{120} = \frac{1}{3}(C_1 + C_2), \qquad (4.9)$$

when $\beta = 30^\circ$ and when the small terms multiplied by α and Δ are neglected. Comparison of the measured values of $\lambda_{30} - \lambda_{120}$ with known values of C_1 and C_2 (Birss and Lee 1960) thus gave the effective multiplicative factor needed for calibration purposes.

The results of the measurements of the forced magnetostriction are shown in table 4.1. The two columns give the values of $C_1' + C_2'$ obtained using the two different equations, 2.63 and 2.64. Only measurements made above 8 KOe. were used in evaluating these constants to ensure that the values of α used would be correct. (Since the predicted values of Δ begin to diverge from the experimental values around 6 KOe. the values of α predicted by the same theory may be considered unreliable below this field magnitude). To indicate the extent of agreement of the theory with the measurements below 8 KOe., values of $\delta\alpha$ and $\delta\Delta$ were estimated from the magnetostriction measurements, using the

TABLE 4.1

Temperature °K	$(C_1' + C_1')$	
	From Eqn. 2.63 $\times 10^{10}$	From Eqn. 2.64 $\times 10^{10}$
213	-1.25	-0.52
131	-1.18	-0.33
92	-0.80	-0.17

(For further details see table 5.12)

values of $C_1' + C_2'$ obtained above 8 KOe. These points were plotted against H and then superimposed, for the purpose of comparison, onto the curves of α and Δ shown in figure 4.8.

As the temperature was lowered, the magnetoresistance of the strain gauge became very large so that very careful alignment of the active and dummy gauges was required. Even so it was found that it was not possible to obtain complete cancellation of this effect, and it is believed that the values for $C_1' + C_2'$ in the two columns of table 4.1 are different for this reason. The explanation of this difficulty may lie in the fact that although it is possible to exactly match the resistance of the active and dummy gauges, the magnetoresistance of the gauges will not, in general, be matched thereby because of the variable amounts of impurities in the resistance wire.

§4.4 Torque Measurements on Gadolinium.

The $(11\bar{2}0)$ specimen of gadolinium, the preparation of which was described in section 3.4, permitted torque measurements to be made to determine the first and second anisotropy constants K_1' and K_2' for gadolinium. Unfortunately the torque meter had been designed with fixed sensitivity, large enough to facilitate accurate measurements on the (111) nickel disc, and this proved too great to permit the measurement of complete torque curves on the gadolinium crystal without damage to the device. However measurements of the slope of the torque curve could still be

made at or near zero torque using otherwise the same general measuring and calibration techniques as described in section 4.11. It was possible to calculate the anisotropy constants from these measurements as has been shown in section 2.1. Equations 2.16 and 2.17 give the dependence of the slope of the torque curves on K_1' and K_2' at $\phi = 0$ and $\pi/2$. A cone of easy magnetisation exists when $|K_1'| < 2|K_2'|$ and equation 2.15 gives the dependence of ϕ_E (the semiangle of the cone of easy directions) on the anisotropy constants. It was possible to measure ϕ_E directly by finding the positions in which the field exerted no torque on the crystal. From symmetry, two such positions are parallel and perpendicular to the hexagonal axis, but over the temperature range for which the cone exists, there are another two positions of zero torque making angles $\pm \phi_E$ with the hexagonal axis. Since the torque meter was limited in the magnitude of the torques that it could accept, such positions were found in practice by gradually increasing the field and simultaneously adjusting its angular position in the plane of the disc so as to keep the torque small or zero. (A similar procedure is necessary when the field is reduced). The values of K_1' and K_2' obtained from the measured slopes were plotted against $\frac{1}{H}$, and the curves obtained were extrapolated to give the effective values of K_1' and K_2' at infinite field. These values have been plotted against temperature on figure 4.9. The variation of the effective values

of K_1' and K_2' against $\frac{1}{H}$ was not linear, so although a maximum field of 14,700 oersteds was used, there may be some error on the values estimated for infinite field. The values obtained compare well, however, with those of Corner, Roe and Taylor (1962) and Graham (1962). Figures 4.10 and 4.11 give the variation of the semi-angle ϕ_E of the easy cone of magnetization with $\frac{1}{H}$ and with temperature respectively. Detailed numerical results for all these measurements on the gadolinium specimen are given in chapter 5.

As already indicated, it was not possible to obtain complete torque curves so that measurements were limited to the determination of torque slopes. This was a disadvantage since to obtain the maximum information the Fourier components of the complete torque curve should be analysed. This is particularly important for gadolinium since there is evidence (Corner Roe and Taylor 1962) that the contribution to the torque from K_3' and possibly higher anisotropy constants is not negligible. Further, the variation of the effective values of K_1' and K_2' with $\frac{1}{H}$ is not linear so that the maximum field available from the 7" Newport magnet did not permit the accurate extrapolation of these curves to $\frac{1}{H} = 0$. In view of these difficulties it was decided not to pursue these torque measurements as part of the present investigation.

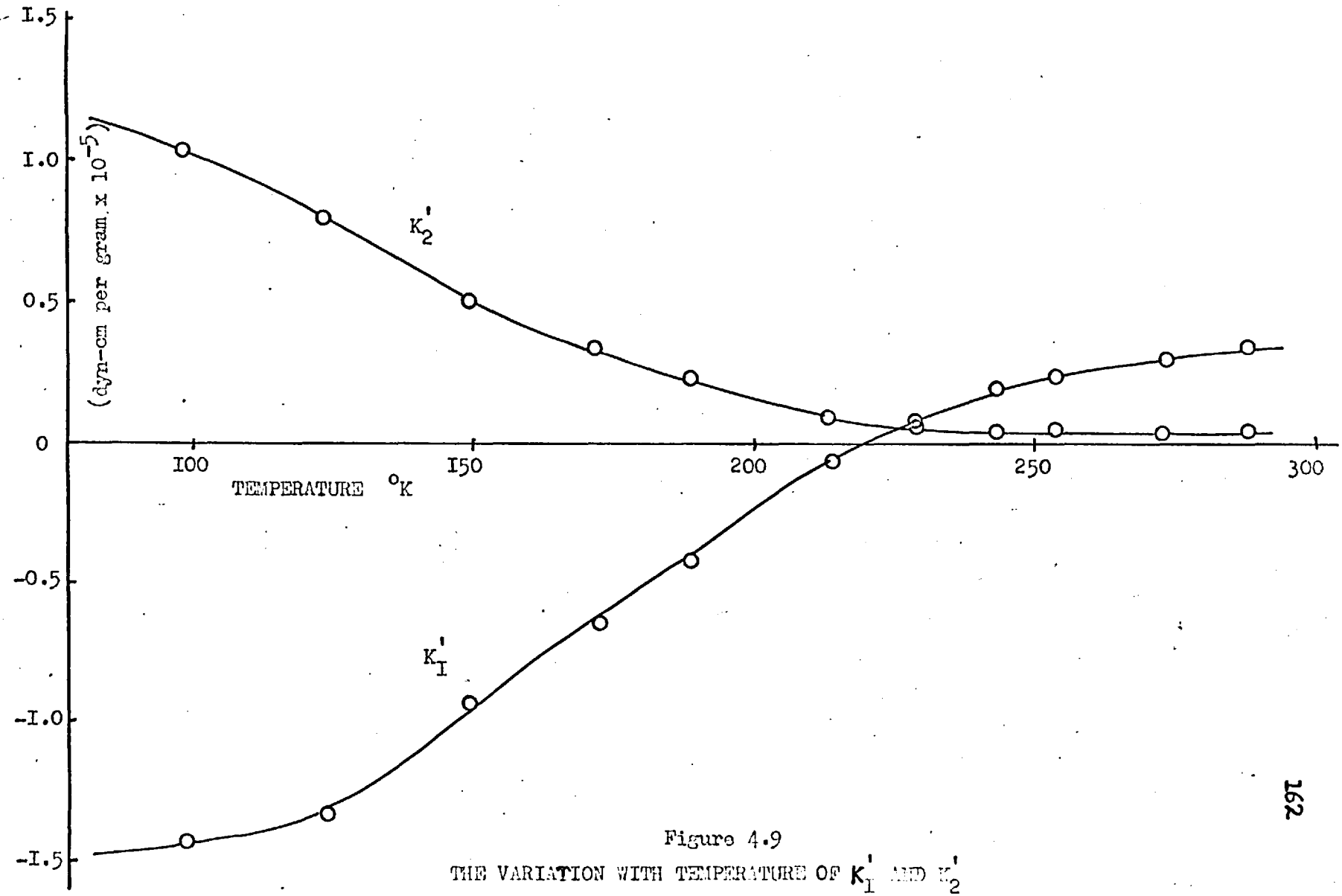


Figure 4.9

THE VARIATION WITH TEMPERATURE OF K_I' AND K_2'

FOR GADOLINIUM

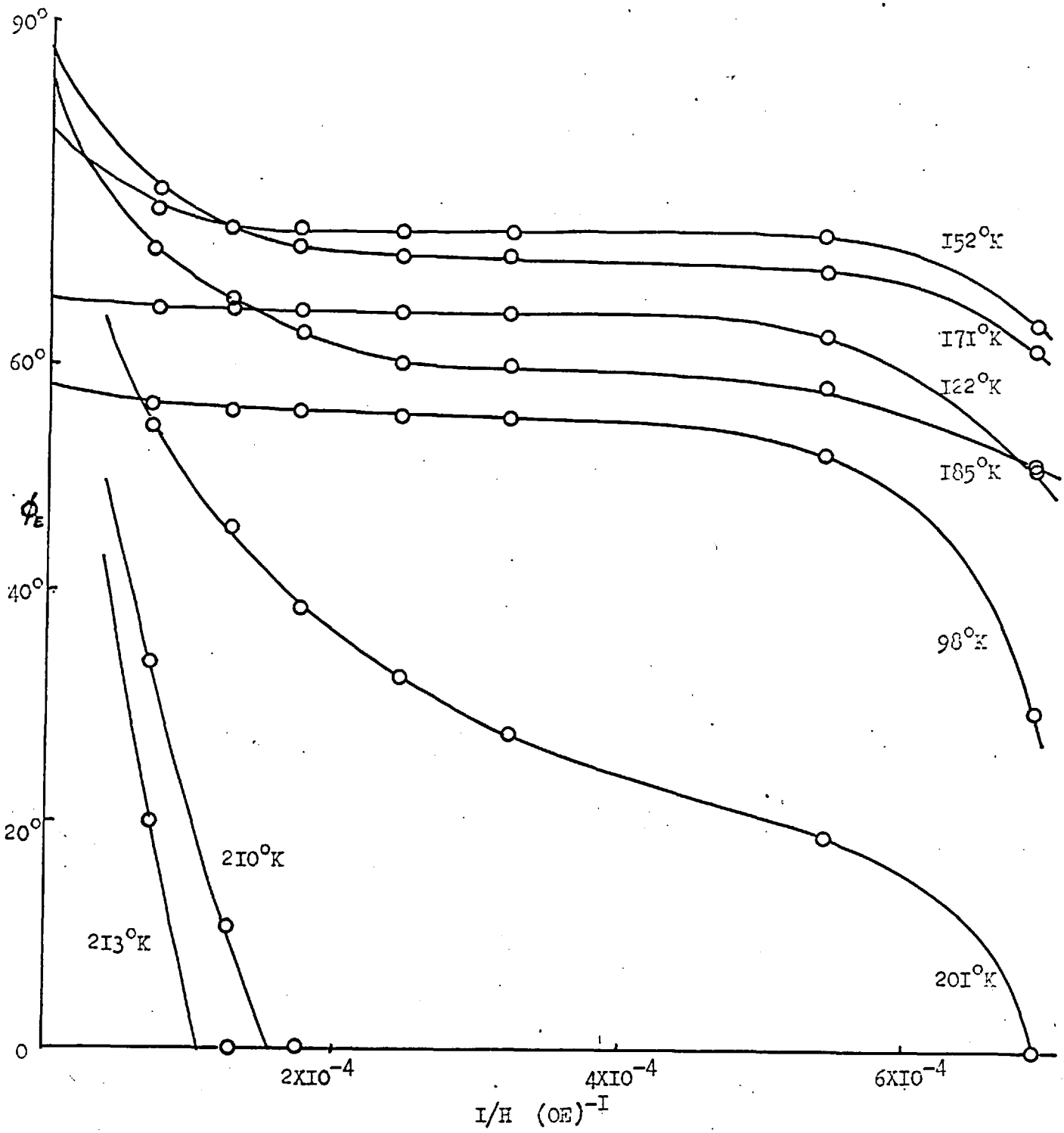


Figure 4.10 THE VARIATION WITH FIELD OF THE EASY CONE ANGLE ϕ_E IN GADOLINIUM

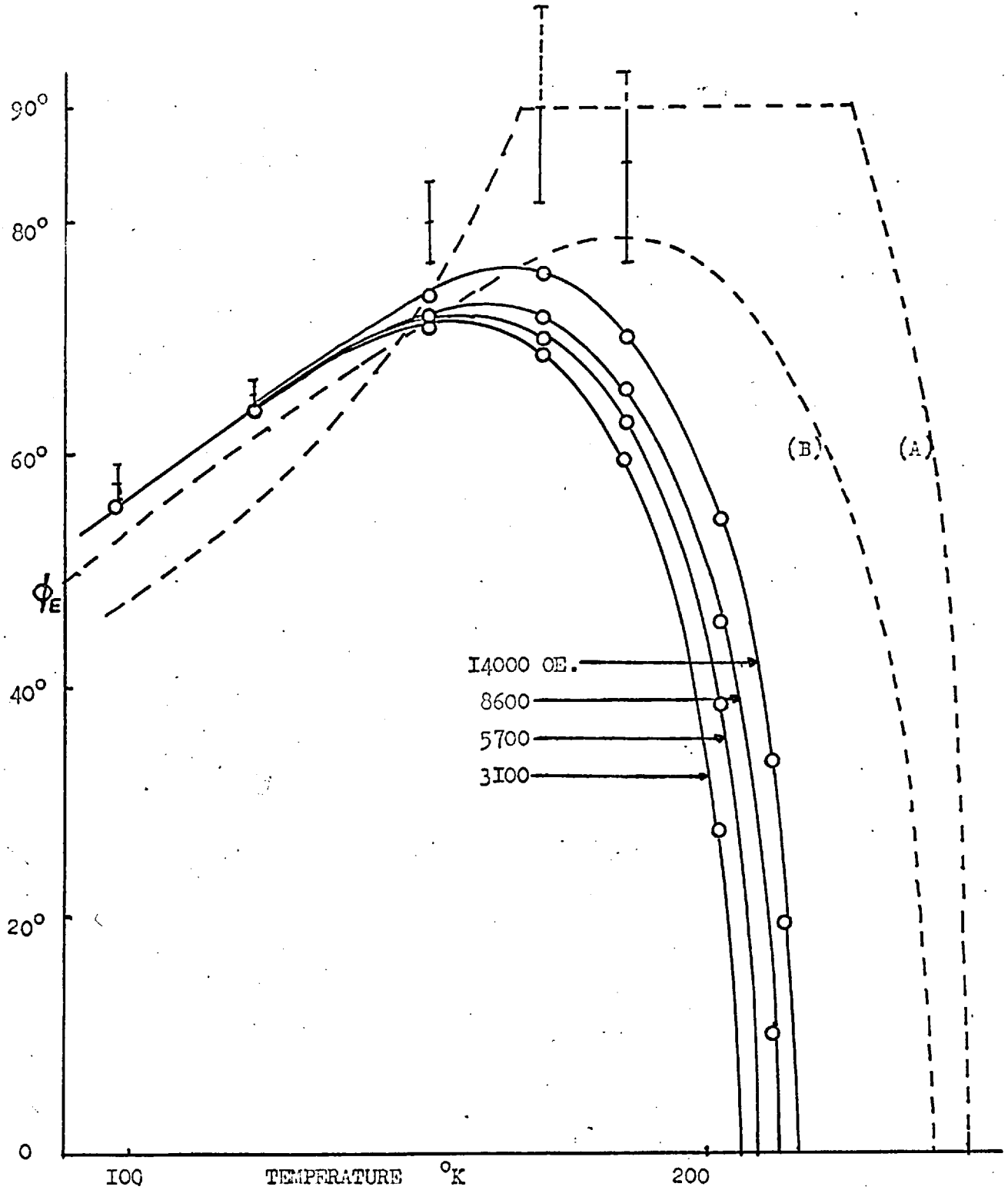


Figure 4.II THE VARIATION WITH TEMPERATURE OF THE EASY CONE ANGLE ϕ_E FOR GADOLINIUM

A, Graham (1962). B, Corner, Roe and Taylor (1962).

§ 4.5 Domain Observations on Gadolinium.

Domain observations were made on a small piece of gadolinium single crystal using the well known magnetic colloid or Bitter figure technique, first discovered by Bitter (1931) and independently by Hamos and Thiessen (1931). Gadolinium reacts fairly readily with water so that the usual colloid preparations based on this solvent could not be used. Xylene was therefore chosen because there can be only a very small percentage of water dissolved in it. No reaction was detected between the xylene-based colloid, prepared as described in section 3.4.2, and the gadolinium specimen. Before domains could be observed the surface of the gadolinium had to be prepared by ion bombardment, as described in section 3.4.1. It is beleived that this process removed a surface layer of polycrystalline gadolinium created during mechanical polishing, and probably also non-magnetic surface impurities which may have been created due to the reaction of the gadolinium with water in the atmosphere. To observe domains the prepared specimen was placed in the special microscope stage shown in figure 4.12. The speciman lay in the brass cup in a recess machined accurately to the shape of the specimen. The magnetic field was applied in such a way that there was a small component of force on the specimen downwards, thus holding the specimen in the recess and hence preventing any lateral displacement. A cover slip placed on top of the cup then permitted a thin

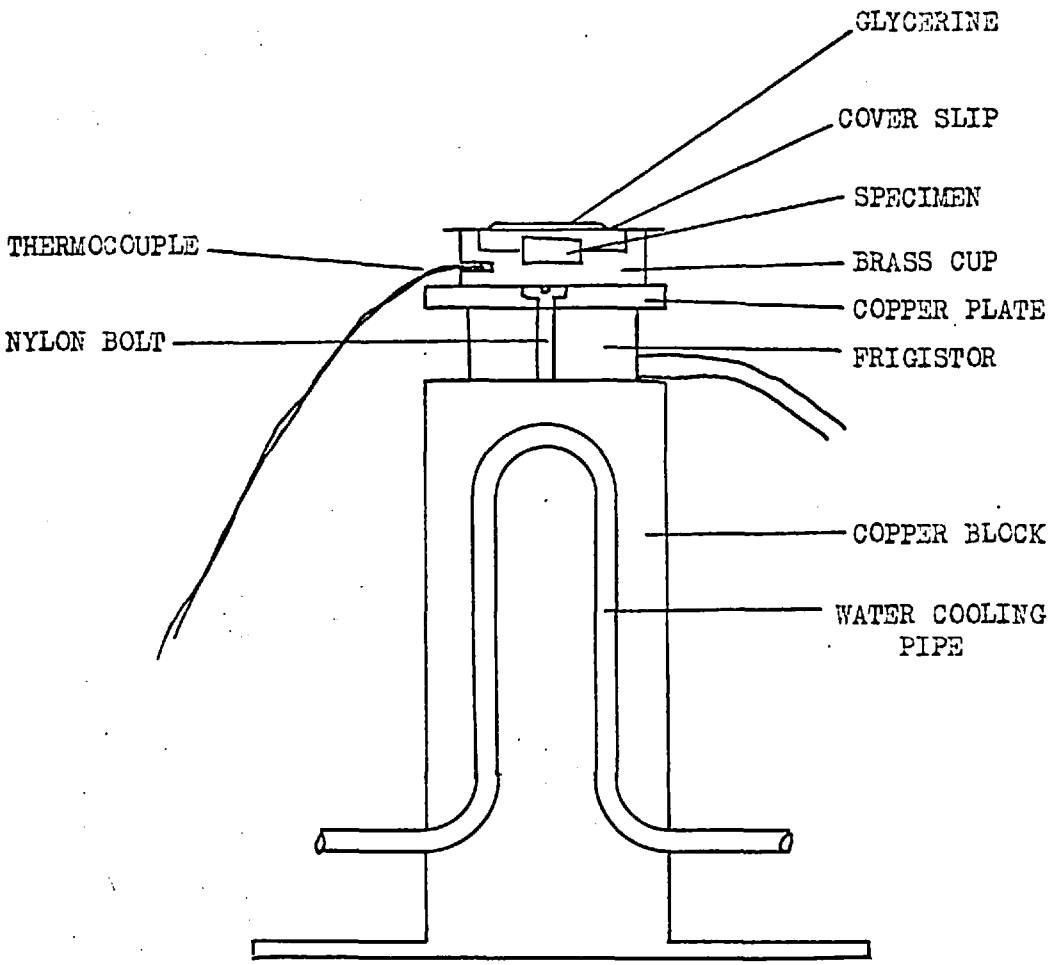


Figure 4.12

MICROSCOPE STAGE FOR DOMAIN OBSERVATIONS

layer of colloid to be introduced between the cover slip and the specimen without evaporation of the colloid occuring. The temperature of the brass cup was controlled by a single 13 amp, 4-couple frigistor unit (similar to those described in section 3.2) with water-cooled hot junctions. The e.m.f. across a copper-constantan thermocouple embedded in the brass specimen cup was measured by a potentiometer whose output was displayed on a Cambridge spot-galvanometer. A photo-transistor attached to the galvanometer scale operated a relay to control the current supply to the frigistor. The temperature of the microscope stage could thus be maintained constant to $\pm$ 1° C at any required temperature down to about -20°C. To prevent atmospheric condensation the cover slip was covered with glycerine.

The domains shown in plate 4.13 were observed at -5°C. It can be seen from figure 4.9 that this temperature is in the region where K_1 is large and positive, with K_2 very small, so that the domains might be expected to be similar of those seen on cobalt and this is in fact the case. However, the magnetization for gadolinium is small at -5°C due to the close proximity of the Curie point (+16°C.) so that Bitter patterns do not form very readily. On application of a magnetic field the domain walls moved in the expected manner, that is the domains with their magnetization in the direction of the applied field grew in width at the expense of those domains whose magnetization lay in the reverse direction. It was

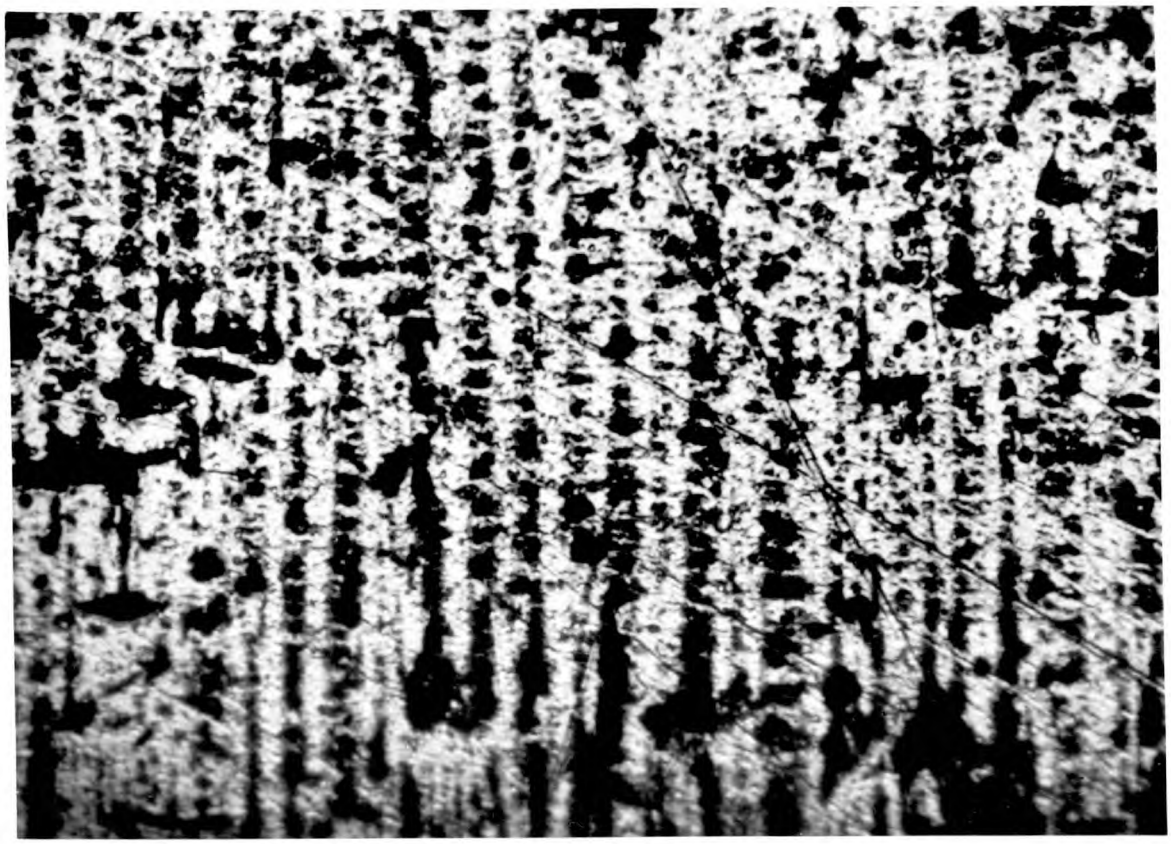


Plate 4.13

DOMAINS ON GADOLINIUM (x320, c-axis vertical)

not found possible, with the techniques and colloid described, to obtain Bitter figures in the interesting region below about -15°C. where a cone of easy magnetization exists.

In view of the low temperatures at which it would be desirable to make domain observations on this material, it was not thought to be worth pursuing further the present observations by the Bitter figure technique.

Chapter Five

NUMERICAL RESULTS

§5.1 Anisotropy Measurements, (111) Nickel.

The torque developed in the (111) specimen gave a reading on the output galvanometer of the measuring system (see §3.2 and §4.2). These readings were not linearly dependent on torque since there was some distortion introduced by the galvanometer amplifier. They were converted to further numbers which were directly proportional to torque by the use of calibration graphs. These latter numbers are listed in tables 5.1 - 5.6 for different temperatures, field magnitudes (H), and field directions (θ). The $6\beta'$ components were obtained from these numbers by Fourier analysis in the following way. Let the range $(0, 2\pi)$ be divided into p equal parts numbered 1, 2, ... r, ... p. Then if $x_r = \frac{2\pi r}{p}$ and the value of the function at x_r is y_r, then

$$a_6 = \frac{2}{p} \sum_{r=1}^{p} y_r \cos 6x_r, \qquad (5.1)$$

and

$$b_6 = \frac{2}{p} \sum_{r=1}^{p} y_r \sin 6x_r \qquad (5.2)$$

where a_6 and b_6 are the sin $6\beta'$ and cos $6\beta'$ components.

From the tables it will be seen that the range actually measured was $(0, \pi)$ and that $p = 36$, so that $x_r = \frac{\pi r}{36}$. The numbers in the tables therefore represent y_r. For convenience equations 5.1 and 5.2 were rewritten in the following way,

$$a_6 = \frac{1}{18} \left[A + \sqrt{\frac{3}{2}}\, B + \tfrac{1}{2} C \right] \qquad (5.3)$$

and

$$b_6 = \frac{1}{18} \left[D + \sqrt{\frac{3}{2}}\, E + \tfrac{1}{2} F \right] \qquad (5.4)$$

since the angles $6x_r$ were multiples of 30°.

The constants A, B, C, D, E and F are given by

$$A = -y_6 + y_{12} - y_{18} + y_{24} - y_{30} + y_{36}$$

$$B = +y_1 - y_5 - y_7 + y_{11} + y_{13} - y_{17} - y_{19} + y_{23} + y_{25} - y_{29} - y_{31} + y_{35}$$

$$C = +y_2 - y_4 - y_8 + y_{10} + y_{14} - y_{16} - y_{20} + y_{22} + y_{26} - y_{28} - y_{32} + y_{34}$$

$$D = +y_3 - y_9 + y_{15} - y_{21} + y_{27} - y_{33}$$

$$E = +y_2 + y_4 - y_8 - y_{10} + y_{14} + y_{16} - y_{20} - y_{22} + y_{26} + y_{28} - y_{32} - y_{34}$$

$$F = +y_1 + y_5 - y_7 - y_{11} + y_{13} + y_{17} - y_{19} - y_{23} + y_{25} + y_{29} - y_{31} - y_{35}$$

The rows of numbers labelled A_6, which represent the amplitude of the $6\beta'$ component, in the tables 1 - 5 were then obtained from

$$A_6 = \sqrt{a_6^2 + b_6^2} \ ,$$

and were converted to torque in dyn-cms per cm^3 by the use of the multiplication factors given (the significance of these factors is discussed in the next parpgraph). This data, plotted against 1/H, is shown in figure 4.5.

The first factor which converts the numbers in the tables to calibration coil current was introduced for convenience in plotting the calibration graphs and is of no other physical significance. The second factor, converting calibration coil current to torque in dyn-cms.

per cm^3., was obtained by using equation 4.1 and dividing by the volume of the specimen. The maximum flux through the coil remained almost constant as the temperature was changed, and a typical value was 25.90×10^4 maxwell turns. (The volume of the specimen was 0.08609 $c\,m^3$).

The anisotropy constants were obtained by fitting equation 4.2 to the curves shown in figure 4.5. The demagnetizing factor, N, had the value 0.955 which was obtained by measuring the ratios of the diameter to the thickness and by then using the data given by Bozorth(1951). The values obtained for K_1 and K_2 were plotted against temperature in figure 4.6 and are also given in table 5.7, together with the values of I_s used in the calculations (Bozorth 1951).

§5.2 Anisotropy Measurements, (110) Nickel.

Numbers derived from the output galvanometer readings of the torque measuring system are given in table 5.8. As in the case for the (111) Nickel specimen, these figures are as read from calibration graphs and are directly proportional to the torque. The $2\beta'$ and $4\beta'$ components were obtained by Fourier analysis of the numbers, with the aid of the following expressions derived from equations corresponding to 5.1 and 5.2 in a similar way to the expressions obtained for $6\beta'$ analysis. Let

$$a_2 = \frac{1}{9}\ (1.0000A + 0.9397B + 0.7660C + 0.5000D + 0.1736E)$$

$$b_2 = \frac{1}{9}\ (0.3420F + 0.6428G + 0.8660H + 0.9848J) \quad (5.5)$$

$$a_4 = \frac{1}{9}\ (1.0000L + 0.9397M + 0.7660N + 0.5000P + 0.1736Q)$$

$$b_4 = \frac{1}{9}\ (0.3420R + 0.6428S + 0.8660T + 0.9848U) \qquad (5.6)$$

where the constants A to U are given by

$$A = -y_9 \quad +y_{18} \qquad L = +y_9 \quad +y_{18}$$

$$B = +y_1 \quad -y_8 \quad -y_{10} \quad +y_{17} \qquad M = -y_4 \quad -y_5 \quad -y_{13} \quad -y_{14}$$

$$C = +y_2 \quad -y_7 \quad -y_{11} \quad +y_{16} \qquad N = +y_1 \quad +y_8 \quad +y_{10} \quad +y_{17}$$

$$D = +y_3 \quad -y_6 \quad -y_{12} \quad +y_{15} \qquad P = -y_3 \quad -y_6 \quad -y_{12} \quad -y_{15}$$

$$E = +y_4 \quad -y_5 \quad -y_{13} \quad +y_{14} \qquad Q = +y_2 \quad +y_7 \quad +y_{11} \quad +y_{16}$$

For b_2				or	For b_4			
$F = +y_1$	$+y_8$	$-y_{10}$	$-y_{17}$	$R = +y_4$	$-y_5$	$+y_{13}$	$-y_{14}$
$G = +y_2$	$+y_7$	$-y_{11}$	$-y_{16}$	$S = +y_1$	$-y_8$	$+y_{10}$	$-y_{17}$
$H = \pm y_3$	$+y_6$	$-y_{12}$	$-y_{15}$	$T = +y_3$	$-y_6$	$+y_{12}$	$-y_{15}$
$J = +y_4$	$+y_5$	$-y_{13}$	$-y_{14}$	$U = +y_2$	$-y_7$	$\pm y_{11}$	$-y_{16}$

The rows of numbers, A_2 and A_4 (representing the $2\beta'$ and $4\beta'$ amplitudes) at the bottom of table 5.8 were then obtained from,

$$A_2 = \sqrt{a_2^2 + b_2^2} \quad \text{and} \quad A_4 = \sqrt{a_4^2 + b_4^2}$$

The conversion factors used to change the readings to dyn cms per c m^3 are also given. These were obtained in the same way as those for the (111) specimen. (The volume of the (110) specimen was 0.00880 cm^3).

From equation 2.12, it can be seen that, for very large fields,

$$K_1 = \frac{8A_2 - 3A_4}{5} \qquad (5.7)$$

The effective values of K_1 given by equation 5.3 were plotted against 1/H and extrapolated to 1/H = 0 (H = ∞). The values of K_1 that were obtained, and which were appropriate to infinite field, are given on the bottom line of table 5.8. These values of K_1 are also plotted against temperature in figure 4.6.

§ 5.3 Anisotropy Measurements on Gadolinium.

Anisotropy measurements on gadolinium were made by measuring the slope of the torque curve at positions of zero torque. The whole torque curve was not measured, for reasons discussed in Chapter 4. Fortunately, owing to the symmetry of the specimen ($11\bar{2}0$), there were two directions of zero torque which were exactly 90° apart (parallel and perpendicular to the c-axis). This meant that the calibration procedure described in chapter 4 could still be followed, although the flux could no longer be maximised through the coil. It can be seen that equation 4.1 still holds so long as the magnet is turned through exactly 90° between measuring the flux and generating a calibration torque in the coil.

Since the torques measured on the gadolinium specimen were much larger than those for the nickel specimen, it was possible to adjust the galvanometer amplifier and attenuator circuit (described in chapter 3) in such a way as to make the galvanometer output exactly proportional to torque. It was thus not necessary to process each separate galvanometer reading to

eliminate the distortion which was encountered in the anisotropy measurements on nickel.

Table 5.9 gives the slopes of the torque curves that were measured for the two mutually perpendicular angular positions of the magnet A and B, which gave zero torque and the slopes are given in divisions of the output galvanometer scale per degree of rotation of the magnet. The readings were plotted against 1/H and the curves that were obtained were extrapolated to 1/H = 0, (H =∞). The values that were obtained in this way have been listed intable 5.10. They were converted first to units of m.A. per degree by use of the calibration scale factor, also listed in table 5.10. These numbers were then converted to dyn-cms per radian per gram with the aid of equation 4.1, and by dividing the torques obtained by the weight of the specimen (0.4667 grms.).

The positions A and B were identified as positions such that the field was parallel and perpendicular respectively with the hexagonal axis, so that the slope of the torque curve at these points was given by equations 2.16 and 2.17. The values of K_1' and K_2' obtained using these equations have been listed in table 5.10 and are also plotted against temperature in figure 4.9. The direction of the cone of easy magnetization was found directly by observing the angular position of the magnet for zero torque, relative to the direction of the c-axis of the specimen. The semi-angle of the cone of easy directions that was found in this way, has been plotted against 1/H for various temperatures in figures 4.10 and 4.11. The curve labelled

$H = \infty$ in figure 4.11 was obtained by extrapolating the curves of ϕ_E verses 1/H to 1/H = 0 to obtain $\phi_{E\infty}$, the cone semi-angle appropriate to infinite field.

§5.4 Magnetostriction Measurements on (111) Nickel.

The figures given in the second, third and fourth columns of table 5.11 respresent the change in the output galvanometer deflection with field (the reference field was 5400 oe), for the three different magnet positions corresponding to $\beta' = 30^\circ$, 75° and 120°. Because of random fluctuations and thermal drift it was not feasible to allow the deflection due to the change in the magnetostriction to occupy more than a small part of the galvanometer scale. Under these circumstances the small amount of distortion due to the galvanometer amplifier was negligible so that, as in the measurements on gadolinium, it was not necessary to process each seperate galvanometer reading. The figures in table 5.11 were therefore directly proportional to $\delta\lambda_{20}$, $\delta\lambda_{75}$ and $\delta\lambda_{120}$ (see § 2.4).

The two columns in table 5.11 labelled X and Y were found directly from the preceeding three columns using

$$X = \frac{3}{2}\delta\lambda_{120} - \tfrac{1}{2}\,\delta\lambda_{30} - \delta\lambda_{75}$$

and

$$Y = \delta\lambda_{120} - \delta\lambda_{30} .$$

X and Y were then plotted against H so that their values at H = 8 koe and 14 koe could be determined accurately. The difference in X and Y between these two field values are given in table 5.12.

The exact strain that these numbers represent was found first by converting them to the change in resistance of the gauge, and then by using the resistance of the gauge and the gague factor to obtain the strain. The conversion factor which gave the change in resistance of the gauge per division of the output galvanometer scale, was found by calibrating the bridge (see§ 4.2). This factor was constant over the range of temperatures at which measurements were made and had the value $4.00 \times 10^{-5}\,\Omega$ per division.

The resistance and gauge factor of the gauges at room temperature was $99.8\,\Omega$ and 2.09 respectively. However, both these quantities change with temperature and in order to determine the effect of this variation, the magnetostriction between $\beta' = 30^{\circ}$ and 120° was measured. Then from equation 2.54 (which neglects the very small contributions from the forced magnetostriction)it can be seen that $|\lambda_{30} - \lambda_{120}| = -\frac{1}{6}(C_1 + C_2)$. The appropriate values for C_1 and C_2, taken from Birss and Lee (1960), were then used to find the effedtive value of the gauge factor. (It was assumed that the resistance of the gauge was constant at $100\,\Omega$) so that the variation of the effective gauge factor included the effect of the change in resistance of the gauge with temperature).

It was felt that the procedure outlined above was preferable to merely accepting the data of Birss and Lee on temperature dependence of gauge factor since both the gauge factor and its variation with temperature is liable to differ between batches, and from gauge to gauge, and to depend on

the exact conditions under which the gauges are fixed to the specimen and subsequantly used. The values of the effective gauge factor that were obtained are tabulated against temperature in table 5.12.

Equations 2.63 and 2.64 were then used to obtain the values of $(C_1' + C_2')$ given in table 5.12, using the values of $(C_1 + C_2)$, $(C_1 - \frac{1}{2}C_2)$, α , and Δ given in the same table. In evaluating $C_1' + C_2'$ it was found that the last terms of both equations 2.63 and 2.64 were negligible so that C_1' and C_2' could not be determined separately.

Finally equations 2.63 and 2.64 were used to obtain the effective values of α and Δ using the values of $(C_1' + C_2')$ already determined. These values for α and Δ are tabulated in the last two columns of table 5.11, and have been plotted against H, and superimposed on the theoretical curves of α and Δ in figure 4.8 so that the theoretical values of α and Δ may be compared with those values found from these experiments below 8 kOe.

TABLE 5.1.

Temperature 92°K									
H (oe)		1,440		1,820		3,100		4,050	
θ		0-90	95-180	0-90	95-180	0-90	95-180	0-90	95-180
0		36.30	..	38.95	-	40,25	..	40.35	
5	95	33.60	14.90	35.40	11.50	36.50	11.65	37.15	12.30
10	100	29.10	18.85	30.20	15.55	31.45	15.90	31.75	16.35
15	105	24.25	23.30	24.30	23.15	24.50	22.95	25.15	22.75
20	110	19.40	27.60	18.75	30.85	17.95	30.20	17.55	29.55
25	115	15.10	31.45	13.15	34.90	12.30	34.35	11.85	33.65
30	120	12.60	32.75	09.85	34.50	09.05	34.45	08.75	33.75
35	125	14.75	30.35	10.25	31.00	09.90	31.20	10.00	30.85
40	130	19,50	26.35	15.70	26.25	15.60	25.85	15.60	25.35
45	135	24.15	21.80	24.45	21.05	24.20	20.15	23.75	19.30
50	140	29.15	17.45	32.75	15.85	31.95	14.10	31.25	13.15
55	145	33.50	14.15	37.10	11.60	36.85	09.75	36.15	09.00
60	150	35.00	12.95	37.15	09.45	37.55	08.25	37.35	07.95
65	155	32.90	16.20	34.20	11.40	35.10	10.95	34.90	11.35
70	160	28.90	21.35	29.65	18.40	30.15	18.65	30.00	19.20
75	165	24.75	26.40	24.75	27.90	24.75	27.95	24.55	28.10
80	170	20.15	31.25	19.75	35.55	18.95	36.05	18.90	35.85
85	175	16.25	35.25	14.65	39.35	14.30	40.25	14.55	40.25
90	180	13.55	36.15	11.30	38.85	11.60	40.35	11.90	40.95
A_6 (divs)		10.24		13.43		14.00		13.90	
1 division = 6.325 m.a. = 1.882×10^{3} dyn-cm per cc.									
$A_6 \times 10^{-3}$ (dyn-cm per cc.)		19.27		25.27		26.35		26.16	

TABLE 5.1 (Continued).

Temperature 92°K								
H (oe)		5,700		8,650		14,000		
θ		0-90	95-180	0-90	95-180	0-90	95-180	
0		40.55		40.10		38.65		
5	95	37.40	13.55	37.35	15.35	36.35	17.55	
10	100	32.65	16.50	32.25	17.45	32.00	18.75	
15	105	25.40	22.25	25.30	21.85	26.15	21.95	
20	110	18.05	28.80	19.25	27.55	20.25	26.45	
25	115	12.25	32.30	13.95	30.45	15.55	28.55	
30	120	09.55	32.40	10.75	30.45	12.60	28.15	
35	125	10.65	29.65	11.95	27.75	13.60	25.75	
40	130	15.65	24.40	16.25	23.00	17.20	21.45	
45	135	23.05	18.35	22.55	17.45	22.15	16.85	
50	140	29.95	12.40	28.70	12.25	27.15	12.65	
55	145	34.50	08.85	32.70	09.30	31.00	10.40	
60	150	36.00	08.35	34.55	09.35	32.25	11.05	
65	155	34.15	11.95	32.95	13.05	31.35	14.95	
70	160	29.95	19.45	29.75	20.70	28.90	21.75	
75	165	24.75	28.60	25.30	28.65	25.70	29.25	
80	170	19.70	35.95	20.75	35.85	22.14	35.65	
85	175	15.45	40.50	17.15	40.00	19.55	39.45	
90	180	13.05	41.15	15.10	40.45	17.75	39.90	
A_6 (divs)		13.14		11.68		9.79		
1 division = 6.325 m.a. = 1.882×10^3 dyn-cm per cc.								
$A_6 \times 10^{-3}$ (dyn-cm per cc.)		24.73		21.98		18.43		

TABLE 5.1 (Continued).

Temperature 92°K						
H (oe)		7,250		10,780		
θ		0-90	95-180	0-90	95-180	
0		40.80		39.50		
5	95	37.50	14.65	36.75	16.65	
10	100	32.85	17.45	32.15	18.30	
15	105	25.75	22.50	26.45	22.15	
20	110	19.35	28.60	19.85	27.15	
25	115	13.35	31.65	14.70	29.75	
30	120	10.70	31.80	11.95	29.65	
35	125	11.85	29.15	13.05	27.00	
40	130	16.80	23.95	16.85	22.40	
45	130	23.05	18.35	22.25	17.45	
50	140	29.75	12.90	28.15	12.75	
55	145	34.15	09.50	32.25	10.65	
60	150	35.85	09.45	33.65	10.55	
65	155	34.25	13.30	32.35	14.50	
70	160	30.65	20.85	29.40	21.55	
75	165	25.75	29.05	25.65	29.30	
80	170	20.75	36.45	21.75	36.10	
85	175	16.40	40.90	18.65	4.00	
90	180	14.85	41.35	16.65	40.45	
A_6 (divs)		12.38		10.72		
1 division = 6.325 m.a. = 1.882×10^3 dyn-cm per cc.						
$A_6 \times 10^{-3}$ (dyn-cms per cc.)		23.30		20.17		

TABLE 5.2

Temperature 131°K								
H (oe)		1,440		1,820		3,100		4,050	
θ		0-90	95-180	0-90	95-180	0-90	95-180	0-90	95-180
0		36.35		38.00		39.15		40.30	
5	95	32.75	09.40	34.45	08.75	36.05	09.30	36.85	09.55
10	100	27.75	13.80	29.00	13.25	29.95	13.30	30.35	13.55
15	105	21.90	21.15	22.15	21.15	22.00	20.30	22.60	20.45
20	110	16.20	28.30	15.65	28.60	14.75	27.50	14.85	27.30
25	115	10.95	32.40	09.80	32.85	08.45	31.95	08.50	31.50
30	120	07.85	32.40	06.55	32.90	05.50	32.35	05.50	31.90
35	125	08.75	29.50	07.80	29.75	07.15	29.25	07.15	28.85
40	130	14.35	24.60	13.70	24.75	13.35	23.85	13.45	23.20
45	135	22.55	19.60	22.50	19.00	21.65	17.25	21.25	16.75
50	140	30.45	14.35	30.95	13.25	30.00	10.95	29.50	10.40
55	145	34.75	10.35	35.50	08.70	35.80	06.60	34.40	06.10
60	150	35.05	08.55	36.05	07.05	36.25	05.65	36.20	05.60
65	155	32.35	10.95	33.30	10.00	33.85	09.30	34.00	09.70
70	160	27.85	17.85	28.50	17.15	28.95	17.35	29.45	17.95
76	165	23.10	25.90	22.80	26.45	22.85	26.45	23.45	27.00
80	170	17.50	33.05	17.35	34.20	17.00	34.25	17.05	34.75
85	175	12.55	36.75	11.55	38.35	11.65	39.10	12.50	39.70
90	180	09.30	36.45	08.60	38.15	8.35	39.65	09.45	40.75
A_6 (divs)		13.23		14.22		14.78		14.68	
1 division = 3.975 m.a. = 1.183×10^3 dyn-cm/cc.									
$A_6 \times 10^{-3}$ (dyn-cm per cc.)		15.65		16.81		17.48		17.36	

TABLE 5.2 (continued)

Temperature 131°K									
H (oe)		5,700		8,650		14,000			
θ		0-90	95-180	0-90	95-180	0-90	95-180	0-90	95-180
0		40.45		40.55		39.90			
5	95	37.05	11.45	37.75	13.00	36.75	15.15		
10	100	31.20	14.00	31.80	15.25	32.50	15.85		
15	105	23.30	20.10	24.85	20.05	25.05	19.30		
20	110	15.50	26.45	16.85	25.65	17.95	24.15		
25	115	09.00	30.35	10.70	28.90	12.20	26.75		
30	120	06.30	30.75	07.60	29.05	08.85	26.55		
35	125	07.85	27.70	08.85	26.35	09.90	23.85		
40	130	13.45	22.05	13.75	21.15	14.15	19.00		
45	135	20.95	15.85	20.50	15.20	19.75	13.85		
50	140	28.50	09.70	27.45	09.50	25.50	09.05		
55	145	33.35	05.95	32.20	06.40	29.95	06.60		
60	150	35.25	06.05	33.85	06.85	31.95	07.75		
65	155	33.85	10.25	32.80	11.60	31.05	12.60		
70	160	29.45	18.55	29.15	19.70	28.55	20.10		
75	165	23.75	27.50	24.50	28.40	24.60	28.35		
80	170	18.05	35.055	19.50	35.46	20.55	35.15		
85	175	13.30	40.15	15.75	40.10	17.65	39.65		
90	180	10.45	41.45	13.60	41.45	15.75	41.05		
A_6 (divs)		13.73		12.72		11.10			
1 division = 3.975 m.a. = 1.183×10^3 dyn-cm per cc.									
$A_6 \times 10^{-3}$ (dyn-cm per cc.)		16.24		15.04		13.13			

TABLE 5.3

Temperature 171°K									
H (oe)		1,440		1,820		3,100		4,050	
θ		0-90	95-180	0-90	95-180	0-90	95-180	0-90	95-180
0		37.60		38.05		39.50		40.05	
5	95	34.75	14.50	35.25	14.30	36.60	14.55	37.75	14.95
10	100	30.35	18.10	30.40	18.05	31.75	17.80	32.05	17.75
15	105	25.25	23.90	24.60	23.85	24.85	23.50	25.35	23.05
20	110	20.30	29.35	18.80	29.00	18.45	28.85	18.60	28.65
25	115	16.50	32.50	14.35	31.70	13.55	32.40	13.40	32.00
30	120	14.05	32.75	12.15	33.05	11.50	32.95	11.25	32.60
35	125	15.10	30.50	13.45	30.85	13.05	30.75	12.85	30.25
40	130	18.55	26.75	18.35	26.65	18.15	26.30	17.80	25.70
45	135	24.95	22.55	25.00	22.05	24.65	21.15	24.15	20.50
50	140	31.25	18.30	31.50	17.45	31.05	16.05	30.85	15.50
55	145	34.95	15.20	35.40	14.05	35.35	12.80	35.00	12.35
60	150	35.40	14.20	36.25	13.25	36.85	12.60	36.75	12.50
65	155	33.30	16.50	34.35	16.15	35.20	16.05	35.45	16.15
70	160	29.60	21.85	30.50	22.00	31.25	22.20	31.60	22.65
75	165	25.30	28.30	25.75	28.80	26.15	29.20	26.75	29.95
80	170	20.85	34.15	20.80	34.85	21.05	35.70	21.75	36.15
85	175	16.65	37.05	16.50	38.35	16.50	39.25	17.35	39.85
90	180	14.20	36.85	13.85	38.25	14.15	39.70	14.75	40.50
A_6 (divs)		10.48		11.33		11.88		11.88	
1 division = 3.062 m.a. = 0.9108×10^3 dyn-cm per cc.									
$A_6 \times 10^{-3}$ (dyn-cm per cc.)		9.543		10.32		10.82		10.82	

TABLE 5.3 (continued)

Temperature 171°K								
H (oe)		5,700		8,650		14,000		
θ		0-90	95-180	0-90	95-180	0-90	95-180	
0		40.55		40.90		40.85		
5	95	37.65	15.90	38.50	17.40	38.50	19.15	
10	100	32.85	18.10	33.25	18.50	33.70	19.10	
15	105	25.65	23.25	26.95	22.95	27.65	22.75	
20	110	19.00	28.25	20.00	27.45	20.65	26.75	
25	115	13.75	31.25	14.60	30.15	15.35	28.90	
30	120	11.55	31.65	12.20	30.35	12.95	28.90	
35	125	13.10	29.30	13.55	28.05	14.15	26.65	
40	130	17.50	24.90	17.75	23.70	17.85	22.60	
45	135	23.90	19.80	23.55	19.00	22.75	18.25	
50	140	30.10	15.00	29.50	14.50	28.20	14.40	
55	145	34.35	12.25	33.45	12.35	32.30	12.65	
60	150	36.45	12.75	35.35	13.30	34.50	14.00	
65	155	35.15	16.75	34.70	17.35	34.05	18.25	
70	160	31.75	23.25	31.80	23.75	31.85	25.15	
75	165	27.15	30.40	27.95	31.15	28.60	31.75	
80	170	22.55	36.85	23.70	37.30	25.25	37.50	
85	175	18.85	40.45	20.60	40.70	22.45	41.00	
90	180	16.10	41.15	17.95	41.75	20.50	42.00	
A_6 (divs)		11.43		10.65		9.63		
1 division = 3.062 m.a. = .9108 x 10^3 dyn-cm per cc.								
A_6 x10^{-3} (dyn-cms per cc.)		10.41		9.699		8.777		

TABLE 5.4

	Temperature 233°K							
H (oe)	1,440		1,820		3,100		4,050	
θ	0-90	95-180	0-90	95-180	0-90	95-180	0-90	95-180
0	+16.10		+17.05		+17.65		+20.65	
5 95	+18.00	-04.05	+19.00	-04.50	+19.90	-05.05	+23.15	-01.75
10 100	+16.85	-02.60	+17.85	-02.85	+18.75	-03.25	+22.20	-00.15
15 105	+13.15	+01.70	+14.15	+01.60	+14.75	+01.50	+18.10	+04.60
20 110	+08.10	+08.00	+08.75	+07.90	+08.85	+08.10	+12.65	+11.20
25 115	+03.20	+14.15	+03.20	+14.55	+03.10	+14.25	+06.75	+17.70
30 120	-00.85	+18.25	-01.10	+18.70	-01.50	+18.90	+01.80	+22.20
35 125	-02.60	+19.25	-02.95	+19.90	-03.40	+20.40	-00.15	+23.70
40 130	-01.60	+17.25	-01.95	+17.85	-02.30	+18.40	+01.05	+21.45
45 135	+01.95	+13.20	+02.00	+13.45	+02.05	+13.35	+05.15	+16.85
50 140	+07.75	+07.95	+07.90	+07.45	+07.95	+07.00	+11.05	+10.05
55 145	+13.65	+02.25	+13.80	+01.55	+14.00	+00.60	+17.20	+03.55
60 150	+17.45	-02.40	+17.80	-03.25	+18.50	-04.60	+21.85	-01.60
65 155	+18.25	-04.70	+19.05	-05.55	+19.80	-06.65	+23.30	-03.55
70 160	+16.40	-04.00	+17.20	-04.60	+17.95	-05.30	+21.35	-02.10
75 165	+12.30	-00.25	+12.80	-00.60	+13.45	-00.80	+17.05	+02.30
80 170	+06.85	+05.25	+07.30	+05.55	+07.25	+05.40	+10.80	+08.90
85 175	+01.85	+11.85	+01.70	+12.15	+01.35	+12.60	+04.35	+16.25
90 180	-02.20	+16.70	-02.65	+17.45	-03.20	+17.80	-00.05	+21.15
A_6 (divs)	11.19		11.82		12.53		12.64	
1 division = 1 m.a. = 0.3007×10^3 dyn-cm per cc.								
$A_6 \times 10^{-3}$ (dyn-cm per cc)	3.364		3.555		3.766		3.801	

TABLE 5.4 (continued)

Temperature 233°K								
H (oe)		5,700		8,650		10,780		14,000	
θ		0-90	95-180	0-90	95-180	0-90	95-180	0-90	95-180
0		+20.35		+20.25		+20.00		+19.80	
5	95	+23.00	-01.45	+23.00	-00.70	+22.85	-00.35	+22.75	-00.25
10	100	+22.20	+00.15	+22.35	+01.20	+22.65	+01.25	+22.45	+01.60
15	105	+17.50	+05.05	+18.85	+05.85	+19.20	+06.50	+19.15	+06.30
20	110	+12.80	+11.70	+13.50	+12.25	+13.85	+12.25	+14.30	+12.65
25	115	+07.10	+17.95	+07.90	+18.30	+08.45	+18.25	+08.70	+18.15
30	120	+02.45	+22.25	+03.25	+22.80	+03.60	+22.45	+04.05	+22.25
35	125	+00.25	+23.60	+01.25	+23.65	+01.90	+23.50	+02.10	+23.30
40	130	+01.40	+21.40	+02.25	+21.45	+02.60	+21.00	+02.90	+20.75
45	135	+05.50	+16.55	+06.05	+16.55	+06.50	+16.20	+06.60	+16.15
50	140	+11.45	+10.10	+11.80	+10.20	+12.20	+10.40	+12.10	+09.85
55	145	+17.55	+03.35	+17.85	+03.95	+17.90	+03.95	+17.75	+04.20
60	150	+21.85	-01.40	+22.05	-00.90	+22.05	-00.65	+22.00	-00.60
65	155	+23.35	-03.75	+23.50	-02.80	+23.45	-02.45	+23.35	-02.20
70	160	+21.55	-01.85	+21.65	-01.25	+21.75	-01.15	+21.35	-00.80
75	165	+17.15	+02.75	+17.00	+03.25	+17.40	+03.55	+17.20	+03.70
80	170	+11.00	+09.00	+10.95	+09.50	+11.30	+09.65	+11.35	+09.80
85	175	+04.85	+16.00	+05.00	+16.25	+05.40	+16.45	+05.05	+16.45
90	180	+00.15	+21.20	+00.90	+21.15	+01.05	+21.35	+01.10	+21.35
A_6 (divs)		12.48		12.10		11.89		11.68	
1 division = 1 m.a. = 0.3007 x 10^3 dyn-cm per cc.									
A_6 (dyn-cm per cc.) x 10^{-3}		3.753		3.639		3.576		3.514	

TABLE 5.5

Temperature 277°K									
H (oe)		1,440		1,820		3,100		4,050	
θ		0-90	95-180	0-90	95-180	0-90	95-180	0-90	95-180
0		27.90		28.20		27.70		27.40	
5	95	29.65	10.15	30.15	8.90	30.00	7.85	29.85	07.75
10	100	28.60	11.65	29.10	10.60	29.15	9.40	29.10	09.20
15	105	25.20	16.10	25.70	15.15	25.55	13.55	25.50	13.65
20	110	21.00	21.65	20.70	20.75	20.25	19.70	20.40	19.20
25	115	16.60	26.80	15.90	26.20	15.40	25.15	15.55	24.85
30	120	13.15	30.15	12.45	29.85	11.45	29.20	11.60	28.95
35	125	12.05	30.90	11.20	30.65	10.25	30.20	10.35	29.95
40	130	13.15	28.95	12.50	28.75	12.00	28.10	11.80	27.75
45	135	16.75	24.95	16.15	24.35	15.90	23.50	15.80	23.05
50	140	21.45	19.60	21.40	18.55	21.55	16.85	21.60	16.75
55	145	26.25	14.45	26.35	12.85	26.60	11.05	27.05	10.65
60	150	29.50	10.45	29.85	8.40	30.35	06.65	30.70	06.65
65	155	30.10	8.55	30.65	6.70	31.15	04.90	31.55	04.40
70	160	28.25	9.40	28.70	7.65	29.25	06.20	29.55	05.80
75	165	24.40	12.75	24.60	11.30	24.60	10.40	25.15	10.05
80	170	19.20	17.85	19.20	16.95	19.30	16.20	19.15	15.95
85	175	14.70	23.40	13.80	23.05	13.30	22.50	13.30	22.50
90	180	11.30	27.75	10.35	27.95	09.25	27.70	09.25	27.50
A_6 (divs)		9.988		10.80		11.41		11.51	
1 division = 0.5000 m.a. = $0.1502 \times 10^{+3}$ dyn-cms per cc.									
A_6 (dyn-cm per cc.) $\times 10^{-3}$		1.501		1.623		1.715		1.729	

TABLE 5.5 (continued)

Temperature 277°K									
H (oe)		5,700		8,650		10,780		14,000	
θ		0-90	95-180	0-90	95-180	0-90	95-180	0-90	95-180
0		27.10		26.90		26.50		25.95	
5	95	29.65	07.90	29.55	07.85	29.25	07.50	29.95	07.20
10	100	29.10	09.40	29.25	09.35	28.95	08.85	28.75	18.70
15	105	25.85	13.75	26.10	13.55	26.00	13.25	25.80	12.95
20	110	20.85	19.30	21.35	19.05	21.50	18.75	21.30	18.50
25	115	15.75	25.05	16.35	24.70	16.40	24.05	16.45	24.00
30	120	12.05	28.85	12.70	29.25	12.70	28.00	12.80	27.65
35	125	10.80	29.85	11.45	29.40	11.45	28.90	11.50	28.55
40	130	12.35	27.45	13.00	27.00	13.00	26.55	12.95	26.00
45	135	16.30	22.85	17.00	22.40	16.85	21.75	16.95	21.05
50	140	22.00	16.35	22.70	15.90	22.55	15.65	22.90	15.05
55	145	27.35	10.25	27.80	09.85	27.85	09.45	27.95	09.05
60	150	31.15	05.70	31.55	05.30	31.55	05.00	31.60	04.55
65	155	32.15	04.15	32.60	03.85	32.45	03.45	32.40	03.10
70	160	30.05	05.65	30.55	05.35	30.40	05.05	30.35	04.75
75	165	25.65	09.95	25.80	09.65	25.65	09.20	25.45	08.85
80	110	19.70	16.10	19.80	15.55	19.50	15.15	19.30	14.75
85	175	13.80	22.70	13.80	22.25	13.50	21.75	13.25	21.60
90	180	09.45	27.45	09.45	26.95	09.05	26.55	08.75	26.35
A_6 (divs)		11.43		11.43		11.38		11.43	
1 division = 0.5000 m.a. = 0.1502 x 10^3 dyn-cm per cc.									
A_6 (dyn-cm per cc.) x 10^{-3}		1.718		1.718		1.711		1.718	

TABLE 5.6

Temperature 347°K							
H (oe)		1,464		1,963		3,154	
θ		5-90	95-180	5-90	95-180	5-90	95-180
5	95	-00.95	+20.20	-00.65	+21.40	+00.30	+20.70
10	100	+01.10	+16.55	+01.85	+17.05	+03.50	+16.00
15	105	+05.30	+10.55	+06.95	+09.95	+09.40	+09.00
20	110	+10.35	+03.80	+12.40	+02.25	+15.55	+01.20
25	115	+15.25	-01.80	+17.35	-03.90	+21.20	-05.15
30	120	+18.05	-04.75	+20.35	-06.70	+24.60	-08.75
35	125	+17.90	-03.90	+20.45	-05.50	+24.40	-08.40
40	130	+14.85	+00.47	+17.25	-01.50	+20.65	-03.55
45	135	+09.95	+06.70	+11.65	+05.10	+14.55	+02.90
50	140	+04.10	+13.80	+05.10	+12.90	+07.25	+10.95
55	145	-01.10	+20.10	-00.28	+19.55	+01.30	+17.30
60	150	-04.00	+24.65	-03.35	+24.40	-02.45	+22.10
65	155	-03-60	+26.25	-03.20	+25.60	-02.35	+23.35
70	160	-00.25	+24.05	+00.40	+23.25	+00.30	+20.55
75	165	+05.60	+19.45	+06.10	+18.40	+05.80	+15.65
80	170	+12.30	12.55	+12.75	+11.65	+12.15	+09.75
85	175	+17.30	+06.05	+18.45	+05.65	+17.80	+03.30
90	180	+20.25	+01.80	+21.50	+01.75	+21.20	+01.20
A_6 (divs)		12.31		12.47		12.66	
1 division = 0.1250 m.a. = 33.05 dyn-cms per cc.							
A_6 (dyn-cm per cc.) x 10^{-3}		0.4069		0.4122		0.4187	

TABLE 5.6 (continued)

Temperature 347°K						
H (oe)		4865		7085		
	θ	5-90	95-180	5-90	95-180	
5	95	+00.65	+18.25	+01.00	+17.10	
10	100	+04.60	+14.15	+05.25	+13.10	
15	105	+10.40	+07.55	+11.90	+06.95	
20	110	+17.40	+00.00	+19.35	+01.00	
25	115	+23.35	-06.35	+25.30	-08.40	
30	120	+26.85	-10.50	+28.95	-12.00	
35	125	+26.50	-10.15	+28.65	-11.50	
40	130	+22.45	-05.70	+24.60	-07.05	
45	135	+15.95	+01.15	+17.85	+00.00	
50	140	+08.15	+09.00	+09.70	+07.70	
55	145	+01.65	+15.85	+02.60	+14.25	
60	150	-02.60	+19.70	-02.75	+18.50	
65	155	-05.20	+21.00	-05.95	+19.50	
70	160	-00.45	+18.50	-01.40	+17.15	
75	165	+04.60	+13.60	+03.90	+12.75	
80	170	+10.45	+07.75	+09.55	+06.80	
85	175	+15.95	+02.95	+14.70	+02.00	
90	180	+18.45	+00.30	+17.50	-00.35	
A_6 (divs)		13.32		13.60		
1 division = 0.1250 m.a. = 33.05 dyn-cm per cc.						
A_6 (dyn-cm per cc.) x 10^{-3}		0.4402		0.4494		

TABLE 5.7

T ^{o}K	I_s	$-K_1$ x 10^5 erg cm^{-3}	$-\frac{1}{18}K_2$ x 10^3 erg cm^{-3}
92	507	5.28	8.42
131	503	3.62	7.94
171	499	2.47	6.23
233	491	0.854	3.19
277	483	0.307	1.65
347	471	-	0.530

TABLE 5.8

T	92°K			131°K		
H(Oe)	4925	8650	14000	4925	8650	14000
θ						
0	15.55	17.00	18.20	17.95	18.95	19.45
10	34.84	32.60	31.75	34.45	33.10	32.55
20	43.90	42.65	41.85	44.75	43.35	42.75
30	43.00	43.95	44.45	45.15	45.70	46.05
40	38.00	39.35	40.20	40.20	41.35	42.05
50	31.70	32.15	32.70	33.25	33.85	34.25
60	25.15	25.05	24.75	26.00	25.70	25.70
70	20.10	19.30	19.05	20.60	19.85	19.70
80	18.05	17.75	17.75	18.75	18.50	18.55
90	21.90	22.05	22.05	23.05	22.95	23.15
100	29.95	29.30	29.25	31.15	30.50	30.50
110	33.55	33.35	33.35	35.05	34.75	34.95
120	31.50	31.75	32.15	33.05	33.45	33.75
130	26.40	26.45	26.35	27.75	27.45	27.60
140	19.95	18.75	18.20	20.25	19.35	18.95
150	13.05	11.00	10.00	13.00	11.33	10.45
160	07.40	05.60	05.15	07.50	06.35	06.05
170	05.95	06.65	07.70	07.55	08.35	09.15
180	15.30	17.05	18.25	17.65	18.90	19.35
A2	07.35	07.81	07.99	07.59	07.93	08.09
A4	1320	13.50	13.56	13.64	13.81	13.89
1 = 5.870 = 17.18 x 10^3 m.a. dyn-cm/cm^3				1 = 4.160 = 12.17 x 10^3 m.a. dyn-cm/cm^3		
K_1 (erg cm^{-3})	5.34 x 10^5			3.67 x 10^5		

TABLE 5.8 (continued)

T	169°K			233°K		
H(oe)	4925	8650	14000	4925	8650	14000
θ						
0	21.45	19.40	19.95	19.60	18.75	17.70
10	35.70	32.55	32.00	33.25	32.25	31.05
20	46.00	42.45	42.10	44.30	43.10	42.30
30	47.75	45.55	45.75	48.15	47.65	46.85
40	43.15	41.45	42.20	43.95	43.75	43.25
50	35.65	33.75	34.15	35.15	34.50	34.00
60	28.05	25.75	25.50	25.70	24.75	23.70
70	22.45	19.65	19.25	18.95	17.75	16.55
80	20.85	18.40	18.30	17.90	17.00	15.85
90	25.30	23.00	23.15	23.50	22.80	21.75
100	33.05	30.40	30.45	32.05	31.25	30.30
110	37.35	34.95	34.95	37.25	36.60	35.75
120	35.70	33.65	33.80	35.65	35.45	34.55
130	29.85	27.50	27.60	28.40	28.15	27.55
140	22.05	19.00	18.85	18.70	17.65	16.35
150	14.50	10.95	10.15	09.15	08.05	05.95
160	09.60	06.45	0.615	04.35	03.50	01.95
170	11.10	09.35	09.70	07.85	07.55	06.25
180	20.85	19.45	19.50	19.00	18.55	17.55
A2	7.60	7.81	7.96	8.587	8.524	8.821
A4	13.81	13.67	13.83	15.53	15.70	16.01
1 = 2.750 = 8.04 x 10^3 m.a. dyn-cm/cm^3				1 = 1.065 = 3.12 x 10^3 m.a. dyn-cm/cm^3		
K_1 $\frac{erg}{cm^3}$	2.42 x 10^5			0.960 x 10^5		

TABLE 5.9

H (Oe)		1440	1820	3100	4050	5700	8650	1400
$T^{o}K$	A	+0.230	+0.306	+0.518	+0.712	+1.003	+1.402	+1.886
288	B	-0.220	-0.337	-0.591	-0.816	-1.077	-1.633	-2.170
273	A	+1.719	+1.921	+2.168	+2.360	+2.515	+2.700	+2.820
	B	-4.050	-4.000	-3.716	-3.550	-3.475	-3.458	-3.408
253	A	+2.200	+2.485	+2.740	+2.860	+2.940	+2.945	+2.790
	B	-3.716	-4.775	-4.608	-4.375	-4.116	-3.850	-3.500
243	A	-2.040	+2.325	+2.530	+2.590	+2.595	+2.515	+2.265
	B	-2.708	-4.008	-4.058	-3.891	-3.683	-3.416	-3.066
228	A	+1.528	+1.793	+1.903	+1.884	+1.812	+1.631	+1.281
	B	-.891	-2.941	-3.091	-3.033	-2.891	-2.666	-2.325
214	A	+0.687	+0.868	+0.896	+0.809	+0.593	+0.321	-0.115
	B	-1.08	-1.92	-2.12	-2.07	-1.985	-1.830	-1.540
188	A	-0.462	-1.250	-1.759	-2.010	-2.375	-2.845	-3.440
	B	-0.115	-0.670	-0.905	-0.910	-0.885	-0.810	-0.610
161	A	-0.740	-2.240	-3.975	-4.420	-4.775	-5.325	-5.925
	B	-0.045	-0.360	-0.580	-0.610	-0.625	-0.585	-0.450
148	A	-1.083	-3.066	-7.100	-7.600	-8.066	-8.800	-9.483
	B	-0.040	-0.310	-0.765	-0.850	-0.930	-0.990	-0.950
123	A	-0.816	-2.716	-9.750	-11.08	-11.66	-12.01	-12.96
	B	-0.040	-0.340	-2.035	-2.365	-2.610	-2.840	-2.945
98	A	-0.600	-2.420	-11.02	-13.00	-13.25	-13.62	-14.47
	B	-0.075	-0.580	-5.100	-6.062	-6.650	-6.975	-6.850

TABLE 5.10

T ^{o}K	A Intercept (divisions per degree)	B Intercept (divisions per degree)	X Factor (ma/div.)	K'_1 x 10^{-5} (dyn-cm per gram)	K'_2 x 10^{-5} (dyn-cm per gram)
288	+3.04	-3.70	7.07	+0.337	+0.037
273	+2.75	-3.50	6.67	+0.287	+0.039
253	+2.20	-3.00	6.67	+0.230	+0.042
243	+1.78	-2.50	6.80	+0.190	+0.041
228	+0.66	-1.60	6.80	+0.071	+0.050
214	-0.65	-1.00	6.75	-0.069	+0.087
188	-4.15	-0.35	6.50	-0.423	+0.230
161	-6.65	-0.25	6.25	-0.652	+0.338
148	-10.25	-0.80	5.85	-0.941	+0.507
123	-14.70	-3.00	5.80	-1.337	+0.805
98	-15.70	-7.00	5.80	-1.428	+1.032

TABLE 5.11

Temperature 213°K

H(Oe) \ β'	30°	75°	120°	X	Y	$\delta H \times 10^{-3}$	$\delta\Delta \times 10^{3}$	$\delta\alpha \times 10^{3}$
1300	-2.78	+0.55	+2.55	-2.98	+0.23	-4.10	-7.07	-5.09
1900	-2.83	-0.05	+2.28	-2.35	+0.55	-3.50	-5.25	-7.47
3000	-1.70	-0.33	+1.48	-2.04	+0.22	-2.40	-4.94	-3.90
4150	-0.88	-0.25	+0.88	-0.63	0	-1.25	-0.87	-1.29
5400	0	0	0	0	0	0	0	0
6650	+0.50	+0.28	+0.68	+0.49	+0.18	+1.25	+0.41	-0.22
8350	+0.85	+0.57	+1.30	+0.95	+0.55	+2.95	+0.87	-2.21
9250	+0.95	+0.75	+1.45	+0.95	+0.50	+3.85	+0.07	-0.82
10650	+1.12	+0.85	+1.90	+1.44	+0.78	+5.25	+0.72	-2.31
11950	+1.32	+1.25	+2.45	+1.76	+1.13	+6.55	+0.64	-4.04
13500	+1.50	+1.35	+2.82	+2.13	+1.32	+8.10	+1.00	-4.72
14000	+1.45	+1.45	+3.05	+2.40	+1.60	+8.50	+1.47	-6.60
	Readings in these 3 columns propnl. to $\delta\lambda_{30}$ etc.							

Temperature = 131°K

H(Oe) \ β'	30°	75°	120°	X	Y	$\delta H \times 10^{-3}$	$\delta\Delta \times 10^{3}$	$\delta\alpha \times 10^{3}$
1300	+0.42	+5.15	-1.35	-7.38	-1.77	-4.10	-22.6	+14.3
1900	-1.48	+2.92	-1.38	-4.25	+0.10	-3.50	-12.1	-2.79
3000	-1.40	+0.97	-1.10	-1.92	+0.30	-2.40	-4.78	-3.66
4150	-0.68	+0.30	-0.68	-1.48	0	-1.25	-3.94	-0.85
5400	0	0	0	0	0	0	0	0
6650	+0.42	+0.05	+0.60	+0.64	+0.18	+1.25	+1.06	-0.81
8350	+0.77	+0.17	+0.92	+0.82	+0.15	+2.95	+0.69	-0.20
9250	+0.80	+1.00	+1.50	+0.85	+0.70	+3.85	0	-4.26
10650	+1.05	+0.42	+1.62	+1.48	+0.57	+5.25	+1.34	-3.45
11950	+1.17	+0.67	+2.25	+2.12	+1.08	+6.55	+2.49	-6.41
13500	+1.35	+0.92	+2.72	+2.48	+1.37	+8.10	+2.90	-8.47
14000	+1.42	+0.97	+2.77	+2.47	+1.35	+8.60	+2.49	-7.98

TABLE 5.11 (continued)

Temperature 92°K								
H(Oe) \ $-\beta'$	30°	75°	120°	X	Y	$\delta H_x \cdot 10^{-3}$	$\delta\Delta \times 10^3$	$\delta\alpha \times 10^3$
1300	+2.55	+8.20	-2.95	-13.90	-5.50	-4.10	-47.9	+54.97
1900	-0.30	+4.65	-0.90	-7.35	-0.60	-3.50	-24.7	+48.18
3000	-1.10	+1.57	-1.08	-4.84	+0.02	-2.40	+16.1	-0.92
4150	-0.65	+0.52	-0.65	-2.97	0	-1.25	-9.9	-0.04
5400	0	0	0	0	0	0	0	0
6650	+0.32	+0.25	+0.65	+0.56	+0.33	+1.25	+1.24	-2.92
8350	+0.95	+0.40	+1.10	+0.77	+0.15	+2.95	+1.34	-0.68
9250	+1.17	+0.32	+1.82	+1.82	+0.65	+3.85	+4.80	-6.09
10650	+1.55	+0.85	+2.27	+1.78	+0.72	+5.25	+3.86	-5.83
11950	+1.85	+1.42	+2.85	+1.93	+1.00	+6.55	+3.70	-8.28
13500	+2.15	+1.60	+3.40	+2.42	+1.25	+8.10	+4.92	-10.48
14000	+2.22	+1.82	+3.65	+2.53	+1.42	+8.50	+5.02	-12.09

TABLE 5.12

Temperature °K	213	131	92
Effective gauge factor	2.22	2.09	1.98
$(C_1 + C_2) \times 10^6$	-159.0	-167.4	-169.5
$(C_1 - \frac{1}{2}C_2) \times 10^6$	-45.50	-43.75	-42.00
$\delta X_{14} - \delta X_9$	+1.6	+1.8	+1.7
$\delta Y_{14} - \delta Y_8$	+1.1	+1.2	+1.1
$\delta\alpha_{14} - \delta\alpha_8$ (radians)	-0.0044	-0.0084	-0.0111
$\delta\Delta_{14} - \delta\Delta_8$ (radians)	+0.00073	+0.00194	+0.00293
$(C_1' + C_2') \times 10^{10}$ (from Eqn. 2.63)	-1.25	-1.18	-0.80
$(C_1' + C_2') \times 10^{10}$ (from Eqn. 2.64)	-0.52	-0.33	-0.17

Chapter Six.

DISCUSSION OF RESULTS AND CONCLUSIONS

§ 6.1 The Anisotropy Measurements.

The measurements of the first anisotropy constant, K_1, using the (110) nickel specimen were undertaken to verify by comparison with existing data that the modified version of the torque meter, together with the temperature control apparatus, was functioning correctly. From figure 4.6 it will be seen that in fact the present results for K_1, lie within the range of existing measurements so that it may be concluded that the apparatus was working satisfactorily.

The primary purpose of the anisotropy measurements on the (111) nickel specimen was the accurate determination of the second anisotropy constant K_2. This was accomplished, but only after an adequate theory for the magnetization process in high fields had been developed. The values for K_2 obtained by previous investigators that existed when the present work was started are summarised in the table below.

$K_2 \times 10^{-4}$ (erg cm^{-3})	Temp.	Method	Reference
+ 5.3	Room	MC	McKeehan (1937), Honda, et al. (1935).
+ 1.09	Room	MC	Nakamura (1955)
- 3.6	20°C	MW	Reich (1956)
- 14 ± 0.5	4.2°K	MW	Reich (1956)
- 6.06	20°C	MW	Barlow and Standley (1958)
+ 2.34	26°C	T	Sato and Chandrasekhar (1958)
+ 31.7	77°K	T	Sato and Chandrasekhar (1958)

(MC, from measurements of magnetization curves; MW, from microwave resonance technique; T, from torque curves.)

This table reveals considerable disagreement between previous measurements and it was therefore thought to be desirable to make the present measurements of K_2. One explanation put forward (Pearson 1960, Anderson and Donovan 1959) for the discrepancies between the values of K_2 given in the table was that experiments by static and by microwave resonance techniques do not, in fact, measure anisotropy constants under the same conditions, and that the former correspond to constant stress and the latter to constant strain. However, it is possible to calculate the difference between the effective value of K_2 at zero stress and at constant strain, and this has been done in appendix A3 where it was found that ΔK_2 was 0.57×10^4 erg cm^{-3}. It is therefore unlikely that this explanation of the discrepancies exhibited in the table is correct, and it might be expected that the data obtained from direct torque measurements would be more reliable. In fact the magnitude for K_2 obtained by Sato and Chandrasekhar, using direct torque measurements, agrees well with the present measurements at room temperature, and it is believed, for the reasons stated in Chapter 4, that an error in sign was made in Sato and Chandrasekhar's measurements.

After the publication of the present results (Birss and Wallis 1964, Appendix A4), further direct torque measurements over a wide range of temperatures were reported by Hofmann (1964a), who used a conventional torque measuring system in conjunction with a single crystal nickel sphere.

However, he obtained (Hofmann 1964b) the expression

$$\Gamma_6 = \frac{1}{18}\left(K_2 - \frac{81}{16}\frac{K_1^2}{HI_s}\right) \qquad (6.1)$$

for the amplitude of the sin $6\beta'$ component of the torque curve, by making the incorrect assumption that the magnetization vector always moves in a plane containing the easy direction and the field direction. Comparison of the above expression with equation 2.35 shows the extent by which his analysis was in error. Hofmann's results nevertheless agree in sign and order of magnitude with the present work. A microwave study of the variation of K_1 and K_2 with temperature has also recently been reported by Rodbell (1964) who used single crystal whiskers and platelets of nickel. He obtained results which agreed in order of magnitude and sign with the present measurements.

From figure 4.6 it can be seen that the variation with temperature of K_2 obtained in the present work becomes progressively more rapid as the temperature is lowered, but that at a temperature of about 100°K this trend is reversed and the variation begins to decrease again. This feature is exhibited even more strongly in the results of Hofmann, where K_2 is actually found to reach a maximum value at about 130°K. (It should be born in mind, however, that these latter results must be to some extent incorrect owing to the method of analysis used). It is thus clear that the variation with temperature of K_2 cannot be explained by assuming that it is proportional to some power (e.g. the 21st) of the reduced magnetization, as has been described in chapter 1,

and another explanation for the temperature variation of K_2 must be found. Such an explanation might be that the second anisotropy constant arises from a pseudomultipole interaction which depends for its existence on the non-alignment of the spins. Such interactions would be similar to the pseudo-dipolar interaction suggested by Van Vleck (1937) for K_1 in nickel. He pointed out thatbecause nickel has cubic symmetry, pseudodipolar interactions cannot lead to any anisotropy when the spins are perfectly aligned. (He also showed that the pseudoquadrupolar and higher order interactions are not allowed unless $S \geq 1$, so that in nickel, where $S \sim \frac{1}{2}$, these interactions may not exist either). Without perfect alignment of the spins he showed that a second-order pseudodipolar contribution to K_1, may appear which is of the same order of magnitude as that due to a pseudoquadrupolar interaction. However, by implication the second-order pseudodipolar anisotropy must presumably decrease as the temperature approaches absolute zero and the spins become more nearly aligned. Although no corresponding decrease in K_1, has been observed as the temperature approaches absolute zero, a similar argument might still be fruitful in explaining any decrease in K_2 with decreasing temperature.

Joenk (1963), using the original Van Vleck theory, amended by spin wave analysis, has evaluated the contributions to $K_1(0)$ and $K_2(0)$ from pseudodipolar, quadrupolar and dipole-quadrupolar interactions. He did not attempt to determine the temperature variation of the anisotropy constants, but found that

$$K_1(0) = K_{1D}(0) + K_{1Q}(0) + K_{1DQ'}(0) + K_{1D'}(0) + K_{1Q'}(0) \quad (6.2)$$

$$K_2(0) = K_{2DQ}(0) + K_{2Q}(0) + K_{2D}(0) \quad (6.3)$$

where the subscripts D and Q indicate the pseudodipolar or pseudoquadrupolar origin of the terms, while the dash indicates a second-order interaction. Joenk assumed that S = ½ for nickel, which meant that all quadropole-like terms were zero, and he was then able to obtain two equations in D (the pseudodipolar coupling constant which is proportional to D_{ij} in Van Vleck's 1937 theory) namely

$$K_1(0) \doteq K_{1D}(0) + K_{1D'}(0)$$

$$= -\frac{9}{8} N S^2 \frac{D^2}{2J} \left\{ \frac{\eta (1 + 0.222\Delta)\Omega_{14}}{(2SZ - \eta)} + \frac{D(3\Omega_{16} - 7\Omega_{14} - 42S\Delta)}{2J\,(2SZ - 1)^2} \right\} \qquad (6.4)$$

and

$$K_2(0) = K_{2D(0)}$$

$$= -\frac{27}{8} N S^2 D^3 \left(\frac{\Omega_{26} + 54S\Delta)}{2J(2SZ - 1)^2} \right) \qquad (6.5)$$

where for f.c.c. nickel the various constants have the following values $\eta = 0.9793$, $\Delta = 1$, $\Omega_{14} = 2$, $\Omega_{16} = \frac{9}{2}$, $\Omega_{26} = -\frac{39}{2}$, $Z = 12$, and $JS = 2.5 \times 10^{-14}$ ergs. Joenk extrapolated the known values of K_1 (T) to obtain K_1 (0) = -8.5×10^5 erg cm^{-3} and was thus able to obtain a value for D from equation 6.4. He chose the negative sign for D (by inspection of equation 6.5) since the best experimental evidence (Sato and Chandrasekhar) indicated that $K_2(0)$ was positive. He then used this value of D in equation 6.5 to obtain the magnitude of K_2 (0) = 0.271×10^5 erg cm^{-3} and concluded that this was not in good agreement with experiment , which indicated at that time that $K_2(0) \approx 4 \times 10^5$

erg cm^{-3}.

From the present measurements of K_2 by torque methods it is clear that the sign of D, obtained by Joenk, must be changed. Further inspection of equation 6.4 shows that the second order term in D^3 is very small so that the magnitude of $D = 3.84 \times 10^{-15}$ erg will be approximately unchanged, and that $K_2(0) \simeq -0.271 \times 10^5$ erg cm^{-3}. Inspection of fig. 4.6 shows that this may now be in fairly good agreement with experiment but that clearly further low temperature measurements are desirable before such an assertion can be made with certainty, especially since the change in trend of the variation of K_2 with temperature only just becomes apparent at the lowest temperatures at which measurements have been made so far.

§6.2 The Theory for the Magnetization Process in a (111) Plane.

In§ 2.2, equations were derived that specified the behaviour of the magnetization vector as a function of the applied field. The calculations are appropriate to the high field or 'single-vector' region, that is the region where the specimen is magnetized as a single domain. In order that the equations could be solved analytically it was necessary to introduce a number of approximations which were only valid for large applied fields and it was shown in§ 2.2 that at first sight these approximations appear to start to break down at fields of about 6 koe. However, more detailed analysis showed, in fact, that the approximations introduced very little error down to 2 koe. There is thus a discrepancy between the

theoretical and experimental torque curves which in fact diverge at applied fields between 5 and 7 koe. It must be emphasised, at this point, that there is no reason to believe that the theory is incorrect at higher fields since experiment and theory agree very well there.

The various possible reasons for the divergence of the theory from experiment will now be discussed separately.

§6.2.1. At first sight, the most likely possibility appears to be that the approximations used in the theory are not valid. As already stated, it has been shown that the approximations made should not introduce substantial errors until the field is reduced to about 2 koe . However, the analysis is fairly complicated so that another method of estimation is desirable to confirm that these calculations are correct, especially since it appears that the approximations themselves become invalid at about the field magnitude where theory and experiment diverge. Full numerical solution, by computer, of the equations that define the position of the I_s vector (equations 2.24) would fulfill this need.

§ 6.2.2. The onset of a multidomain state at a particular field (e.g. 6 koe .) would invalidate the theory below this field magnitude. However, the field at which the specimen becomes saturated may easily be estimated, although the estimate depends on the direction of the applied field, H. If H is along a <112> direction, saturation will occur when H ~ 200 oe, assuming $K_1 = 5 \times 10^5$ erg cm^{-3}. The demagnetizing field

of the specimen has not been taken into account here but it cannot alter, by the order of magnitude required, the field that must be applied externally to obtain saturation. Hence there can be no question of the onset of a general multidomain state which would invalidate the theory at fields as high as 6 koe. This statement must be qualified, because the shape of the specimen was not ideal. An ellipsoidal surface is required for the magnetization to be uniform within the specimen, but the specimen was actually a thin disc, which approximates closely to the required shape. Nevertheless there is a possibility of closure domains persisting in the 'corners' of the disc at fields higher than those estimated for saturation. However the volume involved would be very small so that this can only be a minute contributory cause of the discrepancy.

§6.2.3. The possibility that the torque measuring equipment was not functioning properly must be ruled out as demonstrated by the measurements of K_1, values of which fell within the range of accepted values to be found in the literature. In particular, any variation of the sensitivity of the torque-meter with field could be important. However this point was carefully checked and no change in sensitivity could be detected.

§6.2.4. Any error in the orientation of the (111) plane relative to the surface of the specimen might mean that the field was not applied in the correct plane and consequently that the theory would not apply. Careful X-rays

analysis over a large area of the surface of the disc (chapter 3) showed that the (111) plane was within 15 minutes of the surface, although internal twinning or other irregularities would not be detected by X-ray analysis owing to the very small panetration depth of the X-rays. It is, however, unlikely that a good $6\beta'$ torque curve such as that shown in fig. 4.3 would have been obtained, had such irregularities been present. It must therefore be concluded that neither the present specimen nor the torque meter could be the cause of the observed discrepancy.

§ 6.3 The Magnetostriction Measurements on Nickel.

These measurements were made in the (111) plane so that the theoretical calculations developed to describe the movement of the magnetization vector in high fields could be employed. These calculations enabled the saturation magnetostriction to be predicted, and the difference between the measured and predicted values of the saturation magnetostriction then permitted the forced magnetostriction to be deduced. In principle it is possible to measure both the first and second forced magnetostriction constants separately, however in the (111) plane it was only possible to measure the sum $C_1' + C_2'$. Only measurements between 8 and 14koe were employed to ensure that the theory used was applicable. It was found that the two methods used to determine $C_1' + C_2'$ were not entirely consistent, and it was concluded that the cause of the inconsistencies was the inability to match exactly the active and dummy strain gauges. This difficulty arose because

although it was possible to match the gauges so that changes in resistance arising from temperature changes were exactly cancelled, it was still not generally possible to simultaneously match the gauges for magnetoresistance. This is presumably because of the prescence of variable amounts of impurity in the strain gauge wire. The difficulty was aggravated at the lower temperatures since the magneto-resistance of the gauges become large and very careful angular alignment of the dummy and active gauges was necessary.

From the results it can be ssen that the forced magnetostriction decreases with decrease in temperature, as is expected, since it arises from the degree of disalign-ment of the spins, which will decrease as the temperature is lowered. The magnitude and sign of these results are also in reasonable agreement with the recently published results of Lourens and Alberts (1964), who measured the first and second forced magnetostriction constants of nickel at room temperature and found $h_1' = C_1' = -0.84 \times 10^{-10}$ oe^{-1} and $h_2' = C_2' = -0.33 \times 10^{-10}$ oe^{-1}. Their value of $C_1' + C_2'$ is thus -1.50×10^{-10} oe^{-1}, and may be compared with the results given in Chapter 4 (and in Chapter 5) namely $C_1' + C_2' \simeq -1 \times 10^{-10}$ oe^{-1} at 213°K.

Using the values of $C_1' + C_2'$ obtained in the field range 8 to 14 koe, Δ and α (the in-plane and out-of-plane angles specifying $\underline{I}_s$ relative to $\underline{H}$) were estimated for fields from 8 koe down to 1.5 koe so that the extent of the agreement with values obtained theoretically could be

inspected. From figures 4.8.1 and 4.8.2 it can be seen that the agreement in this field range is better for Δ than for α which reflects the fact that Δ (theoretical) is determined directly from the torque measurements, while α (theoretical) is found from the theory which itself is not particularly reliable below 6. koe. Clearly, if the magnetostriction measurements could be improved it should be possible to use them to measure α directly but it is doubtful if this could be done using a strain-gauge technique.

§6.4 The Anisotropy Measurements on Gadolinium.

The anisotropy measurements on the gadolinium specimen were of a tentative nature. They were undertaken because the specimen was available and the torque measuring apparatus, which was already being used for successful measurements on nickel, was also available. Such measurements as could easily be made were therefore carried out, and in fact the first and second anisotropy constants, K_1' and K_2' were obtained from torque curve slopes around zero torque over a range of temperatures from the Curie point down to $77^{\circ}K$. Measurements of the angle of the easy-cone of magnetization were also made and these measurements agree well with those of Corner Roe and Taylor (1962) and Graham (1963, 1964). However, two features of these experiments were not entirely staisfactory and these will now be discussed.

First, the sensitivity of the torque meter was suitable for measurements on nickel. The volume of the nickel specimen was roughly the same as that of the

gadolinium specimen so that the torques developed on the latter would have been too large for the torque meter. Hence it was only possible to make measurements in field directions where the torque was nearly zero and this only permitted the measurement of the slope of the torque curve and the semi-angle of the easy cone of magnetization. More comprehensive measurements of the complete torque curve would have made it possible to extract the maximum information from the experiments by the use of Fourier analysis. This would also enable the higher-order anisotropy constant to be measured which would be desirable since there is some evidence (Rodbell and Moore 1964) that these higher order constants may not be insignificant.

Secondly, the maximum field available was only 14 koe . The anisotropy constants were found by extrapolating the results obtained to infinite field by plotting them against 1/H and extrapolating to find the interecpt at 1/H = 0. In the case of gadolinium this procedure was unreliable since the variation of the torque slope against 1/H was not linear and this could lead to fairly substantial uncertainties in the intereept at 1/H = 0. This difficulty appears to arise from the large variation with field of the saturation magnetization over a wide temperature range (Nigh Legvold and Spedding 1963) and may clearly only be resolved by making measurements in much higher fields.

For the two reasons just discussed, and because Graham (1964) had already made adequate torque measurements on gadolinium at fields up to 20 koe , it was not considered

expedient to continue with these particular measurements of anisotropy.

§6.5 The Domain Observations on Gadolinium.

Domain observations were made by a colloid technique on a single-crystal gadolinium specimen which was prepared at the same time as the single crystal disc used for anisotropy measurements. Both the preparation of the colloid and the preparation of the surface of the specimen were found to be critical for success. The colloid used has a Xylene base and was prepared in a similar manner to that used by Gustard (1964) for the preparation of acetone based colloids except that the dispersant used to keep the colloid in suspension was Aerosol O.T. (diethylhexyl sulphosuccinate). The surface was prepared by careful polishing and then by ion bombardment. Domains were observed in the region between 273°K and the freezing point of the colloid, and they were similar in form to those seen on cobalt. This was to be expected since both cobalt and gadolinium have (in this temperature range) a large uniaxial anisotropy. Domains on gadolinium were, however, much harder to observe than on cobalt owing to the proximity of the Curie point, which meant that the saturation magnetization was small. In order to increase the sensitivity of the colloid, the particle size was increased with a consequent reduction in detail and this explains the very poor definition shown in figure 4.13. Clearly it would be of interest to make domain observations in the region where there is an easy cone of magnetization. However, such

observations were not possible owing to the high freezing point of the colloid used and owing to difficulties of atmospheric condensation on the specimen. These difficulties would be most easily overcome if the domains were observed by the Kerr-rotation technique although again difficulty may be experienced near the Curie point where the magnetization is small.

§ 6.6 Proposals for Further Research.

A number of ways in which the measurements described here may be extended have been indicated in the foregoing discussion. These will now be summarised and a further suggestion for a connected longer-term experiment will be made.

§6.6.1. The torque measurements on the (111) nickel specimen should be extended to lower (liquid-helium) temperatures. This would establish the low-temperature behaviour of K_2 and also allow a reasonable estimate of $K_2(0)$ to be made for comparison with the estimated theoretical value (Joenk 1963). Such an extension of the present measurements would require the production of somewhat higher applied fields (possibly by the use of a superconducting solenoid) than are currently available, because there is, at 77°K, only a small high-field range over which K_2 may be determined from torque curve amplitudes. This range decreases as K_1 increases and since K_1 will be much larger at 4.2°K, than at 77°K, it will be difficult to measure K_2 accurately here unless the maximum applied field available is increased.

§6.6.2. Improvement and extension of the magnetostriction measurements on the (111) specimen depends on the method of measuring strain and the wire strain gauges used for this purpose were found to be not entirely satisfactory. Extension of the present measurements must therefore await the introduction of a more satisfactory means of measuring the very small strains involved.

§6.6.3. There is clearly scope for improving both the anisotropy measurements and the domain observations on gadolinium. The former measurements again require much higher fields than are available at present, to allow the accurate extrapolation of the effective anisotropy constants to infinite field. When adequately large applied fields become available the torque measurements might be usefully extended to lower temperatures (e.g. 4.2°k).

The domain observations should be extended at least to a temperature where there is a cone of easy directions, so that the effect of this type of magnetization on the domain structure may be studied. It might prove to be possible to obtain the cone angle from the domain configurations to provide confirmation of the cone angle obtained indirectly from the present torque measurements. To do this a new colloid must be developed

since Xylene freezes at $-40^{\circ}C$, a temperature which is too high. Alternatively the magnetic Kerr effect might conveniently be used for domain observations. (Roberts and Bean 1954).

§6.64 The torque meter described in this work was originally designed so that anisotropy measurements might be made at high pressures. The torque meter is particularly suitable for such measurements because of its small volume, because it may be calibrated under working conditions and because it only requires electrical leads to be introduced into the pressure vessel.

Measurements at high pressures would allow a study to be made of the variation of the anisotropy constants with the change in volume of the specimen.

The variation of K_1 with pressure is of use in correcting the temperature dependence of this constant for the effect of thermal expansion. Carr (1958a)drew attention to the fact that before the experimentally measured temperature variation of K_1 could be compared with, for instance, Zener's tenth power law for K_1, the experimental values must be corrected for the effect of thermal expansion. Complete corrections may only be made when the pressure dependence of K_1, is known (Birss 1964). It is therefore suggested that such high-

pressure anisotropy measurements be made on nickel and gadolinium to obtain the variation of the anisotropy constants with pressure. This would provide continuity with present anisotropy measurements made near zero (atmospheric) pressure on these metals.

ACKNOWLEDGEMENTS

I wish to acknowledge the consistent help and encouragement afforded me by my supervisor, Dr R.R.Birss. I am also indebted to many colleagues and friends in particular, S.K.Dey, S.R.Adamson and R.F.Pearson for helpful discussions.

It is a pleasure to thank A.Marotta, K.J.Tauer and R.J.Weiss for supplying the gadolinium single crystal, and the Department of Scientific and Industrial Research for the provision of a maintenance grant.

REFERENCES.

Akulov, N.S. 1928, Z. Physik, 52, 389.
1929, Z. Physik, 57, 249.
1930, Z. Physik, 64, 817, and 59, 254.
1936, Z. Physik, 100, 197.

Aldenkamp, A.A., Marks, C.P., and Zijlstra, H., 1960, Rev. Sci. Instrum., 31, 544.

Anderson, J.C., and Donovan, B., 1959, Proc. Phys. Soc., 73, 593.

Barlow, G.S., and Standley, K.J., 1958, Proc. Phys. Soc., 71, 45.

Becker, R., and Döring, W., 1939, "Ferrogmagnetismus", Springer, Berlin).

Bethe, H., 1933, Handb. d. Physik, 24, 595.

Birss, R.R., 1959, Phil. Mag. Suppl., 8, 252.

Birss, R.R., and Lee, E.W., 1960, Proc. Phys. Soc., 76, 502.
1961, Proc. Roy. Soc., 263, 387.

Birss, R.R., and Wallis, P.M., 1963, Proc. Phys. Soc., 81, 368.
1963, Phys. Let., 4, 313.
1963, J. Sci. Inst., 40, 551.
1964, Proceedings of the International Conference on Magnetism, Nottingham, p.744.
1965, J. Sci. Inst., 42, 322.

Birss, R.R., 1964, "Symmetry and Magnetism", (North-Holland, Amsterdam).

Bitter, F., 1931, Phys. Rev., 38, 1903.

Block, F., and Gentile, G., 1931, Z. Physik, 70, 395.

Block, F., 1932, Z. Physik, 74, 295.

Bozorth, R.M., and Williams, H.J., 1941, Phys. Rev. 59, 827.

Bozorth, R.M., 1951, "Ferromagnetism", (D. Van Nostrand, New York).

1954, Phys. Rev., 96, 311.

Brailsford, F., 1960, "Magnetic Materials", 3rd. Edn. (Methuen, London).

Brenner, R., 1957, Phys. Rev., 107, 1539.

Brooks, H., 1940, Phys. Rev., 58, 909.

Brown, W.F., 1953, Rev. Mod. Phys., 25, 131.

Calhoun, B.A. and Carr Jr. W.J., 1955, Conference on Magnetism and Magnetic Materials, (A.I.E.E., 1956, P.107, New York).

Callaway, J., 1958, "Solid State Physics", (Acad. Press. Inc., New York).

Callen, E.R. and Callen, H.B., 1960, J. Phys. Chem. Solids, 16, 310.

Carr, W.J., 1958a, Phys. Rev., 109, 1971.

Carr, W.J., 1958b, Seminar on Magnetic properties of Metals and Alloys, National Metals Congress and Exposition, Cleveland, (Am.. Soc. for metals).

Corner, W.D., Roe, W.C., and Taylor, K.N.R., 1962, Proc. Phys. Soc., 80, 927.

Croft, G.T., Donahoe, F.J., and Love, W.F., 1955, Rev. Sci. Instrum., 26, 360.

Craik, D.J., and Griffiths, P.M., 1957, Proc. Phys. Soc., B 70, 1000.

Elmore, W.C., 1938, Phys. Rev., 54, 309.

Fletcher, G.C., 1954, Proc. Roy. Soc. A 67, 505.
1955, Proc. Phys. Soc. A 68, 1066.

Friedel, J., 1955, J. Phys. Radium, 16, 829.
1958, J. Phys. Radium, 19, 573.

Gans, R., and Von Harlem, J., 1933, An.. Phys., Lpz., 16, 162.

Garrood, J.R., 1962, Proc. Phys. Soc., 79, 1252.

Gersdorf, R., 1961, Thesis, Amsterdam .

Graham, C.D., 1958, Phys. Rev., 112, 1117.
1962, J. Phys. Soc. Japan, 17, 1310.
1963, J. Appl. Phys., 34, 1341.
1964, Proceedings of the International Conference on Magnetism, Nottingham, p.740.

Gusev, A.A., 1954, Doklady Akad. Nauk, U.S.S.R., 98, 749.

Gustard, B., 1964, Thesis, University of London.

Hámos, L.V., and Thiessen, P.A., 1931, Z. Physik, 71, 442.

Harrison, F.W., 1955, J. Sci. Instrum., 33, 5.

Herring, C., and Kittel, C., 1951, Phys. Rev., 81, 869.

Herring, C., 1960, J. Appl. Phys. Suppl, 31, 3S.

Heisenberg, W., 1928, Z. Physik, 49, 619.
1931, Z. Physik, 69, 287.

Heller, G., and Kramers, H., 1934, Proc. Roy. Acad. Amsterdam, 37, 378.

Honda, K., and Kaya, S., 1926., Sci. Repts. Tôhoku Imp. Univ., 15, 721.

Honda, K., Masumotc, H., and Shirakawa, Y., 1935, Sci. Repts. Tôhoku Imp. Univ., 24, 391.

Hofmann, U., 1964a, Phys. Stat. Sol., 7, 145.

Hofmann, U., 1964b, Exptl. Tech. Physik, 12, 417.

Holstein, T., and Primakoff, H., 1940, Phys. Rev., 58, 1098.

Hozelitz, K., 1952, "Ferromagnetic Properties of Metals and Alloys", (Oxford).

Humphrey, F.B., and Johnston, A.R., 1963, Rev. Sci. Instrum, 34, 348.

Joenk, R.J., 1963, Phys. Rev., 130, 932.

Katayama, T., 1951, Sci. Reps. Tôhoku Univ. A.3, 341.

Keffer, F., 1955, Phys. Rev., 100, 1692.

Keffer, F., and Oguchi, T., 1960, Phys. Rev., 117, 718.

Kittel, C., 1959, J. Phys. Radium, 20, 135.

Kittel, C., and Van Vleck, J.H., 1960, Phys. Rev., 118, 1231.

Klein, N.J., and Smith, R.S., 1950, Phys. Rev., 81, 1111.

Kornetzki, M., 1934, Z. Physik, 87, 560.

Laurens, J.A.J., and Alberts, L., 1964, Sol. State Communications, 2, 141.

Lawton, H. and Stewart, K.H., 1948, Proc. Roy. Soc., A 193, 72.

Lee, E.W., 1955, Rep. Progr. Phys. XVIII, 184.

Mahajani, G., 1929, Trans. Roy. Soc., 228A, 63.

Mason, W.P., (1954), Phys. Rev., 96, 302.

McKeehan, L.W., 1937, Phys. Rev. 51, 136.

Miller, D.S., 1950, Rev. Sci. Instrum., 21, 605.

Nakamura, Y., 1955, J. Phys. Soc. Japan, 10, 937.

Néel, L., 1944a, J. Phys. Radium., 5, 241.
1944b, J. Phys. Radium., 5, 265.

Nigh, H.E., Legvold, S., and Spedding, F.H., 1963, Phys. Rev., 132, 1092.

Osborn, J.A., 1945, Phys. Rev., 67, 351.

Pearson, R.F., 195
1960, Proc. Phys. Soc., 75, 315.

Penoyer, R.F., 1956, Proc. A.I.E.E., Conf. on Magnetism and Magnetic Materials, New York, (Institute of Electrical Engineers) p.365.

Reich, K.H., 1956, Phys. Rev. 101, 1647.

Roberts, B.W., and Bean, C.P., 1954, Phys. Rev., 96, 1494.

Rodbell, D.S., 1964, Proc. Int. Conf. Magnetism, (Nottingham), p.420.

Rodbell, D.S., and Moore, T.W., 1964, Proc. Int. Conf. Magnetism, (Nottingham), p.427.

Rode, V.E., and Herrmann, R., 1964, Soviet Phys. J.E.T.P., 19, 1081.

Sato, H., and Chandrasekhar, B.S., 1956, J. Phys. Chem. Solids, 1, 228.

Shull, C.G., 1955, 'Les Electrons Dans Les Metaux', edited by R.S. Stoops (Coudenberg, Bruxelles), p.227.

Slater, J.C., 1936a, Phys. Rev., 49, 537.
1936b, Phys. Rev., 49, 931.
1959, Rev. Mod. Phys., 25, 199.

Stoner, E.C., 1933, Phil. Mag., 15, 1018.
1938, Proc. Roy. Soc., (London), 165A, 372.
1945, Phil. Mag., 36, 803.
1950, Reps. Prog. Phys., XIII, 83.
1951, J. Phys. Radium, 12, 371.

Spedding, F.H., and Daane, A.H., 1961, "The Rare Earths" (Wiley, New York).

Tarasov, L.P., and Bitter, F., (1937), Phys. Rev., 52, 353

Van Kranendonk, J., 1955a, Physica XXI, 749.
1955b, Physica XXI, 925.

Van Vleck, J.H., 1937, Phys. Rev., 52, 1178.
1956, Conference on Magnetism and Magnetic Materials, Boston-Mass., (A.I.E.E. Special Publication t-91).
1959, J. Phys. Radium,, 20, 124.

Vautier, R., 1954, Thesis, University of Paris.

Von Auwers, O., 1935, Z. Physik, 34, 824.

Vonsovsky, S.V., 1940, J. Phys. Moscow, 3, 181.

Weiss, P., 1907, J. de Phys., 6, 661.

Weiss, P.R., 1948, Phys. Rev., 74, 1493.

Williams, H.J., 1937, Phys. Rev., 52, 747.

Wohlfarth, E.P., 1953, Revs. Mod. Phys., 25, 211.

Zener, C., 1954, Phys. Rev. 96, 1335.

Reprinted from
Proceedings of the Physical Society, Vol. 81, Part 2, No. 520, pp. 368 - 370
1963
Printed in Great Britain by J. W. Arrowsmith Ltd., Bristol 3

APPENDIX A1

The Temperature Dependence of Magnetostriction

In a recent paper Kittel and Van Vleck (1960) have extended the conventional theory of the variation with temperature of the anisotropy of cubic crystals to include that of the magnetoelastic constants. Specifically, if these constants are defined by the equations (see, for example, Birss 1959)

$$V_1^0 = L_0+L_1\alpha_1^2+L_2\alpha_1^4+L_3\alpha_2^2\alpha_3^2 \qquad V_2^0 = L_0+L_1\alpha_2^2+L_2\alpha_2^4+L_3\alpha_3^2\alpha_1^2$$
$$V_3^0 = L_0+L_1\alpha_3^2+L_2\alpha_3^4+L_3\alpha_1^2\alpha_2^2 \qquad V_4^0 = M_0\alpha_2\alpha_3+M_1\alpha_1^2\alpha_2\alpha_3$$
$$V_5^0 = M_0\alpha_3\alpha_1+M_1\alpha_2^2\alpha_3\alpha_1 \qquad V_6^0 = M_0\alpha_1\alpha_2+M_1\alpha_3^2\alpha_1\alpha_2$$

their predicted temperature dependence is given by

$$L_1(T) = [L_1(0)+\tfrac{6}{7}L_2(0)+\tfrac{1}{7}L_3(0)]\zeta^3-[\tfrac{6}{7}L_2(0)+\tfrac{1}{7}L_3(0)]\zeta^{10}$$
$$L_2(T) = L_2(0)\zeta^{10} \qquad L_3(T) = L_3(0)\zeta^{10}$$

$$M_0(T) = [M_0(0)+\tfrac{1}{7}M_1(0)]\zeta^3-\tfrac{1}{7}M_1(0)\zeta^{10} \qquad M_1(T) = M_1(0)\zeta^{10} \qquad (1)$$

where ζ is the reduced magnetization.

The first purpose of this letter is to point out that the calculation of Kittel and Van Vleck is appropriate to constant lattice strain, whereas the reduced magnetization refers to constant stress. The state of strain of a crystalline lattice at temperature T differs from that at $T = 0$ partly because of thermal expansion and partly because of magnetostriction. The normal thermal expansion is supplemented by a change in magnetostriction with temperature to give a deformation of the lattice which is principally an isotropic volume strain, $\omega = \omega(T)$, but is partly an anisotropic deformation

that depends on the direction of magnetization. Since, however, it is observed experimentally that, for the ferromagnetic metals at least (see Callen and Callen 1960), the magnitude of the saturation magnetization depends on ω but not on the direction of the magnetization relative to the crystal lattice, it is possible to express the spontaneous magnetization $I_s(T, \omega)$, at temperature T and volume strain ω, approximately in the form

$$I_s(T, \omega) = I_s(T, 0) + \frac{\partial I_s(T, \omega)}{\partial \omega}\omega$$

where $\omega(0) = 0$. The quantity observed experimentally, $\zeta = I_s(T, \omega)/I_s(0, 0)$, should therefore be replaced in equations (1) by either $I_s(T, \omega)/I_s(0, \omega)$ or $I_s(T, 0)/I_s(0, 0)$, that is by

$$\zeta' = \zeta - \frac{1}{I_s(0, 0)}\frac{\partial I_s(T, \omega)}{\partial \omega}\omega.$$

The second purpose of this letter is to present expressions, corresponding to (1), for the temperature dependence of the magnetoelastic coupling constants for hexagonal materials as derived from the theory of Kittel and Van Vleck. For hexagonal materials the magnetoelastic coupling constants may be defined by the equations

$$V_1^0 = L_0+(L_1-L_3)\alpha_1^2+L_2\alpha_2^2+4L_3\alpha_1^2\alpha_2^2+L_4\alpha_2^2\alpha_3^2+(L_5+L_3)\alpha_3^2\alpha_1^2$$
$$V_2^0 = L_0+(L_2+L_3)\alpha_1^2+L_1\alpha_2^2-4L_3\alpha_1^2\alpha_2^2+L_5\alpha_2^2\alpha_3^2+(L_4-L_3)\alpha_3^2\alpha_1^2$$
$$V_3^0 = M_0+M_1(\alpha_1^2+\alpha_2^2)+M_2(\alpha_1^2+\alpha_2^2)\alpha_3^2$$
$$V_4^0 = \alpha_2\alpha_3(N_0+N_1\alpha_3^2) \qquad V_5^0 = \alpha_3\alpha_1(N_0+N_1\alpha_3^2)$$
$$V_6^0 = \alpha_1\alpha_2[(L_1-L_2-L_3)-(L_4-L_5-L_3)\alpha_3^2+2L_3(\alpha_1^2-\alpha_2^2)].$$

These equations may also be written in the form

$$V_1^0 = \frac{1}{3}(3L_0+L_1+L_2+3L_4+3L_5)Y_{0,0}-\frac{1}{21}(7L_1+7L_2-L_4-L_5)Y_{2,0}$$
$$+\frac{1}{42}(7L_1-7L_2-6L_3-L_4+L_5)Y_{2,2}-\frac{4}{35}(L_4+L_5)Y_{4,0}$$
$$+\frac{1}{105}(L_3-L_4+L_5)Y_{4,2}-\frac{1}{210}L_3Y_{4,4}$$

$$V_2^0 = \frac{1}{3}(3L_0+L_1+L_2+3L_4+3L_5)Y_{0,0}-\frac{1}{21}(7L_1+7L_2-L_4-L_5)Y_{2,0}$$
$$-\frac{1}{42}(7L_1-7L_2-6L_3-L_4+L_5)Y_{2,2}-\frac{4}{35}(L_4+L_5)Y_{4,0}$$
$$-\frac{1}{105}(L_3-L_4+L_5)Y_{4,2}+\frac{1}{210}L_3Y_{4,4}$$

$$V_3^0 = \frac{1}{15}(15M_0+10M_1+2M_2)Y_{0,0}-\frac{2}{21}(7M_1-M_2)Y_{2,0}-\frac{8}{35}M_2Y_{4,0}$$

$$V_4^0 = \frac{1}{21}(7N_0+3N_1)Y_{2,-1}+\frac{2}{35}N_1Y_{4,-1} \qquad V_5^0 = \frac{1}{21}(7N_0+3N_1)Y_{2,1}+\frac{2}{35}N_1Y_{4,1}$$

$$V_6^0 = \frac{1}{42}(7L_1-7L_2-6L_3-L_4+L_5)Y_{2,-2}+\frac{1}{105}(L_3-L_4+L_5)Y_{4,-2}+\frac{1}{210}L_3Y_{4,-4}$$

where the surface harmonics $Y_{n,m}$ are defined in terms of the (Ferrer's) associated Legendre functions of the first kind as follows:

$$\begin{aligned} Y_{n,m} &= \cos m\phi P_n^m(\cos\theta) \quad \text{for} \quad m > 0 \\ Y_{n,m} &= P_n(\cos\theta) \quad \text{for} \quad m = 0 \\ Y_{n,m} &= \sin|m|\phi P_n^{|m|}(\cos\theta) \quad \text{for} \quad m < 0 \end{aligned}$$

and where

$$\alpha_1 = \sin\theta\cos\phi \qquad \alpha_2 = \sin\theta\sin\phi \qquad \alpha_3 = \cos\theta.$$

Consequently, the temperature dependence of the magnetoelastic coupling constants is given by

$$\begin{aligned} L_1(T) &= [L_1(0)-\tfrac{3}{7}L_3(0)-\tfrac{1}{7}L_4(0)](\zeta')^3+\tfrac{3}{7}L_3(0)(\zeta')^{10}+\tfrac{1}{7}L_4(0)(\zeta')^{10} \\ L_2(T) &= [L_2(0)+\tfrac{3}{7}L_3(0)-\tfrac{1}{7}L_5(0)](\zeta')^3-\tfrac{3}{7}L_3(0)(\zeta')^{10}+\tfrac{1}{7}L_5(0)(\zeta')^{10} \\ L_3(T) &= L_3(0)(\zeta')^{10} \qquad L_4(T) = L_4(0)(\zeta')^{10} \qquad L_5(T) = L_5(0)(\zeta')^{10} \\ M_1(T) &= [M_1(0)-\tfrac{1}{7}M_2(0)](\zeta')^3+\tfrac{1}{7}M_2(0)(\zeta')^{10} \qquad M_2(T) = M_2(0)(\zeta')^{10} \\ N_0(T) &= [N_0(0)+\tfrac{3}{7}N_1(0)](\zeta')^3-\tfrac{3}{7}N_1(0)(\zeta')^{10} \qquad N_1(T) = N_1(0)(\zeta')^{10}. \end{aligned} \tag{2}$$

(The coefficients of $Y_{0,0}$ may not be included in relations of this type; this has been discussed by Lee and Birss 1961.)

If the temperature dependence of the elastic compliance moduli S_{11}, S_{33}, S_{12}, S_{13} and S_{44} (see, for example, Birss 1959) is known, then the variation of the spontaneous magnetostriction

$$\begin{aligned} \lambda = {} & Q_0+Q_1\beta_3^2+[Q_2+Q_3\alpha_3^2](1-\alpha_3^2) \\ & +[Q_4+Q_5\alpha_3^2](1-\alpha_3^2)\beta_3^2+[Q_6+Q_7\alpha_3^2](\alpha_1\beta_1+\alpha_2\beta_2)\alpha_3\beta_3 \\ & +[Q_8+Q_9\alpha_3^2](\alpha_1\beta_1+\alpha_2\beta_2)^2+Q_{10}(2\alpha_1\alpha_2\beta_1+\alpha_1^2\beta_2-\alpha_2^2\beta_2)^2 \end{aligned}$$

with temperature may be predicted immediately from (2), since

$$\begin{aligned} Q_0 &= -L_0(S_{11}+S_{12})-M_0S_{13} \qquad Q_1 = -L_0(2S_{13}-S_{11}-S_{12})+M_0(S_{13}-S_{33}) \\ Q_2 &= -L_1S_{12}-L_2S_{11}-M_1S_{13} \qquad Q_3 = -L_5S_{12}-L_4S_{11}-M_2S_{13} \\ Q_4 &= L_1S_{12}+L_2S_{11}-(L_1+L_2)S_{13}+M_1(S_{13}-S_{33}) \\ Q_5 &= L_4S_{11}+L_5S_{12}-(L_4+L_5)S_{13}+M_2(S_{13}-S_{33}) \\ Q_6 &= -N_0S_{44} \qquad Q_7 = -N_1S_{44} \\ Q_8 &= -(L_1-L_2-L_3)(S_{11}-S_{12}) \qquad Q_9 = -(L_5-L_4+L_3)(S_{11}-S_{12}) \\ Q_{10} &= -L_3(S_{11}-S_{12}). \end{aligned}$$

Department of Electrical Engineering,
Imperial College,
London, S.W.7.

R. R. Birss.
P. M. Wallis.

10th December 1962.

Birss, R. R., 1959, *Advanc. Phys.* (*Phil. Mag. Suppl.*), **8**, 252.
Callen, E. R., and Callen, H. B., 1960, *J. Phys. Chem. Solids*, **16**, 310.
Kittel, C., and Van Vleck, J. H., 1960, *Phys. Rev.*, **118**, 1231.
Lee, E. W., and Birss, R. R., 1961, *Proc. Phys. Soc.*, **78**, 391.

APPENDIX A2

MAGNETIC DOMAINS IN GADOLINIUM

R. R. BIRSS and P. M. WALLIS
Imperial College, London

Received 5 April 1963

The ferromagnetic Curie point of gadolinium is at about room temperature and for most of the temperature range down to 0°K the first magnetocrystalline anisotropy constant, K_1, is negative [1,2]. However, immediately below the Curie point there is a range of approximately 30-50°K in which K_1 is positive and in which the domain structure of gadolinium might be expected to be similar to that of cobalt. Since the maximum value of K_1 within this range is only about one twentieth of that for cobalt (at room temperature) and since the spontaneous magnetisation is also low near the Curie point, Bitter patterns of the domains are difficult to obtain and none has previously been reported.

Fig. 1 shows Bitter patterns (magnified 320 times) obtained on a $\langle 11\bar{2}0 \rangle$ face of a single crystal of gadolinium at -5°C. At this temperature water-based colloids are unsuitable and it was found convenient to employ a suspension of magnetite particles in xylene, stabilised with a ten millimolar concentration of sodium di(ethylhexyl) sulphosuccinate.

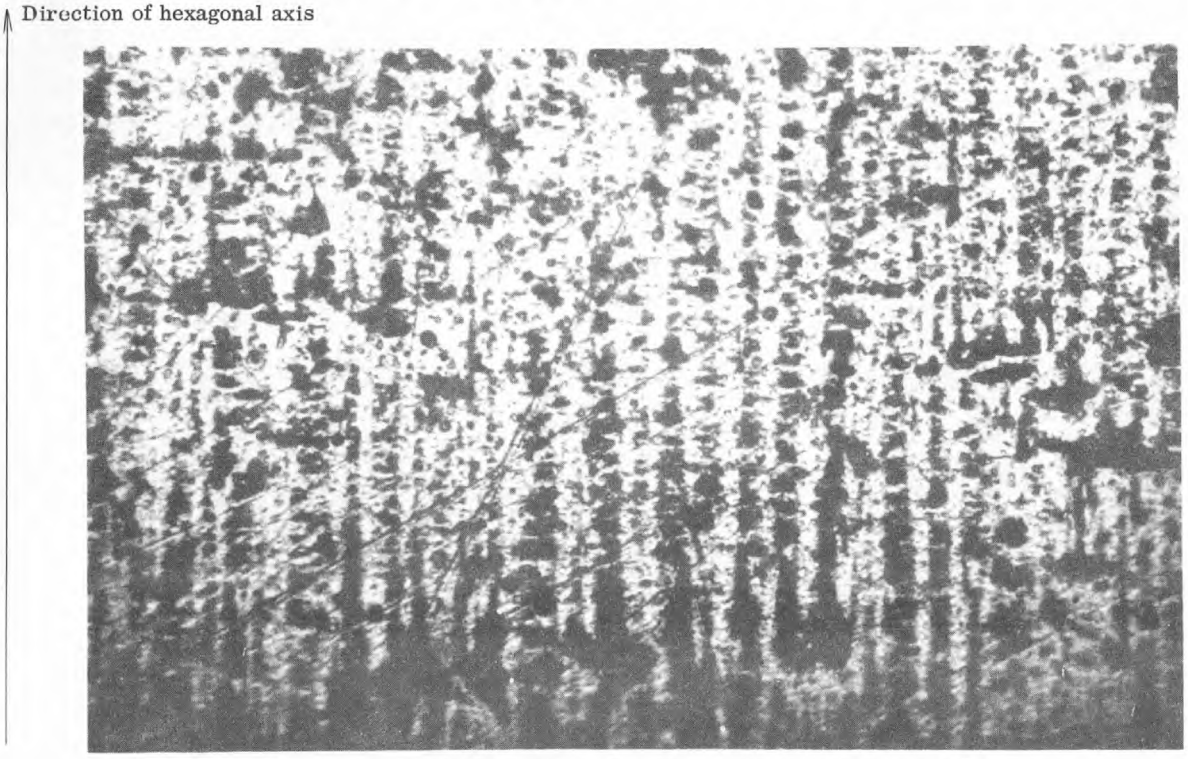


Fig. 1. Bitter patterns (× 320) of ferromagnetic domains on a $\langle 11\bar{2}0 \rangle$ crystallographic plane of a gadolinium single crystal.

On the application of a magnetic field, the walls separating adjacent domains were observed to move in the customary manner, the movement being similar to that obtained with cobalt and other uniaxial ferromagnetic materials.

References

1) W. D. Corner, W. C. Roe and K. N. R. Taylor, Proc. Phys. Soc. 80 (1962) 927.
2) C. D. Graham Jr., J. Phys. Soc. Japan 17 (1962) 1310.

Reprinted from the *Journal of Scientific Instruments*, VOL. 40, pp. 551–556, DECEMBER 1963

APPENDIX A3

A new torque meter or torque magnetometer

R. R. BIRSS and P. M. WALLIS
Imperial College of Science and Technology, London
MS. received 12*th August* 1963, *in revised form* 27*th August* 1963

A torque meter is described which employs the principles used in work with resistance strain gauges to convert small torques developed in isolated specimens directly into electrical signals. The overall sensitivity and the maximum torque that can be measured with this meter can both be altered appreciably by suitable modifications in design, but for the instrument described the overall sensitivity is about 3 dyn cm per cm deflection and the maximum torque is approximately 4×10^3 dyn cm.

The meter has been used to measure the anisotropy torque developed in a (111) single-crystal disk of nickel and hence the second magnetocrystalline anistropy constant K_2. At 23° c the effective values of K_2 appropriate to 7300 Oe and infinite field are respectively $2{\cdot}38 \times 10^4$ and $2{\cdot}53 \times 10^4$ erg cm^{-3}. These results are in excellent agreement with the direct determination of K_2 for nickel by Sato and Chandrasekhar.

1. Introduction

A consideration of the types of torque meter at present in use for measuring small torques, such as the torques developed in the measurement of magnetocrystalline anisotropy and rotational hysteresis in small isolated magnetic specimens, revealed that a somewhat simpler and more convenient torque meter might be developed using the principle employed in work with resistance strain gauges. Such a development is attractive because it allows a particularly simple experimental arrangement: the fractional resistance change resulting from the development of a torque in a specimen may be easily and accurately measured with a Wheatstone bridge.

The normal type of torque meter (Sato and Chandrasekhar 1956), consisting of specimen holder with mirror attached, torsion suspension and torsion head, suffers from certain disadvantages. For stable measurement of a complete torque curve the elastic constant of the suspension must be greater than a limiting value determined by the volume of the specimen and the slope of the torque curve (Harrison 1955) and consequently the maximum sensitivity is limited for stable operation. Although the system is basically simple it would appear that considerable care and patience are needed to obtain accurate results.

These difficulties are reduced, although not eliminated, in a somewhat different type of apparatus first described by Craft, Donahoe and Love (1955) and subsequently modified and improved by others including Penoyer (1956) and Pearson (unpublished). The specimen is suspended from the coil of a moving-coil galvanometer and the torque developed in the specimen is balanced by passing a current through the galvanometer coil. Automatic balancing is achieved by the use of feedback and the sensitivity of this type of instrument appears to be about 1 dyn cm per cm deflection of the indicating instrument. The same principle (of balancing torque against electromagnetic force) is used, with a much higher sensitivity, to measure the anisotropy of thin films (Humphrey and Johnston 1963), but the system used is necessarily complex and the apparatus cumbersome.

In another type of torque magnetometer (Miller 1950), the specimen is supported by an axle mounted in bearings. A phosphor bronze strip, wrapped once round the axle and kept under tension, converts the torque on the axle to a tangential force on the strip which is directly measured with a commercial force-measuring device using the strain gauge principle. The maximum sensitivity is apparently of the order of 10^3 dyn cm per cm. Friction in the bearings limits the sensitivity, and an error due to the rotation of the specimen when torque is developed is also present.

The torque magnetometer described by Aldenkamp, Marks and Zijlstra (1960) avoids bearing friction by the use of a special torsion suspension which incorporates three phosphor bronze strips between two disks. This arrangement makes the suspension relatively rigid to unwanted lateral displacements. A differential transformer and commercial displacement meter are used to measure the rotation between the two disks. It is claimed that there is negligible rotation of the specimen and that the maximum sensitivity is 150 dyn cm per cm.

The torque meter to be described is based on the change in resistance of a wire which occurs when it is strained, a property employed in resistance strain gauges. A torque developed in the system yields an electrical signal via a simple Wheatstone bridge circuit. No feedback network is necessary for stable operation, nor is there a limit, in this respect, to the maximum working sensitivity.

The configuration of resistance wires finally adopted gives the torque meter a number of desirable features. These include:

(i) positive location of the specimen in the magnetic field, with negligible rotation on application of torque;
(ii) insensitivity to unwanted translational forces and torques;
(iii) insensitivity to small changes in ambient temperature and pressure;
(iv) a small volume (~ 12 cm^3), facilitating temperature control and stabilization;
(v) absence of friction from supporting bearings, etc. (since support is entirely by elastic means);
(vi) linearity between the output from the Wheatstone bridge and the torque to be measured.

The use of semiconductor strain gauge elements was considered because they exhibit a much greater resistance change for the same strain. However, the sensing element in the

torque meter has to measure stress rather than strain, and high sensitivity is achieved with a small area of cross section, so that a large strain, and hence a large resistance change, accompanies a given stress. Further factors favouring the use of strain gauge wires are that they are readily available, that they are much easier to manipulate than semiconductor elements of the same cross section and that the magneto-resistance of these wires is small when compared with magneto-electrical effects in semiconductors.

2. General design and apparatus

The basic construction of the torque meter is shown in figure 1. Resistance wires ABCD and EFGH form two adjacent arms of a Wheatstone bridge. A torque on the

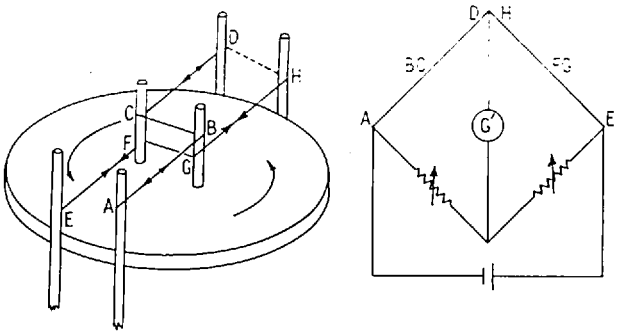


Figure 1. Diagram of principle of torque meter.

two central supports (CF and BG) about the axis of the disk increases the stress in one arm and decreases the stress in the other. Since the resistance of the two arms varies linearly with stress, provided the elastic limit of the wire is not exceeded, small torques produce a proportional out-of-balance current in the galvanometer G'. Detailed inspection of figure 1 reveals that, for this configuration, translational forces, and also torques about the other two perpendicular axes, affect both arms of the bridge equally and so do not contribute to the out-of-balance current. This design also compensates automatically for changes in resistance due to magnetoresistance of the wires in a magnetic field and due to small changes in temperature.

3. Detailed design considerations

The mechanical layout of the torque meter is shown in figure 2. Since a wire will not compress from pressure at its ends, all four wires have to be prestressed, ideally to half the elastic limit. This is done by forcing the two halves of clamp A apart with the differential screw so that the support wires B are made to flex from their bases. The torque from the specimen H and specimen holder C can then be transmitted via the specimen support wires D to produce a strain in the resistance wires E. When not in use the clamp A is closed, removing the stress from the resistance wires and clamping the wires D supporting the specimen so that it can be changed without risk of damage occurring. For calibration purposes a phosphor bronze suspension is attached to the other end of the specimen holder and to the calibration head F. A photograph, 1 cm in diameter, of a circular protractor is cemented centrally on to the top of the torque head so that, with the aid of a microscope, accurately known angular rotations can be applied. A thin coating of Araldite on the support wires B and D insulates them from the resistance wires E. The ends of these resistance wires are terminated mechanically at the tops of the support wires B by wrapping them once round the support wires and then coating them with Durofix. Soldering tags, which are spot welded to the ends of the resistance wires E prior to assembly, are then soldered to copper soldering posts (not shown in the diagram for the sake of clarity). The soldering posts are

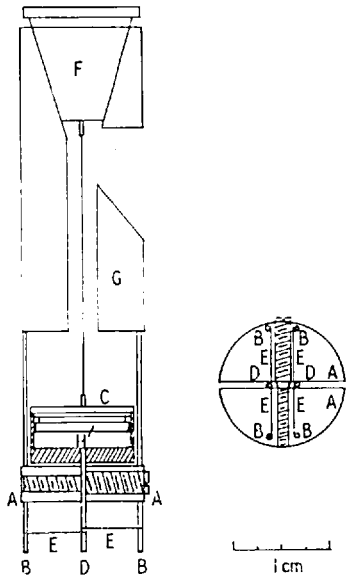


Figure 2. Plan of torque meter. A, clamp jaws; B, D, support wires; C, specimen holder; E, resistance wires; F, torque head; G, main body; H, specimen.

let into the two clamp jaws A and are insulated from them by Paxolin bushes. Electrical connections from the Wheatstone bridge are made to these soldering posts.

A port is provided in the main body G of the instrument, so that the phosphor bronze suspension may be unsoldered and replaced. To gain access to the specimen H, the specimen holder C is made in two halves. In operation these are secured with smears of Durofix which are readily dissolved in acetone when the specimen is to be changed. Within the specimen holder, the specimen is mounted on a thin rubber pad, to provide a small degree of flexibility in the plane of the specimen.

3.1. *Analysis of operation*

Consider a wire of length l and resistance R. If its volume and resistivity remain constant and its length is increased by Δl, it can easily be shown that

$$\frac{\Delta R}{R} = 2\frac{\Delta l}{l}. \tag{1}$$

In practice, since the volume does not remain constant and the resistivity of the wire changes with deformation, the factor 2 is usually nearer 2·2 and must be replaced by a number, denoted by G, called the gauge factor. If a force F is applied to a wire of cross section πr^2, then

$$F = \pi r^2 E \frac{\Delta l}{l}$$

where E is Young's modulus, and

$$\frac{\Delta R}{R} = \frac{GF}{\pi r^2 E}. \tag{2}$$

Now consider the configuration of figure 1 and let a force F in each of the four wires counteract a torque L developed

in the specimen. If the separation of the two central supports is $2a$, then $L = 4Fa$ and

$$\frac{\Delta R}{R} = \frac{GL}{4E\pi r^2 a}. \tag{3}$$

Furthermore, it can be shown that for a bridge with each arm of resistance R, bridge current $2i$ and galvanometer resistance R_g, the galvanometer current is

$$i_g = \frac{i\Delta R}{2(R + R_g)} \quad (\Delta R \ll R)$$

where ΔR is the small change in one of the bridge arms. In the present case both arms change by ΔR but in opposite senses, giving an effective change of $2\Delta R$ in one arm, whence

$$i_g = \frac{iRGL}{4(R + R_g)\pi r^2 Ea}. \tag{4}$$

Hence under these conditions the galvanometer current i_g is proportional to the torque. (In practice, in order to keep R large and yet have wire that is of reasonable cross section, more than one strand of wire is used per arm, the strands being connected in series.)

3.2. *Limits of operation and sensitivity*

The upper and lower limits to the torque that can be measured depend respectively on the breaking strain or elastic limit of the wire and on the smallest value of galvanometer current that can be measured in practice. The upper limit thus depends on the type of wire available, that used being Nichrome wire with a diameter of about 0·0027 cm. It had a Young's modulus of 18×10^{11} dyn cm^{-2} and an estimated elastic limit of 2×10^9 dyn cm^{-2}, corresponding to a fractional change in resistance $\Delta R/R$ of $2{\cdot}4 \times 10^{-3}$. The lower limit for $\Delta R/R$ is more difficult to estimate since it depends on the amount of amplification that can, in practice, be applied to the out-of-balance signal from the Wheatstone bridge. Electrostatic and electromagnetic pick-up and electrical noise originating from electrical contacts, temperature instability, thermal e.m.fs and mechanical vibration limit the maximum sensitivity. A conservative estimate of the lower limit for $\Delta R/R$ for a normal bridge circuit without complicated auxiliary apparatus would be about 10^{-6}, although this limit could be extended, probably by one or two orders of magnitude, depending on the amount of care taken in reducing noise and in developing suitable amplifying equipment.

It may be seen from equation (3) that these practical limits (of 10^{-3} and 10^{-6}) between which $\Delta R/R$ may be measured define upper and lower limits of torque, depending on the factor a which is half the separation of the support wires in figure 1. The value of a used in the present torque meter is 0·2 cm, so that the approximate range of torque that can be measured is from 4×10^3 to 4 dyn cm. For obvious mechanical reasons the factor a cannot be reduced by more than about one order of magnitude, although it could be increased in size to a limit determined only by the maximum desirable size of the apparatus. The lower limit of torque that could be measured with the strain gauge wire at present in use would therefore appear to be between about 10^{-1} and 10^{-2} dyn cm.

For the bridge circuit actually used, in which $R = 60\ \Omega$, $R_g = 40\ \Omega$ and $i = 10$ mA, equation (4) gives the galvanometer currents corresponding to the upper and lower limits of torque as 6 μA and 6×10^{-3} μA. The galvanometer used was a Tinsley type 4500 LS for which these currents give deflections, at 2 metres, of 1307 cm and 1·3 cm respectively, corresponding to an overall sensitivity of about 3 dyn cm per cm deflection. In practice, a galvanometer amplifier with almost full negative feedback is inserted between the bridge and the galvanometer so that the sensitivity can easily be varied.

A simple calculation using equations (1) and (2) indicates that when the elastic limit of the wires is approached, say at 10^9 dyn cm^{-2}, then $\Delta l/l \simeq 5 \times 10^{-4}$. Since $l \simeq 0{\cdot}5$ cm, $\Delta l \simeq 2{\cdot}5 \times 10^{-4}$ cm and the maximum rotation of the specimen is then about 10^{-3} radian or about 3 minutes of arc. Because this rotation is so small it is possible to choose a relatively stiff phosphor bronze suspension so that it may support the weight of the specimen holder, while still contributing a negligible error to the measured torque.

For unwanted torques and translational forces to have no effect on the balance of the bridge, it is important that the wires should be parallel and of the same length, resistance and elasticity. These conditions can in practice never be perfectly fulfilled but careful construction readily reduces unwanted effects to a tolerable level. In particular it was found important that the two parallel planes containing the resistance wires ABCD and EFGH in figure 1 should be as close to one another as possible. If this is not done more torque is transmitted to the arm EFGH nearer to the specimen, due to the relative flexibility of the specimen support wires. Under these circumstances the proper compensation of unwanted effects is not achieved either, for the same reason.

4. The performance of the torque meter when used to study magnetocrystalline anisotropy

To test the performance of the torque meter measurements were made of the second magnetocrystalline anisotropy constant K_2 of nickel, using a single-crystal disk orientated parallel to a (111) crystallographic plane. For this particular orientation, even with a relatively large specimen, the torque is small and may easily be masked by unwanted torques due to inadequacies in the measuring apparatus and from other sources. The determination of K_2 is itself of value since there is disagreement—even as to sign—among the figures already published for this constant.

4.1. *Theory of the measurements*

The magnetocrystalline anisotropy energy density W is given for a cubic crystal by the equation

$$W = K_0 + K_1(\alpha_1^2\alpha_2^2 + \alpha_2^2\alpha_3^2 + \alpha_3^2\alpha_1^2) + K_2\alpha_1^2\alpha_2^2\alpha_3^2 + \ldots$$

where K_1 and K_2 are the first and second anisotropy constants, and the α's are the direction cosines of the magnetization vector relative to the crystal lattice. If it is assumed that the direction of the magnetization vector and that of the magnetic field coincide and lie in the (111) plane (which is only strictly true for $H = \infty$), then it may readily be shown that the torque per unit volume of the specimen is $-\partial W/\partial\theta = -\frac{1}{18}K_2 \sin 6\theta$, where θ is the angle made by the magnetization in the (111) plane with the [110] direction. In order to ensure that the magnetic field is uniform and lies in the (111) plane, the specimen must be an oblate spheroid with its minor axis coinciding with the [111] direction. The disk used had a diameter-to-thickness ratio of about ten and approximated reasonably well to the desired shape.

In practice, there are a number of other contributions to

the torque actually measured with the torque meter. These may be due to:

(i) misalignment of the disk surface relative to the (111) plane. This can occur during the preparation of the disk and should give rise to terms, which depend on K_1, in $\sin 2\theta$, $\cos 2\theta$, $\sin 4\theta$ and $\cos 4\theta$.

(ii) misalignment of the disk (and hence of the (111) plane) relative to the magnetic field. This can occur during the assembly of the apparatus and again should give rise to terms up to $\sin 4\theta$ and $\cos 4\theta$ (Tarasov and Bitter 1937).

(iii) any deviation in the shape of the specimen from that assumed, e.g. variation in thickness or deviation from circular profile.

(iv) any included grains of different orientation within the crystal disk, together with internal stresses giving rise to additional anisotropy.

The main contributions to the unwanted torques include terms only up to $\sin 4\theta$ and $\cos 4\theta$, so that Fourier analysis of the torque curve to determine the terms in 6θ can effectively separate the contribution due to K_2 from that due to K_1. Although terms from random sources such as (iii) and (iv) could conceivably contribute to all even terms including 6θ, such contributions are likely to be very small.

The theory given above assumes H to be very large, so that the magnetization vector may be identified with the direction of the magnetic field. In practice, torque curves are taken at different values of the field and the apparent values of the anisotropy constants so obtained are plotted against H^{-1}. The straight line obtained is then extrapolated to the origin to give the value of the anisotropy constant appropriate to infinite field—a procedure frequently used (Bozorth 1951).

4.2. *The specimen preparation and auxiliary apparatus*

The specimen used for the measurement of K_2 was prepared from the ingot. X-ray back-reflection Laue photographs were used for orientation purposes and to ensure that there were no large areas of disoriented or polycrystalline material. An optically flat surface was polished to within 15 minutes of arc from a (111) plane and a second surface was then ground and polished parallel, within ± 6 minutes, to the first surface. A number of X-ray photographs were taken to find the most suitable area of the resulting slab from which to cut the final disk. Cutting was done using a spark-cutting machine with a hollow copper tool bored to the correct internal diameter (1 cm). The disk was subsequently etched to remove any polycrystalline material created by the polishing and cutting operations.

The apparatus used in the measurements employed the torque meter as already described, with associated centring and levelling support arrangements and with appropriate electrical circuitry. A 4 in. Newport electromagnet was used with 4·4 cm pole gap, giving a field of 7300 Oe at 15 A. The Wheatstone bridge circuit used is shown in figure 3. A galvanometer amplifier is used with negative feedback, primarily so that the damping on the galvanometer can be adjusted to the most convenient level. The impedance of the Wheatstone bridge is otherwise such that the galvanometer used is heavily over-damped, causing considerable delay in taking readings. The arrangement also allows the sensitivity of the circuit to be easily changed. The current through the bridge was kept at 20 mA since it was found that thermal drift became progressively more troublesome as the current was raised above this level.

4.3. *Measurements and results*

Because of slight non-uniformity in the field due to the relatively large pole gap used, it was found important to position the specimen and the torque meter centrally in the magnetic field when the apparatus was initially set up. Before any measurements were made the bridge current was always

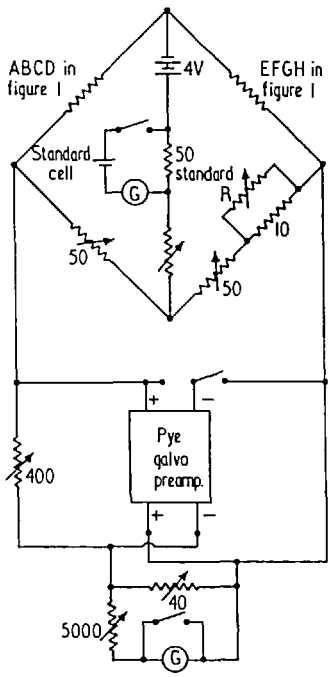


Figure 3. Wheatstone bridge circuit.

standardized by comparing the e.m.f. across the standard 50 Ω resistance with that of the standard cell. The sensitivity of the bridge was also always checked by varying resistance R of figure 3 and noting the galvanometer deflection. The procedure, then, for calibrating the torque meter was to apply accurately known rotations to the torque head and to note the corresponding galvanometer deflections. In order to minimize errors due to possible drift, a galvanometer reading was taken corresponding to a reference zero on the torque head between each reading corresponding to different torque head positions. The relationship between ΔR and the position of the torque head was found to be linear. Measurements of the anisotropy torque were made by noting the galvanometer deflection for different positions of the magnet, a procedure similar to that employed in calibrating the torque meter again being used to minimize the errors introduced by thermal drift.

Figure 4 shows the results which were first obtained without careful alignment of the specimen relative to the magnet pole gap and when full cancellation of unwanted translational forces was not obtained because there was a large separation between the two planes containing the resistance wires. The undesirable effect that this separation has on the operation of the torque meter has been explained in § 3.2. For purposes of comparison, a torque curve obtained by Sato and Chandrasekhar (1956) using a similar (111) nickel sample is superimposed on figure 4, the ordinates of the two curves having been adjusted so that the amplitudes of the components periodic in 6θ (indicated by the broken curve) are the same.

After the necessary modifications had been made to the torque meter the correct centring of it in the pole gap was

found to be no longer so critical and the spurious contributions periodic in 2θ and 4θ could be reduced to a minimum. Greatly improved torque curves were then obtained, especially

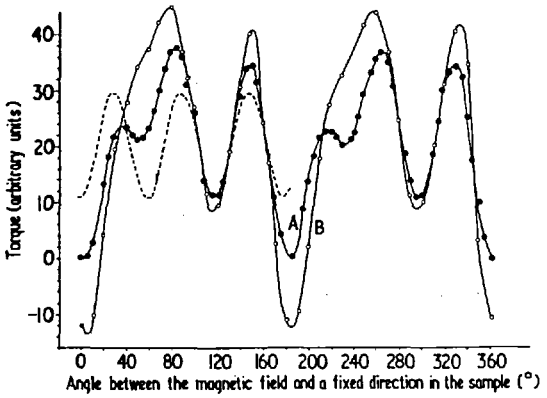


Figure 4. Comparison of a measured torque curve (A) with one obtained by Sato and Chandrasekhar (1956) (B).

at lower temperatures, and a set of curves, measured at $-9{\cdot}5°$ c and at different magnetic field strengths, is shown in figure 5. These curves were subsequently subjected to Fourier analysis and the amplitudes of the components periodic in 2θ, 4θ and 6θ are plotted against H^{-1} in figure 6, where S_n and C_n denote respectively the amplitudes of the $\sin n\theta$ and $\cos n\theta$ components.

The effective amplitude of the $\sin 6\theta$ curve at 23° c and a field of 7300 Oe is 113·8 dyn cm, and, since the volume of the crystal is 0·08609 cm^3, the torque per unit volume is $1{\cdot}322 \times 10^3$ dyn cm, giving a value for K_2 of $2{\cdot}38 \times 10^4$ erg cm^{-3}. The extrapolated value corresponding to infinite field is $2{\cdot}53 \times 10^4$ erg cm^{-3}.

4.4. *Discussion of results*

The values obtained by previous investigators for K_2 for nickel are summarized in the table, together with the temperature at which the measurement was made and the method used.

$K_2 \times 10^{-4}$ (erg cm^{-3})	Temp.	Method	Reference
+5·3	Room	MC	McKeehan (1937), Honda, *et al.* (1935)
+1·09	Room	MC	Nakamura (1955)
−3·6	20° c	MW	Reich (1956)
−6·06	20° c	MW	Barlow and Standley (1958)
+2·34	26° c	T	Sato and Chandrasekhar (1956)

MC, from measurements of magnetization curves; MW, from microwave resonance technique; T, from torque curves.

It may be seen that the present determination of K_2 agrees well with the figure obtained by Sato and Chandrasekhar (1956) at a slightly higher temperature. One explanation put forward (Pearson 1960, Anderson and Donovan 1959) for the discrepancies between the other values of K_2 given in the table is that experiments by static and by microwave resonance techniques do not, in fact, measure anisotropy constants under the same conditions, and that the former correspond to constant stress and the latter to constant strain. However, it is possible to calculate the difference between the effective value of K_2 at zero stress and at constant strain: it is

$$\Delta K_2 = S_{11}\{3L_1(L_2+L_3) + L_2(4L_2+L_3)\} + S_{12}\{3L_1(L_2+L_3) + 5L_2L_3 - L_3^2\} - \tfrac{1}{2}S_{44}(6M_0+M_1)M_1$$

where, for nickel, the elastic compliance moduli are (de Klerk and Musgrave 1955)

$$S_{11} = 0{\cdot}7336 \times 10^{-12}\ \text{cm}^2\ \text{dyn}^{-1}$$
$$S_{12} = -0{\cdot}2744 \times 10^{-12}\ \text{cm}^2\ \text{dyn}^{-1}$$
$$S_{44} = 0{\cdot}8019 \times 10^{-12}\ \text{cm}^2\ \text{dyn}^{-1}$$

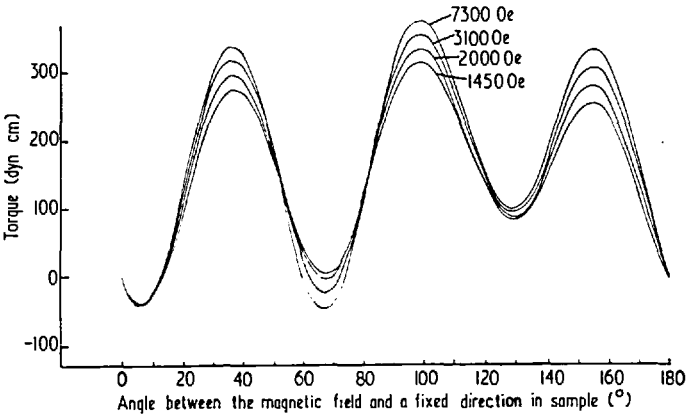


Figure 5. Variation of torque curve with magnetic field at $-9{\cdot}5°$ c.

and the magnetoelastic coupling constants are (Bozorth and Hamming 1953)

$$L_1 = 88{\cdot}36 \times 10^6\ \text{dyn cm}^{-2}$$
$$L_2 = -12{\cdot}67 \times 10^6\ \text{dyn cm}^{-2}$$
$$L_3 = 20{\cdot}11 \times 10^6\ \text{dyn cm}^{-2}$$
$$M_0 = 91{\cdot}03 \times 10^6\ \text{dyn cm}^{-2}$$
$$M_1 = -19{\cdot}20 \times 10^6\ \text{dyn cm}^{-2}.$$

These figures give a value for ΔK_2 of $0{\cdot}57 \times 10^4$ erg cm^{-3}. It is therefore unlikely that this explanation of the discrepancies exhibited in the table is correct, and it is probable that the value of K_2 derived from torque measurements must be accepted as correct. The close agreement of the present results with the work of Sato and Chandrasekhar (1956) is gratifying since they are the only other investigators to have

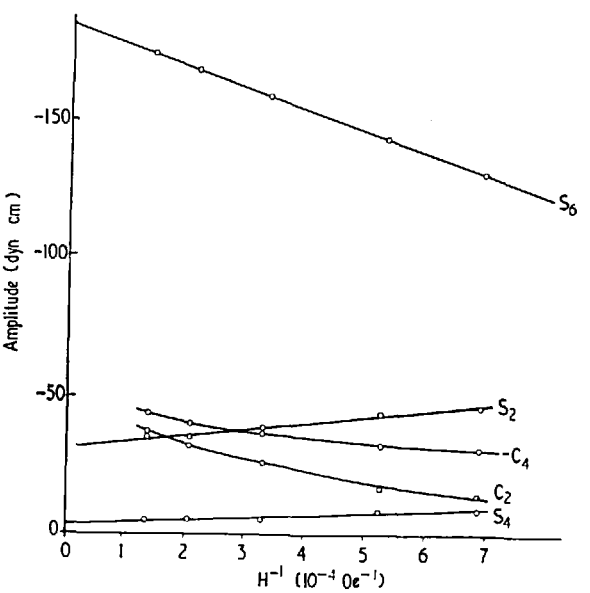


Figure 6. Variation of the periodic components of the torque curves with H^{-3} at $-9{\cdot}5°$ c.

measured K_2 directly using a (111) single-crystal disk. The two sets of values for K_2 derived from measurements of magnetization curves are obtained by estimating the areas under these curves rather than by curve fitting at high fields, and the figures obtained for K_2 are therefore thought to be unreliable—indeed the corresponding estimates for the first magnetocrystalline anisotropy constant K_1 differ by some 25%.

Acknowledgments

One of us (P.M.W.) is indebted to the Department of Scientific and Industrial Research for the provision of a maintenance grant.

References

ALDENKAMP, A. A., MARKS, C. P., and ZIJLSTRA, H., 1960, *Rev. Sci. Instrum.*, **31**, 544.

ANDERSON, J. C., and DONOVAN, B., 1959, *Proc. Phys. Soc.*, **73**, 593.

BARLOW, G. S., and STANDLEY, K. J., 1958, *Proc. Phys. Soc.*, **71**, 45.

BOZORTH, R. M., 1951, *Ferromagnetism* (New York: Van Nostrand), p. 566.

BOZORTH, R. M., and HAMMING, R. W., 1953, *Phys. Rev.*, **89**, 865.

CRAFT, G. T., DONAHOE, F. J., and LOVE, W. F., 1955, *Rev. Sci. Instrum.*, **26**, 360.

DE KLERK, J., and MUSGRAVE, M. J. P., 1955, *Proc. Phys. Soc.* B, **68**, 81.

HARRISON, F. W., 1955, *J. Sci. Instrum.*, **33**, 5.

HONDA, K., MASUMOTO, H., and SHIRAKAWA, Y., 1935, *Sci. Rep. Tôhoku Univ.*, **24**, 291.

HUMPHREY, F. B., and JOHNSTON, A. R., 1963, *Rev. Sci. Instrum.*, **34**, 348.

MCKEEHAN, L. W., 1937, *Phys. Rev.*, **51**, 136.

MILLER, D. S., 1950, *Rev. Sci. Instrum.*, **21**, 605.

NAKAMURA, Y., 1955, *J. Phys. Soc. Japan*, **10**, 937.

PEARSON, R. F., 1960, *Proc. Phys. Soc.*, **75**, 315.

PENOYER, R. F., 1956, *Proc. A.I.E.E. Conf. on Magnetism and Magnetic Materials*, (New York: Institution of Electrical Engineers) p. 365.

REICH, K. H., 1956, *Phys. Rev.*, **101**, 1647.

SATO, H., and CHANDRASEKHAR, B. S., 1956, *J. Phys. Chem. Solids*, **1**, 228.

TARASOV, L. P., and BITTER, F., 1937, *Phys. Rev.*, **52**, 353.

UNWIN BROTHERS LIMITED, WOKING AND LONDON

The temperature variation of magnetocrystalline anisotropy for nickel and gadolinium

APPENDIX A4

R. R. BIRSS and P. M. WALLIS

Physics Laboratory, University of Sussex, Falmer, Brighton, Sussex, England

Abstract. Measurements of magnetocrystalline anisotropy have been made on single crystals of nickel and gadolinium within the temperature range 92°K to 347°K. At room temperature a direct measurement on a (111) nickel disk gives a value of the second anisotropy constant (appropriate to infinite field) of $K_2 = -2.38 \times 10^4$ erg cm^{-3}.

For nickel the variation with temperature of K_1 is in satisfactory agreement with published data but that of K_2 is not. For gadolinium the variation with temperature of the semi-angle of the cone of easy magnetization appears to be in slightly better agreement with the 1962 results of Graham than with those of Corner, Roe and Taylor.

1. Introduction

Although estimates of the value at room temperature of the second magnetocrystalline anisotropy constant K_2 of nickel have been made by several investigators, these estimates are not mutually consistent and differ, in fact, even as to sign. The values of K_2 obtained indirectly from magnetization curves are generally positive, for example, $K_2 = +5.3 \times 10^4$ erg cm^{-3} (McKeehan 1937) and $K_2 = +1.09 \times 10^4$ erg cm^{-3}, (Nakamura 1955). However, Standley and his co-workers have obtained negative values by using a microwave resonance technique, for example $K_2 = -3.6 \times 10^4$ erg cm^{-3} (Reich 1956), and $K_2 = -6.06 \times 10^4$ erg cm^{-3} (Barlow and Standley 1958). It is therefore desirable that direct measurements of K_2 be made by investigating the anisotropy torque in a single crystal disk of nickel orientated so that the plane of the disk is a (111) plane (this being the crystallographic plane in which the first anisotropy constant K_1 does not contribute to the torque). Two such measurements have been made, the values of K_2 obtained being $K_2 = +2.34 \times 10^4$ erg cm^{-3} (Sato and Chandrasekhar 1956) and $K_2 = +2.38 \times 10^4$ erg cm^{-3} (Birss and Wallis 1963). It is now thought, for reasons which are given below, that both these figures, whilst of the correct magnitude, are of the wrong sign and that the actual value (appropriate to infinite field) is $K_2 = -2.38 \times 10^4$ erg cm^{-3}.

The relation usually given (Bozorth 1951, Brailsford 1960, Stoner 1950) for the anisotropy torque in high fields is

$$L = -\frac{dE}{d\theta}, \tag{1}$$

where E is the anisotropy energy density. For a cubic crystal

$$E = K_0 + K_1(\alpha_1^2\alpha_2^2 + \alpha_2^2\alpha_3^2 + \alpha_3^2\alpha_1^2) + K_2\alpha_1^2\alpha_2^2\alpha_3^2 + \ldots,$$

where the α's are the direction cosines of the magnetization relative to the crystallographic axes. L is the torque exerted on the crystal per unit volume of the crystal and θ is the angle (in the plane in which the magnetization rotates) between the direction of magnetization and a fixed direction in the crystal. Since the differentiation is performed relative to axes fixed with respect to the crystal whilst the orientation of the magnetization direction varies relative to the crystal axes, it might reasonably be supposed that equation (1) gives the torque on the crystal, in the direction of θ increasing, when θ is measured from a fixed direction in the crystal to the direction of magnetization. Such optimism would, however, be misplaced for, with this interpretation of the symbols, the torque must be given by

$$L = +\frac{dE}{d\theta}, \tag{2}$$

because it must be in such a direction as to bring an easy direction into coincidence with the field direction when the easy direction makes a small angle with the magnetization. In fact, equation (1) gives the torque on the magnetization when the crystal is fixed whilst (2) gives the torque on the crystal when the magnetization is fixed (by the direction of the field). The reason that the distinction between (1) and (2) is often not important is that the torque usually contains a (leading)term involving K_1, the sign of which may, of course, be predicted in advance from the known position of the easy directions. In the (111) plane, however,

$$L = +\frac{dE}{d\theta} = +\frac{K_2}{18}\sin 6\theta, \tag{3}$$

where θ is the angle made by the magnetization in the (111) plane with a ⟨110⟩ direction. The sign of K_2 can not therefore be determined correctly by using equation (1) and it is thought that both the direct determinations of K_2 mentioned above are in error for this reason. That K_2 is in fact negative is confirmed, as will be shown in § 3, by a comparison of a theoretical estimate of the field dependence of the torque with experiment for low temperatures.

In § 2 data are presented for nickel and gadolinium single crystals within the temperature range 92°K to 347°K.

2. Experimental results

Figure 1 shows a typical torque curve obtained at 347°K with a (111) single-crystal nickel disk for

a field of 1380 Oe (β is the angle the field makes with a $\langle 110 \rangle$ direction). The curves obtained for each value of magnetic field were subsequently subjected to Fourier analysis to separate the amplitude of the term periodic in 6β from other unwanted contributions to the torque (for a discussion see Birss and Wallis (1963)). It was then possible to draw a curve showing the variation of the amplitude, A, of the term periodic in 6β (referred to unit volume of the crystal) as a function of 1/H, where H is the magnetic field strength. Figure 2 shows a selection of such experimental curves appropriate to various temperatures within the range of 92°K to 347°K. For high temperatures the

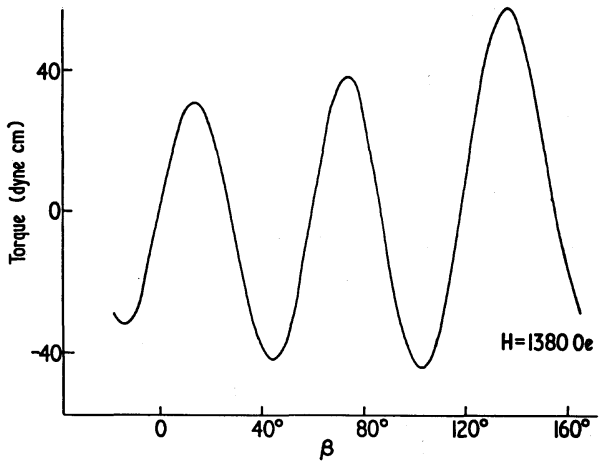


Figure 1. Variation of torque with the angle β between the field and a $\langle 110 \rangle$ direction for the (111) nickel disk in a field of 1380 Oe at 347°K.

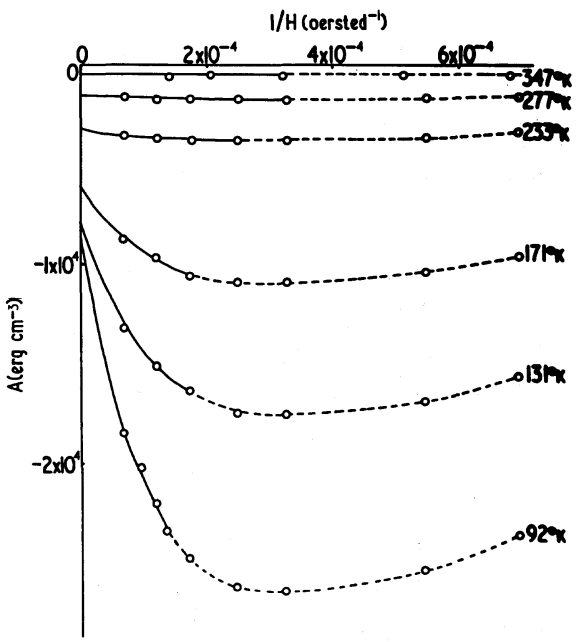


Figure 2. Variation with 1/H of the amplitude A of the component of torque periodic in 6β (referred to unit volume of the nickel crystal) for various temperatures.

torque curves vary little with field at high fields. The reduction in torque at small values of 1/H for low temperatures warrants further discussion, however, and this is attempted in § 3.

A single crystal disk of gadolinium orientated parallel to a $(11\bar{2}0)$ crystallographic plane was also available for torque measurements and it was thought to be of interest to investigate this crystal within a similar temperature range. This would afford a direct comparison with the work of Graham (1962) and Corner, Roe and Taylor (1962) in the interesting temperature region below room temperature in which the easy directions are thought to lie on the surface of a cone surrounding the hexagonal axis. Unfortunately, the torquemeter had been designed with a fixed sensitivity, large enough to facilitate accurate measurements on the (111) nickel disk, and this proved too great to permit the measurement of complete torque curves on the gadolinium crystal without damage to the device. However, it was still possible to determine the orientation of the cone of easy magnetization by finding the positions in which the field exerted no torque on the crystal. From symmetry, of course, two such positions are parallel and perpendicular to the hexagonal axis, but in certain temperature ranges it is also possible to find another two positions of zero torque making angles ψ with the hexagonal axis. Since the torquemeter is limited in the magnitude of the torques it can accept, such positions are found in practice by gradually increasing the magnetic field and simultaneously adjusting its angular orientation in the plane of the disk so as to keep the torque small or zero. (A similar procedure is necessary when the field is reduced.) Figure 3 shows the variation of ψ, the angle for zero torque, with 1/H for various temperatures: the value of ψ obtained by extrapolation to infinite field ψ_∞ may be identified with the semi-angle of the cone of easy magnetization.

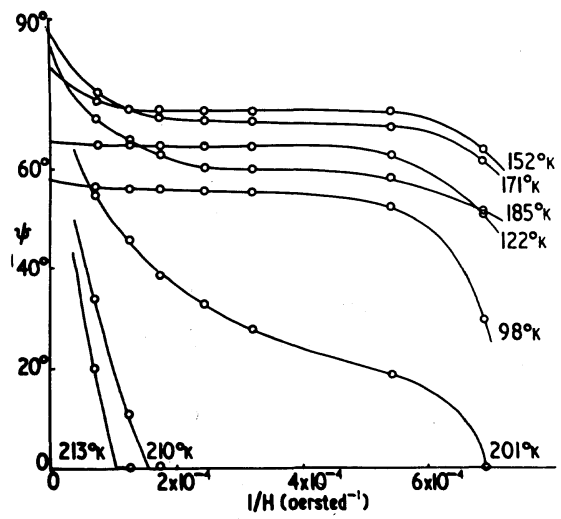


Figure 3. Variation with 1/H of the angle for zero torque ψ at various temperatures, for the gadolinium crystal.

3. Discussion

In equation (3), θ is the angle between the magnetization and a reference direction in the crystal. It is only at infinite fields that the magnetization and the applied magnetic field are strictly parallel. However, at temperatures well below the Curie point it is permissible to assume that in large but finite fields the crystal is magnetized as a single domain, the direction

of the magnetization vector being such as to minimize the sum of the magnetic field energy, the demagnetizing energy, and the anisotropy energy. Thus the direction of the magnetization may be related to both the magnitude and the direction of the field and the variation in torque due to this effect may be calculated. It turns out that in high fields the main contribution is of the form A sin 6β, where

$$A = \frac{K_2}{18} - \frac{[K_1 + \frac{1}{6}K_2]^2}{3(HI_S + k)}, \qquad (4)$$

and powers of 1/H higher than the first have been neglected. The quantity k depends on the demagnetizing energy and can only be calculated exactly when the boundary of the specimen is a surface of the second degree. If the flat disk is assumed to approximate

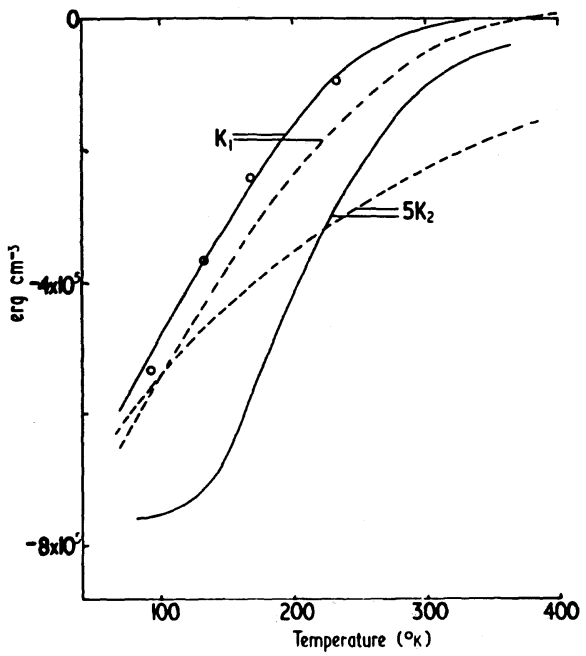


Figure 4. The variation with temperature of K_1 and $5K_2$ for nickel.

to an oblate spheroid with a demagnetizing factor N in the plane of the disk, then, neglecting a small term of order $K_2/9$,

$$k = (4\pi - 3N)I_S^2 - K_1.$$

Since the magnetization does not lie in the plane of the disk it is not possible to correct the torque curve by displacing it parallel to the β axis by an amount L/HI_S (Bozorth 1954) and it is necessary to compare the variation of A with field obtained experimentally with that given by equation (4) to determine the correct value of K_2. This has been done in figure 2 where the broken lines are drawn through the experimental data and the solid curves are calculated from equation (4) using N = 0.955. If equation (4) were modified by the inclusion of terms in $(1/H)^2$ the agreement between theory and experiment would presumably hold to higher values of 1/H.

At low temperatures the value of K_1 is accurately known from the data given by Bozorth (1951), and these values may be used in equation (4). At high temperatures the magnitude of K_1 is much reduced, and any errors in the values given by Bozorth would cause appreciable errors in the slopes of the (A, 1/H) curves since these involve K_1^2. The values of K_1 have therefore been slightly adjusted in obtaining the solid curves shown in figure 2. The extent of the adjustment is shown in figure 4 where the broken curve for K_1 is that given by Bozorth and the solid curve is that used in equation (4). The experimental points are some confirmatory values obtained by replacing the (111) disk with a (110) nickel disk. Also shown, as a solid curve, in figure 4 is the temperature dependence of K_2 (plotted, for convenience, as $5K_2$) deduced from the present investigation. The broken curve corresponds, except for a sign change, with that given by Bozorth (1951).

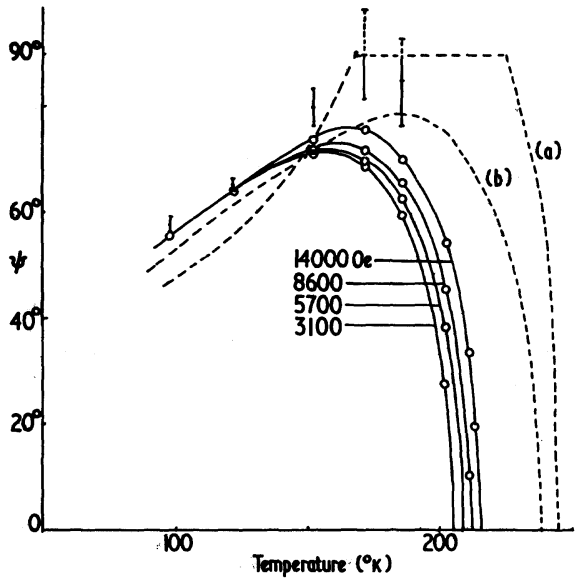


Figure 5. The variation with temperature of the angle for zero torque ψ at various fields, for the gadolinium crystal.

Figure 5 shows the angle for zero torque ψ for gadolinium as a function of temperature for various values of fields. The experimental points on which an error is indicated are of ψ_∞ and these may be compared with the broken curves which are due to (a) Graham (1962) and (b) Corner, Roe and Taylor (1962). Because of the strong dependence of ψ on 1/H above 185°K it would not be realistic to plot experimental points at higher temperatures.

Acknowledgments

The authors wish to thank K. J. Tauer and A. Marotta for kindly supplying the gadolinium single crystal and to acknowledge helpful discussions with G. Gelade, F. W. Harrison, B. C. Hegarty, K. Hoselitz and K. Tweedale. One of us (P.M.W.) is indebted to the Department of Scientific and Industrial Research for the provision of a maintenance grant.

References

Barlow, G. S., and Standley, K. J., 1958, Proc. Phys. Soc., **71**, 45.

Birss, R. R., and Wallis, P. M., 1963, J. Sci. Instrum., **40**, 551.

Bozorth, R. M., 1951, Ferromagnetism (New York: Van Nostrand).

——1954, Phys. Rev., **96**, 311.

Brailsford, F., 1960, Magnetic Materials, 3rd Edn. (London: Methuen).

Corner, W. D., Roe, W. C., and Taylor, K. N. R., 1962, Proc. Phys. Soc., **80**. 927.

Graham, C. D., 1962, J. Phys. Soc. Japan, **17**, 1310.

McKeehan, L. W., 1937, Phys. Rev., **51**, 136.

Nakamura, Y., 1955, J. Phys. Soc. Japan, **10**, 937.

Reich, K. H., 1956, Phys. Rev., **101**, 1647.

Sato, H., and Chandrasekhar, B. S., 1956, J. Phys. Chem. Solids, **1**, 228.

Stoner, E. C., 1950, Rep. Progr. Phys., **13**, 83.

Reprinted from the *Journal of Scientific Instruments*, VOL. 42, pp. 322–325, MAY 1965

APPENDIX A5

A torque magnetometer for a wide range of temperatures

R. R. BIRSS and P. M. WALLIS
Physics Laboratory, University of Sussex, Falmer, Brighton, Sussex
MS. received 27th October 1964, in revised form 17th December 1964

Abstract. This paper describes the modifications made to a torque magnetometer previously described by the authors to permit its use within the temperature range 77–373 °K. These limits are set by the arrangements used for temperature control (also described) and do not represent intrinsic limits of the method. The performance of the device has been checked by measurement of the temperature variation of the first magnetocrystalline anisotropy constant of nickel.

1. Introduction

In a recent paper (Birss and Wallis 1963) a description was given of a new form of torque magnetometer that permitted the measurement of the small torques developed in isolated ferromagnetic samples during measurement of magnetocrystalline anisotropy and rotational hysteresis. The torque-sensing elements were very fine resistance wires arranged in a particularly advantageous balanced configuration (fully described in the original paper), and forming two arms of a Wheatstone bridge circuit. The device had a number of advantages which included insensitivity to unwanted torques and translational forces and to small changes in temperature, pressure and magnetic field. The stability of the torque magnetometer against small changes in the ambient temperature was so good, in fact, that it was felt that the device could be modified to permit its use over an extended range of temperatures. Such a modification proved possible and this paper describes an experimental arrangement that has been used for temperatures between 77 and 373°K. These temperature limits are set by the means used to control the temperature (described in § 3) and there is no doubt that the torque magnetometer itself would work satisfactorily over a much larger range of temperatures.

2. The modified torque magnetometer

Before modification, the torque magnetometer was not particularly suitable for measurements at temperatures other than room temperature because of the method used for calibration. This was effected by rotating a torque head (with microscale) to twist a torsion filament, the resultant torque applied to the specimen (calculated from the modulus of rigidity of the filament) being used for calibration purposes. It would therefore be necessary to determine the variation of this elastic constant with temperature from a separate experiment and a rather elaborate arrangement for temperature control would thus be required for calibration purposes as well as for actual measurements of torque on particular specimens.

The modification to the original design of the torque magnetometer that permitted calibration under working conditions at any temperature was facilitated by the fact that measurements are always made in a large uniform magnetic field. It is therefore feasible to connect a rectangular coil (M in figure 1) rigidly to the specimen holder C and to use the torque developed in the coil when it carries a current in the magnetic field to calibrate the torque magnetometer directly. It is important, for reasons mentioned later, that the demagnetizing field of the specimen should not contribute appreciably to the flux through the coil. The lower end of the coil and the specimen holder are therefore connected by a rigid brass rod N and are separated at their nearest points by at least 9 mm. The top end of the coil is

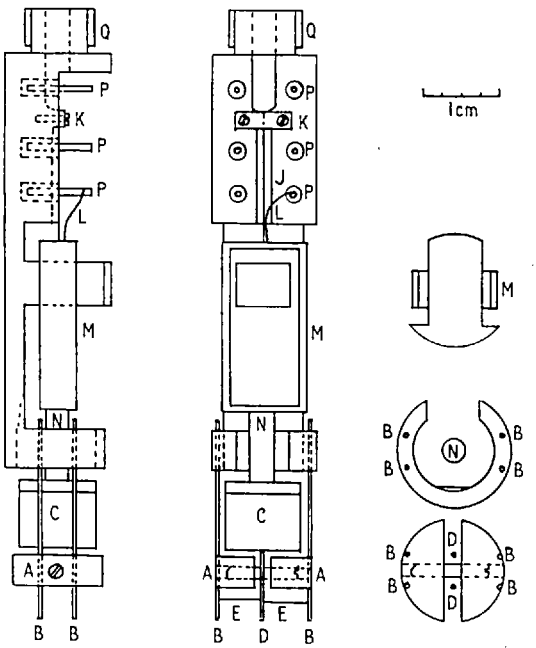


Figure 1. Two elevations, with cross sections, of the modified torque magnetometer.

A, clamp jaws; B, outer support posts; C, specimen holder; D, inner support posts; E, resistance wires; J, phosphor bronze filament; K, filament clamp; L, silver ligament; M, rectangular coil; N, brass connecting rod; P, soldering posts; Q, threaded mounting stud.

connected to a flattened phosphor bronze filament J, which acts both as a suspension and as an electrical connection to the coil. The other electrical connection to the coil is made via a silver ligament L, which carries current between a terminal at the top of the coil and one of the insulated soldering posts P.

A modification is also made to the method of terminating the strain-sensing resistance wires at the outer support posts B. Originally the posts were insulated with a thin layer of

Araldite and the resistance wire was wound round them and anchored with Durafix. Electrical connections were then made separately to the free unstressed end of the resistance wire. This method has the advantage that the state of stress of the wire cannot affect the contact resistance of the electrical connection but it requires a fairly substantial length of non-active resistance wire: this leads to a reduction in that with carefully soldered joints the effect of strain on the contact resistance at the joint is not troublesome.

The specimen, contained by the specimen holder C, was originally mounted on a rubber pad which permitted a small degree of flexibility in the plane of the disk. However, at low temperatures, rubber is unsuitable for this purpose and the specimen was therefore mounted on a pad of asbestos paper.

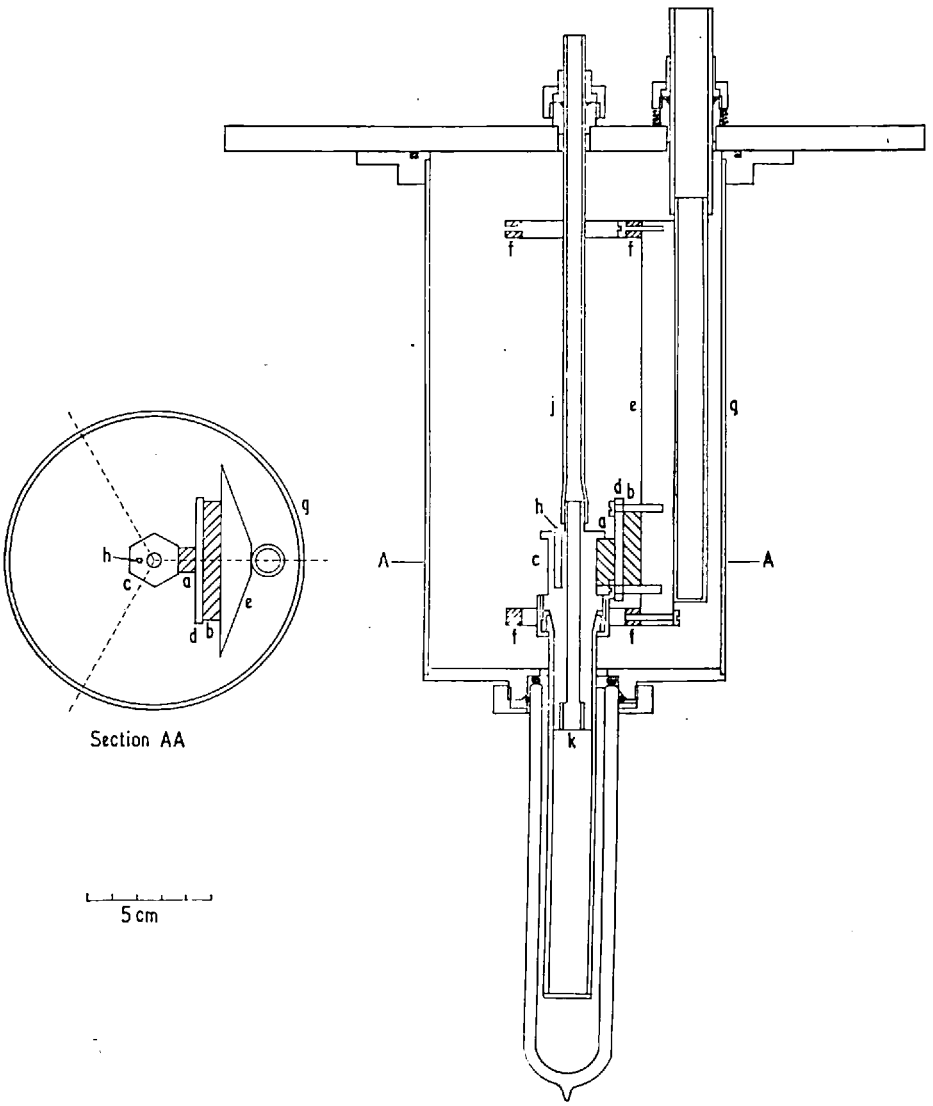


Figure 2. Arrangements for temperature control.

a, first-stage cooling modules; b, second-stage cooling module; c, torque magnetometer housing; d, interstage heat conductor; e, second-stage heat conductor; f, brass rings; g, vacuum vessel; h, drill-hole for platinum resistance thermometer; j, polythene tube; k, threaded hole for mounting torque magnetometer.

sensitivity and also to rather clumsy arrangements for connections to the leads. The modification is to use enamelled Constantan wire (22 s.w.g.) for the support posts B, so that there is no electrical connection between them and the body of the torque magnetometer. The strain-sensing resistance wire can then be soldered directly to the support post, connections from the soldering posts P at the top of the torque magnetometer being made to the other free projecting ends of the support posts. In practice it is found

The procedure adopted to calibrate the torque magnetometer at a given temperature is as follows. A current of the order of 10 mA is supplied to the coil with a magnetic field applied in an arbitrary direction and the magnet is then rotated about the torque magnetometer until the position of minimum torque is reached. A further rotation of the magnet through 90° is then made and the variation in the deflection of the torque magnetometer with current through the coil is observed. Finally the current supply to the coil

is disconnected and the flux through the coil measured with a fluxmeter at the position of minimum torque. Clearly, there must be a negligible contribution to the flux through the coil from the demagnetizing field of the specimen. In addition care is taken in positioning the connecting wires so that the flux measured is due only to the coil and not to the disposition of other parts of the circuit in the magnetic field.

3. Arrangements for temperature control

The temperature of the specimen (and, in fact, of the whole torque magnetometer shown in figure 1, which is attached below the position k in figure 2) is controlled by a unit that employs thermoelectric cooling modules supplied by De La Rue Limited under the trade name of 'Frigistors'. The smallest, standard, 15 A module consists of four thermocouples. Each thermocouple comprises a pair of conducting elements, and the eight elements are connected electrically in series but are arranged so that the hot junctions abut on to an aluminium plate (9 mm × 19 mm) and the cold junctions on to a similar parallel plate. The plates are about 6 mm apart and they are in thermal but not electrical contact with the thermocouple junctions. The overall width of the module, measured across the aluminium plates, is about 7 mm. Heavy-current leads are attached at one end of the module. The maximum heat pumped against zero temperature gradient is 3·5 W and the ultimate temperature difference between hot and cold junctions is 62°C for zero heat pumped. This assumes that the hot junctions are held at 27°C, with the module run at 15 A and 0·4 V. In the temperature control unit there are two stages of cooling modules run in cascade, so that a larger temperature difference can be achieved with normal water cooling of the hot junction of the second stage. The ratio of the numbers of modules in the first and second stages is the suggested one of 1 : 6.

Temperatures above room temperature can be attained by reversing the current through the modules, the upper temperature limit being set by the melting point of the solder used in the construction of the 'Frigistors'. In practice this allows an upper temperature of about 100°C. The temperature range of the unit can be further extended by cooling the 'hot' junctions of the second stage to 77°K with liquid nitrogen. Although the maximum temperature difference between hot and cold junctions is very much reduced at these low temperatures, temperatures between 77°K and room temperature can readily be obtained by using the module with reverse current.

The mechanical layout of the temperature control unit is shown in figure 2. The torque magnetometer is mounted in this unit by screwing the threaded stud Q, at the top of the apparatus, shown in figure 1, into the threaded hole k, shown in figure 2. The cooling modules (a and b) of the first and second stages are arranged with three-fold symmetry round the central copper housing c that contains the torque magnetometer, shown in figure 1. For clarity, only one of the three identical units is shown in the figure. Nylon bolts are used to clamp the second-stage 'Frigistors' between the interstage heat conductor d and the water or liquid-air cooled conductor e adjacent to the 'hot' junction of the second stage. The first-stage 'Frigistors' a are held in position by bolting the three second-stage, 'hot' junction conductors e to two brass rings f which press the three identical units inwards so as to clamp on to hexagonal faces on the housing c. A polished brass vessel g makes it possible to maintain the whole temperature control apparatus under vacuum, whilst a polythene tube j enables the atmosphere within the torque magnetometer housing to be controlled separately. A precalibrated thermocouple is used to measure the absolute temperature of the torque magnetometer and specimen.

The method of clamping the first-stage 'Frigistors' ensures that there are no thermal connections to the first stage due to structural supports. The only thermal connections that remain (apart from convection and radiation) are those provided by the polythene tube j and the leads to the torque magnetometer, the thermocouple and the platinum resistance thermometer—which is located in drill-hole h. Convection and radiation losses are reduced by the use of the polished brass vacuum vessel g evacuated to a pressure of between 100 and 10 μtorr of mercury. To improve heat transfer, the space between the copper housing and the torque magnetometer is not evacuated for temperatures above that of liquid air.

The control system used to maintain a given temperature to within about $\frac{1}{50}$ degC for periods up to four hours is shown schematically in figure 3. The temperature of the torque magnetometer housing is measured with a platinum resistance thermometer which is connected, in series with a variable resistance, into one arm of a Wheatstone bridge circuit. The out-of-balance error signal from the bridge is used to control a continuously variable direct-current power supply (via an a.c. amplifier) to the first stage of the thermoelectric cooling unit. The variable resistance is set to a value that determines the stabilization temperature of the system. The series arrangement of the variable resistance and platinum resistance thermometer ensures that the output impedance of the bridge at balance does not vary with temperature. A separate, manually controlled power unit is used to supply power to the second stage of the thermoelectric cooling unit.

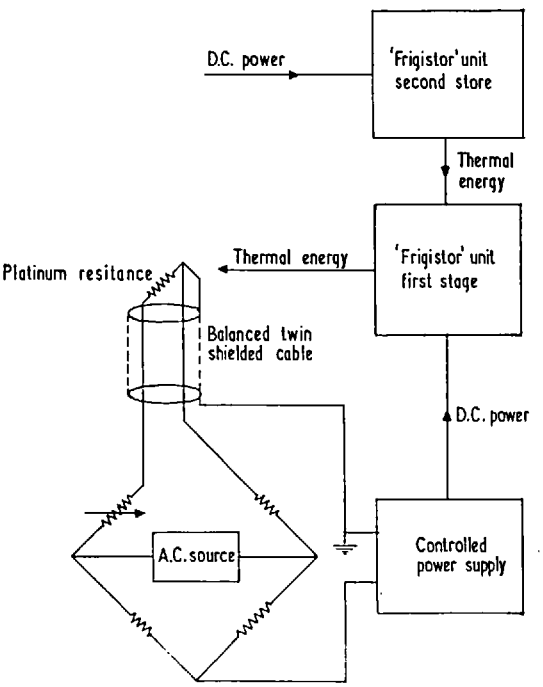


Figure 3. Schematic diagram of the temperature control system.

4. Performance of the torque magnetometer

To test the performance of the torque magnetometer over the temperature range attainable with the equipment described above, measurements were made of the first magnetocrystalline anisotropy constant K_1 for nickel, using a single-crystal disk orientated parallel to a (110) crystallographic plane. In high fields, the anisotropy torque in this plane is given by

$$T = \frac{K_1}{8}(2\sin 2\theta + 3\sin 4\theta) - \frac{K_2}{64}(\sin 2\theta - 4\sin 4\theta - 3\sin 6\theta) \qquad (1)$$

where T is the torque exerted on the crystal per unit volume of the crystal and θ is the angle measured from a $\langle 100 \rangle$ direction to the direction of the magnetization vector.

The torque curves obtained experimentally for various values of applied field were subjected to Fourier analysis to obtain the components periodic in 2θ and 4θ, and hence the effective value of K_1. (The contribution to the torque from K_2 is so small that equation (1) cannot be used to obtain reliable values for this constant.) Equation (1) is strictly true only for very large fields, when the directions of the magnetization vector and the magnetic field coincide and lie in the (110) plane. In practice, this is not quite so and the effective value of K_1 is plotted against the reciprocal of the applied field to obtain, by extrapolation to infinite field, the true value of K_1. Values of K_1 obtained in this way are in good agreement with the known temperature dependence of K_1. At the lowest temperature attainable (77°K), the value of K_1 is almost midway between that obtained by Williams and Bozorth (1939) and by Honda, Masumoto and Shirakawa (1935). It may therefore be concluded that the modified torque magnetometer functions satisfactorily over the temperature range from 77 to 373°K and is likely to do so over a more extended temperature range provided appropriate attention is given to the arrangements for temperature control.

Acknowledgments

The authors wish to thank E. M. Wareham (Measuring Systems) Limited for undertaking the construction of the electronic control equipment mentioned in § 3. One of us (P.M.W.) is indebted to the Department of Scientific and Industrial Research for the provision of a maintenance grant.

References

BIRSS, R. R., and WALLIS, P. M., 1963, *J. Sci. Instrum.*, **40**, 551.

HONDA, K., MASUMOTO, H., and SHIRAKAWA, Y., 1935, *Sci. Rep. Tôhoku Univ.*, **24**, 391.

WILLIAMS, H. J., and BOZORTH, R. M., 1939, *Phys. Rev.*, **56**, 837.

UNWIN BROTHERS LIMITED, WOKING AND LONDON (B3873

APPENDIX B

CIRCUIT FOR THE TEMPERATURE CONTROLLED D.C. POWER SUPPLY FOR FRIGISTOR COOLING MODULES

